Ethobehavioral strategies for the study of fear in mice

Dissertation der Fakultät für Biologie

der Ludwig - Maximilians - Universität München

Andreas Johann Genewsky

Eingereicht am 20. September 2017

München

This page intentionally left blank.

Ethobehavioral strategies for the study of fear in mice

Dissertation der Fakultät für Biologie

der Ludwig - Maximilians - Universität München

Andreas Johann Genewsky

Eingereicht am 20. September 2017

Tag der mündlichen Prüfung 26. Februar 2018

Diese Dissertation wurde angefertigt unter der Leitung meines Doktorvaters *PD Dr. rer. nat. Carsten T. Wotjak* am Max-Planck Institut für Psychiatrie und der Ludwig-Maximilians-Universität München.

Erstgutachter:	**PD Dr. rer. nat. Carsten T. Wotjak**
Zweitgutachter:	**Prof. Dr. Laura Busse**

München 2017

Eidesstattliche Erklärung

Ich versichere hiermit an Eides statt, dass die vorgelegte Dissertation von mir selbständig und ohne unerlaubte Hilfe angefertigt ist.

München, den 8. Juni 2018 Andreas J. Genewsky

(Unterschrift)

Erklärung

Hiermit erkläre ich, *

☒ dass die Dissertation nicht ganz oder in wesentlichen Teilen einer anderen Prüfungskommission vorgelegt worden ist.

☒ dass ich mich anderweitig einer Doktorprüfung ohne Erfolg **nicht** unterzogen habe.

☐ dass ich mich mit Erfolg der Doktorprüfung im Hauptfach .....

und in den Nebenfächern .....

bei der Fakultät für ..... der .....

(Hochschule/Universität)

unterzogen habe.

☐ dass ich ohne Erfolg versucht habe, eine Dissertation einzureichen oder mich der Doktorprüfung zu unterziehen.

München, den 8. Juni 2018 Andreas J. Genewsky

(Unterschrift)

*) Nichtzutreffendes streichen

And I gave my heart to seek and search out by wisdom concerning all things that are done under heaven.

(*Eccles. 1:13 (KJV)*)

To T.R.S & M.J.G.

Danksagung

Der Weg bis zur nun vorliegenden Dissertation ist geprägt von Personen die sich meiner in außerordentlicher Weise annahmen und es mir dadurch ermöglichten eine unerschütterliche Hingabe zu den Naturwissenschaften zu entwickeln. So wurde ich stets in meinen eigenen Bestrebungen bestärkt und respektvoll aber bestimmt zu selbständigem, wissenschaftlichen Arbeiten angeleitet. Ich danke Std. Johann Bründl, Univ.-Prof. Dr. Sébastien Couillard-Després, Univ.-Prof. Dr. Ludwig Aigner, Dr. Bastian Zimmer, Prof. Dr. Marcel Leist, Dr. Sabine Kreissl und Prof. Dr. Olaf Strauß.

Dies allein genügt jedoch nicht um das notwendige Maß an Motivation und Selbstvertrauen aufzubringen, und mein Dank gilt daher in besonderem Maße meinen Eltern, Frau Waltraud Genewsky und Herrn Ernst Genewsky, sowie meinem Bruder Dipl. Ing.(FH) Axel Genewsky die aus mir einen rechtschaffenen Menschen gemacht haben. Für die gemeinsamen Stunden bei handwerklichen Tätigkeiten, auf der Suche nach Pilzen im Wald, in der Werkstatt, im Elektronikkämmerchen und bei der Fischerei, bin ich überaus dankbar.

Für das Ermöglichen meiner Promotion am Max-Planck Institut für Psychiatrie und dem mir entgegengebrachten Respekt und Vertrauen, möchte ich meinem Doktorvater Herrn PD Dr. Carsten T. Wotjak aufrichtig danken. Die Verantwortung in der studentischen Ausbildung, die weitreichende Forschungsfreiheit, die scharfen wissenschaftlichen Diskurse und die betont edukative Betreuung haben nicht zuletzt meinen Wunsch bestärkt, eine weitere akademische Laufbahn zu verfolgen.

Mein Dank gilt auch meinen Arbeitskollegen, den Praktikanten und Studenten die mich während meiner Arbeit begleiteten und besonders meinen Freunden, da sie die Zeit am Institut zu einer unvergesslichen und wertvollen Erfahrung werden ließen.

Insbesondere möchte ich mich bedanken bei Nina Scheithauer, Kasyoka Kilonzo, Dr. Andreea Simona-Bura, Markus Nussbaumer, Paul M. Kaplick, Daniel E. Heinz, Mareen Engel, Dr. Sebastian F. Kaltwasser, Caitlin J. Riebe, Dr. Benedikt T. Bedenk, Dr. Michael Czisch, Dr. Judith Reichel, Suellen Almeida-Correa, PhD. Julien Dine, Dr. Matthias Eder, PhD. Elmira Anderzhanova, Dr. Jan M. Deussing, PhD. Rafael Carvalho Almada, Prof. Oded Klavir und Julia Sulger.

All dies wäre jedoch nur wenig Wert, könnte ich es nicht mit meiner Frau Tabea und unserem Sohn Mats teilen. Ich danke Euch für die Liebe, Kraft und Zuversicht derer Ihr mir zuteil werden lässt.

This page intentionally left blank.

Contents

List of Figures

List of Tables

Listings

Abbreviations & Acronyms

AAV adeno-associated virus
ABR auditory brainstem response
ACA anterior cingulate area/cortex
aCSF artificial cerebrospinal fluid
ACh acetylcholine
ACTH adrenocorticotropic hormone
ADH antidiuretic hormone, *see* AVP
AIC anterior insular cortex
AHA anterior hypothalamic area
AHN anterior hypothalamic nucleus
Amb nucleus ambiguus
AMPA α-amino-3-hydroxy-5-methyl-4-isoxazolepropionic acid
ANS autonomic nervous system
ANOVA analysis of variances
ARAS ascending reticular activating system
Arc arcuate nucleus
ASR acoustic startle response/reflex
AVP arginine vasopressin
BIC brachium of the inferior colliculus
BL6 C57BL/6
BLA basolateral amygdala
BMA basomedial amygdala
BNST bed nucleus of the stria terminalis
bp base pairs
bpm beats per minute
CA1 cornu ammonis, subfield 1
CBT cognitive behavioral therapy
CEA central amygdala
CEl centrolateral amygdala
CEm centromedial amygdala
ChR2 channelrhodopsin-2

CRF corticotropin-releasing factor

CRFR corticotropin-releasing factor receptor

CRH corticotropin-releasing hormone (=CRF)

CoA cortical amygdala

CORT cortisone or corticosterone (depending on the context)

COX cytochrome-*c* oxidase

CNO clozapine-*N*-oxide

CPP conditioned place preference

CS conditioned stimulus

CR conditioned response

CRAC Ca^{2+} release-activated channel

Cre causes recombination

CUN cuneiform nucleus

cyc/deg cycles per degree

DAB diaminobenzidine

dACC dorsal anterior cingulate cortex

DAPI 4',6-diamidino-2-phenylindole

DBS deep brain stimulation

dHPC dorsal hippocampus

DIO 'double-floxed' inverted open reading frame

DLB dark-light box

DMH dorsal medial hypothalamus

DMM dorsomedial medulla

dmPAG dorsomedial periaqueductal gray

dmPFC dorsomedial prefrontal cortex

dlPAG dorsolateral periaqueductal gray

dlPFC dorsolateral prefrontal cortex

DSM-IV Diagnostic and Statistical Manual of Mental Disorders

DZP diazepam

EAA excitatory amino acid

EBL emotional body language

EBT exposure-based therapy

eCB endocannabinoid system

EGFP enhanced green fluorescent protein

EPM elevated plus maze

ER estrogen receptor

FC auditory fear conditioning

FDR false discovery rate

fERG flash electroretinography/electroretinogram

fMRI functional magnetic resonance imaging

FPS fear-potentiated startle

FST forced swim test

GAD generalized anxiety disorder

GIH growth hormone-release inhibiting hormone

GHRH growth hormone-releasing hormone

GnRH gonadotropin-releasing hormone

GR glucocorticoid receptor

HAB high anxiety-related behavior

HB holeboard test

HPC hippocampus

IA inhibitory avoidance

IC inferior colliculus

ICD-10 International Classification of Diseases

icv intracerebroventricular

ICX external nucleus of the inferior colliculus

IHC immunohistochemistry

ILA infralimbic area/cortex

i.p. intraperitoneal

ipRGC intrinsically photosensitive retinal ganglion cells

ITCs intercalated cell masses

LA lateral amygdala

LAB low anxiety-related behavior

LC locus coeruleus

LDT lateral dorsal tegmental nucleus of the thalamus

LED light-emitting diode

LHA lateral hypothalamic area

laser light amplification by stimulated emission of radiation

LCD liquid crystal display

LGd dorsal part of the lateral geniculate nucleus

LGv ventral part of the lateral geniculate nucleus

lPAG lateral periaqueductal gray

LS lateral septal region or lateral septal nucleus/complex

LP lateral posterior nucleus of the thalamus

LTP long-term potentiation

MAFIA mouse anxiety, fear, inhibitory avoidance

MD mediodorsal thalamic nucleus

MDTB Mouse Defense Test Battery

MeA medial amygdala

MEMRI manganese-enhanced magnetic resonance imaging

MGm medial section of the medial geniculate nucleus

MHDS medial hypothalamic defensive system

MPN medial preoptic nucleus

MR mineralocorticoid receptor

MRI magnetic resonance imaging

mPFC medial prefrontal cortex

NAB normal anxiety-related behavior

NAc nucleus accumbens

NE norepinephrine

NMDA *N*-methyl-D-aspartic acid

NTS nucleus of the solitary tract

OCD obsessive-compulsive disorder

OFC orbitofrontal cortex

OKR optokinetic response

OMR optomotor response

ONL outer nuclear layer

OTT one-trial tolerance

PAG periaqueductal gray

PB parabrachial nucleus

PBG parabigeminal nucleus

PCR polymerase chain reaction

PD panic disorder

PeF perifornical region

PET positron emission tomography

PFA paraformaldehyde

PFC prefrontal cortex

PIH prolactin-release inhibiting hormone

PMC pontine micturition center

PMD premammillary dorsal nucleus

POMC pro-opiomelanocortin

PPN pedunculopontine tegmental nucleus

PPT *see* PPN

PrL prelimbic cortex

PRN pontine reticular nucleus

PTSD post-traumatic stress disorder

PV parvalbumin
PVC polyvinyl chloride
PVN paraventricular nucleus of the hypothalamus
PVT paraventricular nucleus of the thalamus
rpm rounds per minute
RE nucleus reuniens
RF radio-frequency
RVM rostral ventral medulla
RVLM rostral ventrolateral medulla
s.c. subcutaneously
SC superior colliculus
SII secondary somatosensory cortex
SSFO stabilized step function opsin
SSRI selective serotonin reuptake inhibitor
SNRI serotonin-norepinephrine reuptake inhibitor
SP sucrose preference test
TMT 2,5-dihydro-2,4,5-trimethylthiazoline
TST tail-suspension test
TRH thyrotropin-releasing hormone
TRP transient receptor potential channel
US unconditioned stimulus
USV ultrasonic vocalization
vg viral genomes
VGCC voltage-gated calcium channel
vlPAG ventrolateral periaqueductal gray
vlPFC ventrolateral prefrontal cortex
VLM ventrolateral medulla
VMH ventromedial hypothalamic nucleus
VSDI voltage sensitive dye imaging
VIP vasoactive intestinal peptide
VTA ventral tegmental area
WCM water cross maze
ZI zona incerta

This page intentionally left blank.

Abstract

Experimental paradigms for the study of anxiety-like behavior in mice, often utilize the avoidance of exposed and brightly illuminated areas. One classical example of such a task is the elevated plus-maze (EPM). The selective bidirectional breeding for extreme behavior on the EPM resulted in two mouse lines, namely high-anxiety behaving (HAB) and low-anxiety behaving (LAB) mice. The core question of this study was, whether the extremes in trait-anxiety of HAB and LAB animals are accompanied by altered innate fear responses. Therefore, two novel, multi-sensory tasks were developed, which assay repeated, innate escape behavior towards an impeding threatening stimulus. Using these two novel tests, it could be demonstrated (a) that HAB animals exhibit exaggerated fear responses which are reflected by a strong but maladaptive escape behavior and an extreme disposition to vocalize, and (b) that LAB animals exhibit a profound deficit in escaping impeding threats. Further, it was discovered that LAB animals suffer from complete retinal blindness, which however, can only in part explain their fear response deficiency. Using manganese-enhanced magnetic resonance imaging (MEMRI), an increased activation of the periaqueductal gray (PAG) in HAB mice, as well as a decreased activation of the superior collicullus (SC) in LAB mice, could be identified. These two midbrain areas are core regions in mediating fear responses. In order to test whether these two brain areas are involved in the generation of both extreme phenotypes, either local injections of the potent $GABA_A$-agonist muscimol within the PAG of HAB animals, or the pharmacogenetic activation using the designer receptor exclusively activated by designer drugs (DREADD) hM3Dq in the SC of LAB have been applied. Thereby, the extreme behavior of both strains could successfully be normalized. This study demonstrated the applicability of tow novel ethologically inspired innate fear assays (Robocat & IndyMaze). Further it was shown that midbrain structures govern the expression of anxiety-like behavior in two strains of mice, which were selectively bred for extremes in trait-anxiety. These findings emphasize the importance of *primordial* midbrain 'emotion' centers, in the generation of affect, suggesting a role which is beyond mere behavioral output.

Zusammenfassung

Experimentelle Paradigmen zur Untersuchung angstähnlichem Verhaltens in Mäusen, stützen sich oft auf die angeborene Abneigung gegenüber besonders exponierten und hell beleuchteten Arealen. Ein klassiches Beispiel für einen solchen Test ist die *elevated-plus maze* (EPM). Die selektive bidirektionale Zucht auf extremes Verhalten im EPM-Test hat zwei Mäuselinen hervorgebracht, zum einen die erhöht ängstlichen Tiere (high anxiety-like behaving, HAB), zum anderen die wenig ängstlichen Tiere (low anxiety-like behaving, LAB). Die Kernfrage dieser Arbeit war, ob sich die extrem unterschiedlichen Niveaus der Eigenschaftsangst von HAB und LAB Tieren auch in den angeborenen Furchtreflexen widerspiegelt. Hierzu wurden zwei neuartige, multisensorische Tests entwickelt, welche angeborenes Fluchtverhalten gegenüber einer herannahenden Bedrohung bemessen, wobei ein besonderers Augenmerk auf die Möglichkeit der wiederholten Testung gelegt wurde. Die Anwendung dieser Verhaltenstests hatte gezeigt, dass HAB Mäuse eine übersteigerte Furcht aufweisen, die sich besonders durch ausgeprägtes, aber jedoch maladaptives Fluchtverhalten auszeichnet und zudem zeigen die Tiere eine auffälige Neigung zur Vokalisation im hörbaren Bereich. LAB Tiere, hingegen, zeigten ein deutliches Defizit, herannahenden Bedrohungen auszuweichen. Diese Beobachtung führte zur Untersuchung der visuellen Fähigkeiten von LAB Mäusen (u.a. mittels Elektroretinographie), und es stellte sich heraus, dass bei diesen Tieren die Photorezeptorschicht der Netzhaut gänzlich fehlt, und sie somit als blind gelten können. Diese Tatsache allein kann allerdings nur teilweise den Phänotyp erklären, da LAB Tiere auch nach einer Kollision mit dem herannahenden Objekt nur in den seltensten Fällen eine Fluchtantwort zeigen. Mittels Mangan-verstärkter Magnetresonanztomographie (*manganese-enhanced magnetic resonance imaging*, MEMRI) konnten des Weiteren eine erhöhte neuronale Aktivität im periaquäduktalen Grau (PAG) von HAB Mäusen, sowie eine reduzierte Aktivität in den Colliculi superiores (SC) von LAB Tieren aufgezeigt werden. Diese beiden Regionen des Mittelhirns stellen wichtige Kerngebiete zur Vermittlung von Furchtantworten dar. Um festzustellen ob diese Hirnregionen für die Präzipitation der extremen Phänotypen von HAB und LAB Tieren verantwortlich sind, wurden zum einen lokale intrazerebrale Mikroinjektionen eines $GABA_A$-Agonisten (Muscimol) im PAG von HAB Mäusen durchgeführt, zum anderen wurde die pharmakogenetische Aktivierung neuronaler Zellen im SC von LAB Mäusen angewendet. Beide Vorgehen haben auf erfolgreiche Art die extremen Verhaltensweisen der jeweiligen Mäuseline normalisiert. Diese Arbeit hat die Anwendbarkeit zweier neuartiger, an ethologischen Grundsätzen angelehnter Verhaltenstests zur Untersuchung angeborenen Furchtverhaltens (Robocat & IndyMaze) dargelegt. Überdies konnte gezeigt werden, dass Mittelhirnstrukturen die Ausprägung von angstähnlichem Verhalten zweier Mäuselinen, welche auf extreme Unterschiede in ihrer Eigenschaftsangst gezüchtet wurden, bestimmen. Diese Ergebnisse unterstreichen die Wichtigkeit der uranfänglichen Emotionszentren des Mittelhirns bei der Erzeugung von Affekt, und deuten auf eine Rolle dieser Zentren hin, die über den bloßen Verhaltensoutput hinausgeht.

A time to weep, and a time to laugh; a time to moan, and a time to dance.

Eccles. 3:4 (KJV)

Chapter 1

Introduction

Animal studies founded the basis of natural sciences throughout the centuries. Be it Luigi Galvani's discovery of bioelectricity in the 18th century, or the very recent leap in understanding the three-dimensional representation of the world within the hippocampus and entorhinal cortex (O'Keefe and Dostrovsky, 1971; Fyhn et al., 2004). As animals have served zoologists to grasp the organization of living matter, animals also served to understand the emergent properties of cells and tissues, giving rise to complex physiological & behavioral processes, such as reproduction, digestion, secretion and courtship display.

As Lorenz (1958) describes, the morphological similarities between a whale's flipper, a bat's wing and a man's arm are obvious and point to a common phylogeny. Further, K.Z. Lorenz notes the striking similarities between different species carrying out the same behavior (scratching in dogs and birds) and involving the same motor patterns. This suggests a common *phylogeny of behavior*. It is justifiable to assume that not only observable states are subject to evolution, but also internal subjective phenomena. The affective states *viz.* social joy, expectancy, anxiety, anger, sadness, sexual excitement and nurturance (Panksepp and Biven, 2012, p. xi) have to be understood as emergent properties of the cellular nature of the brain. These subjective internal states of mind are those which trouble the mentally ill and form the focus of psychiatric practice. Pathological alterations of affect manifest as anxiety disorders (e.g. generalized anxiety, social anxiety, panic), depressive disorders, obsessive-compulsive disorders, impulse-control disorders and addictive disorders. Inspired by cognitive sciences, modern psychiatric research concentrates on the cerebral control of affects. This is owed to the circumstance that the human neocortex is the origin of highly complex socio-emotional processes e.g. pride, shame, confidence, guilt or jealousy (Panksepp and Biven, 2012, p. xi). But the overwhelming primordial emotions are piloted by the diencephalon and mesencephalon. The study of the neural circuits which mediate those emotions in animals will lead to a targeted pharmacological modulation of affective symptoms in psychiatric disorders.

The way a layperson but also a psychiatrist, typically attempts to obtain information about the mental state of another person, happens via verbal communication. Hereby, it is of the essence that both partners use the same language. The use of animals in the study of affective neuroscience lacks this possibility, and one has mostly to rely

on observable measures as we are dealing with private minds. When the Nobel Prize winning ethologist Niko Tinbergen noted, 'subjective phenomena cannot be observed objectively in animals, it is idle to claim or deny their existence' (Tinbergen, 1951, p. 5), he brought up a painful subject. It is not enough to merely rely on observation alone, but it is necessary to establish physiological (e.g. heart rate, blood pressure, electromyography) and neurophysiological correlates of emotion. Here, I want to emphasize that a strict denial of an anthropomorphic conception, will lead to insufficient findings at most. Questions in behavioral neuroscience need to be approached with a *biocentric anthropomorphism* (Bekoff, 2000), and answered with ethologically inspired (Pellman and Kim, 2016) experimental strategies. The question if animals have emotions is a peculiar one. The complexity of animal affective states, forms a continuum and increases as a function of the social capabilities and cerebral development. *Emotion* is a word from the human language. It describes subjective phenomena which can only be felt and communicated by humans. Thus, whether animals have emotions or not, is a semantic question.

The present work discusses the study of negative affect, with special emphasis on defensive responses. In the introduction I will describe the affective states resembling the feelings of Fear, Anxiety & Panic. Subsequently, we explore the bodily changes which accompany these emotions and dwell on the underlying brain regions and their connectivity. Further, I will cover the pathologically altered states of fear and anxiety in humans, and briefly discuss the current treatment strategies. We will see in detail how the amygdala, periaqueductal gray and the superior colliculus are involved in the generation of defensive responses, and how established animal models aid the understanding of anxiety disorders. Finally, I will present selected methods in neuroscience which permit the *dissection* of neural circuits and ultimately advance our understanding how the brain gives rise to complex behavioral patterns.

1.1 Definition of Fear, Anxiety & Panic

The conceptual distinction between Fear, Anxiety & Panic is usually not made in our everyday life. However, strictly speaking, these words describe quite different conditions. The word fear stems from the Anglo-Saxon words *fær* (fear) or *vār* (ambush) (Donald and Chambers, 1872, p. 176). It describes the affective states and behavioral patterns which are elicited with respect to a clear, threatening stimulus. The behavioral repertoire of fear has the sole purpose to increase the distance between the subject and the threat. Pathologically altered fear precipitates as specific phobias (e.g. arachnophobia) or as an exaggerated fear response in the case of post-traumatic stress disorder (PTSD). It is important to note that neither specific phobias nor PTSD can be effectively treated with classical anxiolytics like alprazolam, diazepam or lorazepam (Sartory et al., 1990; Guina et al., 2015).
Anxiety, on the other hand, is mainly characterized by worries about distant or potential threats. It is an important cognitive process, which is strongly modulated by learning. In contrast to caution, anxiety intensifies the drive to retreat in order to seek

a safer environment. The word anxiety stems from the Latin words *anxietas* (Donald and Chambers, 1872, p. 18) or *angustia* (narrowness). Those words in turn can be derived from the Latin roots *anxi* or *ango*, both of which can be translated as *to choke* or *to strangle* (Wandruszka, 1981, p. 15). The occurrence of exaggerated anxiety in combination with constant ruminations about illusionary threats, indicates an anxiety disorder. For the classification of anxiety disorders the International Classification of Diseases (ICD-10) (World Health Organization, 1992) and DSM-IV (American Psychiatric Association, 1994) suggest besides phobia or PTSD also obsessive-compulsive disorder (OCD), panic disorder (PD), somatoform autonomic dysfunctions and generalized anxiety disorder (GAD). One major challenge in dealing with anxiety disorders, is the vicious circle of self-reinforcing avoidance. The patients do not expose themselves to any not fully-controllable environmental or social (agoraphobic) setting. This leads to isolation, as they associate their bodily integrity with avoidance and they will not leave their 'safety-zone'.

The third category is panic. Panic typically describes strong, undirected and uncontrollable fear reactions, which serve to evade life-threatening imminent danger. Along with flight, it includes defensive aggression. The word panic is derived from the Greek word *panikōs* 'belonging to Pan', the ancient Greek pastoral god, terrifying the nymphs with blind roar. In the year 2010 the horrifying incident of crowd panic at the 'Love Parade' in Duisburg, North Rhine-Westphalia, Germany (Helbing and Mukerji, 2012), has sadly shown the dramatic outcome of a stampede. The sudden feelings of intense terror, imminent death, loosing control and intense vegetative symptoms out of context are characteristic for pathological panic attacks. Patients usually develop a strong anxiety and avoidance reaction to places were they once suffered a panic attack. For example, a person who suffered a panic attack on a bridge, might have another episode only in expectation of being forced to cross a bridge. Interestingly, spontaneous and unexpected panic attacks are proceeded by cardiorespiratory instabilities, already one hour before the onset (Meuret et al., 2011). Panic disorders are characterized by the recurrent occurrence of sudden, unexpected panic attacks which manifest as feelings of intense anxiety and discomfort which climaxes within minutes. A further hallmark of this disorder is the fear of panic attacks and a high co-morbidity with agoraphobia (increased fear of unprotected environment, often with a strong social component).

1.2 Bodily Changes in Negative Affect: *Physiology of Emotion*

Affective states manifest in various forms of observable 'bodily' changes - the emotional body language (EBL). For the human being it is of uttermost importance to 'sense' and understand another person's internal state, as the dynamics within a group of people rely on highly developed social cues. As mentioned earlier, language serves as an important medium to communicate these internal states. Apart from words, non-verbal cues transport most of the unconsciously perceived information and constitute emotional

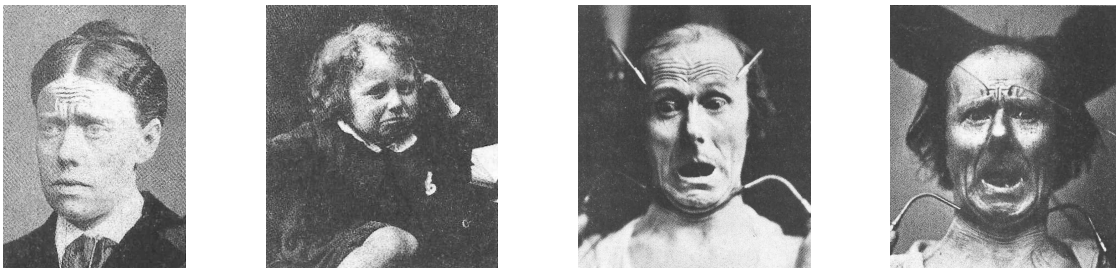

(a) (b) (c) (d)

Figure 1.1 | Facial Physiognomy of Anxiety & Fear
(**a**) Man with oblique eyebrows, (**b**) boy with drawn down corners of the mouth, (**c**) man with electrically provoked facial expression of fear or terror (**d**). (Darwin, 1872, pp. 181, 302, 303)

communication and decision making. Here, I summarize the bodily changes which occur with respect to negative internal states. I will make a gross distinction between clearly observable or behavioral, and non-behavioral signs of intense emotions.

Mimic Expressions of Emotion

The physiognomy of emotions in man and animals was first comprehensively described by Darwin (1872) who has greatly summarized also previous work of Bulwer (1644), Bell (1806), Gratiolet (1854) and Duchene de Boulogne (1862). Broadly speaking, based on Darwin's findings, one can divide the observable bodily changes in mimic and behavioral[†] expressions. While the mimic component gives information about the quality of the emotion, the behavioral component (e.g. *crouch* or *flight*) can also tell the direction of a threat (de Gelder, 2006). The mimic expressions of negative affect and 'low spirits' are quite different for anxiety/worry and fear/horror. The facial signs of worry are depicted in Fig. 1.1a, where we see an obliquity of the eyebrows, namely a raise of the inner ends, as well as a drawing down of the corners of the mouth (*see* Fig. 1.1b). Terrified facial expressions are dominated by the action of the *musculus platysma myoides*, the *muscle of fright*, which wrinkles the skin of the neck and strongly depresses the jaw (*see* Fig. 1.1c,d). But also oblique eyebrows and a strong tension in the muscles around the eye (*see* Fig. 1.1d). Facial expression are mediated via the *nervus fascialis* (cranial nerve VII), whose motor output is situated within the medulla. Afferent fibers to the facial nucleus arise from the ventro-caudal periaqueductal gray (PAG), the nucleus of Darkschewitsch and the rostral occulomotor nucleus (Panneton and Martin, 1979). Facial nerve paralysis renders patients unable to display facial expressions of emotions (Coulson et al., 2004).

Of course not only humans are able to show facial expression, but also monkeys, apes, horses, rodents and many more. Langford et al. (2010) showed that the facial expression − the grimaces − of mice change with respect to *physical* pain (*see* Fig. 1.2). Although

[†]Darwin used here the term habitual (in the sense of *'concerning the habitus'*) which is ambiguous as it can be confused with 'habituation', therefore the term *behavioral* will be used instead.

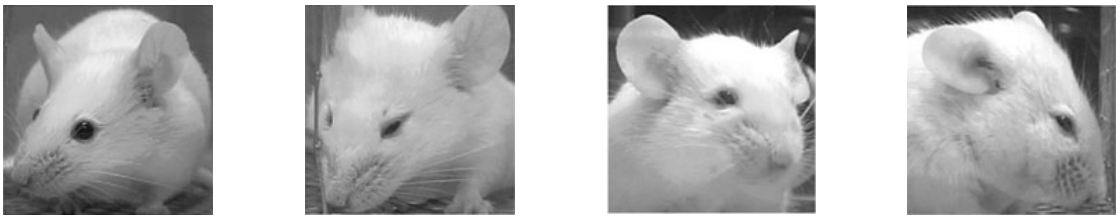

(a) normal **(b)** orbital thightening **(c)** nose bulge **(d)** ear position

Figure 1.2 | Murine Facial Physiognomy of Pain
(**a**) Normal animal, (**b,c,d**) and animals experiencing physical pain while displaying various types of facial expressions. (Langford et al., 2010)

pain cannot be considered to be an emotion, we know from auditory fear conditioning (*see* animal models of fear & anxiety) that mice typically squint their eyes in anticipation of the aversive unconditioned stimulus, which in turn clearly resembles a negative affect.

Behavioral Expressions of Emotion

Freezing & Flight The most distinct behavioral expressions of negative affect constitutes the two movement behaviors i.e freezing and fleeing (Blanchard and Blanchard, 1969). A simple example of both behaviors, with respect to their phylogeny, comes from the horse *Equus ferus spp.* and the donkey *Equus africanus spp.*. Both animals are closely related and share many common social behaviors. But they are also very distinct with respect to their flight response. While horses tend to bolt in the presence of an uncertainty, a donkey will freeze. This resulted in the donkey's reputation of being stubborn, although we just see a shift from an active towards a passive fear response. This striking difference is attributed to the different ground conditions (prairie or mountainous regions) in which both species developed (Goodwin, 2007). Both behaviors are adaptive in a way, that they promote self-preservation and constitute the last resort in response to an imminent inescapable threat. Similarly those behaviors are also present in humans and become evident in patients who suffer from anxiety disorders and especially during a panic attack. Levine (1997) reported a patient who was suffering from panic disorder and entered a full-blown anxiety attack during a therapy session and '*appeared paralyzed and unable to breathe*' and '*her heart was pounding wildly, and then seemed to almost stop*'. When the therapist tried to relieve her of this state by exclaiming loudly, that a tiger is chasing her (an admittedly unsettling approach), '*her legs started trembling in running movements*' and '*she let out a bloodcurdling scream*'. The transition from freezing (tonic immobility) to flight (collapsed immobility) and ultimately fight, is termed the defensive cascade (Volchan et al., 2017) and forms a continuum, which is dependent on the imminence of the threat e.g. the distance to a predator (Fanselow and Lester, 1988). With decreasing distance to a potential threat, the involvement of brain areas which govern the behavioral outcome, gradually changes from initially higher regions (like prefrontal cortex and anterior cingulate area), over subcortical (septo-hippocampal system, amygdala and hypothalamus) to the brainstem (periaqueductal gray) (McNaughton and Corr, 2004). While the cortical and subcortical areas mediate caution or attentive immobility,

the midbrain areas trigger undirected flight attempts (panic-like), reflected as fleeing, jumping and galloping but ultimately also defensive attacks (e.g. biting, scratching).

(a) startle **(b)** piloerection **(c)** pupil dilation **(d)** defecation

Figure 1.3 | Behavioral Expression of Intense Emotion in Cats
(**a**) Cat startling in response to exposure to snake-like object (cucumber). (**b**) Piloerection in a terrified cat due to the exposure to a dog. Adapted from (Darwin, 1872, p. 127). (**c**) Maximal pupil dilation due to intracerebral electrical stimulation of the perifornical region. Adapted from Hess (1954), p. 27. (**d**) Electrical stimulation within the Septum pellucidum induces defecation. Adapted from Hess (1954), p. 30.

Startle Response Closely related to the aforementioned defensive responses, is the acoustic startle response/reflex (ASR). In its classical sense, it is not considered to be a behavioral component of emotions, however, it is strongly modulated by negative affects, resulting in being 'jumpy' or 'nervous'. The ASR generated in reaction towards loud (>80 dB) acoustic stimuli e.g. a hand-clapping or a sudden voice from behind etc. is a clear sign of being scared. The acoustic input reaches the brain via the cochlear nuclei (*for review see* Koch and Schnitzler, 1997) which sends glutamatergic projections to the caudal pontine reticular nucleus (PnC), which in turn projects onto premotor and motor neurons, resulting in the typical jumping/startle response. The ASR is decreased by a short acoustic signal presented 30-500 ms before the actual startle pulse − this phenomenon is termed pre-pulse inhibition. It involves a regulatory circuit composed of the inferior and superior colliculus, as well as the pedunculopontine tegmental nucleus (PPT). Another though positive modulation happens via conditioned fear, what we know as fear potentiated startle. Direct glutamatergic input from the central amygdala (CEA) and the PAG facilitate the startle response as an effect of e.g. conditioned fear. Similar to the acoustic startle response is the visual startle (Stitt et al., 1976), which can be also described as a directed flight response evoked by short (e.g. looming) stimuli. Recently, this sort of visual evoked startle response has gained attention as an Internet phenomenon, where cats were deliberately scared by snake-like objects (*see* fig 1.3a). Finally there is also the tactile startle response, which one can vividly imagine if for example a Great Green Bush-Cricket (*Tettigonia viridissima*) lands in someones neck. The felt perception of the rather heavy impact combined with the sensation of the legs (tarsi) grasping for hold, immediately imposes a strong biological meaning and likely leads to a profound startle response.

Piloerection To make someone's hair to stand on end, hair-raising, goosebumps, horripilation or simply piloerection − these words all describe the erection of hair in response

to intense emotions. Hair follicles are connected via a small band of smooth muscles, called the *musculus arrector pili*, to the connective tissue of non-glabrous skin (Tansey and Johnson, 2015). This muscles are innervated by the sympathetic nervous system but also react to epinephrine secretion from the adrenal medulla. Stimulation of α_{1A}-adrenoreceptors, activates phospholipase C, inositol triphosphate, calcium-calmodulin pathway and ultimately phosphorylates the myosin-light chain, thereby leading to the contraction of the muscles and raising of the hair (Puetz and Pfitzer, 2009). Piloerection can be pharmacologically induced by selective α_{1A}-adrenoreceptor agonists in rodents and man (Stephens, 1986; Alsene et al., 2006; Kikuchi-Utsumi et al., 2013). However, phenylephrine applied systemically does not lead to piloerection (Stephens, 1986), but injected locally it does (Siepmann et al., 2012). This seemingly simple mechanism is complicated by the fact, that already Brücke (1935) described on the one hand a stimulating action of subcutaneous injection of acetylcholine on the pilomotor system (Coon and Rothman, 1940; Burn and Rand, 1965), but more importantly an inhibitory action of acetylcholine on piloerection elicited by electrical sympathetic ganglia stimulation. This inhibition could be overcome by local injection of 'adrenaline'. Similar observations on the interplay between noradrenaline and acetylcholine were made at the nictitating membrane (Burn et al., 1959). These findings lead to the hypotheses, that in the case of pilomotor muscle innervation, the postganglionic neurons of the sympathetic branch are (a) cholinergic, (b) co-release acetylcholine and via presynaptic autoreceptors exert an effect on noradrenergic transmission ('cholinergic-link') or (c) release noradrenaline via an 'axon-reflex'. It is certain that postganglionic sympathetic fibers co-release many different neuropetides (Gibbins, 1991; Elfvin et al., 1993) and can differentiate from noradrenergic to cholinergic (Schotzinger and Landis, 1988). Moreover, there is evidence, that cultured sympathetic neurons co-release acetylcholine and noradrenaline (Furshpan et al., 1986). How fear and terror activates the pilomotor response cannot be entirely described at the moment.

Pupil Dilation Similar to the *musculus arrector pili*, the pupillary dilator muscle is contracted in response to intense emotion and sympathetic activation via the same signaling cascade. The contraction of this muscle leads to an increased pupillary diameter. The sympathetic nerve fibers arise from the superior cervical ganglion. The antagonist of the pupillary dilator muscle is the iris sphincter muscle which is innervated by the parasympathetic system originating at the Edinger-Westphal nucleus, situated within the close vicinity of the ventrolateral PAG (vlPAG). If activated by acetylcholine the sphincter muscle reduces the pupillary diameter. The iris muscles are a beautiful example for the balance of adrenergic and cholinergic (resp. sympathetic and parasympathetic) signaling combined with tissue-specific receptor expression. Adrenergic and metabotropic acetylcholine receptors exhibit both intrinsic activity, moreover, the afferent sympathetic and parasympathetic fibers are tonically active (Rossier et al., 1999; Nelson et al., 2005). If now the constitutive activity of the iris sphincter muscles is blocked via the action of the inverse muscarinic agonist atropine (e.g. mydriatic eye drops), the pupils will dilate. This dilation, due to inhibition of parasympathetic drive, is

also observed in many cognitive processing tasks in humans. As Steinhauer et al. (2004) have demonstrated, the pupil diameter is dependent on cognitive load during mathematical processing paradigms and increases with difficulty (summation vs. subtraction). Visser et al. (2013) have applied the pupil dilation response in combination with human fear conditioning and report an increase in pupil size as a result of successful fear memory formation. It is tempting to link 'fear' with pupil size directly, but as stated in the beginning, intense emotions reduce the pupil size and most likely also in human fear-conditioning a dilated pupil size indicates high levels of attention and cognitive load.

Micturition & Defecation Less obvious signs of emotional disturbances are defecation and micturition. In situations of negative affect or emotional stress, animals and humans show increased defecation and micturition/urination, which even can serve as a measure of individual differences in emotionality (Hall, 1934). Gastrointestinal motor activity and colonic transit, one might think, is also heavily dependent on sympathetic and parasympathetic activity. However, there is a strong line of evidence which links the activation of the sympathetic nervous system to decreased defecation. Systemic treatment with clonidine, an α_2-adrenoreceptor agonist, drastically decreased defecation in rats during restraint (wrapping) stress (Doherty and Hancock, 1983; Yamamoto et al., 1998). Overstimulating the cholinergic system with muscarine directly or unspecifically with organophosphate nerve agents (e.g. sarin), which block the degradation of acetylcholine within the synaptic cleft, leads to defecation, vomiting, lacrimation, salivation and sweating. An explanation for the constipating effects of α_2-adrenoreceptor activation is given by Scheibner et al. (2002). They found evidence for the α_{2A}-adrenoreceptor functioning as a heteroreceptor on cholinergic nerve terminals within the enteric nervous system and thereby inhibiting the acetylcholine release. However, there is compelling evidence that the 41-amino-acid peptide corticotropin-releasing factor (CRF) (Vale et al., 1981; Bale and Chen, 2012) acting on the CRF receptor type 1 ($CRFR_1$) is mediating the stress-induced colonic motor stimulation.

Central administration of CRF in mice dose-dependently stimulates distal colonic transit (*for review see* Taché and Perdue, 2004) and defecation (Martínez et al., 2004). Central administration of the unspecific CRH antagonist α-helical $CRF_{9\text{-}41}$ (Williams et al., 1987) or the selective $CRFR_1$ antagonist NBI-35965 (Martínez et al., 2004), prevented the stress-induced increased fecal excretion in rats and mice respectively. Moreover, $CRFR_1$ deficient female mice produced less fecal boli during an open-field test (Bale et al., 2002). The stimulating effect of centrally administered CRF on colonic transit cannot be abolished by bilateral hypophysectomy or ardenalectomy but by truncal vagotomy and ganglionic blockade by the nicotinic acetylcholine receptor blocker chloroisondamine − indicating a central activation of the parasympathetic innervation of the colon (Lenz et al., 1988a). Further, systemic treatment with CRF induced increased colonic transit (Lenz et al., 1988a; Lenz et al., 1988b; Miampamba et al., 2002), which could not be blocked by truncal vagotomy or chloroisondamine, indicating an independent mechanism in the periphery.

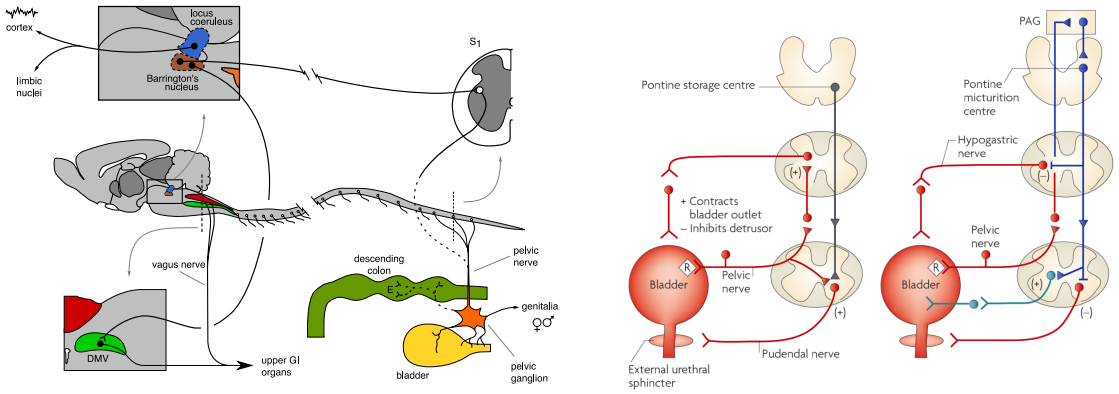

(a) vagal outputs of the PMC **(b)** interplay of PAG and PMC

Figure 1.4 | Brainstem Circuits for the Control of Micturition & Defecation
(**a**) The pontine micturition center (PMC, Barrington's nucleus) sends direct projections to the locus coeruleus (LC), the lumbosacral segments of the spinal cord and the dorsal motor vagal nucleus. Adapted from Pavcovich et al. (1998). (**b**) *left panel*: The 'guarding reflex' (involuntary sphincter control) is initiated via bladder tension sensing receptors at the pelvic nerve, which leads to an inhibition of the detrusor muscle and an activation of the sphincter muscle. *right panel*: Bladder distension information is relayed via the PAG to the pontine micturition center (PMC), enabling higher brain areas (prefrontal cortex) to control excitatory inputs to the PMC and thus the 'voiding reflex'. The PAG forms a critical switch in the voiding circuit, as it constitutes a fully 'on' or 'off' function. [Adapted from Fowler et al. (2008)]

This can be explained by the expression of $CRFR_1$ in neurons of the myenteric plexus (Taché et al., 2004). In the case of micturition, a detailed explanation for the action of stress is not as straightforward. The research of the British surgeon Frederick James Fitzmaurice Barrington (1884-1956) culminated in the description of the *pontine micturition center* (PMC), also called *Barrington's nucleus*. Barrington (1925) performed lesions on a little medullar region close to the locus coeruleus and the laterodorsal tegmental nucleus (*see* Fig. 1.4a). These lesions rendered cats unable to empty their bladder completely, or on the opposite, disregarding their desire to void. The tissue tension is sensed by transient receptor-potential (TRP) channels within the bladder and relayed via the PAG to the PMC (*see* Fig. 1.4b *right panel*). One region of the PMC ('M' region) is projecting towards the preganglionic parasympathetic neurons of the lumbosacral spinal cord, which innervates the bladder; the other 'L' region projects to the urethral-sphincteric motor neurons in Onuf's nucleus. More recent findings consider the Barrington's nucleus to be involved in the control of the lumbosacral parasympathetic system in general, which includes the bladder and the distal colon (Pavcovich et al., 1998) and thereby mediating the stress induced changes on micturition and colon transit. Despite whether voiding is 'mechanically' necessary (bladder filling controlled by the PAG and PMC), the question if it is safe to void or socially appropriate is handled by the PAG and most likely by the medial prefrontal cortex (mPFC). Growing evidence from human neuroimaging studies implicates the mPFC as a major regulating brain area in various conditions of bladder filling (*for review see* Griffiths and Fowler, 2013). An increased activity of the PAG

might also play an important role in people who suffer from paruresis (also known as 'avoidant paruresis', 'shy bladder syndrome' or 'psychogenic urinary retention'). This condition is characterized by the inability to empty the bladder in the real or imaginary presence of others.

Vocalization Throughout the animal kingdom the generation of acoustic signals plays an important role for social interaction. The complexity of acoustic stimuli varies greatly, ranging from courtship songs in invertebrates (Bennet-Clark and Ewing, 1968), to the more complex syllables of songbirds, over the resemblance of language and identity information transmission in bottlenose dolphins (Janik et al., 2006) and finally the human language.

Rats produce two very distinct types of ultrasonic vocalization (USV): the long 22-kHz calls typically signal distress e.g. in anticipation of unavoidable aversive stimuli (Brudzynski et al., 1993) and on the contrary the 50-kHz calls are emitted if rats are tickled (Panksepp and Burgdorf, 2003) which signals positive affect. The vocal repertoire of mice is not less complex. Both, male and female mice are known to ultrasonically interact during male courtship display (Neunuebel et al., 2015). Newborn mice signal distress, due to separation of the dam, with USV calls in the range of 40-80 kHz (Zippelius and Schleidt, 1956). But mice are also capable of producing sonic, audible squeak-like sounds (Coburn, 1912; Whitney, 1970; D'Udine et al., 1982), mostly with respect to fearful or painful stimuli or as a result of agonistic behavior. Both signals originate from the larynx, but the production mechanism differ remarkably: While the ultrasonic sounds are produced in a whistle-like manner by the specially constricted larynx (Johnson et al., 2010) which was recently described as intra-laryngeal planar impinging jets (Mahrt et al., 2016), the audible squeaks are produced by the vibrating vocal cords with a fundamental frequency between 2-10 kHz and a harmonic series exhibiting formant structure (Roberts, 1975a; Roberts, 1975b; Roberts, 1975c; Roberts, 2009). The neuronal circuits which mediate vocalization in rodents are mainly described for ultrasonic vocal events. To what extent those circuits differ, cannot be completely assessed. However, transection of both, the inferior and superior laryngeal nerves in infant rats, abolished or hampered ultrasound vocalization, but did not affect audible squeaking (Wetzel et al., 1980). Roberts (1975a) showed earlier, that transection of the superior laryngeal nerve in adult rats, strongly attenuated ultrasound vocalization, and to a large extent also audible sounds. Recently, Pascual-Font et al. (2011) mapped very elegantly the projections from the nucleus ambiguus (Amb), within the medulla, to the larynx of the rat. The neurons within the Amb fire very closely timed to ultrasound events (Yajima et al., 1982), and afferent projections to the Amb arise from the lateral periaqueductal gray (Ennis et al., 1997; Arriaga et al., 2012). Electrical and chemical stimulation of the PAG in cats leads to vocalization (hissing and growling) (Bandler and Carrive, 1988) and bilateral chemical lesions of the nucleus retroambiguus in decerebrate cats abolished PAG-stimulation induced vocalization (Shiba et al., 1997).

Non-behavioral and Cardiorespiratory Expressions of Emotion

Facial Coloring There is a certain set of non-behavioral signs of intense negative affect which are only part of human physiology. Besides the mimic facial expression in the human face, one can infer the internal states from facial coloring and sweating. The blood flow in the human face is tightly regulated. With increasing ambient and ultimately body temperature, the sympathetic nerves which innervate the human facial area actively discharge (Nordin, 1990) and lead to vasodilatation. Moreover, arousing stimuli (electrical median nerve stimulation) promote a sudden increase in the supraorbital sympathetic discharge rate. The discharges of the supraorbital sympathetic nerve are rhythmically linked to a increase in forehead skin conductance which indicates sweating. Most strikingly, mental arithmetic tasks readily increased supraorbital discharge and increase skin conductance, indicating the link between an internal state and the coloring ('reddening') of the skin (Drummond, 2003). Despite this known correlation there is no clear evidence for the receptors which mediate this vasodilatation, but most likely there is involvement of the β_2-adrenergic receptor (Drummond, 1997). Pallor (cutaneous vasoconstriction), on the other side, is hypothesized to serve as a protective mechanism in order to decrease possible blood loss (vasoconstriction happens in the extremities as well), due to injury (Hoskins et al., 1916; Blessing, 2003). It is induced in rabbits within 1-2 seconds upon a negative conditioned auditory or a painful stimulus. This vasoconstriction is dependent on the CEA (Yu and Blessing, 1999) and the pre-sympathetic neurons in the rostral ventrolateral medulla (RVLM) and the raphe magnus/pallidus parapyramidal region. Inactivation of the raphe magnus with muscimol inhibits vasoconstriction triggered by amygdala/hypothalamic stimulation (Nalivaiko and Blessing, 2001).

Sweating The 'purposivists' view about emotional sweating is that sweat glands in palms and soles are recruited in situations where our defensive system is activated to increase friction and ultimately aid running or climbing (Adelman et al., 1975; Asahina et al., 2015). However, sweat also serves as an important communication signal among many animals and to a certain extent also to humans (Chen et al., 2006; de Groot et al., 2014). The research on 'fear sweat' or German 'Angstschweiß' may have found its origin with Karl von Frisch's (von Frisch, 1942) work on the warning signal released from the skin of minnows. The olfactory and chemical communication in humans, however, works entirely different. Human sweat glands are cutaneous exocrine glands which can be divided according to their mode of secretion into: apocrine (parts of the cell constitute the secrete), eccrine (excretion via exocytosis) and apoeccrine (a mixture of both; *see* Sato et al., 1987). Apocrine and apoeccrine cells are only found at the axilla, mammary, perineal and genital region, whereas eccrine cells are most densely located around the palms and soles. Eccrine cells are mediating the psychophysiological skin conductance response and are most important for psychophysiological measures. Eccrine cells are innervated by the sympathetic divisions of the autonomic nervous system, whereby the nature of the postganglionic fibers is cholinergic (*see* piloerection), but also noradrenergic

fibers can be found in the close vicinity. The brainstem control of electrodermal activity happens via the reticular formation in the brainstem (Roy et al., 1993). Interestingly, patients with locked-in syndrome can learn to control their skin conductance and thereby control external devices (Blain et al., 2006; Falk et al., 2010).

Cardiac Signs Among the strongest subjective feelings during intense emotional states is the 'pounding heart'. The regulation of the heart rate (adjusting it to the physiological needs to come) is an important feature of our body. This regulation is complex and tailored to the species. Therefore I will focus mainly on results which were obtained in rodents, with a focus on mice.

Healthy mice typically have a heart rate ranging from 400 to 800 beats per minute (bpm). A frequent shift from low to high rates (high heart rate variability) which is strongly linked to bouts of movement, indicates a non-frightened state. Constant high rates with very little variability (low heart rate variability) indicate states of high fear or stress. Mice which underwent auditory fear conditioning display a marked tachycardia (Herrmann and Carran, 1972) and a decreased heart variability in response to the conditioned tone (Stiedl and Spiess, 1997). The unspecific β-adrenoreceptor blocker sotalol (low blood-brain barrier permeability) completely abolishes the tone-induced increase in heart rate. Intraperitoneal injections of the unspecific β-adrenoreceptor agonist isoproterenol (10 μg/kg) increases the heart rate to its maximum (Kim et al., 2008). In the ex-vivo mouse artrial preparation, vagal stimulation elicits a pronounced and reversible bradycardia (Choate et al., 2001). However, the typical conditioned fear-induced bradycardia (*heart-rate conditioning*), known from rabbits and rats, has not been observed so far in mice. If rats are re-exposed to a previously negatively conditioned environment, they display a marked increase in freezing and mean arterial blood pressure, but an initial decrease in heart rate (Carrive, 2006) followed by a tachycardic response. The fear induced bradycardia is turned into a strong tachycardia by systemic delivery of atropine. This indicates a simultaneous activation of the parasympathetic and sympathetic afferents to the heart (Iwata and LeDoux, 1988), while the parasympathetic branch keeps a break on the heart rate as the animal expects the aversive stimulus. In rabbits a loud unconditioned auditory stimulus is enough to induce bradycardia and hypotension (Sheldon et al., 2007), similar to processes which induce a vaso-vagal syncope in humans − another sign of intense emotions. However, in humans the hypotension is due to vasodepression and independent from the heart rate (Connolly et al., 2003), whereas in rabbits, artificially pacing the heart abolished hypotension (Sheldon et al., 2007).

Other Reactions Stage fright or performance anxiety are typical examples were the salivary glands seem to be inhibited, which results in a dry mouth. The salivary glands (parotid, submandibular and sublingual) are innervated by parasympathetic and sympathetic fibers. Activation of the parasympathetic branch stimulates saliva secretion via muscarinic M1 and M3 receptor and increases glandular blood flow. Sympathetic stimulation on the other hand neither stimulates salivation, nor does it inhibit salivation at the level of the glands. But increased sympathetic drive might induce vasoconstriction

in glandular regions, whereby simply the movement of water across the apical membrane is limited. However, the 'dry mouth' in anxiety seems to be an effect of higher brain areas, and a central inhibition of the primary salivary centers in stressful situations is suggested (Proctor and Carpenter, 2007).

Among Walter B. Cannons observation of the bodily changes upon fear (Cannon, 1929, p. 66-79) there is 'emotional glycosuria' (elevated levels of glucose in urine) which could be either achieved by physical pain, severe emotional stress, electrical stimulation of the splanchnic nerves (projecting to the adrenal glands) or injection of adrenaline. Now we know that this glycosuria can be traced back to adrenaline's various action sites which control the blood sugar level: (a) inhibition of insulin release via α-adrenergic receptor at the pancreas (Porte, 1967), (b) stimulation of glycogenolysis in the liver (Sutherland and Cori, 1951) and muscles (Richter et al., 1982; Raz et al., 1991), and (c) inhibition of insulin-mediated-glycogenesis (Raz et al., 1991). The excess in blood sugar is reflected with an increased excretion of glucose. So far there is no literature which describes the changes in blood glucose due to acute stress with high temporal resolution. Walter B. Cannon also observed increased coagulation in animals which were severely stressed (Cannon, 1929, p. 132-156). This observation lead to the identification of various hemostatic responses upon acute and chronic stress, which seem to depend mostly on the increased sheer forces in blood vessels due to increased blood pressure (Austin et al., 2013). Finally Cannon observed a hemoconcentrating (increase in red blood cells) effect upon acute emotional excitement (Cannon, 1929, p. 178-192). This effect can be explained by a strong adrenaline and noradrenaline mediated contraction of smooth muscles which surround the spleen in several athletic mammals (e.g. cats), but the human spleen is only of very limited capacity to expel blood (Stewart and McKenzie, 2002). The aforementioned bodily changes are accompanied and governed in part by a profound activation of the autonomic nervous system and neuroendocrine responses. These will be covered in chapter 1.5 separately.

1.3 Fear & Anxiety Disorders

With a 12-month prevalence of 14.0%, anxiety disorders are the most frequent mental disorders in the European population, followed by insomnia (7.0%) and major depression (6.9%) (Wittchen et al., 2011). According to the Diagnostical and Statistical Manual of Psychiatric Disorders 5^{th} Editions (DSM-5) (Falkai and Wittchen, 2015) and the International Classification of Diseases 10^{th} Edition (ICD-10) (World Health Organization, 1992), the term 'anxiety disorder' comprises several distinguishable conditions, like separation anxiety disorder (F93.0), selective mutism (F94.0), specific phobias (F40.X, e.g. animal type F40.218, natural environment type F40.228, blood F40.230, injection F40.231, medical care F40.232, injury type F40.233, etc.), social anxiety (F40.10), panic disorders (F41.0), agoraphobia (F40.0) and generalized anxiety disorder (GAD, F41.1). Formerly, post-traumatic stress disorder (PTSD) as well as obsessive-compulsive disorder (OCD) were included in the anxiety disorder category but have now been classified

separately in the DSM-5. As a core symptom, all anxiety disorders have excessive fear and anxiety reactions >6 months in duration in common. Whereas FEAR describes the emotional and physiological reactions towards imminent, real or perceived threats, ANXIETY relates to the anticipation of distant, unpredictable and indefinite threats. In daily language use anxiety can be quite conveniently described as a '*Circulus vitiosus: The fear of anxiety, leads to anxiety of fear.*' (Uhlenbruck, 1983). The patients themselves control the extent of their disorder with often pronounced avoidance behavior. This course of conduct is unfortunately self-reinforcing in a way that for example patients suffering from social anxiety avoid public places and learn to avoid them also in the future, as they were safe while staying at home. When these avoidance reactions disable the patients to a level where job loss and social isolation is at risk, they typically seek medical attention. However, these constraints have strong inter-individual differences, as again, a mild social anxiety might not affect a writer, but will certainly hinder a ticket inspector of public transportation. The age at onset of anxiety disorders is typically childhood or adolescence, but for phobias and especially separation anxiety, a rather early onset between 7 and 14 years of age (Kessler et al., 2007b) has been reported. However, the course of the disease is often chronic-recurrent and panic disorder, agoraphobia and generalized anxiety disorder have been found to have a later age-of-onset distribution in the early-mid twenties. Most anxiety disorders occur more often in females than in men (ratio 2:1), but also a profound contribution of genetic factors of up to 48% heritability (twin study) has been suggested (Hettema et al., 2001). This familial component of anxiety disorders is further substantiated by the notion that in family studies high odds ratios of ≈4 (phobias), ≈5 (panic disorder) and ≈6 (generalized anxiety disorder) have been observed among directly related family members (Shimada-Sugimoto et al., 2015). But anxiety is a '*complex trait*' and the identification and validation of 'anxious genes' (Morris-Rosendahl, 2002) in recently identified susceptibility loci (Otowa et al., 2016) that increase the risk for anxiety disorders, has yet to be conducted. Other risk factors, like stress (Risbrough and Stein, 2006) and adverse childhood experience (Sareen et al., 2013) have been implicated. Anxiety disorders are highly comorbid with other psychiatric diseases, like major depression, bipolar and substance abuse (Merikangas and Swanson, 2010). But also physical disorders like cardiovascular conditions and respiratory diseases co-occur with anxiety disorders. This heterogeneity is likely the cause why anxiety disorders are often misdiagnosed in primary care settings (Vermani et al., 2011). The neuropathophysiological causes of anxiety disorders cannot be comprehensively outlined to date. Functional neuroimaging studies of unmedicated patients suffering from e.g. panic disorder combined with symptom-provocation cannot be conducted for obvious reasons (despite rare exceptions, *see below*). However, a plethora of preclinical research, mainly dealing with rodent models of fear & anxiety disorders, has suggested several key brain circuits involved in the acquisition, retention, expression, consolidation, re-consolidation and extinction of fear memories (e.g. Pavlovian auditory fear-conditioning) or the expression of innate fear reactions (e.g. predator odor avoidance). These circuits comprise the amygdalar nuclei, the hippocampal formation, the hypothalamic nuclei, the PAG, the superior colliculus, the septo-hippocampal system

and the prefrontal cortical regions (for a detailed description of these circuits, *see the following section*). Differential activation in some of these circuits could be demonstrated in anxiety patients, as well as in artificially induced fear & anxiety producing situations in healthy subjects. In arachnophobic patients (spider phobics), several functional neuroimaging studies consistently reported an increased activation of the amygdala, and to some extent the insular and prefrontal cortex, in response to images depicting spiders (Dilger et al., 2003; Schienle et al., 2005; Goossens et al., 2007a; Goossens et al., 2007b; Schweckendiek et al., 2011). Lipka et al. (2014) even reported an activation of these structures when subliminal (masked) stimuli where used. Goossens et al. (2007b) could demonstrate a reduction of amygdala hyperfunction after exposure-based therapy. In a case report, Pfleiderer et al. (2007) describe a patient who experienced a spontaneous panic attack during a fMRI session where also an increased amygdala activation was observed. Despite these rare examples, where either a phobic-fear provoking stimulus was used or a panic attack was triggered, there are many other functional imaging studies which try to challenge the 'fear matrix' using e.g. angry/fearful faces or negative words in healthy subjects or patients suffering from anxiety disorders. Findings from these studies associate anxiety disorders with an increased activity in the amygdala and insular cortex, while prefrontal cortical areas (vlPFC, dlPFC, dmPFC, ACA) seem to be hypoactivated (*for review see* Etkin, 2010). Technical limitations, however, hamper the simultaneous imaging of lower brain areas and cortical structures. In addition, the small nuclei of the brainstem are surrounded by structures with markedly different density (bone and fluid), which is the reason why functional imaging studies of these areas are rare. The seminal work of Mobbs et al. (2007) is an exception. Here the authors have applied a virtual active avoidance task on humans, where the healthy subjects learned to flea a predator, which was able to chase, capture and inflict pain (mild electric shock). As the 'Pacman-like' virtual predator grew closer, functional MRI revealed a shift from prefrontal cortical and amygdalar regions towards the PAG. Additionally the imminence-driven PAG activation increased with the subjective experience of dread, and was negatively correlated with confidence of escape. Another recent study by Wendt et al. (2017) could successfully replicate these findings. A recently published meta-analysis of human fear conditioning (uninstructed only), combined with fMRI (Fullana et al., 2016), analyzed the data of 27 independent studies yielding a pool of total 677 healthy adult participants. The study identified a consistent activation of several regional clusters in response to differential fear conditioning, including the anterior insular cortex (AIC), dorsal anterior cingulate cortex (dACC), secondary somatosensory cortex (SII), dorsolateral prefrontal cortex (dlPFC), as well as the septo-hypothalamic zone and periaqueductal gray (PAG). Moreover, several clusters showed a significant deactivation, including the ventromedial prefrontal cortex (vmPFC), hippocampus (HPC) and orbitofrontal cortex (OFC). Therefore this study substantiates the aforementioned 'fear network', however, most notably a consistent activation of the amygdala could NOT be characterized. This might be partially explained by technical constraints (fMRI protocols not tailored for the detection of amygdala activation, Mechias et al., 2010) and the possibility that '*human fMRI fear-conditioning experiments generally do not evoke consistent*

responses within the classical amygdala defense/threat detection circuitry' (Fullana et al., 2016) in healthy volunteers. The fact, that the amygdala is undoubtedly involved in the regulation of fear responses, but also in the generation of the subjective affect, is most convincingly demonstrated by a subset of patients suffering from the rare, recessive, genetic disorder known as Urbach-Wiethe syndrome (Urbach and Wiethe, 1929; Hofer, 1973). The core symptoms of the disease involve hoarseness of speech and skin lesion, due to depositions/infiltrations of proteinaceous material in the mucous membranes (Thornton et al., 2008). In rare cases, this disease involves a complete focal bilateral amygdala lesion. One of these cases is the patient known as SM (Tranel and Hyman, 1990; Adolphs et al., 1994) who is unable to experience and exhibit any form of fear since an age of 10 years (consistent with the course of her amygdala pathology) (Feinstein et al., 2011). Current treatment strategies for anxiety disorders involve cognitive behavioral therapy (CBT), including exposure-based therapy (EBT), and pharmacological treatment. While CBT is especially effective for treating specific phobias, most anxiety disorders are treated best pharmacologically. Traditional antidepressants (selective serotonin reuptake inhibitor SSRI, serotonin-norepinephrine reuptake inhibitor SNRI) are considered as a first-line pharmacological treatment for anxiety disorders (Ravindran and Stein, 2010), as the drugs can be very safely used. As a second-line treatment the highly efficacious benzodiazepines are recommended (Craske et al., 2017), but the potential abuse and the risk of dependence limit their applicability.

1.4 Brain Circuits Involved in the Generation of Fear in Rodents

Fear responses critically contribute to the survival of an individual. Theses behavioral programs need to be executed with low latency to ensure effectiveness. Highly adaptive regulatory systems ensure that autonomic changes, freezing, fleeing, jumping and defensive attacks are only triggered in the appropriate context. Thus, it is not surprising that many areas in the mammalian brain deal with the regulation and execution of defensive responses. Beyond the fear-related areas of the limbic system (amygdalar complex, hypothalamus, septo-hippocampal system) also the midbrain superior colliculus (SC) and brainstem periaqueductal gray (PAG) are strongly involved in the precipitation of fear. In addition, the autonomic nervous system and the circuits for homeostatic regulation situated within hypothalamus are key regulators in order to adapt physiological processes to possible escape and defense scenarios.

Amygdala

The amygdala (from *Greek* ἀμυγδαλέ 'almond') is a bilateral almond-shaped (in humans) nucleus found in the temporal lobe of vertebrates and was originally described by Karl Friedrich von Burdach almost 200 years ago (Burdach, 1822). Since then, the amygdala has been recognized to constitute the central hub for the processing and regulation of fear-related stimuli or behavior respectively. The amygdala with its ascending and

descending connections is well-conserved throughout evolution and even non-mammalian animals have been found to possess amygdala like structures (*for review see* Janak and Tye, 2015).

Choi and Kim (2010) have demonstrated in a beautiful manner, how severely a transient inactivation of the amygdala changes behavior. In their experiments they have asked food-deprived rats to forage a food pellet in a large arena. The food pellet, however, was guarded by a robot (*Robogator*) programmed to move towards the rat, once the animal surpassed a certain limit before the food was in reach. The lesioned animals failed to exhibit any form of fear reaction, however, they were not consuming the food on the spot, but rather retrieved from the arena before. One might interpret this behavior as unaffected 'precaution'.

The amygdala can be divided into five main areas − the central amygdala (**CEA**), comprised of the centromedial (CEm) and centrolateral (CEl) amygdala, the medial amygdala (**MEA**), the basolateral amygdala (**BLA**), comprised of the basal (BA) and lateral (LA) amygdala, basomedial amygdala (**BMA**), and the cortical-like amygdala (**COA**) which consists of many nuclei mainly responsible for the evaluation of e.g. predator olfactory cues. From a developmental neuroanatomical point of view, the CEA and MEA are of subpallial/striatal origin, while the BLA, BMA and COA are pallial/cortical structures (Swanson and Petrovicha, 1998; Pabba, 2013). This distinction becomes more apparent if the afferent and efferent connections and the respective roles in mediating behavior are considered. The BLA receives sensory inputs from auditory and pain related thalamic nuclei (Ottersen and Ben-Ari, 1979; Ottersen, 1981) (for a detailed description of the amygdala's role in auditory fear-conditioning *see next section*), as well as the multi-sensory temporal (McDonald et al., 1996) and especially the auditory cortical areas (McDonald, 1987; McDonald and Jackson, 1987; Romanski and LeDoux, 1993a). Additionally the BLA receives inputs from the prelimbic (PrL) prefrontal cortex (Vertes, 2004) and even forms reciprocal connections to the PrL and the infralimbic (ILA) prefrontal area (Hoover and Vertes, 2007). Projections from the ILA, however, project not directly towards the BLA, but to a specific GABAergic group of neurons located between the BLA and CEA, termed *massa intercalata* or intercalated masses/cells (ITCs) (*for review see* Millhouse, 1986). The ITCs have been implicated in extinction memory formation, a process where a newly formed memory trace can suppress the expression of previously acquired fear associations (Royer and Paré, 2002). The reciprocal connections between the ventral hippocampus (vHPC) and the BLA are thought to mediate, in concert with the prefrontal cortex, the contextual fear regulation (Pitkänen et al., 2000; Orsini et al., 2011). Moreover, there is evidence that the ventral tegmental area (VTA) sends dopaminergic projections towards the BLA (Ford et al., 2006), however, the role of these neurons is not known so far. It is further hypothesized that the BLA receives inputs from the perirhinal, entorhinal and parahippocampal cortices, most sensory related cortical areas and certain hypothalamic nuclei as well (conveying e.g. homeostatic information, Sah et al., 2003). The BLA forms numerous reciprocal connections with cortical areas and hippocampal regions, but the behavioral output is mainly directed

to the central amygdala. The BLA also has an intimate connection with the nucleus accumbens (NAc) and is involved in the regulation of appetitive behavior and reward (Everitt et al., 1999). More prominently, however, is the connection with the bed nucleus of the stria terminals (BNST). The BNST is a very heterogeneous and complex brain region and plays a role in e.g. addiction, aggression, and importantly, in sustained fear or anxiety-like behavior (*for an excellent review see* Lebow and Chen, 2016). Therefore one may reduce the function of the BLA to the integration of multi-sensory and fear-modulating inputs and the convergence of emotionally 'tagged' memory traces for proper (mid latency) response selection. For a rodent this could mean to gradually (decision making PFC; context vHPC) overcome innately fearful situations (e.g. novel foraging grounds) in order to gain better access to resources.
The CEA receives projections from the BLA as mentioned above but also from the insular cortex and posteromedial ventral thalamic nucleus (the thalamic gustatory nucleus) (Nakashima et al., 2000) where possibly viscerosensitive and homeostatic information is relayed. In line with these afferents is also the strong projection from the parabrachial nucleus (PB) (Ottersen, 1981), a brain region known to relay visceral, cardiorespiratory and nociceptive information. Another prominent projection towards the CEA is sent by the paraventricular thalamic nucleus (PVT) (Turner and Herkenham, 1991), which has been shown to be strongly involved in fear processing especially at later stages after a fear memory has been formed (Do-Monte et al., 2015; Yates, 2015). The CEA also forms reciprocal connections with the periaqueductal gray (Rizvi et al., 1991). It is considered to comprise the behavioral output stage of the amygdalar complex. The major efferent projections reach the lateral hypothalamus (LH), where autonomic parameters like arterial pressure and heart rate are affected (LeDoux et al., 1988), and the PAG, where flight, freezing and vocalization can be elicited (Tovote et al., 2016; Sugiyama et al., 2010). Some minor projections centers are the zona incerta (ZI) (Roger and Cadusseau, 1985), and the PB.
Like in humans, a lesion of the amygdala in rodents also leads to a complete absence of fear responses e.g. conditioned freezing (Kim et al., 1993). For the sake of completeness it shall be briefly mentioned that the amygdala processes not only aversive signals, but also reacts to rewarding stimuli (Setlow et al., 2002; Everitt et al., 2003; Ambroggi et al., 2008).

Recent studies, however challenge the prevailing but one-sided view of the amygdala. Amir et al. (2015) discovered, using the semi-naturalistic mechanical predator ('Robogator', Choi and Kim, 2010) mentioned above, that the majority of the recorded BL amygdala principal neurons (type-1, 88 %) decrease their firing rate, once the rat approaches the threat in order to retrieve the food pellet. If the rats reached the sensor range, the Robogator initiated a movement, which elicited escape responses. Even during the escapes, type-1 BL amygdala neurons remained silent. The authors summarize that '*threat proximity and reward availability did not consistently predict BL activity. Instead, BL activity co-varied with behavior, even though threat and reward levels were clamped at low or high levels*'. In a recent review article Paré and Quirk (2017) developed

a new conceptualization of the role of the amygdala in which they state that the amygdala simply *opposes behavioral engagement*, which precipitates in increased measures of fear.

Periaqueductal Gray

The PAG is the major orchestrator of defensive responses (freezing & fleeing) in mice and man. It is a ventricular gray matter and forms the upper end of the spinal cord (Bandler et al., 1991). As such it surrounds the cerebral aqueduct which connects the third and the fourth ventricle. Adjacently located to the PAG are the superior colliculus (SC), the midbrain reticular nucleus (formation), the posterior hypothalamic nucleus (PH), the inferior colliculus (IC) and dorsal raphe nucleus. Moreover, several distinct nuclei are interwoven within the PAG namely some of the preganglionic centers of cranial nerves (III, IV, V), the Edinger-Westphal nucleus (pupil constriction) and the Nucleus of Darkschewitsch (reflexive gaze). The PAG can be subdivided along its dorsoventral axis in dorsomedial (dmPAG), dorsolateral (dlPAG), lateral (lPAG) and ventrolateral (vlPAG) subdivisions. The dmPAG is not often considered exclusively e.g. most bilateral treatments to the dlPAG also affect the dmPAG, therefore if not explicitly stated otherwise, dorsal PAG (dPAG) refers to both areas.
If rats are confronted with a predator (cat) the cells within the PAG are strongly stimulated and express the neuronal activity marker *c-fos* (Canteras and Goto, 1999). If rats receive gradually increasing, electrical stimulation within the PAG, they initially display a freezing response which develops into a strong undirected flight responses (galloping) at higher intensities (Brandão et al., 1999). Stimulation of the PAG, with either excitatory amino acids (EEA) or by means of electrical current, also induces freezing and flight responses in the decerebrate animal (Keay and Bandler, 2001). Also the human PAG is activated if a 'threat' is approaching the proximal distance. Mobbs et al. (2007) showed very elegantly that the confrontation with a virtual threat (computer game), which was previously associated with a mild electric shock, the participant's PAG was markedly activated while they were trying to escape. That the PAG can even alter a persons affective state has been already shown impressively in the late 1960's by Nashold et al. (1969). In search for a deep brain stimulation (DBS) based treatment to alleviate chronic pain, they electrically stimulated the PAG in awake patients. As a strong side-effect, the patients reported sensations of anxiety, distress, panic or even imminent horror of death. In the following I will outline the main connectivity of the PAG and thereby derive the circuitry which produces the distinct behavioral responses.

The ascending afferents from the ventral horn of the spinal cord preferentially terminate in the dPAG whereas ventral and dorsal horn afferents project towards the lPAG and the vlPAG (Beitz, 1982; Meller and Dennis, 1986). Predominately, the upper cervical (C1-C4) and sacral (S1-S3) regions project to the vlPAG and lPAG (Keay et al., 1997). The spinal afferents are considered to carry nociceptive signals directly to the PAG. In an elegant study, Clement et al. (2000) has combined retrograde labeling of PAG-projecting spinal neurons with *c*Fos immunohistochemistry and observed their acti-

vation upon several distinct noxious stimuli. Other ascending inputs contain projections from the medullary and pontine reticular formation with slightly preferred innervation of the vPAG & vlPAG over the dPAG (Beitz, 1982; Meller and Dennis, 1986). These include the catecholaminergic afferents of the nucleus of the solitary tract (NTS), caudal and rostral ventrolateral medulla (VLM) and dorsomedial medulla (DMM) (Herbert and Saper, 1992). These regions might be involved in the bradycardic response evoked by noradrenaline microinjections in the dPAG/vlPAG (Pelosi and Corrêa, 2005; Pelosi et al., 2008) which has been shown to be vasopressin dependent (Pelosi et al., 2008). However the most prominent projections towards the PAG arise from diencephalic, mesencephalic and telencephalic regions which substantiates the notion that the PAG is an output region. Various subregions of the hypothalamus, which have been demonstrated to play a major role in the regulation of defensive reactions or fear responses, project extensively towards the PAG. While glutamatergic dl/lPAG neurons preferably receive glutamatergic afferents from the ventromedial hypothalamus (Tong et al., 2007; Kunwar et al., 2015), the lateral hypothalamic area (LHA) sends projections to the dl/l-PAG and vlPAG, both onto GABAergic and glutamatergic neurons equally (Tovote et al., 2016). Moreover, the VMH seems to exhibit a topographical innervation of the PAG with the ventrolateral VMH (VHMvl) targeting mostly the caudal PAG, the dorsomedial VMH (VMHdm) targeting mostly the rostral PAG and the anterior VMH (VMHa) projecting towards the lPAG (Canteras et al., 1994). Other tracing studies showed that the LHA and the associated perifornical region (PeF) project preferentially towards the vPAG (Beitz, 1982; Meller and Dennis, 1986) (for the role of the PeF in panic *see* Johnson and Shekhar, 2012).

Neurons which are positive for the transcription factor steroidogenic factor 1 (SF1), have been found to constitute a large portion (≈60%) of the VMH, and a part of these neurons send contralateral projections towards the dPAG and the anterior hypothalamic nucleus. With a carefully designed experiment Wang et al. (2015) could demonstrate that the projection-specific optogenetic activation of $SF1^+$ VMH → dl/l-PAG neurons led to a robust increase in immobility without affecting avoidance learning, suggesting a mere motor output driving function of this projection. This was further substantiated as the pharmacogenetic inhibition of the dPAG did not alleviate memory formation in a predator avoidance task, even though the inhibition abolished fear responses at the training day (Silva et al., 2016). However, several other studies have demonstrated that a direct dPAG stimulation leads first to immobility followed by escape attempts (panic-like) in a concentration/stimulus intensity dependent manner (Schenberg et al., 1990; Coimbra and Brandão, 1993; Ullah et al., 2015; Deng et al., 2016). Other prominent diencephalic inputs to the PAG arrive from the dorsal premammillary nucleus (PMD) (has been reported to modulate fear responses, Blanchard et al., 2003) and the zona incerta (ZI). The mesencephalic inputs to the PAG arise mainly from the SC and IC; some retrograde tracing studies suggest also the parabigeminal nucleus (PBG), VTA and substantia nigra (SN) as afferents to the PAG (Beitz, 1982; Meller and Dennis, 1986), but all three regions massively project to the overlying superior colliculus and a diffusion of the retrograde tracer into the SC might be the cause for

the observed labeling. The SC (*see next section*) and IC relay multisensory inputs to the periaqueductal gray, which might permit a fast response-selection (Redgrave and Dean, 1991). The telencephalon sends vast afferents towards the PAG, of them only those arising from the PrL, anterior cingulate area (ACA), CEA and BNST will be discussed. Increased prelimbic cortex activity has been implicated in promoting conditioned fear responses (Vidal-Gonzalez et al., 2006) and especially the projections towards the BLA are thought to play a major role (Bukalo et al., 2015). However, the PrL sends strong projections towards the dmPAG, and recent efforts have demonstrated that silencing this pathway reduces the previously established (social defeat) social avoidance (Franklin et al., 2017), which can be interpreted as a decrease in defensive responses. The ACA has been implicated in pain processing, regulation of affect and social behavior (Devinsky et al., 1995). It strongly projects towards the lPAG (*see* http://connectivity.brain-map.org/projection/experiment/112514202), and on-site optogenetic stimulation of the ACA has been shown to reduce pain thresholds in rodents (Gu et al., 2015). Also the BNST sends projections towards the PAG, but neither for the ACA nor for the BNST, there have been projection specific manipulations or recordings which could otherwise provide an indication about the behavioral role of these connections. The CEA sends GABAergic projections towards the vlPAG, which disinhibit local GABAergic neurons and in turn allow glutamatergic PAG efferents to activate the behavioral repertoire known as freezing (Tovote et al., 2016). The executive circuits which mediate the freez-

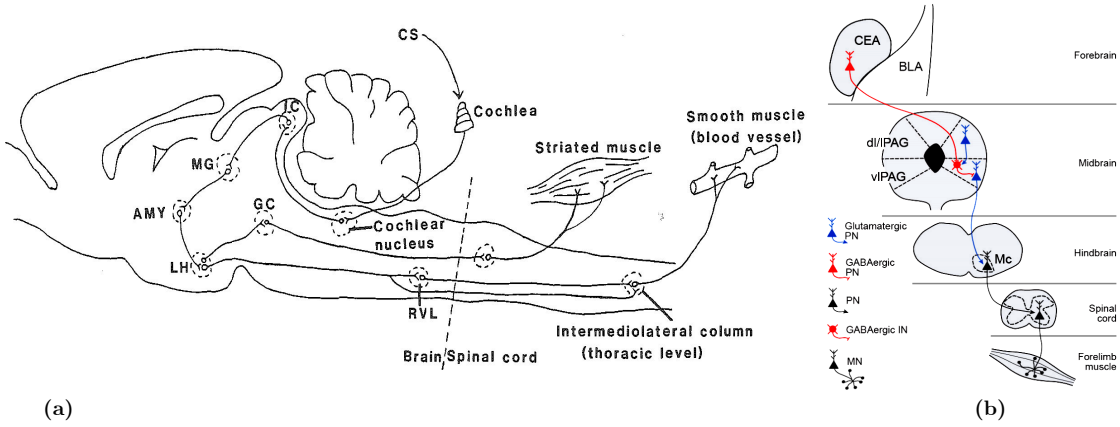

Figure 1.5 | Midbrain Circuits of Freezing Behavior
(**a**) Thalamoamygdaloid pathways mediating learned fear responses in the rat. AMY, amygdala; CS, conditioned stimulus; GC, central gray = periaqueductal gray; IC, inferior colliculus; LH,lateral hypothalamus; MG, medial geniculate nucleus; RVL, rostral ventrolateral medulla. Adapted from LeDoux (1987). (**b**) Schematic representation of the freezing pathway. CEA, central amygdala; BLA, basolateral amygdala; PAG, periaqueductal gray; Mc, magnocellular part of the medulla; PN, projection neuron; IN, interneuron; MN, motor neuron. Adapted from Tovote et al. (2016).

ing response have been proposed by LeDoux (1987) (*see* Fig. 1.5a) and conclusively investigated by Tovote et al. (2016) (*see* Fig. 1.5b). The ventrolateral PAG sends glutamatergic projections towards the magnocellular part of the ventral medulla, which synapse onto cholinergic premotor neurons, which in turn synapse on motor neurons

within the spinal cord (*see also* Mantyh, 1983). An activation of this pathways subsequently leads to a freezing response. Tovote et al. (2016) could also disprove the hypothesis (Vianna et al., 2001; Vianna and Brandão, 2003) that the vlPAG mainly expresses conditioned fear. The question how the facilitation of a movement behavior is generated from this circuit cannot be resolved at the present time but there is evidence that the dorsolateral PAG might be one of the effector sites (Kim et al., 2013; Chen et al., 2015). Another route for the expression of innate and conditioned freezing, namely the connection between the vlPAG and the lateral cerebellar pyramis, has recently been described by Koutsikou et al. (2014) and underlines the cerebellum's recent acknowledgment in the regulation of emotion (Schutter and van Honk, 2005; Strata, 2015).

In general, the efferents of the PAG have been demonstrated to innervate more than 80 different brain regions (Meller and Dennis, 1991; Cameron et al., 1995a; Cameron et al., 1995b). The brain areas with strongest innervation are by far the midbrain reticular nucleus (MRN) and pontine reticular nucleus (PRN) which likely mediate the increase in alertness, vigilance and arousal, which is accompanied with increased PAG activation, via the '*ascending reticular activating system*' (ARAS) (Steriade, 1996). The descending reticular projections might modulate the cardiovascular tone and even produce motor output. Other strong projections target the LHA and the posterior hypothalamic nucleus. These areas are involved in the homeostatic regulation of the organism and in the execution of the respective behavioral patterns (e.g. feeding) whereby the reciprocal nature of the hypothalamic $\rightleftharpoons$ PAG projection might infer that these projections carry feedback information. Similarly the efferents towards the parabrachial nucleus (PB), dorsal medial hypothalamus (DMH), mediodorsal thalamic regions (MD), CEA, and BNST, might function as feedback mechanisms or (especially the thalamic projections) bring the behavioral state into awareness. As mentioned, the stimulation of the dPAG causes a gradual shift from immobility to flight and an amygdala lesion abolishes a fear reaction towards a predator (*see section before*). Notably, Kim et al. (2013) showed that the concurrent stimulation of the dPAG remains without any effect if the amygdala is lesioned, which strongly states that the fear-mediating (but not the panic-like) function of the PAG, stems from its projection towards the amygdala, which functions as a downstream target of the PAG in this case (Kim et al., 2013). The role of the PAG being a unique hub for generating 'primal emotional tone' which ultimately influences 'prosencephalic sites' to mediate aversive responses has received more attention recently (Motta et al., 2017). The prevailing opinion, however, considers the PAG mainly as an output region, which is nonetheless reflected by its vast descending projections towards the medulla oblongata (as mentioned above) and the pons within the hindbrain. These projections are thought to mediate the accompanying physiological changes of defensive reactions. Changes in cardiovascular tone are mediated via efferents reaching the rostral ventrolateral medulla (RVLM) (Lovick, 1993) and PB (Nosaka et al., 1993). As seen before, the PAG-medulla projections also mediate motor output in the form of freezing but also vocalization. Especially vocalization is a rather complex motor program which involves muscular activity in the larynx, oral cavity, face and also in the chest

to control exhalation. It has been shown that the premotor nuclei are orchestrated by circuits within the medullary parts of the reticular formation. And stimulation within the reticular formation produces complete phonations not only isolated components of vocalization (*for review see* Jürgens, 2009). Transection experiments further highlighted the PAG to be the pivotal brain region which mediates vocalization, as a cut behind the PAG causes mutism in cats, dogs and squirrel monkeys (Adametz and O'Leary, 1959; Skultety, 1962; Jürgens and Pratt, 1979).

Another important function of the PAG is its role in mediating inhibitory pain modulation. Electrical stimulation of sites nearby or within the PAG of rats has been shown to eliminate all reactions towards painful stimuli (Reynolds, 1969; Mayer et al., 1971), while other responses towards visual and auditory stimuli remained unaffected. The main projections which are implicated in the antinociceptive effects of PAG stimulation are the descending pathways via the rostral ventral medulla (RVM) to the dorsal horn of the spinal cord (*for review see* Loyd and Murphy, 2009). This descending inhibitory pain pathway is also the main site of action for the analgesic effects of opioids (*for review see* Basbaum and Fields, 1984). During the direct confrontation with an imminent predator where injuries are likely, it has been demonstrated that the pain threshold is elevated. This phenomenon is termed *stress-induced analgesia* and the PAG has been found to play a major role also in the mediation of this specific adaptive response (*for review see* Butler and Finn, 2009).

Taking all these findings into consideration, one can describe the function of the PAG as being the major orchestrator of defensive reactions towards imminent threats by generating low latency behavioral responses. The fast responses are only possible as sensory information is reaching the PAG almost directly via the SC and IC. On the contrary there is only rudimentary understanding of the PAG as an emotional relay for subcortical structures so far.

Superior Colliculus

The superior colliculus (SC) is a bilateral mammalian midbrain structure which forms together with the IC the *corpora quadrigemina*. This is self-explanatory if the rodent brain is observed from above; then the four 'little hills' are apparent. The rostral 'bumps' form the SC. The evolutionary developmental origin of the SC is the optic tectum which is the main visual processing area in all non-mammalian vertebrates like amphibians, fish, reptiles and birds. As such, the SC receives direct sensory input from retinal ganglion cells (optic nerve) and exhibits a retinotopic organization (Sperry, 1963; Graybiel, 1975). Analog to this, the inferior colliculus receives projections from the cochlear nucleus and exhibits a tonotopic organization. However, the SC is a multisensory modality integration center, and while retinotectal afferents mainly target the superficial SC layers, the deep layers of the SC receive inputs from the lateral substantia nigra reticulata (SNr)(*see submitted manuscript* 'Nigrotectal pathway controls threat detection at the

level of the superior colliculus', Appendix 5.4.4), the parabigeminal nucleus (PBG), locus coeruleus (LC), brachium of inferior colliculus (BIC), external nucleus of the inferior colliculus (ICX), parabrachial nucleus (PB), zona incerta (ZI), pontine trigeminal nuclei, cuneiform nucleus (CUN), lateral dorsal tegmental nucleus (LDT), pedunculopontine nucleus (PPN) and medullary nuclei (paragigantocellularis lateralis, gigantocellularis) (Edwards et al., 1979; Jiang et al., 1997). Neurons within the SC have been found to respond to a wide variety of sensory modalities, and notably visual, auditory and somatosensory (tactile) information converges onto the same neurons (Meredith and Stein, 1986). Another strong input, mainly to the ventral motor-related part of the SC, arises from the motor cortex (Fries, 1985). It is believed, that this projection serves to guide visual attention and controls reflexive visually-guided saccades in primates (Pierrot-Deseilligny et al., 1991). Whether this projection fulfills a similar function in rodents is currently not known.

The efferent projections of the SC are also different for the superficial and deep layers. The superficial (visual related) layers project to the visual thalamic nuclei, namely the lateral posterior nucleus of the thalamus (LP), the dorsal and ventral part of the lateral geniculate nucleus (LGd, LGv) but also the nucleus of the brachium of the inferior colliculus, parabigeminal nucleus and midbrain reticular nucleus (Holstege and Collewijn, 1982). The deep layers of the SC on the contrary send most of their projections towards the dorsomedial and dorsolateral PAG, the nucleus reuniens (RE), zona incerta, pontine and medullary reticular formation and the mediodorsal thalamic nucleus (Graham, 1977; Sparks and Hartwich-Young, 1989).

Generally, the SC enables an animal to direct its primary sensory organs like eyes, pinnae and the head in response to a wide variety of cues. In primates the function of the SC is supposed to be limited to gaze shifts or shifts in visual attention, but stimulation experiments in cats and rodents revealed complex behavioral patterns controlled by the SC. Sahibzada et al. (1986) have electrically stimulated the SC of rats and observed freezing and contralateral orientating responses which turned into ipsilateral escape bouts followed by running and jumping with increasing currents. Similarly, the injection of excitatory amino acids (glutamate) into the SC caused a battery of defensive reactions (Dean et al., 1988) which excludes the possibility that electrical stimulation affected only fibers *en passage*. These observations suggest that the SC generates immediate behavioral responses in order to evade rapidly approaching threats, but the SC has been also implicated in predatory pursuit and hunting (Furigo et al., 2010). In this context the nigrotectal pathway (SNr→SC) has been shown to modulate innate fear responses elicited by the SC by attenuating threat detection (*see submitted manuscript* 'Nigrotectal pathway controls threat detection at the level of the superior colliculus', Appendix 5.4.4). Mice show a robust freezing & flight response if a dark looming disk (simulating a rapidly approaching predator e.g. bird of prey) is presented above them on a screen (Yilmaz and Meister, 2013). Shang et al. (2015) identified a parvalbumin positive (PV^+) but EXCITATORY group of neurons within the superficial layers of the SC, which, when activated produce a rapid flight & freezing response predominantly in male mice, accompanied by autonomic activation. Moreover, they could demonstrate

that those neurons exclusively respond to visual looming stimuli and that the projection towards the parabigeminal nucleus mediates the flight response. We have come across the redundant organization of crucial survival promoting circuits already several times (*see* PAG), thus it is not surprising that also the SC follows this logic. Wei et al. (2015) have reported a CaMKIIα-positive population of neurons within the intermediate layers of the SC which when activated elicits freezing. A selective optogenetic inhibition of these cells reduces the defensive responses towards looming stimuli. Further, they could demonstrated that these neurons project towards the lateral posterior nucleus of the thalamus and synapse onto amygdala-projecting neurons. Additionally, temporarily inactivation the amygdala using muscimol resulted in a complete absence of defensive responses evoked by SC optogenetic stimulation. Similar to the PAG, this suggests that the SC has an important role in integrating ascending information and translating it to defensive behavior.

1.5 The Autonomic Nervous System and the Hypothalamus

For the sake of completeness it is only just to describe in addition, the autonomic nervous system (ANS) in general, as well as the humoral or endocrine part of the stress response, namely the activation of the hypothalamus-pituitary (HPA) axis. As covered in the sections before, the affective states are accompanied by the initiation of various physiological and behavioral responses. These reactions cause a sudden increase in metabolic activity (e.g. during flight) and subsequently nutritional and thermoregulatory requirements which are fulfilled by two main homeostatic counter-regulatory systems (ANS & HPA). I have covered the involvement of the sympathetic and parasympathetic branches of the ANS already for certain aspects of the expression of negative affect. On purpose, the ANS was not introduced in the classical manner so far, as already John Newport Langley was aware of the oversimplification when he coined the term '*autonomic*' nervous system (Langley, 1903; Langley, 1921). I rather focused on different physiological functions and highlighted the partly antagonistic roles of the sympathetic and parasympathetic systems, which are sometimes contrary to expectations. It is important to remember that the functional segregation into the extreme 'fight-or-flight' and 'rest-and-digest' conditions might be partially practical, but indeed specific subsets of both systems can be activated independently. This fine-tuned neuronal control of physiological processes gives rise to the diverse bodily sensations which accompany human emotions (Nummenmaa et al., 2014). Even today, the classification into the sympathetic and parasympathetic branches of the ANS is not entirely certain for some of the nerves. A recent example is the discovery of Espinosa-Medina et al. (2016) where the authors disproved a more than 100-years old dogma and demonstrated that the outflow of the sacral part of the ANS belongs in fact to the sympathetic and not to the parasympathetic subdivision. This finding was, however, challenged by leading scientists of the field (Neuhuber et al., 2017). I will provide an overview on the general functions of the ANS and HPA

axis in this section, based on the following literature: Ulrich-Lai and Herman (2009); Castro et al. (2010); Jänig (2010); Lang (2010); Horn and Swanson (2013). The ANS

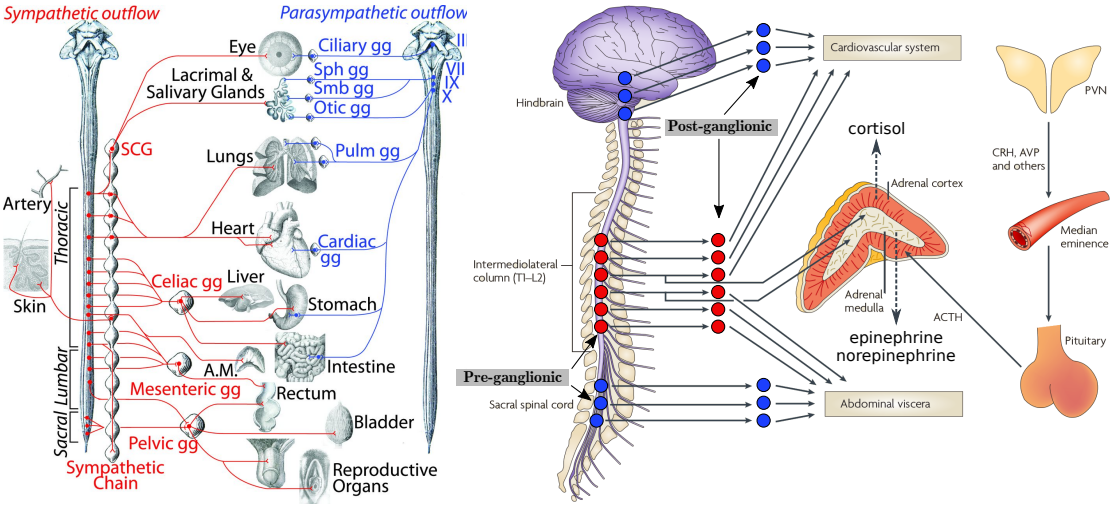

(a) Revised anatomy of the ANS

(b) Sympatho-adrenomedullary & HPA axis

Figure 1.6 | Revised Autonomic Nervous System and HPA Axis
(**a**) The revised anatomy of the autonomic nervous system. **Spinal** sympathetic (red, left) and **cranial** parasympathetic (blue, right) branches of the ANS. III oculomotor nerve; VII facial nerve; IX, glossopharyngeal nerve; X, vagus nerve; A.M., adrenal medulla; gg, ganglion; Pulm, pulmonary; SCG, superior cervical ganglion; Sph, sphenopalatine; Smb, submandibular. [Adapted from Espinosa-Medina et al. (2016)] (**b**) The sympatho-adrenomedullary (*left panel*) and hypothalamic-pituitary-adrenocortical (HPA) (*right panel* axes [Adapted from Ulrich-Lai and Herman (2009)]

can be divided into the cranial parasympathetic and the spinal sympathetic division (*see* Fig 1.6a). In contrast to the somatic motor system where the premotor neurons are located in the ventral horn of the spinal cord, the cell bodies of the analogous autonomic 'motor' neurons are located in special ganglia and thus are called *post-ganglionic* neurons. In the case of the sympathetic branch, these ganglia are mostly located in the paravertebral sympathetic chain with segmental organization, with only six exceptions (superior/middle cervical, celiac, superior/inferior mesenteric ganglia and the **adrenal medulla**). Each ganglion innervates several different target organs, whereby in the case of the adrenal medulla, the preganglionic cells innervate intra-adrenal chromaffin cells. The pre-ganglionic afferents arise from the ventral root of the spinal cord and reach their target ganglion via small 'communicating' branch-like nerves - the *rami comunicantes*. The parasympathetic system is organized very differently. Each ganglion is in very close proximity to one specific effector organ, and the preganglionic afferents arise from the cranial nerves within the brainstem. Generally, it is thought that the neurotransmission within the ANS is solely based upon two main neurotransmitters namely acetylcholine (ACh) and norepinephrine (NE). Whereas ACh is the neurotransmitter in all preganglionic and also parasympathetic postganglionic neurons, norepinephrine is released from sympathetic postganglionic cells (e.g. chromaffin cells). However, it has become evident that the neurotransmission is in fact much more complex which is indicated by the vast occurrence of neuropeptides such as calcitonin-related peptide, dynorphin, enkephalin,

galanin, neuropeptide Y, somatostatin, substance P and vasoactive intestinal peptide (VIP) in pre- and postganglionic neurons (Jänig, 2006). Moreover, the tissue specific expression of various types of α- and β-adrenoreceptors as well as metabotropic acetylcholine receptors (M1-M4), suggest a complex scenario which is far from being easily understood.

As several functions of the ANS have been discussed already, I just want to emphasize the distinguished role of the sympathetic (splanchnic nerve) innervation of the adrenal medulla and the resulting epinephrine & norepinephrine release into the blood stream by secretory chromaffin cells. This is sometimes called the *fast* stress response. In contrast to this direct sympatho-adrenomedullary response stands the *slow* stress response, via the activation of the hypothalamic-pituitary-adrenocortical (HPA) axis (*see* Fig 1.6b). The hypothalamus is the most critical brain area involved in the regulation of the *milieu intérieur* as Claude Bernard (†1878), the founder of regulatory physiology, has called the internal environment (Holmes, 1986). This involves direct physiological control and complex behaviors. With precise electrical stimulation within the hypothalamus of cats, Walter Rudolf Hess could observe a highly diverse repertoire of reactions all governed by such a small brain area (*see* table 1.1).

Table 1.1 | Physiological and Behavioral Changes due to Electrical Stimulation of the Hypothalamus (Hess, 1954)

Physiological	arterial blood pressure, heart rate, respiratory rate, body temperature, blood sugar level
Reflexive	defecation, micturition, salivation, sneezing, vomiting, jawing, pupillary dilation
Behavioral	licking, sniffing, feeding, freezing, flight, defensive attacks, aggression, rage, reproduction

The paraventricular nucleus (PVN) of the hypothalamus, is a thin layer of neurons surrounding the ventral part of the third ventricle. Ventral to the hypothalamus originates the pituitary stalk (*infundibulum*), which bears the anterior pituitary (*adenohypophysis*) and the posterior pituitary (*neurohypophysis*). The hypophysis is the major neuroendocrine release site. The dorso-rostral part of the pituitary stalk is called the median eminence (*eminentia mediana*) and the portal venous blood stream connects the median eminence with the adenohypophysis. The origin of the adenohypophysis is not neural, but during embryonic development cells of the anterior pituitary placode, within the oral ectoderm, start to thicken and form a small excrescence − the Rathke's pouch. As a separating mesenchymal membrane is missing, the Rathke's pouch is in direct contact with the developing ventral diencephalon and later becomes the posterior pituitary (Scully and Rosenfeld, 2002). Within the PVN there are two main groups of cells, the magnocellular and the parvocellular neurons. The magnocellular neurons project via the pituitary stalk towards the neurohypophysis and directly release vasopressin (also called: antidiuretic hormone ADH; adiuretin; arginine vasopressin AVP) or oxytocin into the inferior hypophysial artery. The anterior pituitary

is regulated indirectly via hormones released from the parvocellular cells of the PVN, but also from the arcuate nucleus (Arc, a brain region below the PVN). These neurons send their axons towards the fenestrated hypophysial portal vein system in the median eminence where they secrete liberins (releasing hormones, releasing factors) and statins (release-inhibiting hormones) e.g. thyrotropin-releasing hormone (TRH, thyroliberin), gonadotropin-releasing hormone (GnRH, gonadoliberin), corticotropin-releasing hormone (CRH, corticoliberin), growth hormone-release inhibiting hormone (GIH, somatostatin), growth hormone-releasing hormone (GHRH, somatoliberin, from the Arc) and prolactin-release inhibiting hormone (PIH, dopamine, from the Arc)[†]. Carried via the blood stream, those hormones reach their cognate receptors within the anterior pituitary whereby the release of the respective trophic ('nourishing') and tropic ('driving','changing' Steinberg, 1952) hormones is regulated. In the case of CRH, the target cells are the *corticotropes* which in turn liberate adrenocorticotropic hormone (ACTH, corticotropin). Within the corticotropes ACTH is synthesized via the cleavage of pro-opiomelanocortin (POMC), a 241 amino acid long peptide which, in addition to ACTH, is also the precursor for several other peptide hormones. Once released, the main function of ACTH is to stimulate the release of glucocorticoid steroid hormones (mainly cortisol or corticosterone, CORT) from the *zona fasciculata* of the adrenal cortex. The physiological functions of released CORT are vast and range from immuno-suppressive to gluconeogenesis stimulating (hence the name) and fear memory altering (Pugh et al., 1997). This multi-staged cascade offers the possibility of minute, physiological fine-tuning of CORT release via e.g. the glucocorticoid receptor (GR) and mineralocorticoid receptor (MR) which mediate the regulative negative feedback within the anterior pituitary, the PVN and limbic structures.
In general the function of the HPA-axis, with respect to defensive responses, is to prepare the organism for increased metabolic activity, physical confrontation where high levels of arousal are necessary, and ultimately injury and blood-loss.

1.6 Animal Models and Model Organisms of Anxiety Disorders

The term *animal model* refers to a system which allows to observe behavioral or physiological responses in a highly reproducible manner, enabling the study of the underlying biological mechanisms. An animal model consists of the combination of (i) a model organism, (ii) a specific testing situation (iii) and a defined readout. The model organism can be a wild-type animal with known disposition to show e.g. increased anxiety-like behavior, specific mouse lines which have been established via selective breeding in order to augment specific behavioral traits, pharmacologically induced models or genetically modified animals. The readouts most likely are the number, duration or quality of a certain displayed behavior but also physiological parameters, like heart

[†]The melanotropin-release-inhibiting-hormone has been deliberately omitted as the literature is very vague on this subject.

rate, or CORT release etc.. The testing situation comprises a paradigm which reliably and preferentially in a repeated manner evokes the specific behavior. The quality of an animal model is typically assessed via its adherence to the following criteria: face validity (how well does the animal model phenomenologically reproduce the human disease), etiological validity (how similar are the inducing factors/stimuli between the animal model and the human disease), construct validity (how similar are the underlying physiological processes) and predictive validity (how well does the animal model translate to the human disease with respect to treatment responsivity). In this section I will give a short summary of the most prominent animal models and model organisms for the study fear & anxiety in mice (*for review see* Campos et al., 2013; Calhoon and Tye, 2015).

Experimentally Induced or Conditioned Fear & Anxiety Tests

Auditory Fear Conditioning

Probably the most widely applied paradigm to study fear reactions in rodents is *fear conditioning*. Recent attempts to better conceptualize the terms used in basic research on the *fear system* (LeDoux, 2014) suggest the use of THREAT CONDITIONING, instead. This is owed to the fact that *fear* describes a subjective (human) feeling which cannot be readily adopted to describe animal affects. Nonetheless I will continue to use the conventional term *fear* throughout the thesis.

Fear conditioning is a special form of Ivan Petrovich Pavlov's well known classical conditioning (Pavlov and Anrep, 1927) - it *involves learning that certain environmental stimuli predict aversive events* (Maren, 2001). More specifically, talking about auditory fear conditioning, the innoxious conditioned stimulus (CS) - the stimulus to which the animal will be conditioned - consists of a tone (e.g. 9 kHz at 80 dB SPL, 20 seconds duration) and is paired with a noxious, unconditioned stimulus (US) e.g. a brief, mild electric shock (0.3-1.5 mA) to the animal's feet. Already after a single pairing, the emotional responses which are usually evoked by the US alone (e.g. accelerated heart-rate, increased blood-pressure, flight attempts, immobility) are linked to the innoxious CS and can be now evoked by the CS alone. In the case of an auditory fear-conditioned mouse, upon the onset of the tone, the animal would show most prominently an immobility response, called *freezing*. To successfully link the CS to the US, it is necessary that the tone onset precedes the foot-shock (18 seconds) and most effectively both stimuli terminate simultaneously. The neural circuits which mediate the formation, storage and expression of the auditory fear-memory have been the subject of extensive research over the past 50 years and are well described (*for review see* LeDoux, 2000; Maren, 2001; Paré et al., 2004; Fanselow and Poulos, 2005; Davis, 2006; Kim and Jung, 2006; Pape and Pare, 2010; LeDoux, 2012; LeDoux, 2014). In brief, the core integration center where the information about the CS and US converges is the lateral amygdaloid nucleus (LA). Auditory information about the CS reaches the LA via auditory thalamic nuclei, namely the medial section of the medial geniculate nucleus (MGm) as well as the posterior intralaminar nucleus (PIN) (LeDoux and Farb, 1990). But also the auditory cortical regions send

prominent projections towards the LA (Romanski and LeDoux, 1993b). It is necessary to highlight the discrepancy of the PINs role in relaying auditory versus tactile information. In the original publication by LeDoux and Farb (1990), the PIN was said to merely relay auditory information. In a more recent publication published by Lanuza et al. (2008), the MGm/PINs role changed and was said to relay *somatosensory and nociceptive information to the LA*.

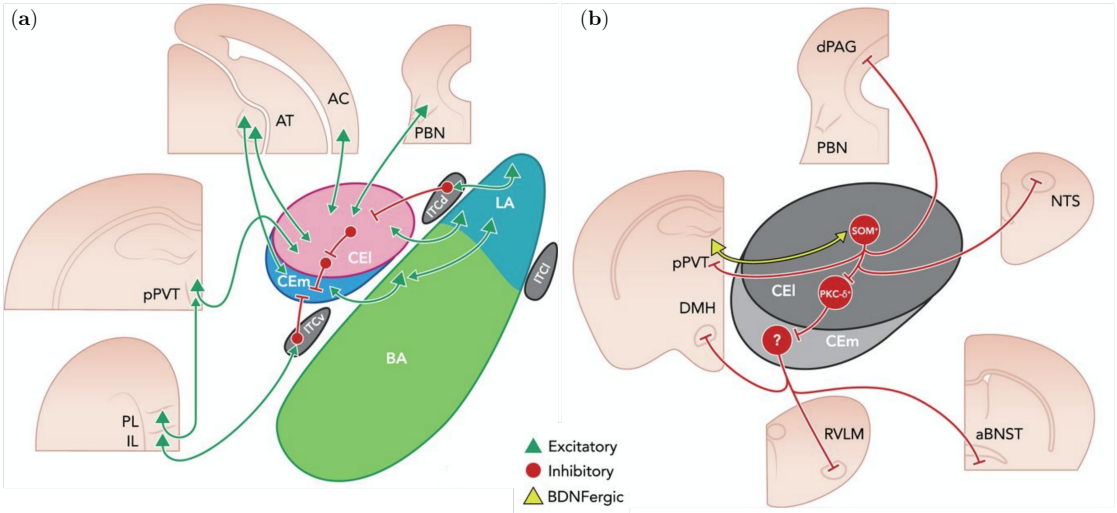

Figure 1.7 | Inputs and Outputs of the Rodent Amygdalar Circuit
(**a**) Intra- and extra-amygdalar CEA inputs. (**b**) Intra- and extra-amygdalar CEA outputs. See text for a detailed description. CEl centrolateral amygdala, AC auditory cortex, AT auditory thalamus, pontine parabrachial nucleus, LA lateral amygdala, IL infralimbic prefrontal cortex, PL prelimbic prefrontal cortex, pPVT posterior paraventricular thalamus, ITCv/d ventral/dorsal intercalated cell mass, CEm centromedial amygdala, dPAG dorsal periaqueductal gray, NTS nucleus tractus solitarius, DMH dorsomedial hypothalamus, RVLM rostral ventrolateral medulla, aBNST anterior bed nucleus of the stria terminalis, SOM+ somatostatin-expressing, PKC-δ+ protein kinase C-delta-expressing, BDNF brain-derived neurotrophic factor. [Adapted from Keifer et al. (2015)]

An alternative site of convergence for CS and US has been hypothesized to be the MGm/PIN complex itself (Weinberger, 2011). Studies in-*vitro* demonstrated a strong potentiation of the MGm-LA synapse upon fear conditioning, which is partly due to an increase in presynaptic transmitter release (Shinnick-Gallagher and McKernan, 1997). The information from the LA is then relayed to the centrolateral amygdala (CEl) and via recurrent inhibitory projections towards the centromedial amygdala (CEm) (*see* Fig 1.7a). It has been shown previously that a net-disinhibition of the CEm output, due to an interplay of protein-kinase-C-delta positive (PKC-δ+) ON, PKC-δ+ OFF and somatostatin-positive (SOM+) (*see* Fig. 1.7b) neurons, leads to the expression of conditioned freezing (Haubensak et al., 2010; Ciocchi et al., 2010). A recent paper by Fadok et al. (2017) demonstrated that the activation of corticotropin-releasing hormone-positive (CRH+) neurons in the CEl is necessary for displaying conditioned flight responses. The GABAergic long-range projections from the CEm and CEl, targeting the vlPAG (Tovote et al., 2016), have been shown to mediate the conditioned freezing response via

the dis-inhibition of vlPAG GABAergic interneurons. These in turn activate glutamatergic projections towards the magnocellular part of the ventral medulla and ultimately glutamatergic premotor neurons projecting to the spinal cord. Interestingly, opposing sexually divergent expression of conditioned fear was recently reported by Gruene et al. (2015).

Fear-potentiated Acoustic Startle Response

While freezing is the most easily observable conditioned response (CR) in rodents, a high degree of experience is necessary to distinguish mere immobility from a real freezing response (in particular in mice), which is otherwise displayed in the anticipation of pain. Therefore different approaches have been undertaken to better separate immobility from freezing, for example by incorporating appetitively motivated tasks like leverpressing for a rewarding stimulus (water, food) (Mast et al., 1982; Quirk, 2002). Another readout for the assessment of successful fear-memory formation is the fear-potentiated acoustic startle response/reflex (ASR) (*see* Fig. 1.8) (*for review see* Davis, 1980; Davis, 1984).

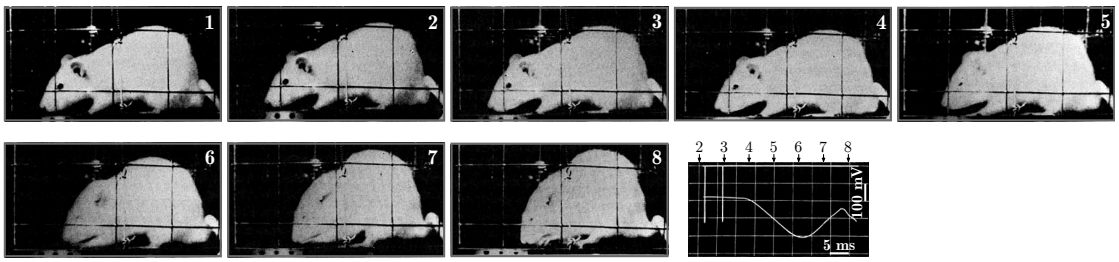

Figure 1.8 | Prototypic Acoustic Startle Response in a Rat
[Adapted from Davis (1984) p. 292]

An acoustic stimulus, consisting of a brief white noise (12-50 ms length) with 90-120 dB sound pressure level (SPL), elicits a profound startle response, mediated mostly by contractions of the extremities followed by the neck and trunk muscles which results in an overall shorting of the body. The response is typically measured using piezoelectric transducers in voltage mode combined with rectification and amplification (1000x). The typical amplifier circuit of a San Diego Instruments Startle Apparatus is depicted in figure 1.9. The startle response in mice is a highly robust measure, which has been shown to undergo only moderate (-20%) long-term habituation in the course of 5 days of repeated testing (Azzopardi et al., 2013; Pilz et al., 2014). However, the ASR is not inert to modulating influences. The presence of a previously negatively conditioned stimulus (e.g. pairing a visual or auditory cue with an aversive footshock) increases the ASR. This phenomenon is known as the fear-potentiated startle response (FPS) mentioned above (Brown et al., 1951; Davis and Astrachan, 1978). While the FPS paradigm has been mainly applied to rats, there is convincing evidence that also mice show an increased ASR in response to a conditioned light stimulus (McCaughran et al., 2000). However, most notably there seem to be strong strain differences involved in developing a FPS response. Falls et al. (1997) could demonstrate that DBA/2J mice develop a profound

FPS response, while C57BL/6J mice were almost unaffected. A major pitfall of this study is the fact that both stimuli (startle stimulus and CS) where of the same modality - namely auditory signals. Despite the fact that DBA/2 and C57BL/6 differ in their absolute hearing capabilities (Willott et al., 1984) (Falls et al., 1997 controlled for this), especially the DBA mouse line is highly prone to develop even fatal audiogenic seizures (Hall, 1947). Thereby is it likely that the FPS response observed by Falls et al. (1997) can be at least partially attributed to an increased/non-linear excitability of auditory-related brain areas. An interesting study by McCaughran et al. (2000), however, could show that DBA/2J but not C57BL/6J can form a robust FPS response when a the light of 7 watt house lamp (10 s) was co-terminated with a 0.5 mA footshock (1 s) for at least five trials.

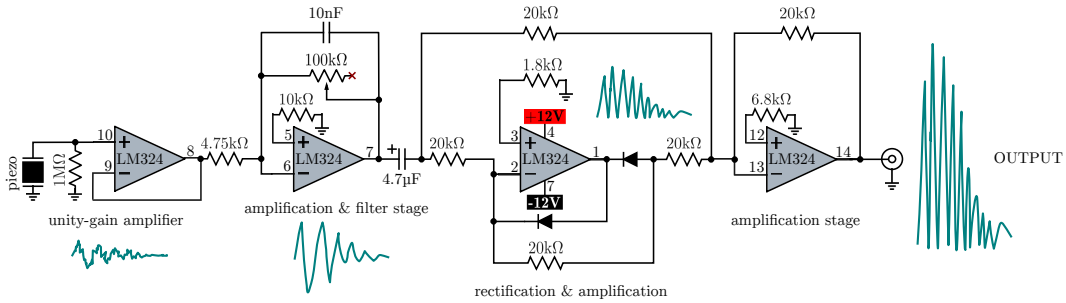

Figure 1.9 | SDI Startle Apparatus Amplifier Circuit
Circuit diagram has been obtained through careful electrical analysis of an existing device. [Genewsky]

Active & Passive Avoidance Task

Two other very important paradigms to asses acquired fear are the active and passive avoidance tasks. While these tasks are generally considered to involve a learning process (e.g. at least one encounter with the aversive stimulus), they are ultimately based on the animals natural avoidance to noxious stimuli. In an active avoidance testing procedure an animal learns to display a specific behavior in order to avoid punishment (e.g. mild foot shock). Usually these experiments are carried out in a specific shuttle box with two compartments connected via a smaller passage and equipped with independently electrifiable grid floors. The animals are acclimatized for several minutes to the apparatus, before an auditory stimulus (CS, e.g. white noise) sounds or a visual stimulus lights up, approx. 5-10 seconds prior the onset of an electric foot shock (US, 0.3 mA, <10 seconds). One testing session can consist of up to 100 trials with approx. 20-60 seconds inter-trial intervals. After four sessions, mice have readily acquired a profound avoidance (preemptive response within 10 seconds after CS onset) behavior (>80%) in response to the CS and the number of received foot shocks is minimal (Bovet et al., 1969). If the animals do not react to CS, they can still move to the other compartment and escape further punishment (shuttle once the US is present). However, the interpretation of the active-avoidance task with respect of anxiolytic action is not trivial. Typically, benzodiazepines modulate the performance during 'acquisition' phase

e.g. in the first session and it has been repeatedly shown that alprazolam, diazepam and midazolam facilitate avoidance 'learning' in rats (Fernández-Teruel et al., 1991; Savić et al., 2005). However, it has to be noted that benzodiazepines effectively decrease freezing rates whereby a shift from passive to active fear-coping strategies takes place which is independent from any form of learning.

In passive avoidance tasks, the animals are forced to inhibit a behavioral response and otherwise receive a punishment, usually in the form of an electric footshock. Typically these tasks are learned within a single trial (other than active avoidance tasks). Prototypic examples of passive avoidance in mice are step-down or step-through inhibitory avoidance tasks. Here, mice are placed either on an electrically isolating platform within an apparatus containing an electrified grid floor (step-down) or within a shuttle-box with an electrified grid in the connecting tunnel. The main measure in these behavioral procedures is the latency it takes for the animal to 'step-down'/'step-through' the grid and receive immediate punishment. Thereby an avoidance memory is formed during the training session which leads to increased latencies in the following retention test on the consecutive day. Pre-training administration of benzodiazepines has been shown to drastically decrease step-down latencies in mice (Nabeshima et al., 1990). But whether benzodiazepines directly change the valence of the situation or more likely exert their apparent 'anxiolytic' effect by affecting the memory formation, cannot be answered readily. Growing evidence, however, suggest, that at least during operant conditioning tasks − like step-down avoidance and if non-reinforced also the concomitant safety-learning − benzodiazepines severely affect hippocampal information processing (Micale et al., 2017).

Geller-Seifter & Vogel Conflict Test

In the paragraph before we have seen how the animal's intrinsic exploratory drive creates a conflict (passive avoidance) as staying in a certain compartment or on a platform and the likelihood to receive a shock act against each other. This approach-avoidance or conflict situation is the core principle in the following models. In the Geller-Seifter conflict test (Geller et al., 1962), food-deprived animals have the chance to gain access to nourishment by pressing a lever within the behavioral apparatus. Once the animals have reached a stable performance (e.g. 30 lever presses for one pellet), a mild footshock is applied whenever the animal attempts to consume. This reinforced phase of the experiment is signaled by an auditory stimulus. During one testing session, several reinforced and non-reinforced phases alternate. Thereby a conflict is experimentally established, as animals have access to food on the one hand, but risk punishment. It has been shown that anxiolytics (e.g. Diazepam 1 mg/kg) strongly increase the number of leverpresses even during the punishment phase. Similar to the Geller-Seifter conflict test, but simpler and also more popular is the Vogel conflict test (Vogel et al., 1971). Here, the animals are water-deprived and usually only 1 hour per day or during the testing procedure they have access to a water (*ad libitum*). In the behavioral apparatus they receive a mild footshock once they start licking at the electrified watter bottle. In

this test the animals do not have to learn a novel task, as the water bottle is usually very similar to the one in their homecage. Anxiolytics like diazepam (1 mg/kg), have been shown to drastically increase the number of lickings/shocks per session (Umezu, 1999). The benefit of the experimentally induced conflict and motivation are their stability over time which allows repeated testing, different from most exploratory based tasks. Therefore especially the Vogel conflict test has a pivotal role in pharmacological testing.

Unconditioned or Innate Fear & Anxiety Tests

In animal models of conditioned or acquired fear the experimenter can precisely control the modality and intensity of the applied stimuli. Brightness, sound-pressure level and current are adjusted to yield the maximally desired effect. This approach minimizes undesired variances and leads to highly robust behavioral readouts. Moreover, in the case of the auditory fear-conditioning, fear-potentiated startle and active avoidance paradigms, the onset of the fear-eliciting impulse is known, whereby the correlation of physiological, neurophysiological and behavioral measures is permitted. The ethological relevance of the applied stimuli - with respect of the *house mouse* being the subject of study - is oftentimes disregarded and the experimental animal becomes less important. This abstraction bears the risk that behavioral results are misinterpreted and even loose their translational value. Ethologically relevant fear & anxiety tests are based on innate behaviors and are inextricably linked to the physiology and anatomy of the model organism.

Elevated Plus Maze

The elevated plus maze (EPM) (Pellow et al., 1985) makes use of a rodents' innate fear of high, open and brightly lit spaces opposed to their preferred stay in dark and protected compartments. The EPM consists of two crossed (90°) arms, whereby one arm is equipped with shielding walls (closed arm) and the other one is left unprotected (open arm). At the intersection of the arms, the walls are opened (center). Additionally the open arms are evenly illuminated with >300 lux white light to increase the aversiveness. Typically, the mouse or rat is placed in the center at the beginning of the experiment, whereon once released the animal usually immediately retrieves into one of the closed arms. After a certain latency the animals starts to explore the maze and eventually explores the open arms. Anxious animals spend less time on the open arms than less anxious animals do. Benzodiazepines like chlorodiazepoxide have been shown to significantly increase the time spent on the open arms (Pellow et al., 1985; Calzavara et al., 2005). The duration of the test is limited to 5-10 minutes, but longer periods may be necessary to assess pharmacological modulations in highly anxious animals. Notably, the EPM readout is sensitive to the size, acoustics and illumination of the experimental room, as these parameters heavily influence the aversiveness of the open arms (Violle et al., 2009). Moreover, repeated EPM testing is complicated by the fact that certain kinds of 'carry-over' effects seem to change the animals response in consecutive trials. One example is the 'one-trial tolerance' (OTT) (File et al., 1990), an

effect where anxiolytics lose their effectiveness on EPM behavior from the first to the second trial (*for review see* Carobrez and Bertoglio, 2005). Besides the OTT, another important factor, which limits repeated testing, is the decreased motivation to explore the open arms between trials.

Light-Dark Box

Similarly, to the EPM, the dark-light box (DLB) test (Crawley and Goodwin, 1980), is based on a rodents' innate avoidance of open spaces. The apparatus is very simple as it only consists of two compartments: the dark compartment which is constructed of black, dulled PVC with no or only infrared illumination, and a brightly white-lit light compartment made of white and glossy PVC. Both compartments are connected via a small dark tunnel. The test can be carried out at two different modes: (a) as an emergence task, where the animals are placed in the dark compartment, and the latency it takes for the animal to step into the light compartment as well as the number of transitions and overall time in the compartments are measured; or (b) as a withdrawal task, where the animals are placed in the light compartment. It has been shown that benzodiazepines (clonazepam, diazepam, flurazepam, chlorodiazepoxide) strongly increases the locomotor activity and number of transitions (Crawley, 1981) in this task, but also a profound strain-dependency plays an important role (Griebel et al., 2000). The test duration is typically limited to 5-7 minutes in mice.

Open Field Test

The open-field test (Hall, 1934; Christmas and Maxwell, 1970) (*for review see* Bailey and Crawley, 2009), assesses a rodent's locomotor activity within a brightly illuminated (>200 lux) square (60×60 cm, mice) or circular arena (ø 60 cm, mice). Naïve animals typically display a pronounced *wall-hugging* behavior in a novel environment, which is described as *thigmotaxis*. Thereby, the time the animal spent in the center (e.g. inner 50% area) of the arena is low. The anxiolytics diazepam (0.8 mg/kg) and buspirone (0.3 mg/kg) have been shown in rats to significantly increase the number of entries into the central zone without affecting overall motor activity (Siemiątkowski et al., 2000).

Novelty-induced Suppression of Feeding

The novelty-induced suppression of feeding (also *hyponeophagia* or *novelty-suppressed feeding*) test is based on an animals innate behavior to forage and consume food only under safe conditions. Animals which have been food-deprived for 24h before the task are placed in a novel environment (e.g. type III cage, 425×266×155 mm) filled with bedding. In the center of the arena is the food platform, consisting of a circular piece of Whatman paper mounted on a plastic petri-dish to increase the salience and visibility. The food platform is baited with the animals standard food (e.g. food pellet). The food should be fixed to the petri-dish using a rubber band in order to hamper animals from carrying the food away (Samuels and Hen, 2011). Once the animals are introduced to the behavioral setup, the latency until the animal grasps and bites into the pellet

is recorded. It has been demonstrated that the latency to feed in a novel environment can be significantly reduced by diazepam (0.3 mg/kg) in mice (Iijima et al., 2012). The novelty-induced suppression of feeding task has been found to be an excellent paradigm especially in measuring stress-induced changes in anxiety (e.g. mouse model of PTSD, Siegmund and Wotjak, 2007), as the accompanying anhedonia-like behavior goes in line with increased novelty fear.

Ethologically Inspired Testing Situations

Despite the established and standardized tests mentioned above, there have been several attempts to develop ethologically relevant testing situations for the study of fear in rodents (*for review see* Pellman and Kim, 2016). These tests stand out in a way, as they put the model organism into the focus and consider its different sensory and behavioral biological capabilities. By mimicking real-world situations, the evoked behavioral repertoire is more complex and likely involves a larger part of the fear system, than learned CS-US associations ever can. Following this line of reasoning a little further, one can start to question learned fear paradigms entirely and the remarks by Bolles, 1970 (pp. 32-33) seem apt:

> Thus, *no real-life predator is going to present cues just before it attacks. No owl hoots or whistles 5 seconds before pouncing on a mouse. And no owl terminates his hoots or whistles just as the mouse gets away so as to reinforce the avoidance response. Nor will the owl give the mouse enough trials for the necessary learning to occur. What keeps our little friends alive in the forest has nothing to do with avoidance learning as we ordinarily conceive of it or investigate it in the laboratory.*

Therefore, the study of innate fear responses using ecologically relevant stimuli is possibly the most naturalistic approach, and shall be covered in the following paragraph.

Prey animals, like mice and rats, show increased sensitivity to predator-derived odors and react with avoidance, increased arousal and even display defensive responses, upon detection. One of the most widely studied odorants is 2,5-dihydro-2,4,5-trimethylthia-zoline (TMT), a component found i.a. in the urine of red foxes (*Vulpes vulpes*), the natural predator of mice (*for comprehensive review see* Fendt et al., 2005; Apfelbach et al., 2005). TMT has been found to induce aversion and immobility responses (freezing) in rodents (Endres and Fendt, 2009). It has been also shown to augment anxiety-like responses in standard testing situations like EPM, namely decreasing the time spent on the open arm (Hacquemand et al., 2013). Some authors suggest that odorants used at high concentrations, exert their repelling effects via an activation of trigeminal nerve fibers (Brand, 2006), and thereby leading to unspecific fear responses. However, Ayers et al. (2013) have demonstrated, using bulbectomized rats, that the freezing response evoked by TMT is dependent on an intact olfactory bulb. The neural circuits that mediate the odor-evoked fear responses have been elegantly identified by Root et al. (2014). Here, the authors

have optogenetically inhibited, previously TMT odor-primed circuits within the cortical amygdala, and could successfully abolished TMT-evoked avoidance responses. Regarding the pharmacological modulation of fear responses induced by predator odors, very little is known so far, but Blanchard et al. (1990) have demonstrated a reduction in active risk-assessment induced by cat odor in rats, upon treatment with diazepam. Not to be ignored, however, is the rather high technical effort in order to control the spatial diffusion and temporally precise application of TMT, which drastically limits its applicability. A much better temporal and spatial control is offered with the use of visual fear evoking stimuli. Besides ground-dwelling predators, mice have to fear birds of prey, which can approach almost silently from great heights with extreme velocity (>140 km/h *Falco peregrinus*, Alerstam, 1987). Therefore neuronal circuits which bypass conscious perception and allow the initiation of flight responses with ultra-low latency have evolved (*see* section *Superior Colliculus*). The use of looming visual stimuli to robustly evoke flight and freezing responses in mice, has been demonstrated by Yilmaz and Meister (2013). Here, the authors have used a LCD screen which was mounted above a small arena equipped with a shelter. The animal was placed in the arena for 10 minutes to acclimatize. Subsequently, a dark looming disk at a speed of 35°/s was repeatedly projected onto the screen and the behavioral responses were video taped. However, the authors also report that they have observed great differences the disposition to either show flight or freezing responses in the same mouse line but stemming from two different animal facilities. This suggests that the evoked behavior might be robust among a specific breed of mice, but rearing conditions greatly affect the behavioral repertoire and care must be taken to use well-handled animals in combination with standardized housing conditions.

The use of isolated stimulus modalities offers the possibility to probe specific sensory-related fear circuits for their behavioral effect and allows to further dissect their connectivity using e.g. optogenetics (Wei et al., 2015). But simulating real-world scenarios requires the application of complex multimodal stimuli. A very interesting technique to mimic a foraging situation has been demonstrated by Choi and Kim (2010). Here the authors have used a 4-wheeled robot which was programmed to move forward once a movement was detected by its ultrasonic sensors. The robot was placed in a large longitudinal arena, and food-deprived rats where asked to forage food pellets which were placed in the close vicinity of the robot. This setup allows the study of active risk assessment behaviors as well as flight responses, without the need of noxious stimuli. The ultrasonic range finders emit pulsed (20 Hz) signals in the 50 kHz range. Surprisingly, mice and rats are not disturbed by this auditory stimulus, possibly due to the lack of any biological significance (no whistle-like sound profile).

For the purpose of simulating real-world predator encounters, which cover several sensory modalities, including olfactory cues, several groups have developed testing situations which incorporate the use of other actual predatory animals. One famous example is the use of the venomous pit viper 'Urutu' *Bothrops alternatus* (Almada and Coimbra, 2015). Here, the mice are placed in a large arena which offers several possibilities to retrieve (ladder, burrow), for three consecutive days in order to acclimatize. On the fourth day, the mice are confronted with a sated snake. The behavioral repertoire

evoked by this stimulus is possibly the most complete: alertness, freezing, defecation, exophthalmus, micturition, oriented escapes (e.g. towards the burrow), running, jumping but also active risk assessment which even includes approaching the snake (personal communication. Almada RC). However, ethical concerns strongly limit the applicability of such a task, and the testing outcome is not only dependent on the behavior of the mouse, but is also strongly affected by the snake. In order to avoid this additional variable, the Mouse Defense Test Battery (MDTB) has been developed (Griebel et al., 1997; Blanchard et al., 2003; Griebel and Beeské, 2011). The MDTB utilizes a mouses' natural aversion to rats, as rats are known predators of mice (Nikulina, 1991) and have been found to possess a pronounced *muricide* (mouse killing) behavior (Karli, 1956). The MDTB is conducted within a large longitudinal arena (W0.4×H0.3×L3.0 m) which is separated along its length via a median wall yielding a 6 m long track. After a 3 minute acclimatization period the mouse is confronted with a hand-held stimulus rat (anesthetized or freshly killed) which is used to chase the mouse. Several behavioral readouts are possible using this test: flight, contextual anxiety (jumping), defensive aggression (biting) and risk assessment. The MDTB has been found to reliably show the effect of various anxiolytics including diazepam, whereby at low doses of 1 mg/kg DZP the most sensitive measure was risk assessment, which was significantly decreased (Griebel et al., 1998). But, again also the MDTB, utilizes another animal which has to be anesthetized or even killed, simple to conduct the test. It is questionable to what extent this use of rats complies with the Animal Welfare Act or whether it presents a 'reasonable cause', but certainly it is not entirely without ethical concerns.

In conclusion, there are many available ethologically inspired testing situations which allow the assessment of innate fear. However, none of them offers a multimodal sensory stimulation and simple implementation, permits the use of naïve animals (not food or water deprived) and does not depend on the use of other animals (e.g. cats, snakes or rats) to evoke the defensive reactions.

Model Organisms for the Study of Fear & Anxiety

The International Mouse Strain Resource (www.findmice.org, accessed 03.04.2017, Eppig et al., 2015) currently lists almost 500 inbred mouse strains of which more than 160 are kept as live stock worldwide. Strain differences have been reported numerously with many of the above mentioned fear & anxiety testing procedures with for e.g. 129/Sv, 129S1/SvImJ, BALB/c, DBA/2J, and C3H/He while C57BL/6 being the comparator strain (*for review see* Sartori et al., 2011a). The per definition high genetic similarity between the individuals of one strain (>98.6%, Davisson, 1996) fosters the search for the hereditary basic principals which mediate the alterations in emotional behavior.

However, up to today only a very limited number of possible treatment strategies for anxiety disorders have been suggested based on academic preclinical research with inbred mouse strains and strain differences. One of the best examples is the suggested application of L-DOPA (Haaker et al., 2013) and a promising role of dietary zinc-restriction (Whittle et al., 2010; Whittle et al., 2016) in order to enhance fear-extinction learning

and prevention of the return of fear. The understanding of spontaneously occurring behavioral phenotypes in inbred mouse lines is of keen interest in the field of behavioral genetics. But the unknown selection criteria in combination with the likely complex or multifactorial genetic cause, render inbred mouse strains a challenging model organism to understand fear & anxiety in humans.

An alternative approach is the selective bi-directional breeding strategy where individuals from an outbred mouse line are selected for further breeding with respect of their performance in a typical anxiety test as selection criterion. After several generations, the behavioral responses are amplified and extreme behavioral traits precipitate. To my knowledge, the only established mouse lines so far which have been selectively bred specifically for extremes in anxiety-related behavior are the hyperanxious HAB (high anxiety-related behavior) and hypoanxious LAB (low anxiety-related behavior) mice (Krömer et al., 2005). Other selective breeding attempts have been made (Szego et al., 2010) but are not taken into account, as subjective and non-standardized selection criteria have been applied. In the following I will focus on the HAB and LAB mouse lines and their comparator mouse line CD1 or NAB (normal anxiety-related behavior) which have been established later-on via selective breeding for an intermediate anxiety phenotype. Moreover, I will emphasize anxiety/fear-related behavioral phenotypes and mostly neglect results from genetic and proteomic studies. Additionally, only comparisons between HAB vs. NAB/CD1 and LAB vs. NAB/CD1 are taken into account, as the manifestation of high-anxiety and low-anxiety phenotypes, via selective breeding, most likely involved different complex multigenic changes. Thus a direct comparison of HAB against LAB is inappropriate. Table 1.1 summarizes the behavioral and physiological phenotypes of HAB and LAB mice compared to NAB/CD1.

With respect to the original selection criterion (time spent on the open arm of the EPM) HAB and LAB mice have shown to display a highly robust phenotype: whereas HAB mice typically spend less that 5% on the open arm showing a clear avoidance behavior, LAB animals with >60% OAT can be described almost as 'risk-taking' (Krömer et al., 2005; Bunck et al., 2009; Erhardt et al., 2011; Avrabos et al., 2013; Yen et al., 2013; Füchsl et al., 2014). Equally, the other anxiety measures are modulated in the same directions, however, with slightly less congruence. Likewise the fear responses (freezing and odor avoidance) show a clear-cut difference between HAB and LAB (Sotnikov et al., 2011; Sartori et al., 2011a; Yen et al., 2012), where HAB animals show more pronounced reactions than LAB. Interestingly, also the autonomic responses (heart rate, heart rate variability) of HAB mice are exaggerated, indicating changes in anxiety/fear related pathways beyond mere locomotor circuits. On the contrary, the acoustic startle response is drastically increased in LAB mice whereas HAB animals show a decrease. This has been hypothesized to reflect a state of hyper-arousal in case of LAB (Yen et al., 2012; Yen et al., 2013) and a shift to a more passive coping style in HABs (Yen et al., 2012). It has to be mentioned that differences in locomotor activity can be a confounding factor in many behavioral tests. Therefore, the heightened levels of locomotion seen in LAB mice (Krömer et al., 2005; Yen et al., 2013; Yen et al., 2015) have to be critically assessed, and it is remarkable that only one study (Yen et al., 2013) so

Table 1.2 | Physiological & Behavioral Phenotypes of HAB and LAB mice

Modality	Test	Measure/Param.	HAB	LAB	References
Anxiety	EPM	time on open arm	- -	++	(Krömer et al., 2005; Bunck et al., 2009) (Erhardt et al., 2011; Avrabos et al., 2013) (Yen et al., 2013; Füchsl et al., 2014)
	EPM	open arm latency	++	•	(Krömer et al., 2005)
	DLB	time in light comp.	•	+	(Krömer et al., 2005)
	USV	no. of vocalizations	++	- -	(Krömer et al., 2005)
	IA	step-down latency	++	n.a.	(Yen et al., 2012)
Fear	TMT	odor avoidance	+	•	(Sotnikov et al., 2011)
	FC	contextual, freezing	++	- -	
	FC	cued, freezing	++	- -	(Sartori et al., 2011b; Yen et al., 2012)
	TM	FC, HR during CS	++	n.a.	(Gaburro et al., 2011)
	TM	FC, HRV during CS	-	n.a.	(Gaburro et al., 2011)
	ASR	105-115 dB	-	++	(Yen et al., 2012; Yen et al., 2013)
Locomotion	DLB	line crossings	- -	++	(Krömer et al., 2005)
	DLB	rearing	- -	++	(Krömer et al., 2005; Yen et al., 2013)
	HB	rearing	-	++	(Yen et al., 2013)
	OBS	homecage activity	•	+	(Krömer et al., 2005)
	TM	homecage activity	•	n.a.	(Gaburro et al., 2011)
	OF	distance	•	++	(Yen et al., 2013)
	OF	mobility time	- -	++	(Yen et al., 2013)
Stress Reactivity	TMT	CORT release	•	•	(Sotnikov et al., 2011)
	FST	CORT release	- -	•	(Sotnikov et al., 2014)
	DEX	CORT release	- -	•	(Sotnikov et al., 2014)
Depression	TST	immobility	•/+	- -	(Krömer et al., 2005; Bunck et al., 2009) (Yen et al., 2013)
	FST	immobility	•/++	- -	(Krömer et al., 2005; Bunck et al., 2009) (Sah et al., 2012; Sotnikov et al., 2014) (Schmuckermair et al., 2013)
	SP	sucrose intake	- -	n.a.	(Sah et al., 2012)
Addiction	CPP	cocaine-induced	+	n.a.	(Prast et al., 2014)
Spatial Navigation	WCM	relearning	•	- -	(Yen et al., 2013)
Physiology		fluid intake	n.a.	++	(Keßler et al., 2007a)
		urine osmolarity	n.a.	- -	(Keßler et al., 2007a)
	IHC	GAD65/67 in amygdala	++	n.a.	(Tasan et al., 2011)
	VSDI	LA-CEA signal prop.	++	-	(Avrabos et al., 2013)

ASR acoustic startle response, CS conditioned stimulus, CORT corticosterone, CPP conditioned place preference, DEX dexamethasone-suppression/CRH-stimulation test, DLB dark-light box, EPM elevated plus maze, FC fear conditioning, FST forced swim test, HB holeboard test, HR heart rate, HRV heart rate variability, IA inhibitory avoidance, IHC immuno-histochemistry, OBS observation or visual scoring by experienced experimenter, OF open field, SP sucrose preference test, TMT 2,5-dihydro-2,4,5-trimethylthiazoline, TM telemetry, USV ultrasonic vocalizations, VSDI voltage-sensitive dye imaging, WCM water cross-maze. - - strong decrease; - slight decrease; • no change; + slight increase; ++ strong increase; n.a. not applicable.

far reported the distance traveled by HAB, NAB and LAB on the EPM - which was surprisingly only significantly altered compared to HAB but not to NAB. Generally speaking, in emotional demanding situations, the mobility of HAB animals is decreased, likely due to their innate passive fear coping strategy, while LAB animals also show increased activity in their homecage. Other, in terms of anxiety, notable physiological alteration in HAB and LAB animals is the different information flow within the amygdalar nuclei. Avrabos et al. (2013) have demonstrated, using voltage sensitive

dye imaging in acute slice preparations, that the neuronal signal propagation from the lateral amygdala to the central amygdala is strongly increased in HAB mice. These findings might explain the shift towards more passive fear coping strategies as it has been suggested by Gozzi et al. (2010). Interestingly, the opposite observation, namely a decreased signal propagation, could be made with LAB animals. Concerning the amygdala, Tasan et al. (2011) has reported a strongly increased GAD65/67 immunoreactivity in HAB animals in glutamatergic principal neurons, which could reflect a tonic activation of the amygdalar nuclei in HAB animals. Taken together, the HAB and LAB mouse lines constitute ethological valid mouse models of anxiety-related behavior. Moreover, molecular targets of anxiety-related disorders found in psychiatric patients have been found to be equally regulated in HAB animals (Hambsch et al., 2010; Erhardt et al., 2011).

1.7 Current Methods in Neuroscience for Circuit Mapping

The intimate relationship between structure and function is a core principle in biology. It proves true for various distinct levels e.g. amino acid residues ▷ binding cavities; cell surface receptor expression ▷ neuropharmacological profile; neuronal subpopulations ▷ functional cluster; neuronal network ▷ behavior. The understanding how specific neuronal subtypes (defined by either morphology, connections, electrophysiological properties or molecular markers) give rise to networks which ultimately govern behavioral responses, is a key interest in experimental neuroscience. The techniques which allow the interrogation of neuronal networks are vast and a overview is given in figure 1.10.

Strategies to Measure Tonic Changes in Neuronal Activity

Psychiatric disorders develop over years as the brain can compensate for certain alterations. Only when the patient seeks medical attention because coping with his or her condition is not possible any longer, one may refer to this state as a psychiatric disease. Therefore, in order to elucidate altered brain activity which lasted a significant amount of an animals life span, a 'snap shot' of the entire brain activity would not be informative. In fact, to solve this issue, one needs either approaches which allow the measurement of neuronal activity over long time periods, approaches which allow to draw indirect conclusion on neuronal activity based on tonic metabolic compensatory changes or simply approaches which can integrate brain activity.

In-*vivo* Electrophysiology

Long-term in-*vivo* electrophysiological extracellular measurements in freely moving rodents have become a standard technique in experimental neuroscience. Technical advances in small animal surgical procedures, preamplifier miniaturization and wafer-based silicon electrode design rendered massively paralleled recordings with more than 512 electrodes in freely moving rodents feasible (Csicsvari et al., 2003; Berényi et al., 2014; Scholvin et al., 2016). In-*vivo* electrophysiology allows the recording of extracellular spike

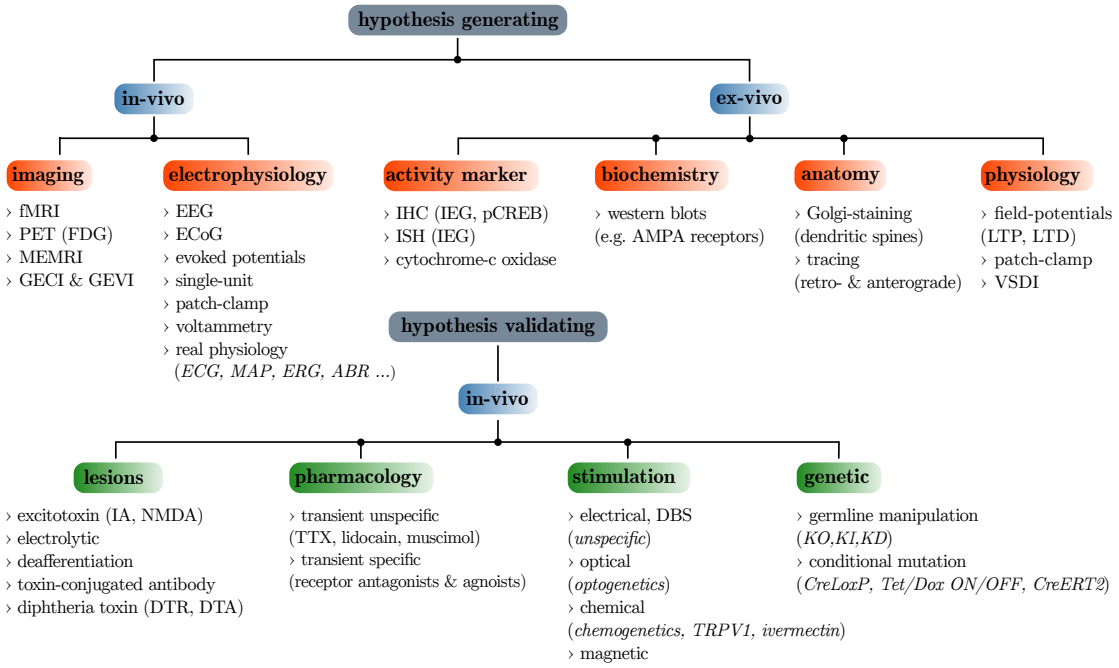

Figure 1.10 | An Experimental Neuroscientist's Toolbox

ABR auditory brainstem response; AMPA α-amino-3-hydroxy-5-methyl-4-isoxazole propionic acid; Cre **c**auses **re**combination; DBS deep brain stimulation; Dox doxycycline; DTA diphteria toxin fragment A; DTR diphteria toxin receptor; ECG elelctrocardiography; ECoG electrocorticography; EEG electroencephalography; ERG electroretinography; ERT2 tamoxifen-binding domain of the human estrogen receptor variant 2; FDG fludeoxyglucose (^{18}F; fMRI functional magnetic resonance imaging; GECI genetically encoded calcium indicators; GEVI genetically encoded voltage indicators; IEG immediate early gene (e.g. *c-fos, Zif268, ARC*); IHC immunohistochemistry; ISH in-*situ* hybridization; KD knock-down; KI knock-in; KO knock-out; loxP locus of crossover in phage P1; LTD long term depression; LTP long term potentiation; MAP mean arterial blood pressure; MEMRI manganese-enhanced MRI; NMDA *N*-methyl-D-aspartic acid; PET positron emission tomography; Tet tetracycline; TRPV1 transient receptor potential vaniloid 1; TTX tetrodotoxin; VSDI voltage sensitive dye imaging.
[Adapted from Wotjak and Pape (2013)]

waveforms at sampling frequencies of approx. 30'000 Hz per electrode and depending on the analog or digital filter settings as well as the reference electrode placement, permit conclusions not only on individual neurons (single units, 600-6'000 Hz) but also on larger clusters (local field potentials (DC-300 Hz). Usually electrophysiological experiments involve a repeated stimulus presentation, whereby unrelated neuronal activity and noise are strongly reduced. For the assessment of changes in tonic activity over long periods of time, a stimulus presentation would not make sense, as stimulus perception might change as well and the results are impossible to analyze. Moreover, for an accurate measure of firing frequency, one would need to ensure, that the signals of one recording electrode can be ascribed to a constant number of neurons. However, even with sophisticated spike-sorting techniques and electrodes in stereotrode (McNaughton et al., 1983) or tetrode (Gray et al., 1995) configuration the number and signal characteristics of neurons to be recorded of, vary over the time course of several weeks (Voigts et al., 2013).

Thus it is evident that in-*vivo* electrophysiological measurements are, despite the unsurpassed spatiotemporal resolution, not the first method of choice to investigate tonic alteration in neuronal network activity.

Cytochrome-*c*-oxidase Activity

Cytochrome-*c* oxidase (COX, ferrocytochrome c oxygen oxidoreductase, Complex IV) is a large mitochondrial transmembrane (inner mitochondrial membrane) protein and an integral part of the mammalian mitochondrial electron transport chain (figure 1.10). In short, complexes I, III and IV are proton pumping enzymes which generate the electromotive force and ultimately drive complex V (F_1F_0-ATP synthase) which synthesizes adenosine triphosphate. Complex II couples the tricarboxylic acid cycle (TCA, Krebs cycle) to the respiratory chain by catalyzing the succinate-to-fumarate conversion. Complexes I+II generate ubiquinol which is a membrane-embedded electron carrier, while complex III produces the soluble cytochrome *c*. Cytochrome *c* in turn is oxidized by complex IV to reduce molecular oxygen, which is the ultimate electron acceptor (Sazanov, 2015). As a result of this tight coupling between cellular metabolic activity and oxidative phosphorylation, it could be demonstrated that mitochondrial enzymatic activity can serve as a reliable marker for neuronal activity (Wong-Riley et al., 1978; Wong-Riley, 1979). The most metabolically demanding process in neurons, is keeping the ion balance intact. Every action potentials cause the sodium and potassium concentrations to vary, and the Na^+/K^+-ATPase uses ATP to actively remove sodium ions from the cytoplasma while pumping potassium ions inside. Neurons with tonically increased firing rates therefore have an increased mitochondrial enzymatic activity. The seminal work by Ehrlich (1885),Ver-

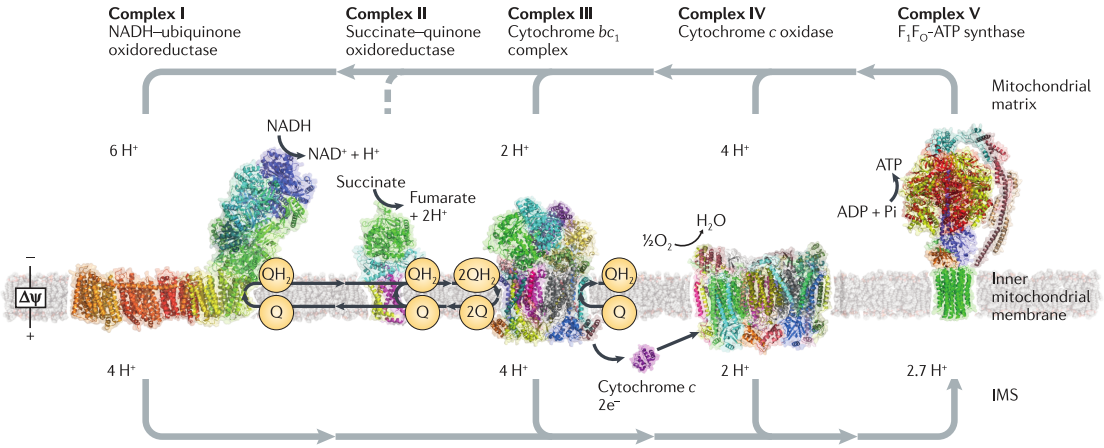

Figure 1.11 | The Electron Transport Chain
[Adapted from Sazanov (2015)]

non (1911a), Vernon (1911b), Battelli and Stern (1912) allowed the identification of tissue regions with high metabolic activity using the 'nadi' (dimethyl-*p*-phenylenediamine + α-naphtol) reagent which gets oxidized to the dark colored indophenol. Later on, Keilin and Hartree (1938) could identify cytochrome *c* oxidase as being the enzyme which catalyzes this reaction. The refinement of the enzymatic color reaction (Burstone, 1959;

Seligman et al., 1968) allowed the ultrastructural localization of COX activity using 3,3'-diaminobenzidine (DAB). However, it has to be noted that the DAB labeling can vary between different staining procedures as the incubation time of the different reagents as well as the temperature are crucial. Therefore precise COX standard series have to be incorporated in every experiment (Gonzalez-Lima and Cada, 1994; Melendez-Ferro et al., 2013). Several studies have successfully applied COX activity to asses long-lasting neuronal activity changes upon learning and memory formation (Poremba et al., 1998; Conejo et al., 2010) but also with a mouse model for post-traumatic stress disorder (Henes and Wotjak, 2009).

Manganese-enhanced Magnetic Resonance Imaging (MEMRI)

Magnetic resonance imaging (MRI) has become a pivotal method in daily clinical practice. The theoretical concepts of MRI are complex and a detailed description of the operating principle can be found elsewhere (Ridgway, 2010; Currie et al., 2013). In (simplified) brief: the MRI method makes use of the nuclear magnetic resonance phenomenon of hydrogen atoms. A hydrogen atom consists of only a single proton which in turn has an angular momentum, called *spin*. Thereby the spinning, charged particle possesses a magnetic moment and the hydrogen atom can be seen as a *bar magnet*. If tissue, which naturally contains high concentrations of hydrogen, is placed in a strong, homogeneous magnetic field B_0, the spin vectors of all protons align either parallel or anitparallel to B_0. Moreover, those spin vectors oscillate with their characteristic *Larmor* frequency (42.576 MHz/T for ^{1}H) parallel to B_0, but out-of-phase. If additionally a brief, electromagnetic radio-frequency (RF) pulse (f = resonance frequency of hydrogen = *Larmor* freq.) is applied at 90° to B_0, the spin vectors are deflected, precession is maximal and importantly the protons precede now in phase, resulting in a strong, oscillating, transverse magnetization, which can be picked up by a pair of receiver coils close to the sample. Once the RF pulse is terminated, the precession movements desynchronize quickly (transverse, T_2-relaxation) and the oscillation is dampened as the spin vector approaches the direction of B_0 again (longitudinal, T_1-relaxation). In order to gain XYZ-coordinate information, several gradient coils (for slice-, phase- and frequency-encoding gradients) are used in addition, which allow later on the demodulation and decomposition to result in a 3D reconstruction of different tissues within the sample. Tissue specific contrasts based on differences in water content or tissue specific relaxation times allow the delineation of structures deep inside the organism. Differences in relaxation times in biological tissues arise most importantly from *dipole−dipole* interactions between either protons and electrons or protons only. The stronger these interactions are, the more magnetic relaxation will be induced which ultimately leads to short relaxations times. The interaction strength is dependent on the distance between the dipoles: intramolecular (within one molecule) interactions are stronger than intermolecular (between molecules) ones. Moreover, the relative motion of the molecules with bound hydrogen is important: if the molecular movements are close to the Larmor frequency, the energy transfer between the dipoles and thus the induced relaxation is maximal. For

example in T_1-weighted MRI images (this simply means with an emphasis on T_1 contrasts) fat typically is very bright due to its short T_1-relaxation times, while water has a long T_1-relaxation time and filled cavities (e.g. bladder, ventricles) appear dark. There are only two protons in a water molecule and compared to lipids this means that most *dipole−dipole* interactions have to happen intermolecular ($\Rightarrow$ little induced relaxation). Moreover, free water has a high molecular motion, higher than the Larmor frequency ($\Rightarrow$ again little induced relaxation). Fat on the contrary has a high hydrogen content and lower molecular mobility, thus the relaxation time of fat is short. In order to increase tissue contrasts, several contrasting agents have been in use for years including gadolinium (Gd^{3+}), iron oxide (FeO) and manganese (Mn^{2+}/Mn^{3+}) (Lauterbur et al., 1978; Mendonça-Dias et al., 1983). Contrast agents for MRI studies have to interfere with the relaxation (transverse or longitudinal) times of hydrogen protons − as these are the only measures in MRI. Thus compared to e.g. X-ray or PET, the effects of MRI contrast agents can only be observed indirectly. Manganese, like gadolinium, exerts its positive contrast enhancing effects via a shorting of the T_1-relaxation time (manganese enhanced MRI = MEMRI). This is achieved via a strong electron-proton dipole−dipole interaction of the five free electrons of manganese (in high-spin state, paramagnetic) and hydrogen protons.

Manganese is an important cofactor of almost 100 known enzymes in the animal kingdom (Andreini et al., 2008) e.g. Mn-type superoxid dismutase in human mitochondria or glutamine synthetase in the mammalian brain (Wedler et al., 1982). Prolonged manganese-deficiency in rats is correlated with decreased bone mineralization and increased Ca^{2+} serum levels (Strause et al., 1986) indicating an interaction with Ca^{2+} homeostasis. Excess intake of Mn^{2+} or overexposure typically leads to severe extrapyramidal symptoms (similar to Parkinson's disease) which have been described as *manganism*. This profound neurological effect can be explained by manganese's high availability to the central nervous system and specific accumulation: substantia nigra > striatum > hippocampus > frontal cortex (Zheng et al., 1998). Manganese can enter cells and mitochondria in its bivalent or trivalent form (complexed with transferrin) via the active transporters Na^+/Ca^{2+} exchanger (Frame and Milanick, 1991), Na^+/Mg^{2+} antiporter (Günther et al., 1990) and the divalent metal transporter 1 (DMT1) (Gunshin et al., 1997; Bartelle et al., 2013), receptor mediated endocytosis (Suárez and Eriksson, 1993), voltage-gated Ca^{2+} channels (VGCC) (Kita et al., 1981; Drapeau and Nachshen, 1984; Gach et al., 1986; Narita et al., 1990; Shibuya and Douglas, 1993; Salomone et al., 1995; Simpson et al., 1995; Quattrini et al., 2001), possibly *N*-methyl-D-aspartate (NMDA) receptors (Brouillet et al., 1993) or Ca^{2+} permeable α-amino-3-hydroxy-5-methyl-4-isoxazolepropionic acid (AMPA) receptors (Savidge and Bristow, 1997). Other routes e.g. via Ca^{2+} release-activated (CRAC) Ca^{2+}-like channels (e.g. Orai-2) and certain transient receptor potential channels (TRP) (Bouron et al., 2015) are possible. Inside the cell, excess manganese has several non-specific effects simply due its close resemblance to calcium.

However, there is growing evidence that in the case of neurotoxicity, manganese might exert its adverse effects on neural cell viability by either causing mitochondrial

dysfunction via increasing oxidative stress/mitochondrial permeability transition or augmenting the autoxidation of catecholamines (*for review see* Martinez-Finley et al., 2013). Consequently, manganese serves as a MRI contrast agent which is taken up by neurons partly via activity dependent mechanisms (AMPA receptors, NMDA receptors, VGCC). Thereby, MEMRI allows the non-invasive mapping of tonic neuronal activity changes in-*vivo* in laboratory animals. It is important, however, to ensure minimal toxicity while assuring a high central loading with manganese. For mice this can be achieved by fractionated *intraperitoneal* manganese injections of 30 mg/kg over the course of 8 days every 24 hours (Grünecker et al., 2010) or continuous infusion using osmotic minipumps (Poole et al., 2017). Notably, manganese containing contrast agents for human clinical use (e.g. Teslascan®, LumenHance®) have been discontinued. Several studies up to date have beautifully applied the MEMRI technique to detect regional differences in brain activity in rats, gerbils, mice, monkeys, rabbits and song birds. Using in-*vivo* MEMRI, several groups have detected long lasting changes in neuronal activity e.g. upon induced hearing loss in mice or rats (Yu et al., 2005; Gröschel et al., 2011; Gröschel et al., 2016), in a model of epilepsy (Alvestad et al., 2007), during opiate administration and withdrawal (Sun et al., 2006), upon cocaine administration (Lu et al., 2007), upon 2,5-dimethoxy-4-iodoamphetamine (DOI) administration in a mouse model of schizophrenia (Malkova et al., 2014), in αCaMKII heterozygous knockout mice, during voluntary running (Eschenko et al., 2010), during whisker stimulation (Schroeder et al., 2016), associative taste learning (Gildish et al., 2012), in selective breeding lines for extremes in Pavlovian fear learning (McGuire et al., 2013), with repetitive transcranial magnetic stimulation (Fa et al., 2011), in alcohol-preferring rats (Dudek et al., 2016) and in spatial learning (Tang et al., 2016). However, another important characteristics of manganese (once taken up by neurons) hinders the interpretation of the aforementioned findings − anterograde axonal transport and trans-synaptic trafficking. Hans Tjälve and colleagues demonstrated that the radioactive isotope $^{54}Mn^{2+}$ is transported from the olfactory receptor neurons to the secondary olfactory neurons and accumulates in the telencephalon and diencephalon (Tjälve et al., 1995; Tjälve et al., 1996). With elegant experimental design Sloot and Gramsbergen (1994) have demonstrated that manganese is transported in neurons exclusively in an anterograde manner via microtubles. Bearer et al. (2007) has further shown that the trans-synaptic transmission of manganese is activity dependent. These findings led to the application of MEMRI for anterograde trans-synaptic tract tracing in-*vivo*, and several groups have made use of this technique. Among these, Kevin C. Chan and colleagues have studied the connections from the retina towards higher brain areas (Chan et al., 2011; Chan et al., 2012) and finally achieved the layer-specific and topographic brain mapping of retinal, callosal, cortico-subcortical, trans-synaptic and intracortical horizontal connections in the rat visual system (Chan et al., 2014). Taking the dynamics of Mn^{2+} into account, one has to consider the possibility that the activity dependent uptake of manganese, the effective axonal transport and the probably less effective synaptic release, likely leads to an increased accumulation of manganese in the projection terminals of tonically active brain regions.

Strategies to Modulate Neuronal Activity

Since Santiago Ramón y Cajal and Camillo Golgi have described the cellular fine structure of the central nervous system, the complexity of the brain, given by its hundreds of different cell types and their even more inscrutable interconnections, has become obvious. Understanding the brain circuits which lead to the emergence of specific behaviors and emotions is one of the most fundamental tasks in experimental neuroscience. But deciphering these networks is preceded by the functional inquiry of individual or groups of neurons. In order to transiently and reversibly modulate the activity of neuronal cells, several techniques have been established which differ mostly in their mode of operation, specificity, degree of invasiveness and temporal precision. In the following sections I will describe the most commonly used methods to alter neuronal activity and establish causality in behavioral experiments, while emphasizing the implementation in freely moving mice and rats.

Electrical Stimulation

The use of electrical brain stimulation originated with Luigi Galvani's discovery of bioelectricity in the 18^{th} century. Later, Fritsch and Hitzig (Fritsch and Hitzig, 1870; Fritsch and Hitzig, 2009) could show for the first time that electrical stimuli applied to the cortex could reproducibly evoke movements. The electrical stimulation of the human brain has been carried out extensively by Penfield and Boldrey (1937), who have established the somatotopic organization of the cortex. The seminal work of Hess and Brügger (1943), Hunsperger (1956) and Fernandez de Molina and Hunsperger (1959) demonstrated the applicability of electrical microstimulation to change behavior and emotion in cats and rhesus monkeys, and Delgado (1977) ultimately treated patients with neurological disorders (*for review see* Zago et al., 2008; Clark et al., 2011). Electrical microstimulation finally found its way into daily clinical practice as deep brain stimulation (DBS) within the subthalamic nucleus in the treatment of advanced Parkinson's disease (Limousin et al., 1998). The application of deep brain stimulation (DBS) has been expanded since then to the treatment of depression (Mayberg et al., 2005), intractable cluster headache (Leone et al., 2004) and obsessive-compulsive disorder (Nuttin et al., 2003). Electrical microstimulation is usually carried out with implanted and often multipolar metal electrodes. It is important that those electrodes have a good high frequency response and can not be polarized. Therefore, stainless steel, tungsten, gold or platinum are the most often applied materials. The stimulating effect is elicited by passing anodal or cathodal current through the electrodes, in the range of 0.1-100 μA with pulse widths of 50-200 μs and frequencies ranging from 20 Hz to 500 Hz, which are delivered in trains of 1-5 seconds in length (Perlmutter and Mink, 2006). The electrical field displaces charged ions (Na^+, K^+, Cl^- and Ca^{2+}), leading to changes in the local extracellular and intracellular (e.g. axon plasma) ion concentration and thereby is changing the membrane potential which ultimately might trigger an action potential. With low frequencies and large currents the neurons follow the stimulation pattern and this setting has been traditionally used to e.g. activate the medial forebrain bundle

(Zacharko et al., 1983) or to activate brain regions in general (Hess and Brügger, 1943; Hunsperger, 1956; Fernandez de Molina and Hunsperger, 1959; Milad et al., 2004; Vidal-Gonzalez et al., 2006). In contrast to this rather direct way of stimulation, stands the classical DBS approach, where high frequency and low current is used to activate but also inhibit neurons or even disrupt (Chiken and Nambu, 2016) information flow. The stimulation settings for DBS are tailored to the patient (e.g. severity of disease) and the specific brain region and most importantly to alleviate the symptoms most effectively (e.g. tremor). Thereby, the directly imposed effects are less understood. Moreover, all extracellular electrical stimulation techniques have in common that it is impossible to ascribe the behavioral or therapeutic effect to the nearby cell bodies (neural or glial) only, as fibers *en passage* are stimulated to the same extent. Neither a cell-type specificity can be achieved which is the reason why electrical microstimulation in experimental neurosciences is less important nowadays. However, in thalamocortical pathways where neuronal firing rates are extremely high and intraburst firing frequencies up to 400-1000 Hz (Llinás and Steriade, 2006) can be seen, electrical microstimulation is the only technique which can mimic these ultrafast dynamics. For example in a mouse model of acute fear and fear extinction, DBS within the mediodorsal thalamic nucleus has been shown to either decrease (DBS at 100 Hz) or increase conditioned fear responses (DBS at 416 Hz) which was ascribed to the differences in thalamocortical coupling (Lee et al., 2011).

Chemical & Pharmacological Manipulation

While the use of pharmacological or dietary means to alter the state of mind in order to alleviate pain was known since antiquity (Chivukula et al., 2014), the use of chemicals to intentionally alter neuronal activity is an invention of the 20^{th} century. The discovery of chemical synaptic transmission by Otto Loewi at Easter Monday in the year 1920 (Koelle, 1986) through the identification of acetylcholine (*Vagusstoff*) paved the way for the pharmacological modulation of neural activity. Without knowing the synaptic mechanisms Hans Adolf Krebs noted that *brain and retina have an increased respiration in the presence of glutamic acid* (Krebs, 1935). Takashi Hayashi based his work on the results of de Barenne (1933) and discovered the convulsive effects of various chemicals and neurotoxins, including glutamate, by intracerebral microinjections in dogs, monkeys and also humans (Hayashi, 1954). These discoveries led to the development of chemostimulation which one of the most important techniques to transiently modulate neuronal activity in target brain areas and ultimately modulate behavior (Miller, 1965). The brain area of interest is typically targeted with guide cannulae with outer diameters of 460 μm, which end several hundred microns above the area of interest, in order to avoid mechanically damaging the target area. Clogging of the guide cannula is avoided by the use of 'dummy cannulae'. Prior to the e.g. behavioral experiment the dummy is removed and a 33 gauge injection cannula targeting the exact brain area of interest is inserted trough the guide. Infusion of 50-500 nl per injection site at injection speeds of 50-100 nl/min is carried out using precision micropumps while the animals are anesthetized. One major drawback of this technique is the fact that every injected

substance will diffuse differently according to its lipophilicity and size. A simple mixture of a dye and the substance for post-mortem histological analysis, therefore can only result in a very rough estimate of the affected brain region. Moreover, the temporal precision of intracerebral injections is within the range of seconds to hours depending on receptor affinity and clearing mechanisms and thus only rather long lasting changes in brain activity can be assessed. However, the intracerebral injection of neurotransmitters and analogs (e.g. NMDA) can readily distinguish between pre- and postsynaptic effects if the receptor expression profiles are known allowing even rudimental cell-type specific manipulations.

Genetic Interference

With the advances in murine genome modification (Capecchi, 1989), the full sequencing of the mouse genome (Chinwalla et al., 2002) and projects like the Allen Brain Atlas (Lein et al., 2007), thousands of differentially or region-specific expressed genes within the mouse brain were identified. These developments fostered the generation of thousands of transgenic mouse lines which paved the way for cell type- and region-specific control of gene-expression. The most popular expression system for this purpose is certainly the 'Cre-*loxP*' system (Sauer and Henderson, 1988; Tsien et al., 1996). In this system a cell type-, region- or tissue-specific promoter is controlling the expression of the Cre recombinase (Cre = causes recombination). The enzyme Cre is a 38-kDa protein, naturally encoded by the bacteriophage P1, which allows the site-specific recombination at 34-bp *loxP* sites. Cre can excise pieces of DNA which are flanked by *loxP* (lox = locus of crossover) sites ('floxed') allowing an e.g. cell type restricted knockout or, if the 'floxed' site encloses a STOP codon before an exogenous transgene, a cell-type specific rescue. Alternatively, a viral mediated gene transfer of so called 'double-floxed' inverted open reading frame (DIO) sequences can be employed. Here, the exogenous transgene is flanked by two different pairs of flox-sites, and following Cre excision it will be inverted and recombines again, which permits expression (Cre-dependent viral vector).
Two examples of cell-type specific knock-out animals are (1) the $CB1^{f/f;NEX\text{-}Cre}$ also called Glu-$CB1^{-/-}$ or less frequent NEX-CB1 and (2) the $CB1^{f/f;Dlx5/6\text{-}Cre}$ also called GABA-$CB1^{-/-}$ or less frequent DLX-CB1 (Monory et al., 2006). On the one hand, Glu-$CB1^{-/-}$ mice lack the cannabinoid receptor type 1 (CB1) on specific glutamatergic neurons (*see below*) and originated from a crossbreed of $CB1^{f/f}$ animals, where the gene encoding for CB1 is flanked with flox-sites, and Nex-Cre animals (Goebbels et al., 2006). The latter express Cre in place (knock-in gene replacement) of the developmental cortical glutamatergic forebrain neuron marker *Nex* (Schwab et al., 2000). On the other hand, GABA-$CB1^{-/-}$ mice lack the CB1 receptor on a subset of GABAergic neurons (*see below*) and were generated via a crossbreed of the already mentioned $CB1^{f/f}$ mouse line and the Dlx5/6-Cre mouse line (Monory et al., 2006). The latter expresses Cre recombinase under control of the I56i and I56ii intergenic enhancer sequences of the murine *Dlx5/Dlx6* genes (Zerucha et al., 2000), and ultimately results in Cre expression in GABAergic forebrain neurons.

But these techniques do not allow any temporal control of expression. With the introduction of the mutated ligand binding domain of the human estrogen receptor (ER), Cre can be rendered being inducible (Cre-ER^{T2}) via systemic administration of tamoxifen (Metzger and Chambon, 2001) or local infusion of endoxifen (Benedykcinska et al., 2016). Using these approaches various genes which directly modify the excitability of the target network can be expressed or deleted. For example the deletion of NR1 subunit of the NMDA receptor in parvalbumin positive neurons decreases gamma-oscillations and inhibits fear learning in mice (Carlé N et al., 2011). Minett et al. (2014) conditionally deleted $Na_V1.7$ sodium channels in a mouse model of chronic neuropathic pain and rendered the animals hypoaesthesic. Silencing synaptic transmission in a specific neuronal subpopulation can be achieved by using Cre-dependent expression of the tetanus light chain molecule which cleaves synaptobrevin (Lee et al., 2015). Cre recombinase expression can also be achieved by using adeno-associated viruses (AAV), whereby no or only a very limited range of cell-type specificity is possible due to AAV's small packaging capacity. However, the mere genetic modification of neuronal activity using Cre recombinase is permanent and a reversible modification would be desirable. Another system which has no cell type specificity per se, but good temporal control and reversibility is the tetracycline-regulated expression system (Gossen and Bujard, 1992). Here the exogenous transgene is under the control of the tetracycline response element. In a *tet-OFF* system the tetracycline transactivator (tTA) can only bind and activate the TRE (tetracycline responsive element) if tetracycline or doxycycline is absent. In *tet-ON* systems the reverse tetracycline transactivator (rtTA) activates and binds TRE in the presence of the antibiotic. Various ways of controlling neuronal excitability have been established which utilize the tet-system e.g. hyperpolarizing neurons via the overexpression of the inwardly rectifying potassium channel $K_{ir}2.1$ (Yu et al., 2004). A combination of Cre and tet systems is a powerful approach to transiently alter gene expression (Lee et al., 1999; Shimizu et al., 2000). Besides those methods mentioned above there are other novel approaches like the remote and reversible inhibition of neurons by regulated stabilization of otherwise actively destabilized $K_{ir}2.1$ channels (Auffenberg et al., 2016).

Pharmacogenetic Manipulation

An improvement of the genetic approaches to alter neuronal excitability are chemo- or pharmacogenetic techniques. Broadly speaking, pharmacogenetic strategies utilize the sole and exclusive activation of mostly engineered receptors by artificial ligands. Here I will focus mainly on designer receptors which are exclusively activated by designer drugs (DREADDs) (*for review see* Sternson and Roth, 2014; Urban and Roth, 2015; Roth, 2016). The DREADD system is comprised of designer receptors which evolved via directed molecular evolution from human muscarinic acetylcholine receptors in a way that they possess highest affinity towards the otherwise pharmacologically inert (Weiner et al., 2004) molecule clozapine-*N*-oxide (CNO), insensitivity to acetylcholine, and low constitutive activity. So far two main designer receptor types have been most commonly

used: the stimulating hM3Dq which is based on the human G_q-protein-coupled M_3 receptor, and the inhibiting hM4Di based on the G_i-protein-coupled human M_4 receptor. Binding of CNO to hM3Dq leads to the activation of the G_q alpha-subunit which ultimately affects the membrane potential of neurons via the phospholipase C (PLC) pathway. In brief: the activation of membrane-bound PLC leads to the hydrolysis of the lipid precursor phosphatidylinositol 4,5-bisphosphate (PIP_2), the membrane-bound diacylglycerol (DAG) and the small and mobile inositol 1,4,5-triphosphate (IP_3). IP_3 rapidly diffuses through the cytosol and when it reaches the endoplasmatic reticulum it activates the *IP_3*-gated Ca^{2+}-release channels, which in turn lead to a fast release of calcium from the ER into the cell lumen. This calcium spike leads to store-operated calcium entry via Ca^{2+}-release activated Ca^{2+} channels. Besides depolarizing the cell, the increased calcium levels (already by IP_3-receptor activation) allow the protein kinase C (PKC, calcium-dependent) to translocate from the cytosol to the plasma membrane where PKC gets further activated by DAG. Once activated PKC phosphorylates several downstream targets e.g. ERK1/2 (extracellular signal-regulated kinase), ROCK (Rho-associated protein kinase) and CaMKII (Ca^{2+}/calmodulin-dependent protein kinase II) (Berridge, 1993; Berridge, 1998). Besides the rather subtle depolarization due to Ca^{2+} from the stores, the expression of hM3Dq at presynaptic sites offers an alternative mechanism of neuronal activation: presynaptic modulation of neurotransmitter release can occur via protein kinase C-mediated phosphorylation of proteins of the exocytotic release machinery directly (Boehm and Kubista, 2002; Kubista and Boehm, 2006), but also via the aforementioned CaMKII activation as it was shown that this kinase phosphorylates syntaxin, VAMP (vesicle-associated membrane protein), SNAP-25 (synaptosomal-associated protein 25) and synaptotagmin (Hirling and Scheller, 1996) which ultimately increases the neurotransmitter release probability. In addition specific isoforms of PKC can directly phosphorylate presynaptic *N*-type calcium channels whereby the calcium current is increased (*for review see* Tedford and Zamponi, 2006). Moreover, it is likely that IP_3-receptor mediated calcium release from stores can directly increase neurotransmitter release. Thus the activation of hM3Dq leads to an increased neurotransmitter release of neurons, which is sufficient to alter behavior in-*vivo* (e.g. Krashes et al., 2011; Cai et al., 2014; Betley et al., 2015; Urban et al., 2016). Alexander et al. (2009) has shown that the PLC inhibitor (U73122) completely abolishes the CNO-induced neurophysiological effects.

Binding of CNO to hM4Di leads to several distinct mechanisms by which the output or postsynaptic plasticity (e.g. in response to learning) of the targeted neuron is diminished: (a) $G_{\beta/\gamma}$ mediated activation of the G-protein coupled inwardly-rectifying potassium channel and subsequent hyperpolarization (Armbruster et al., 2007), (b) presynaptic inhibition of neurotransmitter release via a direct interaction of $G_{\beta/\gamma}$ and the high voltage-activated (HVA) N- and P/Q-type Ca^{2+} channels (McKinney et al., 1993; Levey et al., 1995; Schneider et al., 1997; Dolezal and Tucek, 1998; Tedford and Zamponi, 2006; Brown and Sihra, 2008; Zamponi and Currie, 2013) and (c) the $G_{\alpha i}$ mediated inhibition of adenylyl cyclase (Sadana and Dessauer, 2009). Several studies to date have demonstrated the inhibition of neuronal firing, altered behavioral responses as well

as hippocampal remapping upon the activation of hM4Di in-*vivo* (Sasaki et al., 2011; Zhu et al., 2014; Miao et al., 2015). Typically CNO is dissolved in DMSO and stored in stocks (75-100 mM) at -20°; doses of 0.5-6 mg/kg have been effective if applied 45 minutes (i.p.) prior to the experiment. Alternative approaches are the local application via guide cannulas 5-30 minutes before the experiment (Silva et al., 2016; Franklin et al., 2017) or the chronic application via osmotic minipumps (Whissell et al., 2016).

Despite the convincing results obtained with DREADDs in the field of behavioral experimental neuroscience, there have been also critical reports which note the back-metabolism of clozapine-*N*-oxide to the antiypsychotic clozapine (Jann et al., 1994; Chang et al., 1998; Loffler et al., 2012), demonstrate ligand-independent functional changes in neurons simply due to DREADD expression (Saloman et al., 2016), or question the activity and blood-brain permeability of CNO entirely (Gomez et al., 2017). Therefore, the incorporation of CNO-treated controls in every DREADD experiment is critical. Moreover, as mentioned above, the mechanisms by which DREADDs exert their either activating or inhibiting modulation upon neuronal output is governed by complex intracellular signaling cascades. Within local polysynaptic circuits (e.g. the Schaffer collaterals) when the expression of DREADDs is not limited to one population of neurons, the effect of their activation is difficult to assess beforehand and might even lead to effects opposite to what has been expected. This has been recently described by López et al. (2016).

Optical Manipulation

The use of light pulses to precisely manipulate neuronal activity is an invention of the early 1970's, when Fork (1971) applied 488 nm laser pulses to reversibly activate *Aplysia californica* abdominal neurons. The further advancement of this technique led to the development of infrared neural stimulation (*for review see* Thompson et al., 2014). Another more popular mechanism to optically alter neuronal activity is light-dependent release of *caged* glutamate (Lester and Nerbonne, 1982) with high temporal fidelity in the millisecond time scale and micrometer spatial resolution (*for review see* Callaway and Yuste, 2002). With the establishment of viral vector mediated gene-transfer, modifications to the e.g. ion channel repertoire of the neurons in questions in-*vivo* became feasible. This sparked the invention of several 'light switches' of neuronal excitability like engineered photoswitchable K^+ channels (Banghart et al., 2004) or opsin/rhodopsin based approaches (Zemelman et al., 2002; Zemelman et al., 2003). The ectopic expression of microbial rhodopsins − coined *optogenetics* − has become the 'gold standard' technique for remote and reversible control of neuronal excitability (Boyden et al., 2005; Li et al., 2005; Nagel et al., 2005; Ishizuka et al., 2006; Bi et al., 2006) (*for review see* Boyden, 2011; Deisseroth, 2015). In the meanwhile the standard optogenetic actuator repertoire comprises more than 10 different opsins: channelrhodopsin-2 ChR2/H134R (Nagel et al., 2005), ChETA ChR2/E123T (Gunaydin et al., 2010), VChR1 (Zhang et al., 2008), C1V1 (Yizhar et al., 2011), stabilized step-function opsin C128S/D156A (Yizhar et al., 2011),

halorhodopsin eNpHR3.0 (Gradinaru et al., 2010), archaerhodopsin (Chow et al., 2010; Han et al., 2011), Chronos & Chrimson (Klapoetke et al., 2014) and Jaws (Chuong et al., 2014). In the following I will only focus on channelrhodopsin. Channelrhodopsin-2 (ChR2) is a directly light-gated cation-selective membrane channel found in the green algae *Chlamydomonas reinhardtii*. It is comprised of the microbial opsin channelopsin-2 *Chop2* and the covalently linked *all-trans* retinal (Nagel et al., 2002; Nagel et al., 2003). The wavelength which yields maximal photocurrents is at $\approx$ 460 nm. Once light has activated ChR2, mainly Na^+ and K^+ ions can pass the membrane along their concentration gradient, leading to a depolarization of the target cell. The resulting photocurrent and ultimately the effectiveness of the activating opsin in evoking action potentials if expressed in excitable cells, is largely dependent on the kinetics of the opsin. Slow kinetics allow more channelrhodopsins to get activated by the same photon flux. For example for ChR2 ($\tau_{\text{off}} = 18$ ms Fenno et al., 2011) a photocurrent saturation light intensity of $\approx$ 10 mW/mm^2 was reported (Lin et al., 2009), while for the stabilized step function opsin (SSFO) C128S/D156A ($\tau_{\text{off}} = 29$ min, Fenno et al., 2011) light intensities less than 100 μW/mm^2 are sufficient to evoke action potentials reliably. An advantage but also a drawback of ChR2 is its high photocurrent. Overactivation of neurons depolarizes them very strongly almost immediately. If in addition the stimulation frequency is set >30 Hz and the neurons do not receive strong inhibitory GABAergic projections (Dine et al., 2016), the stimulated neuron likely undergoes a 'depolarization block'. This means that the necessary hyperpolarization for the voltage-gated sodium channel to become de-inactivated, fails to appear and no further action potentials occur, despite the cell being depolarized. The delivery of light into the brain of freely moving small animals (mouse, rats) requires special equipment like fiber light guides (multimode optical silica fiber) and implanted fiber stubs (ø200 μm) or guide cannulas which target the brain region of interest. The incoupling of light into such fibers leads to coupling efficacies of <0.05 % if incoherent light sources like LEDs and mercury arc lamps are used, but reaches >90 % if one uses coherent light sources like diode pumped solid state lasers (DPSS). The fibers used for optogenetics typically have a numerical aperture >0.22NA and most commonly 0.39NA. This yields acceptance/emission angles of ≈25 - 45° (Aravanis et al., 2007), which means that the light is conically spread. The fact that the light intensity within the brain decays rapidly due to scattering and absorption strongly limits the effective area one can manipulate with optogenetics − taken heat production into account. Therefore, algorithms which model the three-dimensional heat production inside neural tissue, dependent on stimulus intensity and stimulation frequency have been developed (Stujenske et al., 2015) which greatly ease the setting of the appropriate stimulation parameters. However, it has to be mentioned, that with optogenetic stimulation one entrains an entire neuronal population and synchronizes their firing rhythms (with exception of SSFOs). This is a highly unnatural situation and can lead to seizure-like activity with unpredictable outcome. Therefore, it is necessary to combine optogenetic stimulation with electrophysiological recordings to determine the physiological firing frequencies of the neurons in question before an artificially activation is attempted and to monitor the neuronal activity during stimulation.

1.8 Aims of the Study

In contrast to panic research, preclinical fear & anxiety studies focuses mainly on prefrontal cortical as well as amygdalar circuits. This is owed to the fact that the extremely popular auditory fear conditioning paradigm led to the generation of a plethora of knowledge how conditioned fear memories are acquired, consolidated, extinguished and re-consolidated. As one of the key symptoms of anxiety disorders being ruminating thoughts about potentially fearful but distant events, the higher brain areas are certainly important structures in the generation of general anxiety. But it has to be noted that midbrain structures like the PAG and the SC have instructive roles in the generation of fear. These midbrain but also medullary structures further function as a first-line interface between the sensory (auditory, visual, tactile) or viscero-sensory (heart rate, blood-pressure, energy metabolism etc.) systems and the higher brain areas. Moreover, they even are able to generate low-latency physiological and behavioral responses which bypass the immediate conscious awareness about those processes. The strong ascending afferents from lower brain areas towards thalamic nuclei but also the amygdala, suggest that those higher *fear centers* depend to a certain degree on these ancient emotion centers. Therefore, the involvement of midbrain areas in the generation of fear & anxiety disorders via e.g. decreased thresholds to respond to threatening stimuli, is easy to imagine, and a similar role might be attributed to them in the context of somatic symptom disorders.

The aim of this study was to **establish a causal link between the anxiety-like phenotypes of two mouse-lines which have been selectively bred for extremes in trait anxiety (HAB and LAB mice) and their respective midbrain (PAG and SC) neuronal activity**. Hereby, it became evident that standard behavioral testing paradigms for fear & anxiety responses are insufficient to probe the involvement of brainstem areas (e.g. high controllability), while other paradigms which do so, have to be considered unethical (e.g. life predator exposure). In order to assess species-specific fear responses, it is pivotal to consider the animals sensory capabilities, its habitat and its natural predators. Therefore, one part of this thesis was the **development of novel ethologically inspired testing paradigms** (Robocat, IndyMaze) for the study of fear in mice.

The conclusive implementation of these experiments demanded the assessment of the animals' visual capabilities and thus the optomotor response and flash-evoked electroretinograms were conducted in addition. Initially, we aimed to assess the visual function using home-cage activity monitoring in combination with shifting the light-cycle. The rationale was that visually impaired animals might exhibit deficits in photoentrainment. Therefore, this thesis also includes the **design, construction and validation of a simplified microwave-based motion detector** for home cage activity monitoring in mice. In search for appropriate testing paradigms to repeatedly assess fear responses, while conducting in-*vivo* electrophysiological recordings, another procedure – the **Moving Wall Box task – was developed** which could be validated using conditional cannabinoid receptor type 1 knock-out animals. Beyond the frame of this thesis stands

my keen interest to understand the neuronal circuits which mediate the physiological and behavioral aspects of negative affect. This attempt, however, can only be satisfyingly tackled with the use of combined in-*vivo* optogenetic manipulation and electrophysiological recordings. Therefore, this thesis further contains the **design, construction and validation of a low-cost motorized combined electrical and fiber-optic rotary joint for physiological recordings**.

This page intentionally left blank.

Yea, though I walk through the Gey Tzalmavet, I will fear no rah; for Thou art with me; Thy shevet and Thy staff they comfort me.

Tehillim 23:4 (OJB)

Chapter 2

Material and Methods

2.1 Animals

In this thesis (including manuscripts found in the appendix) adult (3-8 months), male mice of the following strains have been used: Glu-CB1$^{-/-}$)(N=9), GABA-CB1$^{-/-}$)(N=9), Glu-CB1$^{+/+}$(N=9), GABA-CB1$^{+/+}$(N=10), C57BL/6N (N=22), NEX-ChR2 (N=1), HAB (N=111), NAB (N=108), LAB (N=110), CD1 (N=16), resulting in a total number of 405 animals.

All animals were bred in the animal facilities of the Max Planck Institute of Biochemistry, Martinsried, Germany. The animals were group-housed (2-4 animals per cage) under standard housing conditions: 12h/12h inverted light-dark cycle (light off at 8 AM), temperature 24°C, food and water *ad libitum*.

Experimental procedures were approved (55.2-1-54-2531: 44-09, 188-12, 142-12, 133-06, 08-16) by the State of Bavaria (Regierung von Oberbayern, Munich, Germany). Animal husbandry and experiments were performed in strict compliance with the European Economic Community (EEC) recommendations for the care and use of laboratory animals (2010/63/EU).

2.2 Drugs

The anxiolytic diazepam (Diazepam-Lipuro®, Braun Melsungen, Germany) was dissolved in physiological saline (vehicle) and injected systemically (1 mg/kg, i.p.) using a volume of 100 μl per 10 g body weight. Muscimol MUSC (Sigma-Aldrich, #M1523) and fluorescently-labeled muscimol (fMUSC) (Bodipy®TMR-X conj. Thermo Fisher Sc. M23400) was dissolved in artificial cerebrospinal fluid (aCSF) (Baarendse et al., 2008). MUSC itself has a molecular weight of 114.1 g/mol whereas the fMUSC (MW 607.46 g/mol) is 5.324× heavier. In previous experiments with MUSC, we found a concentration of 10 ng/100 nl (876.4 μM) most effective, therefore we have used 53.24 ng/100 nl fMUSC to achieve the same physiological effect. As the fMUSC is poorly water-soluble, we dissolved 1 mg in 1.878 ml aCSF to reach a final ready to use concentration of 876.6 μM. Whereas the EPM experiments where conducted using MUSC, the vocalization experiments only involved fMUSC. The vocalization experiment was carried out using a

crossover design: half of the animals received fMUSC on the first day, whereas the other half received VHC (aCSF). On the next day the treatment was switched. 1-3h after the experiment the animals which received fMUSC were transcardially perfused (4 % PFA), whereas the remaining animals received another injection of fMUSC on the following day and were also perfused 1-3h after the injection.

2.3 Behavioral Tests

2.3.1 Elevated Plus Maze

The elevated plus maze (EPM) apparatus consisted of two open (L30×W5 cm) and two closed (L30×W5×H15 cm) arms which were connected via a central platform (L5×W5 cm). All parts of the EPM were made of dark gray PVC. The apparatus was elevated 37 cm above a table (H50 cm), which was placed in the center of the dim illuminated experimental room. The light intensity (luminous flux) at the open arms was 7 lux. Before the experiment every subject was tested for the disposition to emit sonic vocalizations by lifting them 3 times from the grid cage top (Whitney, 1970). At the beginning of each trial, the animal was placed near the central platform facing a closed arm. Each trial lasted for 30 minutes and was video tapped. The animals behavior was analyzed using a behavioral tracking software (ANY-maze, Stoelting CO., USA) and the percentage of time spent on the open (OA) and closed (CA) arm and the central zone (time in center) as well as the total distance traveled were determined. In order to render these results comparable to other EPM experiments found in the literature, the data (except latency) of the first 5 minutes of each trials is reported. Other behavioral parameters which were analyzed by an experienced observer, blind to the experimental conditions, included number and duration of stretched-attend postures (SAP) within the first 15 minutes of each trial, and the latency for the first full entry to the open arm (all four paws) within the entire 30 minutes exposure. After the trial the fecal boli on the EPM apparatus were counted. In between the trials the apparatus was cleaned with tap water containing detergent, and was subsequently dried with tissues.

2.3.2 Robocat Task

The Robocat is a four-wheeled robot (Lego Mindstorms), equipped with ultrasound range finders and programmed to advance for 25 cm (speed 25 cm/s) once a movement has been detected within the sensor range of 50 cm. Despite the name suggests, no extra effort has been invested to disguise the robot as a cat, except two little cardboard ears. The task is conducted within a longitudinal arena (H35×W50×L150 cm, whereby the robot is placed 125 cm away from the start compartment (H35×W50×L12.5). The access to the arena is provided via a sliding door, operated by the experimenter, and the natural exploratory drive (neither bait, nor food or water deprivation used) ultimately leads to the mouse-robot encounter. Once the mouse triggers the robot, its movements typically evoke a robust flight response and the mouse retrieves to the start compartment. All animals were first pre-exposed to the entire setup with unrestricted

access to the arena (sliding door opened). On the following consecutive 3 days each animal was subjected to habituation trials which consisted of 10 minutes acclimatization within the start compartment and 10 minutes of free exploration in the arena. The test trial on day 4 was conducted in identical manner, except that the Robocat was placed in the arena. During the test trial, the animals typically activated the Robocat several times. All trials were video taped and the behavior was analyzed offline by an experienced observer, blind to the experimental conditions. The behavioral readouts were flight (activation + retrieval), bypass (activation but tolerance to the approaching Robocat) or collision, and were counted if observed at least once. Only animals which activated the Robocat at least once were considered for analysis.

2.3.3 IndyMaze Task

The IndyMaze (*see* Mouse Anxiety Fear Inhibitory Avoidance Task MAFIA, Scheithauer, 2016) is conducted within a longitudinal arena (H35×W16×L150 cm), which is divided into six equidistant (25 cm) sectors. To one end of the arena, a small custom-made microdialysis cage (H30×W16×L25 cm), equipped with bedding material, is connected to serve as a home compartment. The arena itself is slightly tilted towards the home compartment. For the task, each animal is first placed into the home compartment and has a maximum of 30 minutes to step (with four paws) into the arena (latency 1st entrance). Once the animal entered the arena, the time to reach the last sector is taken (latency for end-exploration). After the end exploration, the animals typically retrieve to the home compartment or are gently forced by the experimenter. With low latency the animals re-enter the arena but this time a styrofoam ball (Ø15cm , 100 g) is introduced at the last sector, which is allowed to roll (25 cm/s) towards the animal once it passed the midline (75 cm). The animals can either respond with (a) a preemptive flight response or a retrieval once the ball has hit them (both counted as fear responses), or (b) they are overrun by the ball and continue to explore the arena. The threat exposure part of the behavioral paradigm is carried out for a maximal duration of 30 minutes or once the animals has encountered the ball three times. The behavior is scored online by the experimenter during the task.

2.3.4 Optomotor Response

In order to assess the visual performance of male C57BL/6N, CD1, HAB, NAB and LAB mice (N=12), the animals' optomotor response (Abdeljalil et al., 2005) has been tested using the rotating drum task. The task is based on the mouses' predisposition to fixate on moving vertical black/white stripes and follow their rotation with short movement bouts, involving the entire head. By decreasing the stripe width, higher visual acuity is necessary to resolve the stripes. The apparatus consisted of a rotating cylinder (drum, Ø33 cm, height 35 cm), whose inner walls were lined with an alternating black/white stripe pattern using a stripe width of 2.88 cm, giving a spatial frequency of 0.05 cycles per degree (cyc/deg, r=16.5 cm, arc length per black/white cycle 5.76, angle 20°). During the task, the animals were placed within the center of the drum

on a Ø11.5 cm fan grid which was mounted 16 cm above the bottom. The rotation of the drum was controlled via a custom-built microprocessor-based motor driving circuit which operated a geared motor. The rotational speed of the drum was set to 2.5 rounds per minute (rpm). For the task the animals were placed into the drum for 1 minute to acclimatize (bright illumination 500 lux) and subsequently the drum started to rotate for 60 seconds clockwise, followed by a 30 seconds break and than rotated in counter-clockwise direction for additional 60 seconds. Than, the background illumination was decreased to 3 lux and the cycle started from the beginning. All experiments were videotaped and analyzed offline (if possible blind to the strains, CD1, HAB, NAB, LAB), whereas every head movement was scored as an optomotor response if it was directed into the same rotational direction as the drum. This modified version of the original task (Abdeljalil et al., 2005) does certainly not allow to make detailed statements regarding different levels of visual acuity, especially under varying light conditions (insufficient time for dark-adaptation), though it is sufficient to asses the general visual performance of the mouse strains in question.

2.4 Physiological Measurements

2.4.1 Electroretinography

In order to asses the retinal function of male C57BL/6N, CD1, HAB, NAB and LAB animals (N=6), flash-evoked electroretinographic (fERG) measures in the anesthetized animals have been employed. Therefore the animals were dark-adapted for $>$ 3 h prior to the experiment. Under dim red light (650 nm) illumination, the animals were weighed and received analgesic treatment (200 mg/kg Novalgin/Metamizol s.c. in saline in a concentration to obtain 100 μl/10 g of body weight) and subsequently transferred from their home-cage to the anesthesia chamber (isoflurane 4 %). After reaching surgical tolerance, indicated by the absence of the eye-lid and paw-withdrawal reflex, the animals were transferred to a modified stereotaxic frame were the anesthesia was maintained with isoflurane (2-3 % in oxygenated air, using an oxygen concentrator, EverFlo). The body temperature was monitored and controlled (37.5°C) using an animal temperature controller (WPI Inc. #ATC2000) in combination with a small rodent rectal temperature probe (WPI Inc. #RET-3) and a small heating-pad (15×10 cm) with built-in RTD sensor (WPI Inc. #61830) with an additional silicone pad to ensure maximal heat transfer (WPI Inc. #503573). For the analgesic treatment to have an effect, the animals was allowed to reach a stable anesthesia for >15 min, while the eyes were kept moisturized with 0.9 % (w/v) physiological sodium chloride solution (saline). Subsequently the pupils were dilated maximally using 2.5 % phenylephrine (Sigma #P6126, in PBS, pH adjusted to 7.0) and 1 % (w/v) atropine (Sigma # A0132, in PBS, pH adjusted to 7.0) and the eyes were henceforward kept moisturized using 1 % methyl cellulose (Carl Roth #8421) in saline. The ERG electrodes were custom made using Ø200 μm uncoated gold wire wound to form Ø3 mm loops and were placed gently on the eyes of the animal. A stainless steel wire wrapped around the animals tail served as the ground electrode. All

signals were bandpass filtered at 0.1-300 Hz and sampled at 30 kHz using the Open-Ephys (Siegle et al., 2017) system in conjunction with a headstage based on the Intan RHD2132 integrated extracellular amplifier circuit. The animals left eye was covered with a piece of lightproof black PVC and additionally shielded from the right side using aluminum foil. The animals right side was stimulated using a Ping-Pong ball which was cut in half (Green et al., 1997) and illuminated with a white LED (Osram Oslon LUW CN7N) which was controlled via a custom-made constant current source. Thereby scotopic and photopic (3 lux background illumination) measurements were carried out which involved the display of 32 light flashes (per condition) of 40-180 μs length at a frequency of 1 Hz at three different light intensities. The light intensities were measured (65 lux, 225 lux, 420 lux) using a hand-held lux meter (Iso-Tech ILM 1335) and the respective log $\Phi{\cdot}\text{rod}^{-1}{\cdot}\text{s}^{-1}$ values were calculated using the following relation:

1 photopic lux = 650 photoisomerizations $(\Phi){\cdot}\text{rod}^{-1}{\cdot}\text{s}^{-1}$ (Pugh et al., 1998).

All 32 acquired responses per condition were averaged and the datasets were further analyzed using custom Python2.7 scripts.

2.4.2 Acoustic Measurements & Analysis

During the normal animal care taking procedures, it was realized that HAB mice have a strong disposition to vocalize in the audible hearing range, if lifted at their tails (e.g. at changing cages) and especially when they loose grip from a grid cage top. Although there have been previous attempts to standardize this cage-grid vocalization test (Whitney, 1970), the tail-suspension test (TST) was employed, a behavioral test which typically aims to assess depression-like behavior in mice (Steru et al., 1985). For this test, the animal was affixed roughly 2 cm above the tail root to a Ø5 mm vertical stainless steel rod (20 cm above ground) using heat sterilization tape. The test was carried out within a sound-attenuating chamber. Other tapes can be used, but it was found that this sort of material is characterized by its rather low adhesion to murine skin and its excellent removeability, without introducing skin irritations. The test duration is 5 minutes, and the animals vocalization was monitored using high-quality sonic/ultrasonic recording equipment (Avisoft UltraSoundGate USG 116-200, condenser microphone CM16/CMPA). Offline analysis was carried out using custom written Python2.7 scripts.

2.5 Standard Laboratory Procedures & Analysis

2.5.1 Stereotaxic Implantation and Virus Injections

All stereotaxic surgical procedures were carried out similarly and shall be briefly described. Specifics for cannulae implantations and virus injections are provided if necessary. Before the surgery, the animal was weighed and analgesic treatment (200 mg/kg Novalgin/Metamizol in saline, s.c.) was administered 15 minutes prior to any other interventions. During this time, all surgical instruments have been heat sterilized and wiped with 70 % ethanol. Than the animal was transferred to the anesthesia induction cham-

ber and slowly anesthetized with isoflurane (0-4 % in oxygenated air, EverFlo Oxygen Concentrator). The absence of the eyelid and paw withdrawal reflex indicated surgical tolerance and the animal was transferred to the stereotaxic frame (Leica Biosystems, AngleTwo), where it was fixed using non-rupture/non-traumatic ear bars and a snout clamp. The anesthesia was kept constant with 2-2.5 % isoflurane, while the animals body temperature was constantly monitored and controlled (37.5°C) using a rodent rectal probe, heating blanket and a animal temperature controller (WPI Inc. ATC2000). The eyes were kept moisturized using eye ointment (Bepanthen® eye and nose ointment). Further the animals head was shaved using either serrated scissors or an electric shaver. Excess cut hair was removed with cotton swabs soaked with lidocaine (Sigma #L7757, 10 % (w/v) in 70 % ethanol) which in addition exerted an additional cutaneous analgesic effect. Using sharp scissor, the skin above the skull was opened from 1 mm caudal to lambda to 2 mm rostral to bregma. The periosteum was removed with clean cotton swabs soaked in lidocaine solution followed by 3 % hydrogen peroxide. Now, using a small and stiff probe the AngleTwo system was calibrated with the position of bregma and lambda and medial-lateral (ML) and dorsoventral (DV) deviations were corrected if necessary to read less than 50 μm utilizing the manufacturing tolerances of the mouse skull adapters' dove tail rails. The anterior-posterior (AP) coordinate of lambda was noted. In order to correct the skull rotation, two contra-lateral coordinates on the skull surface were targeted (ML ±2.0 mm, AP -1.82 mm) and the respective DV coordinates were noted. If a deviation >50 μm was noticed, the ear bars were released and the initial rotation was corrected. Once the position of the skull was sufficiently accurate, implantation or virus injection was conducted. After these procedures the animals were weighed and their general health and healing status was assessed and recorded on a daily basis for 5 consecutive days and in addition the animals received post-surgical analgesic treatment (1 mg/kg Metacam in saline, s.c., daily).

Viral Injections For viral injections, a 5 μl Hamilton syringe (7634-01/00) equipped with a blunt 33 gauge needle or a 10 μl WPI Inc. syringe (NANOFIL) equipped with a 34 gauge beveled needle (NF34BV-2) in conjunction with a motorized micropump (WPI Inc. UMP3) and the respective micropump controller (WPI Inc. MICRO4) was used. The injection rate was set to 80 nl/min. For the experiments involving the pharmacogenetic manipulation of the SC in LAB mice, 350 nl of adeno-associated-virus serotype-5 (AAV), expressing either the active DREADD (AAV5-CaMKIIα-hM3Dq-mCherry, #AV6333, N=12) or just the reporter fluorophore (controls, AAV5-CaMKIIα-mCherry, #AV4809c, N=12), have been injected (ML ±0.9 mm, AP -3.64 mm, DV -1.75 mm). All viruses were purchased from the Gene Therapy Center Vector Core of the University of North Carolina, Chapel Hill and were diluted, using 350 mM NaCl solution, to reach a target titer of 1.7×10^{12} vg/ml. For the injection, first, the target drilling site was marked with a pencil on the skull surface, and the skull was penetrated using a Ø0.5 mm burr with counterclockwise concentric movements until the intact dura mater becomes visible. Using a hypodermic needle, whose foremost sharp tip was gently bent to the outside by tipping it onto a polished stainless steel surface in order to form a micro-miniature

hook-like instrument, was used to first remove the remaining skull pieces and secondly to open the dura at the site of injection. The injection needle was slowly lowered to reach the target site and the injection was initiated. After the injection the needle was raised for 100 μm and left for additional 10 minutes in order to allow the virus to diffuse. Subsequently, the needle was removed and the procedure was repeated on the contralateral side. During the injection the wound was kept moisturized using saline, in order to prevent brain tissue from sticking onto the needle and to aid the subsequent cutaneous suture. After the injection, using resorbable, sterile, surgical needled suture material (VetSuture fastPGLA 5/0, 13 mm reverse cutting needle 3/8), the wound was closed with 4-6 intermittent stitches, and treated with iodine solution (BRAUNOL®). The incubation time for the virus to reach stable expression was >5 weeks.

Guide Cannula Implantation & Local Muscimol Injections For the local injection of muscimol within the lPAG of HAB mice (N=14), two 3.0 mm long, 26 gauge guide cannulae (WPI Inc.) have been implanted using an angle of ±25° at ML ±1.02 mm, AP -4.25 mm and DV -1.55 mm. As the internal injection needle had a length of 4.0 mm, the ultimate injection site was ML ±0.6 mm, AP -4.25 mm and DV -2.45 mm. One skull screw per hemisphere above the hippocampus (ML ±1.5, AP -1.27) allowed a mechanically stable attachment of the cannulae to the skull using dental cement (Paladur®, Heraeus-Kulzer). Iodine solution (BRAUNOL®) was used to disinfect the wound. After the implantation, dummy injection needles with a dust cap and a length of 3.5 mm were inserted into the guide cannulae in order to prevent clogging. The animals were allowed to recover for more than 2 weeks after the surgery.

Local Muscimol Injections The injection of MUSC or fMUSC or vehicle (aCSF) before the EPM and vocalization task was conducted in the slightly anesthetized (2-2.5 % isoflurane) animal. The injection was carried out using an ultra micropump (WPI Inc. UMP3) and the injection rate was set to 100 nl/min whereby volume of 100 nl was injected. 45 minutes after the injection, the animals were subjected to the behavioral paradigm.

2.5.2 Histology

For histological verification of injection and implantation sites, the animals were deeply anesthetized using a mixture of ketamine (50 mg/kg, Essex Pharma GmbH, Germany) and xylazinhydrochloride (5 mg/kg, Rompun, Bayer Health Care, Germany) injected systemically (100 μl per 10 g body weight, i.p.). Subsequently the animals were given an overdose of isoflurane to induce respiratory arrest (final anesthesia) and transcardially perfused with cold physiological saline followed by 4% (w/v) paraformaldehyde (PFA) in phosphate buffered saline (PBS, final concentrations in mM: 136.89 NaCl, 2.68 KCl, 10 Na_2HPO_4, 1.76 KH_2PO_4; pH adjusted to 7.4 using HCl). The brains of the animals were post-fixed in PFA solution for >24 h at 4°C. In order to prevent the implant tracks from collapsing upon removal, the entire heads of the animals were post-fixed for >48 h, for the verification of optic fiber and electrode placements. The brains were further

placed in 30% (w/v) sucrose in PBS solution for >36 h at 4°C for cryoprotection in order to increase tissue rigidity. Subsequently the brains were dry dabbed and carefully frozen by repeatedly dipping the brain, held at the medulla, into the cold 2-methylbutane on dry ice and stored at -80°C. Coronal tissue sections of 35 μm, cut in several series, were prepared using a cryostat (Thermo Scientific Microm HM560). Sections were collected directly on microscopy slides (SuperFrost®, Menzel-Gläser, Germany). For proteinaceous fluorophores the specimens were covered and preserved using antifade mounting medium (VECTASHIELD® HardSet H-1500, VECTOR Laboratories, UK) containing the nuclear counter stain 4',6-diamidino-2-phenylindole (DAPI). Some series were stained using the standard Nissl staining method in order to reveal the gross anatomical structures. In brief, the specimens were dehydrated using (in v/v) 80 %, 90 %, 2×100 % ethanol (30 seconds per step), stained in 0.1 % (w/v) cresyl violet solution in double distilled water acidified with 300 μl glacial acetic acid for 30 seconds. Subsequently the specimens were differentiated in 100 % isopropyl alcohol (for 30 seconds)followed by 100% xylene for (>5 min). The cresyl violet stained sections were covered and preserved using DPX mounting medium. For the preparation of retinal section the eyes of the perfused animals were removed and stored in 4 % PFA at 4°C and the retinas were extracted. Retinal sections (30 μm) were obtained (Ivanova et al., 2013) using a cryostat and the specimens were stained with haematoxylin and eosin.

2.5.3 Genotyping for *Pde6b^{rd1}*

The genotyping for *Pde6b^{rd1}* was carried out according to Chang et al. (2013). In brief, genomic DNA was extracted from tail biopsies (BL6, CD1, HAB, NAB, LAB, N=4 per strain) by adding 100 μl 50 mM NaOH aqueous solution to each sample (per 1.5 mL reaction tube) followed by 30 minutes incubation at 99°C. Subsequently the samples were allowed to cool down and 30 μl of 1 M Tris-HCl aqueous solution was added per sample. Finally the samples were thoroughly vortexed and cell debris was removed by brief centrifugation and the samples were stored at -20°C. For the polymerase chain reaction (PCR), 2.5 μl PCR buffer (Thermo Scientific, ThermoPrimeTaq 10x Buffer) , 2.5 μl $MgCl_2$ (25 mM), 1 μl deoxynucleoside triphosphate (dNTP, 10 mM) mix (Thermo Scientific, 18427-088), 1 μl dissolved G1 primer, 1 μl G2 primer, 1 μl XMV primer, 0.2 μl *Taq* DNA polymerase (Thermo Scientific, ThermoPrime, #AB-0301/B) and 14.8 μl double distilled water was mixed with 1 μl of genomic DNA solution.

The primer sequences were as follows: G1 (5'-CCTGCATGTGAACCCAGTATTCT ATC-3'), G2 (5'-CTACAGCCCCTCTCCAAGGTTTATAG-3') and XMV (5'-AAGCTA GCTGCAGTAACGCCATTT-3'). The idea of this three primer design is that while G1 and G2 result in a PCR product of 240 base pairs (bp) from normal non-mutant animals, G2 and XMV generate a larger (560 bp) product from the *rd1* mutant allele.

The thermal cycler PCR protocol consisted of the following steps: denaturation for 3 minutes at 95°C, followed by 34 cycles of annealing (30 seconds, 55°C) and extension

(1 minute, 72°C) terminated with a final cycle at 72°C for 5 minutes and the subsequent incubation at 4°C. The amplified DNA was analyzed using agarose gel electrophoresis and a subsequent ethidium bromide staining.

2.5.4 Manganese-enhanced MRI

For a detailed description of the MEMRI data acquisition, data processing and analysis *see* Grünecker et al. (2010). In brief the animals (HAB N=31, NAB N=26, LAB N=30) were injected with a nontoxic dose of manganese chloride (30 mg/kg in saline, i.p.) for eight consecutive days prior to the scanning procedure. The MRI experiments were performed in a 7T MRI scanner (Avance Biospec 70/30, Bruker BioSpin, Ettlingen, Germany) at 24 h after the last injection, while the animals were anesthetized with isoflurane ($\approx$ 2 % in oxygenated air). T_1-weighted images were acquired using a three-dimensional gradient echo pulse sequence (repetition time TE = 50 ms, echo time TE = 3.2 ms) using a matrix of 128×128×128 at a field of view of 16×16×18 mm^3 yielding a final resolution of 125×125×140.6 μm^3. Each voxel was imaged 10 times and averaged. In addition three-dimensional T_2-weighted images were acquired using a rapid acquisition relaxation enhanced pulse sequence (TR = 1 s, TE = 10 ms) with the same spatial resolution as mentioned above, whereby each voxel was imaged twice. This resulted in a total imaging time of 2 hours per animal. The reconstructed images (Paravision, Bruker BioSpin, Ettlingen, Germany) were further analyzed using the statistical parametric mapping package SPM6 *. The acquired images of all animals was spatially normalized to a common single animal template. Following a pairwise voxel-based comparison between HAB vs. NAB and LAB vs. NAB (FDR p<0.001, cluster extent >20) using a 3-level full-factorial design revealed the differential manganese accumulation.

2.5.5 Statistical Analysis

All data are presented as mean values ± standard error (SEM). Statistical analysis has been performed using GraphPad Prism 5.03. One way analysis of variance (in some cases for repeated measures) was followed either by Bonferroni post-hoc analysis or Dunnett's Multiple Comparison post-hoc test (indicated in the text). Two-way analysis of variance (ANOVA for repeated measures) was followed by Bonferroni post-hoc analysis. Non-parametric analysis was carried out using the Mann-Whitney U test. Contingency tables were analyzed using χ^2 test if the tables were of sufficient size, otherwise the Fisher's exact test was used. A p<0.05 was considered statistically significant. All statistical comparisons were carried always between HAB and NAB or LAB and NAB (if not indicated otherwise).

*http://www.fil.ion.ucl.ac.uk/spm/

This page intentionally left blank.

For in much wisdom is much grief: and he that increaseth knowledge increaseth sorrow.

Eccles. 1:18 (KJV)

Chapter 3

Results

3.1 Anxiety-like Behavioral Assessment of HAB, NAB, LAB mice on the Elevated Plus Maze

The elevated-plus maze (EPM) is considered to be a robust assay for the detection of altered anxiety-like behavior in mice. However, the standard test duration rarely exceeds 5-10 minutes (Komada et al., 2008), whereby strong inter-individual differences in anxiety-like behavior and especially their pharmacological modulation, are masked due to stringent cut-off criteria. In order to overcome this issue, we have extended the testing duration to 30 minutes and re-evaluated the behavior of HAB, NAB and LAB mice on the EPM, while focusing on the initial 5 minutes for all parameters (except latency) to provide largely comparable measures (see Fig 3.1a). As the manifestation of high-anxiety and low-anxiety phenotypes, via selective breeding, most likely involved different complex multigenic changes, a direct comparison of HAB against LAB is inappropriate. Therefore, we only compared HAB and LAB to the common NAB control.

Using this approach, the pronounced anxiety-like phenotype of HAB animals surfaced clearly, as more than 45% of all animals did not enter the open arm, even within the extended testing duration of 30 minutes. On the contrary all LAB animals readily explored the open arm with low latencies (75.1±39.6 s vs. 1009.0±153.0 s). A one-way ANOVA revealed significant group differences ($F_{2,22}$=15.07, p<0.0001; a detailed listing of all performed statistical tests is given in the Appendix in table 5.2). These distinct behavioral traits were also reflected by the percentage of time the animals spent on the open arm, where LAB animals stood out with 53.6±11.3% compared to 2.4±0.8% of NAB ($F_{2,22}$=26.25, p<0.0001). Additionally, LAB animals showed an overall increase in locomotor activity (1400.0±171.7 cm vs. 723.0±60.8 cm, $F_{2,22}$=22.49, p<0.0001). On the contrary, HAB animals spent more than 85% of the time in the closed arm ($F_{2,22}$=28.98, p<0.0001), as they also avoided staying in the central zone (13.0±2.3 % vs. 33.8±4.0 %, $F_{2,22}$=12.96, p=0.002). These observations are consistent with previous reports of HAB, NAB and LAB behavior on the EPM (Krömer et al., 2005; Bunck et al., 2009; Erhardt et al., 2011; Avrabos et al., 2013; Yen et al., 2013; Füchsl et al., 2014). As an additional measure to complement the traditional EPM parameters, the display of stretched-attend postures (SAP) (Grant and Mackintosh, 1963) was analyzed, which is

a form of active risk assessment behavior. It was previously shown that the number of SAPs decreases upon anxiolytic treatment (Kaesermann, 1986) and increases with the anxiogenic 5-$HT_{2C/1B}$ receptor antagonist mCPP (Grewal et al., 1997). Moreover, the display of SAPs depend on the presence of an imminent threat or a potential threatening situation (Pinel et al., 1989). LAB animals showed a significantly decreased number of SAPs in the first 5 minutes of the test (20.7±5.9 vs. 63.0±4.3), whereas HAB animals were not different from NAB ($F_{2,19}$=29.84, p<0.0001). Looking at the overall duration of displayed SAPs, HAB animals showed slightly increased measures (222.4±16.8 s vs. 158.0±15.2 s), whereas LAB animals spent on average only 33.7±12.3 seconds displaying SAPs ($F_{2,19}$=32.74, p<0.0001). Over the course of the first 15 minutes, however, NAB animals could adapt to the EPM and the duration of displayed SAPs decayed. On the contrary, HAB animals even showed a slightly elevated non-decaying response after 15 minutes and a repeated-measures two-way ANOVA revealed a significant group × time interaction ($F_{2,28}$=3.587, p=0.0410). This observation can be ascribed to the HAB's maladaptive high-anxiety phenotype. In addition, HAB animals showed higher autonomic arousal which was reflected by significantly increased defecation (11.6±1.2 vs. 7.7±0.7, $F_{2,21}$=4.779, p<0.0195).
Before the animals where placed on the EPM, every subject was tested for the disposition to emit sonic vocalizations by lifting them 3 times from a grid cage top (Whitney, 1970). Animals which vocalized at least once, were counted as 'vocalizers'. Whereas none of the NAB or LAB animals emitted a single call, 47% of HAB animals strongly vocalized and emitted multiple calls (χ^2=15.61, p=0.0004).

In order to investigate to which extent the extreme phenotype of HAB mice can be modulated with traditional anxiolytics, we have applied diazepam (DZP) at 1 mg/kg i.p., or vehicle (saline) in a separate cohort of HAB animals (2× N=13). The effect of DZP on the behavior of HAB animals on the EPM was studied subsequently. None of the classical EPM parameters were sensitive to DZP treatment, except the locomotor activity, which was slightly increased (t_{24}=2.174, p=0.0398). Notably, it has been shown previously that DZP can decrease locomotor activity as a side-effect (Chaouloff et al., 1997). Also neither the number nor the duration of SAPs during the first 5 minutes of the test, were significantly altered by DZP treatment. However, during the first 15 minutes of the test, the non-decaying development of SAP duration over time of vehicle treated animals, was transformed to a decaying response in DZP treated mice, resembling the NAB phenotype. Repeated measures two-way ANOVA combined with Bonferroni post-hoc testing, revealed a significantly different SAP duration for DZP treated animals at 10-15 minutes (45.8±9,8 s vs. 94.3±15.5 s) after test onset (interaction: $F_{2,28}$=3.587, p=0.0410; over time: $F_{2,24}$=6.468, p=0.0033). The anxiolytic effect of DZP was accompanied by a significant decrease in defecation (1.5±0.5 vs. 5.8±1.2, t_{24}=3.344, p=0.0027) and a marked decrease in the disposition to vocalize during a 5 minute tail-suspension test (TST) (3 out of 13 vs. 9 out of 13, two-sided Fisher's exact test p=0.0472). The higher incidence of vocalizers, compared to the data shown in figure 3.1d, is most likely due to prior injection stress.

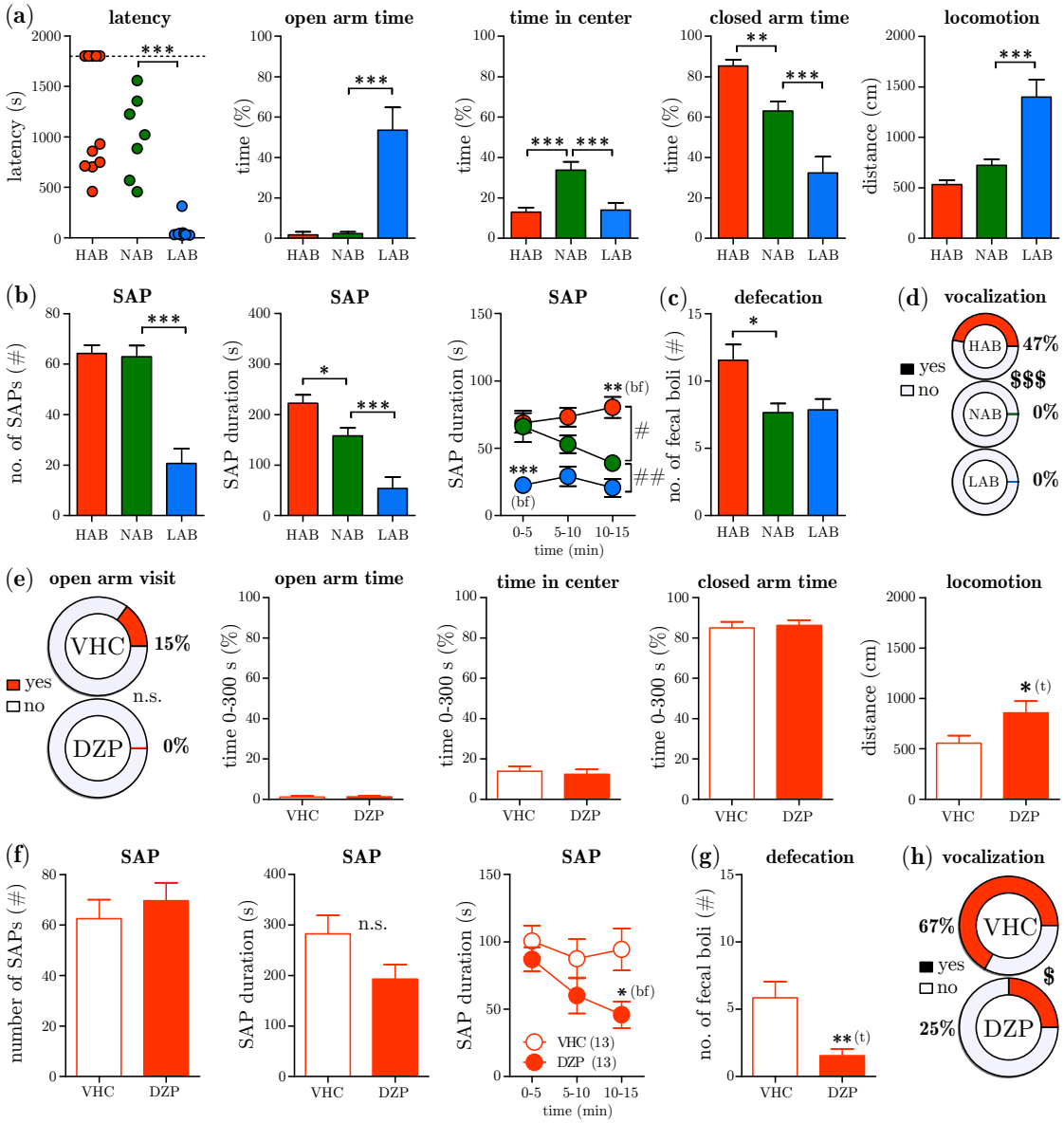

Figure 3.1 | Behavioral Assessment of HAB, NAB, LAB Mice on the EPM
(**a**) Using the standard EPM but with an extended cut-off time of 30 min the following behavioral parameters were assessed for HAB (N=11), NAB (N=7) and LAB (N=7) animals: the latency to enter the open arm, open arm time (0-5 min), central zone time (0-5 min), closed arm time (0-5 min) and the distance the animals have moved (0-5 min). (**b**) In addition to the classical EPM parameters we have also investigated the display of stretched-attend postures (SAP) which serves as a measure of active fear coping: the number of SAP's during the first 5 min of the task, the total duration of SAP's during the first 5 min of the task, and the total duration of SAP's in 5 minute bins during the first half of the experiment. (**c**) As an indirect measure of autonomic arousal serves defecation (number of fecal boli) while the animals are exposed to the EPM. (**d**) Disposition to emit sonic vocalizations. (**e**) Another cohort of HAB animals were treated with diazepam (1 mg/kg, i.p.) (N=13) or vehicle (saline, N=13) and subjected to the EPM and again the standard EPM parameters were assessed. (**f**) Stretched-attend posture display of HAB animals during EPM with diazepam/vehicle treatment (0-5 min). (**g**) Defecation of HAB animals during EPM with diazepam/vehicle treatment. (**h**) In order to assess the disposition to vocalize in standardized manner, the diazepam/vehicle treated HAB animals were subjected to a 5 min tail-suspension test, while audio signal were recorded and scored offline. Asterisks indicate significance values obtained by t-tests (t) or 1-way ANOVA followed by Newman-Keuls Multiple Comparison/Bonferroni post-hoc (bf) tests, * p<0.05, ** p<0.01, *** p<0.01; dollar signs indicate significance values obtained by χ^2 tests, \$ p<0.05, \$\$\$ p<0.001; hashes indicate group effects obtained by 2-way ANOVA, ## p<0.01. Values are given as mean±SEM.

Taken together, HAB, NAB and LAB animals show the expectable, robust behavior on EPM, according to their selective breeding. But traditional EPM measures fail to reveal the anxiolytic properties of diazepam, and other, ethological more relevant measures as autonomic arousal, vocalization and active risk assessment have to be considered in order to establish a comprehensive readout for anxiety-like behavioral phenotypes in mice.

3.2 Two Novel Ethologically Inspired Testing Situations for the Study of Fear in Mice

The behavioral measures obtained on the EPM are indicative of an approach-avoidance situation which became manifest differently in HAB and LAB mice. The term 'anxiety' test for the EPM infers an inner conflict which misleadingly points towards higher cognitive processes, mediated for example by the prefrontal areas. Looking at avoidance behavior separately, it becomes obvious that there is a strong subcortical component which is in a continuum to flight and panic-like reactions, involving most likely the amygdala, ventromedial hypothalamus, periaqueductal gray and the superior colliculus. Therefore, we were interested if the altered anxiety-like behavior of HAB and LAB is accompanied by changes in fear responses as it has been suggested previously to be the case with conditioned fear (Sartori et al., 2011a; Yen et al., 2012). In order to circumvent learning mediated effects, we focused on innate fear upon acute confrontation with a (potential) threat.

Paradigms which asses general innate fear levels should incorporate multisensory stimuli and allow for repeated testing and temporally confined exposure. In lack of appropriate testing situations, we have developed two novel paradigms: the Robocat, which is based on a previously published design by Choi and Kim (2010), and the IndyMaze, which is inspired by a popular movie (Spielberg and Marshall, 1981) (for a detailed description of both tests *see* chapter *Materials & Methods*). The different behavioral readouts obtained in the Robocat task are depicted in figure 3.2a. The mouse could either activate the Robocat and subsequently display a flight response, activate the Robocat but simply bypassing it or activate the Robocat and collide with it. The innate fear responses of HAB (N=7), NAB (N=6) and LAB (N=9) mice were assessed using the Robocat task. Figure 3.2b depicts the percentage of animals which displayed the respective behaviors at least once during a 10 minute exposure to the Robocat. During this trial the animals activated the Robocat several times (HAB 2.4±0.4, NAB 3.5±0.6, LAB 10.8±2.1). HAB animals were not able to adapt to the Robocat's activation and showed a flight response at all encounters (Fisher's exact p=0.021), they never bypassed (Fisher's exact p=0.0047) nor collided with it. On the contrary NAB animals, displayed a well-balanced behavioral profile: the minority of all animals feared the Robocat (33%) or got hit by the it (17%), while 83% of all NAB mice tolerated and bypassed the threatening stimulus. This is contrasted by the behavior of LAB mice: no single animal fled upon the Robocat's movement, but all bypassed it. Most strikingly however, is the significantly increased collision rate of 89% (Fisher's exact p=0.011, a

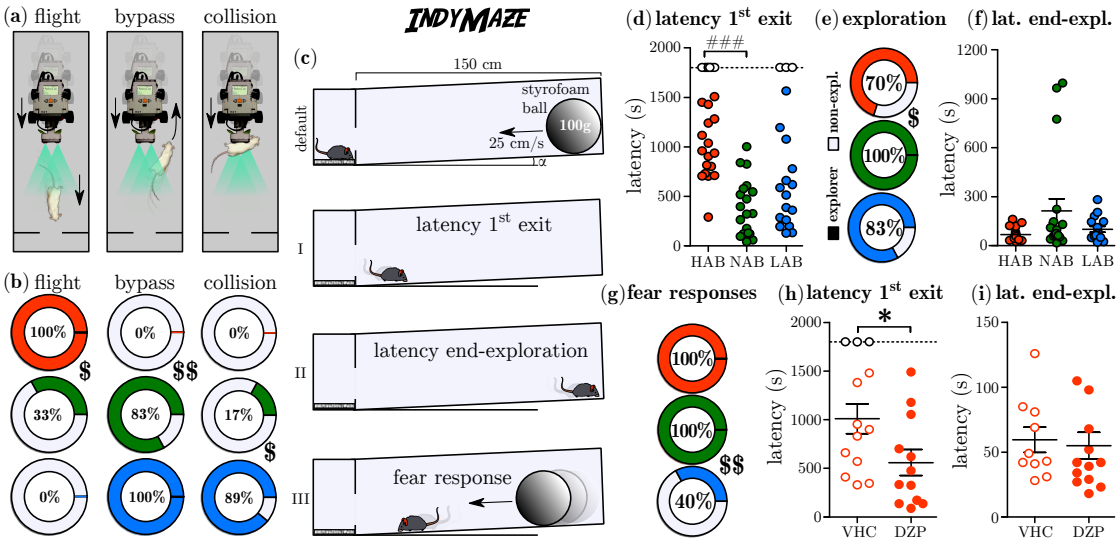

Figure 3.2 | Two Novel Ethologically Inspired Testing Situations for the Study of Fear in Mice

(**a**) The three different behavioral measures obtained in the Robocat task, whose appearance have been scored: flight, bypass and collision. (**b**) Using the Robocat, we have investigated the fear responses of HAB (N=7, red), NAB (N=6, green) and LAB (N=9, blue) animals (Fisher's exact). Values are percentages of animals which showed the respective behavior at least once. (**c**) Schematic description of the IndyMaze (default) operational procedure as well as the different obtained behavioral measures (latency to 1st exit I, latency for end-exploration II and flight response III). Using the IndyMaze we have tested different cohorts of HAB (N=24), NAB (N=19) and LAB (N=20) animals (**d**) Quantification of the latency to 1st; non-filled circles indicate animals which did not leave the start arm, HAB (N=7), NAB (N=0) and LAB (N=4), those animals were excluded from the 1-way ANOVA. (**e**) Quantification of the number of animals which explored the arena. (**f**) Quantification of the latency for end-exploration without the non-explorers shown in *d*. Note: If the animals left the start compartment, they all explored the arena to its end. (**g**) Quantification of the occurrence of fear responses at least once during 3 encounters of the approaching styrofoam ball (this includes preemptive fear responses, as well as fear responses after the ball had hit the animal). (**h**) Another cohort of HAB animals were treated with diazepam (1 mg/kg, i.p.) (N=13) or vehicle (saline, N=12) and subjected to the IndyMaze, and the latency to 1st exit was quantified. (**i**) Latency for end-exploration (corrected for non-explorers) for DZP/vehicle treated HAB animals. Asterisks indicate significance values obtained by Mann-Whitney test, * = p<0.05; dollar signs indicate significance values obtained by χ^2 or Fisher's exact tests, \$ p<0.05, \$\$ p<0.01, \$\$\$ p<0.001; hashes indicate significance values obtained by 1-way ANOVA followed by Newman-Keuls Multiple Comparison test, ### p<0.001. Values are given as mean±SEM.

detailed listing of all performed statistical tests is given in the Appendix in table 5.3). Indeed, the Robocat task revealed extreme differential fear responses between HAB and NAB. But it became also evident that the high degree of controllability (allowing a bypass or withdrawal from the arena to avoid activation/confrontation) is not suitable to ask whether NAB and LAB show different levels of fear. Because an inability to express fear, and a high degree of adaptation would result both in a decreased level of observable fear. In order to avoid this confounding variable we have developed the IndyMaze. In this test an animal is confronted with a rolling (25 cm/s) styrofoam ball (100 g) in a slightly tilted and narrow tunnel. Therefore, every trial involves a direct encounter with the threatening stimulus. The operational procedure is depicted in figure 3.2c. First, the animals are free to enter the arena, which gives the latency to first exit, a measure comparable to other emergence tasks. This measure corresponds to the exit latency on the EPM and thus can be considered as a parameter to assess changes in anxiety-like behavior. HAB animals showed strongly increased latencies to exit the home compart-

ment (977.4±79.2 s vs. 392.1±66.1 s) whereas LAB animals were not different to NAB ($F_{2,50}$=12.64, p<0.0001). A significant amount of HAB animals even never left the home compartment (Fig. 3.2e) within 30 minutes ($\chi^2{}_{2,N=62}$=6.671, p=0.0356). This is again indicative of an increased anxiety-like behavior. Once all animals have left the home compartment, they explored the entire arena (Fig. 3.2f) with equal low latency (HAB 68.8±10.1 s; NAB 213.1±72.8 s; LAB 100.4±18.2 s). Looking at the fear responses (Fig. 3.2g), which included preemptive flight responses or a retrieval after the ball has hit the animals, it is evident that both HAB and NAB are able to respond appropriately towards impeding threatening stimuli, whereas 60% of LAB animals exhibited significant deficits ($\chi^2{}_{1,\ N=27}$=13.11, p=0.0014). In order to test whether the behavioral readouts obtained using the IndyMaze can be modulated with anxiolytics, another cohort of HAB animals was treated with diazepam (DZP, 1 mg/kg, N=13) or vehicle (VHC, saline, N=12) and subjected them to the IndyMaze task. The DZP treatment could significantly decrease the latency to 1st (VHC 1011.0±153.4 s vs. DZP 595.5±133.5 s; Mann-Whitney, two-tailed, $U_{\mathrm{n1=208,\ n2=117}}$=39.00, p<0.0363), indicative of an anxiolytic effect, while leaving latency for end-exploration unaffected. However, DZP treatment was INEFFECTIVE in modulating the fear responses (fear responsivity: VHC 100%, DZP 100%).

In summary, both tasks, the Robocat and IndyMaze, have proven to be valid tools to assay innate fear responses in mice. In addition, the IndyMaze task permits also the parallel assessment of anxiety-like behavioral phenotypes. Using both tasks, we could demonstrate again that HAB animals show increased DZP-sensitive, anxiety-like behavior which was accompanied by maladaptive levels of fear. In contrast, LAB animals were shown to possess a strong deficit to escape impeding imminent threats.

3.3 Complete Retinal Blindness in LAB Mice

The severe deficit in avoiding impeding threats, observed in LAB mice, raised the question whether these animals have intact vision. In order to assess the visual capabilities of LAB mice, their home-cage activity was monitored (*see manuscript in press* 'A simplified microwave-based motion detector for home cage activity monitoring in mice', Appendix 5.4.1, figure 5.5b) for 6.5 consecutive days, while on day 3 the light cycle was shifted. This manipulation led to a strong photoentrainment of the home-cage activity in CD1 control animals, while LAB animals where unable to adapt to the new light cycle (Appendix 5.4.1, figure 5.5d). However, there are cells, other than the photoreceptors, which respond to the photoentraining signals, namely the intrinsically photosensitive retinal ganglion cells (ipRGC) (Güler et al., 2008; Hatori et al., 2008). Therefore, changes in photoentrainment do not necessarily mean a loss of visual function.

A standard test for visual acuity in mice is the assessment of the optomotor response (Thaung et al., 2002; Prusky et al., 2004; Abdeljalil et al., 2005). This test is based on the tracking behavior of mice in response to horizontally moving stripes. For this test, mice are placed on a fixed platform within a rotating cylinder lined with stripes of different width to probe visual acuity (Fig. 3.3a *inset*). We slightly modified this testing procedure

in order to fit it to all five mouse lines (BL6, CD1, HAB, NAB and LAB) in a way that we have used only one, relatively large grating (0.5 cycles/degree) and in addition scored every head movement if it was concordant with the cylinders rotational direction. Therefore, we have used this test to assess vision in general, rather than visual acuity. In order to avoid potential saturation effects due to different light sensitivities between pigmented (BL6) and albino (CD1, HAB, NAB, LAB) animals, we further used two different light intensities of 500 lux and 3 lux. However, the different light conditions did not lead to an increased performance of the albino animals (with lower illumination also the contrasts decrease and the level of difficulty increases), and we therefore based our statistical analysis only on results obtained at 500 lux background illumination. Using this approach, we could observe significant differences revealed by one-way ANOVA ($F_{4,54}$=93.13, p<0.0001, a detailed listing of all performed statistical tests is given in table 5.4) in performance among the various strains (Fig. 3.3a). In general, BL6 mice outperformed all other strains by far (Bl6 16.9±0.9 OMR/min), whereas among the albino animals HAB animals showed the strongest responses (5.5±0.8 OMR/min). Both, CD1 (2.6±0.7 OMR/min) and NAB (2.4±0.5 OMR/min) animals responded equally, but LAB animals failed to show any clear optomotor responses (0.2±0.1 OMR/min). However, as LAB mice also have been reported to exhibit certain phenomenological similarities to ADHD (Yen et al., 2013), we could not exclude the possibility that these animals could perceive the visual stimuli, but in fact were simply unable to attend to the visual stimuli and therefore failed to show an appropriate response.

To exclude this possibility, the retinal function of all five mouse strains was investigated using flash electroretinography (fERG) measurements in the anesthetized animal. The fERG setup (depicted in Fig. 3.3b *top*) consisted of a differential amplifier usually used for in-vivo extracellular neural recordings (Siegle et al., 2017), whereby the reference electrode was placed on the shaded eye. The other eye was stimulated with a custom built miniature eyecup, equipped with a white LED, in combination with a custom built LED driver. This setup allowed the reliable detection of electroretinographic signals and the dissection of the b-wave component of fERG (eg. 3.3b *bottom*). The fERGs acquired in scotopic (dark-adapted for >3h) as well under photopic conditions at three different light flash intensities (0.23, 128 and 1.69 log photoisomerizations$\times$rod$^{-1}\times$s^{-1}), showed strong deflections for BL6, CD1, HAB and NAB (N=6, each) animals (Fig. 3.3c). However ,tauin LAB animals there was no detectable electrophysiological response. These effects were shown to be highly significant by two-way repeated measures ANOVA (scotopic, Group $F_{4,25}$=14.38, p<0.0001; photopic, Group $F_{4,25}$=8.77, p=0.0001; Fig. 3.3d). To further determine the cause for the total absence of electroretinographic responses, a histological analysis of retinal sections of all strains (N=3, each, right eye) was conducted and a complete absence of the outer nuclear layer (ONL) and the subjacent inner/outer segments was observed in LAB animals (Fig. 3.3f). As the founder strain for LAB animals (CD1) is known to exhibit incidences of a *rd1* retinal degeneration (Serfilippi et al., 2004), we employed a polymerase chain reaction (PCR) genotyping screening for all strains (N=4, each, tail biopsy) (Chang et al., 2013). The test (Fig 3.3g) revealed that LAB animals exhibit a homozygous mutation in the *Pde6b*$^{\mathrm{rd1+/+}}$ allele which is

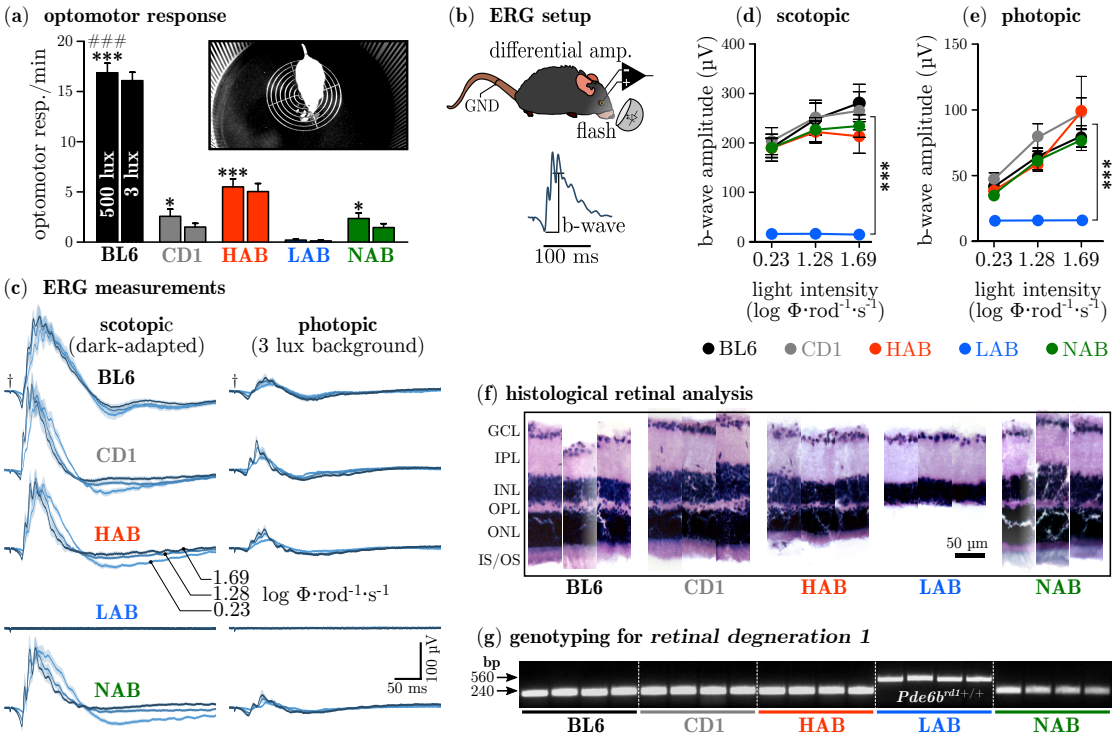

Figure 3.3 | Complete Retinal Blindness in LAB Mice
(**a**) Optomotor responses (OMR) measured in BL6, CD1, HAB, NAB, LAB (N=12, each) under 500 lux (left bar) or 3 lux (right bar). Inset shows a HAB animal within the OMR setup. Significance values obtained by one-way ANOVA followed by Newman Keuls Multiple Comparison are indicated by asterisks compared to LAB or by hashes for BL6 compared to all other mouse lines. (**b**) Simplified overview of the setup for measuring electroretinography in the anesthetized mouse. (**c**) Electroretinograms of BL6, CD1, HAB, NAB, LAB (N=6, each) measured at scotopic and photopic conditions a three different flash intensities. (**d**) Quantification of scotopic ERG measurements. Asterisks indicate significant group effect obtained by two-way ANOVA followed by Bonferroni post hoc test. (**e**) Quantification of photopic ERG measurements. Asterisks indicate significant group effect obtained by two-way ANOVA followed by Bonferroni post hoc test. (**f**) Histological analysis of 30 μm retinal sections of BL6, CD1, HAB, NAB, LAB (N=3, each, right eye only) stained with haematoxylin and eosin. IS/OS inner/outer photoreceptor segments; ONL outer nuclear layer; OPL outer plexiform layer; INL inner nuclear layer; IPL inner plexiform layer; GCL ganglion cell layer. (**g**) Polymerase chain reaction (PCR) screening for $Pde6b^{rd1+/+}$ allele, *retinal degeneration 1*. Significance values are indicated by asterisks and hashes (details for the statistical tests are given in the respective part of the figure legend): * p<0.05, ** p<0.01, *** p<0.001, ### p<0.001. Values are given as mean±SEM.

indicative of the retinal degeneration 1 mutation which leads to blindness shortly after birth. Therefore it is conclude that LAB animals (tested at an age of 3-6 month of age) suffer from complete retinal blindness, which is the reason for the inability to escape impeding threatening stimuli, like the Robocat (Fig. 3.2b). But blindness does not explain why still only 40% of LAB animals showed a flight response even after hit by the ball in the IndyMaze task (Fig. 3.2g).

3.4 Reversing the Low-anxiety Phenotype of LAB Mice

The severe deficit in avoiding impeding threats of LAB mice during the Robocat task is certainly explained by their retinal degeneration. However, using the IndyMaze, where retrievals (after the ball had hit the animal) were also counted as fear responses, it became

obvious that LAB mice also showed a strongly decreased responsivity towards tactile stimuli. Therefore, it was necessary to determine whether this behavioral abnormality can be ascribed to differential activity in a certain brain area.

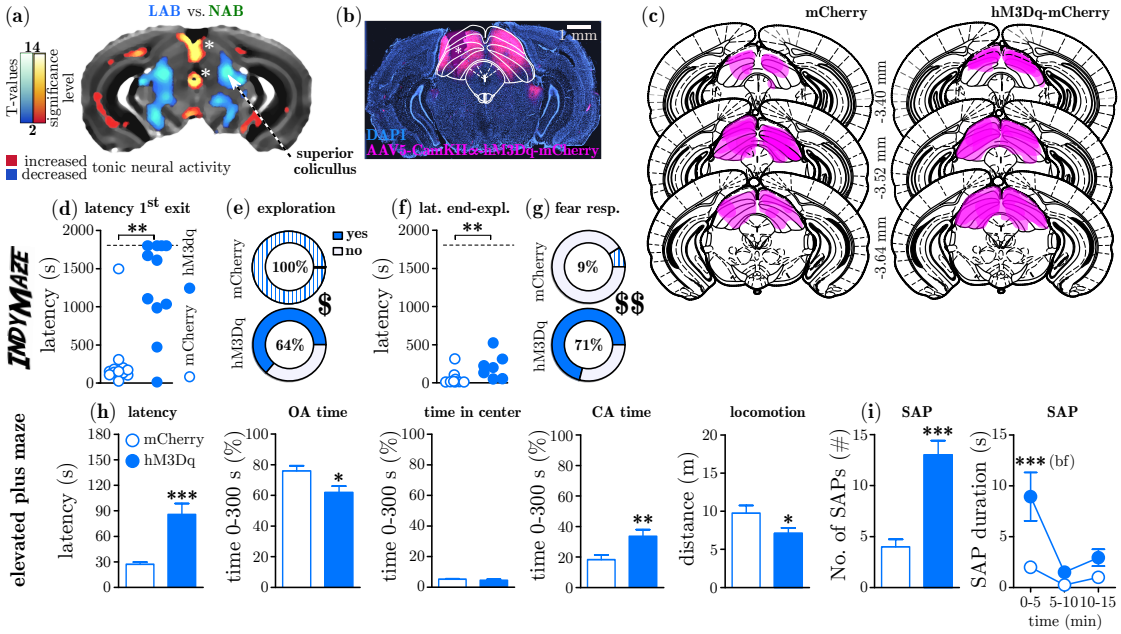

Figure 3.4 | Reversing Low-anxiety Phenotype of LAB Mice
(**a**) Manganese enhanced MRI (MEMRI) of LAB (N=30) vs. NAB (N=26) animals showed a significantly decreased accumulation of Mn^{2+} within the superior colliculus of LAB. Warm colors indicate increased accumulation, cold colors indicate decreased accumulation. The color brightness indicates the significance values. Asterisks mark signal artifacts within the aqueduct and above the superior colliculus due to line differences in brain templates. (**b**) Exemplary brain section depicting extent of viral expression (*magenta*) at the level of the superior colliculus. Shown in *cyan* is the nuclear 4',6-diamidino-2-phenylindole (DAPI) counterstain. Overlaid are the outlines of the SC and PAG. Asterisk marks tissue lesion which occurred during sectioning. (**c**) Schematic representation of the extent of viral expression in control (mCherry, N=12) and experimental (hM3Dq-mCherry, N=12) LAB mice. The effect of hM3Dq activation within the SC was studied using the IndyMaze task. Shown is the latency to 1st exit (**d**), the percentage of animals which explored the arena at all (**e**), latency to end-exploration (**f**) and the percentage of animals which showed a fear response to the ball (**g**). All animals were all treated with 1 mg/kg clozapine-N-oxide (CNO) 45 minutes before the test. (**h**) In addition the same animals were tested for the behavior on the EPM (30 minutes), and latency to emerge, open arm (OA) time, time in the center, closed-arm (CA) time and locomotion was assessed within the first 5 minutes. (**i**) Moreover the active risk assessment parameters, number of stretched-attend postures (SAP)(0-5 min) and the duration of SAPs over time (0-15 min) were scored. Asterisks indicate significance values obtained by Mann-Whitney test if not stated otherwise, * p<0.05, ** p<0.01, *** p<0.001; dollar signs indicate significance values obtained by Fisher's exact tests, \$ p<0.05, \$\$ p<0.01. Significance values obtained by 2-way repeated measures ANOVA, followed by Bonferroni post-hoc test are indicated with *bf*. Values are given as mean±SEM.

In order to investigate the tonic neuronal activity changes in LAB mice compared to NAB, manganese-enhanced magnetic resonance imaging (MEMRI) in anesthetized HAB (N=31), NAB (N=26) and LAB (N=30) animals were employed (FDR p<0.001, cluster extent >20), using a 3-level full-factorial design based on a voxel-wise analysis (for the complete MEMRI data set *see* Appendix section 5.3, Fig. 5.1). The results obtained by pairwise comparison of MEMRI data suggested a decreased accumulation of manganese within the ventral parts of the motor-related layers of the superior colliculus (lateral to the periaqueductal gray) in LAB mice compared to NAB (Fig. 3.4a).

This structure receives strong inputs from the primary and secondary somatomotor areas (Allen Brain Atlas, Connectivity, exps. 180719293, 180709942). In order to assess the functional relationship of this brain region in the generation of the LAB behavioral phenotype, the recently developed 'designer receptors exclusively activated by designer drugs' (DREADD) approach (Armbruster et al., 2007) was employed. The activating DREADD hM3Dq fused to the reporter protein mCherry was expressed under the control of the CaMKIIα promoter using adeno-associated viral vectors (AAV5-CaMKIIα-hM3Dq-mCherry) or the empty control virus (AAV5-CaMKIIα-mCherry) within the SC (ML $\pm$0.9 mm, AP -3.64 mm, DV -1.75 mm). An exemplary image of the virus expression is shown in figure 3.4b. This approach resulted in the labeling of the entire SC (Fig. 3.4c). After an incubation period of >5 weeks, all animals were subjected to the IndyMaze. On the testing day each animal was injected (i.p.) with 1 mg/kg clozapine-*N*-oxide (CNO, in DMSO) 45 minutes before each trial. Experimental animals expressing hM3Dq showed a significantly (Mann-Whitney $U_{\mathrm{n1=94,\ n2=182}}$=16.00, p=0.0023, a detailed listing of all performed statistical tests is given in table 5.5) increased latency to leave the start compartment (1282.0$\pm$185.4 s vs. 265.5$\pm$113.6 s), indicative of an increased anxiety-like response (Fig. 3.4d). Moreover, only 64% of hM3Dq animals left the start compartment (Fig. 3.4e) within 30 minutes (Fisher's exact, p=0.0373). Also the latency was increased for end exploration (216.0$\pm$62.7 s vs. 51.0$\pm$25.3 s; Mann-Whitney U test; $U_{\mathrm{n1=86,\ n2=104}}$=8.00, p=0.0046; Fig. 3.4f). Strikingly, the fear responsivity (Fig. 3.4g) was clearly increased to 71% of mice transfected with hM3Dq, compared to 9% in mCherry controls (Fisher's exact, p=0.0095). In order to asses whether this pharmacogenetically induced fear, is also reflected by changes in anxiety-like behavior, these animals were treated again one week later before the exposure to the EPM (Fig. 3.4h). Similar to the emergence component of the IndyMaze, hM3Dq animals treated with 1 mg/kg CNO showed an increased (85.6$\pm$12.9 s vs. 27.4$\pm$2.4 s) latency to access the open arm ($U_{\mathrm{n1=69.5,\ n2=183.5}}$=3.500, p=0.0002). This was accompanied by a slightly decreased percentage of time spent on the open arms (61.9$\pm$4.2 % vs. 76.0$\pm$3.3 %, $U_{\mathrm{n1=183,\ n2=93}}$=27.00, p=0.0178), an increased percentage of time spent in the closed arms (33.6$\pm$4.3 % vs.18.3$\pm$3.0, $U_{\mathrm{n1=100.5,\ n2=175.5}}$= 22.50, p=0.0081) as well as decreased locomotor activity (7.1$\pm$0.7 m vs. 9.7$\pm$1.0 m, $U_{\mathrm{n1=179,\ n2=97}}$=31.00, p=0.0337). All these observed measures reflect an increase in anxiety-like behavior, which however, could be explained by an increased passivity due to unspecific effects of the active DREADD. Therefore the increase in the number of active risk assessment, namely stretched-attend postures (Fig. 3.4i) in hM3Dq animals (13.0$\pm$1.4 # vs. 4.0$\pm$0.7 #) is of particular importance ($U_{\mathrm{n1=56.5,\ n2=174.5}}$=1.5, p=0.0002). In addition, also the duration of SAPs was increased (8.9$\pm$2.4 s vs. 2.0$\pm$0.6 s) within the first 5 minutes of the EPM task with significant interaction, demonstrated by a repeated measures 2-way ANOVA ($F_{2,38}$=3.59, p=0.0375). These results show that even in blind LAB animals, an elevated neuronal activity within the SC precipitates as an increased anxiety-like behavioral phenotype. Moreover, the pharmacogenetic stimulation of the SC could restore in part, the deficits in fear response to tactile stimuli.

3.5 Reversing the High-anxiety Phenotype of HAB Mice

Similar to LAB mice, the possible underlying neural circuitry generating the maladaptive fear response and increased anxiety-like behavior in HAB mice was investigated using the MEMRI approach. A prominent brain structure found to exhibit increased

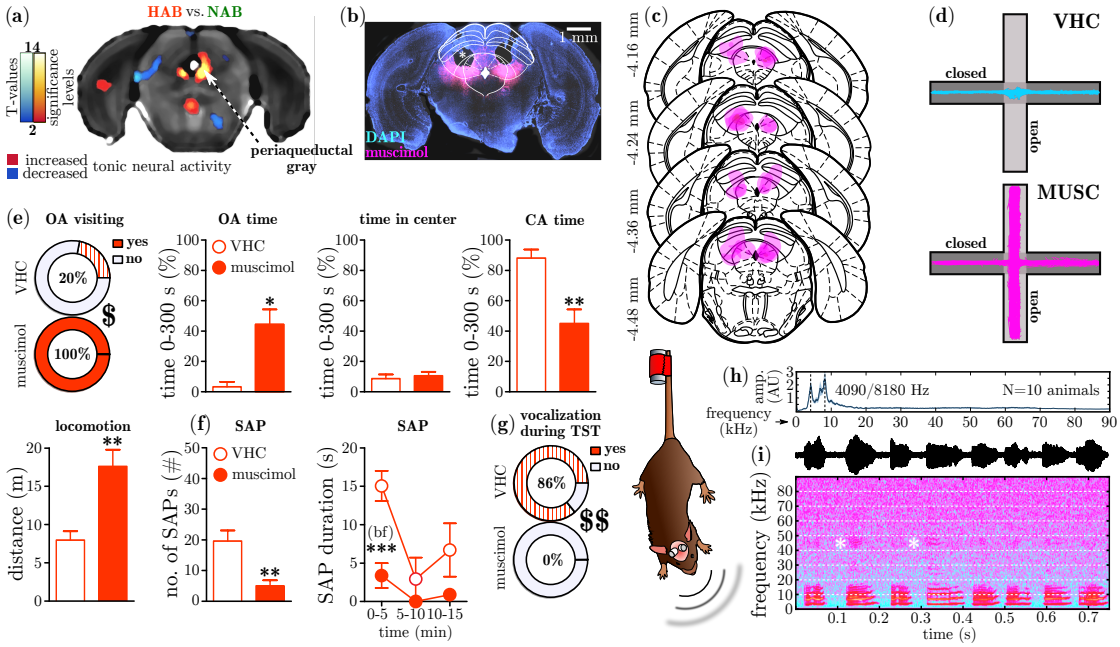

Figure 3.5 | Reversing High-anxiety Phenotype of HAB Mice
(**a**) Manganese enhanced MRI (MEMRI) of HAB (N=31) vs. NAB (N=26) animals showed a significantly increased accumulation of Mn^{2+} within the periaqueductal gray of HAB. (**b**) Exemplary brain section depicting extent of fluorescently labeled muscimol (MUSC) diffusion (*magenta*) at the level of the periaqueductal gray. Shown in *cyan* is the nuclear DAPI counterstain. Overlaid are the outlines of the SC and PAG. Asterisk marks tissue lesion due to cannula placement. (**c**) Schematic representation of the extent fluorescently labeled MUSC diffusion N=14. (**d**) Exemplary movement trace of a vehicle (VHC) and MUSC treated HAB mouse on the EPM. (**e**) VHC (N=5) or MUSC (N=6) treated HAB animals were tested for their behavior on the EPM (30 minutes), and the percentage of open arm (OA) visiting animals, OA time, time in the center, closed-arm (CA) time and locomotion was assessed within the first 5 minutes. (**f**) Moreover the active risk assessment parameters, number of stretched-attend postures (SAP)(0-5 min) and the duration of SAPs over time (0-15 min) were scored. (**g**) Finally, all animals (N=14) have been treated with VHC and MUSC in a crossover design and subjected to a 5 min tail-suspension test (*see* cartoon), in order to assay the disposition to vocalize. (**h**) Spectral analysis of vocal call emitted by HAB (N=10). Depicted is the average (black) together with the SEM (blue). Dashed horizontal lines indicate the dominant frequency at 4090 Hz and the first harmonic at 8190 Hz. (**i**) Exemplary call of a HAB animal. *Top panel*: Hull curve of raw signal. *Lower panel*: Sonogram of the same call. Note the formant structure of the harmonics. Asterisks denote rare and slight ultrasound artifacts within the 40-50 kHz range, which occur due to the expelled air itself. Asterisks indicate significance values obtained by Mann-Whitney test if not stated otherwise, * = p<0.05, ** = p<0.01, *** = p<0.001; dollar signs indicate significance values obtained by Fisher's exact tests, $ = p<0.05, $$ = p<0.01. Significance values obtained by 2-way repeated measures ANOVA, followed by Bonferroni post-hoc test are indicated with *bf*. Values are given as mean±SEM.

manganese accumulation, suggesting tonically increased activity, was the ventrolateral, lateral and dorsolateral periaqueductal gray (Fig. 3.5a; for the complete MEMRI data set *see* Appendix section 5.3, Fig. 5.1). In order to assess the functional relationship of the PAG in the generation of the HAB behavioral phenotype, we implanted guide cannulae targeting the dl/lPAG (ML ±0.6 mm, AP -4.25 mm, DV -2.45 mm, needle protruded 500 μm) and injected 53.24 ng/100 nl (per hemisphere) of fluorescently labeled musci-

mol (MUSC), a potent $GABA_A$-agonist (45 minutes before each experiment) which is comparable to 10 ng in 100 nl of ordinary muscimol. An exemplary image depicting the muscimol diffusion is shown in figure 3.5b. The extent of muscimol diffusion of all animals (N=14) is shown in figure 3.5c and comprised besides the lPAG, the dlPAG and partly the deep layers and also the intermediate gray layers of the SC. In order to test whether increased GABAergic signaling within the lPAG changes the extreme anxiety-like behavior of a 'vocalizer enriched' HAB mice cohort, we have tested vehicle (aCSF, N=6) or MUSC (N=5) treated HAB mice (one VHC and two MUSC animals have been excluded due to deficient infusion) for their behavior on the EPM. While only 20% of VHC treated animals accessed the open arm, all MUSC animals readily did so (Fisher's exact, p=0.0152, a detailed listing of all performed statistical tests is given in table 5.6). Further, MUSC treated animals spent significantly ($U_{\mathrm{n1=16,\ n2=50}}$=1.000, p=0.0116) more time on the open arm (44.4±9.4 % vs. 3.2±3.2 %), less time in the closed arm (45.0±9.3 % vs. 88.1±5.8 %, $U_{\mathrm{n1=44,\ n2=22}}$=1.000, p=0.0087) and showed increased locomotion (17.6±2.2 m vs. 8.0±1.2 m, $U_{\mathrm{n1=15,\ n2=61}}$=0.0, p=0.0043). These observed measures indicate a decrease in anxiety-like behavior, which however, could be confounded by the increased activity. Therefore, a decrease of active risk assessment (shown above to be sensitive systemic diazepam treatment) in MUSC treated HAB mice (Fig. 3.5f), namely number of SAPs (5.0±3.5 # vs. 19.6±3.4 #, $U_{\mathrm{n1=45,\ n2=21}}$=0.0, p=0.008) is of great importance. Moreover, the duration of SAPs was significantly decreased within the first 5 minutes of the EPM task with significant group effect, demonstrated by a repeated measures 2-way ANOVA ($F_{1,9}$=13.71, p=0.0049). Finally, all animals were tested two times on two consecutive days for their disposition to vocalize during a 5 min TST, using a crossover design. Half of the animals received either VHC or MUSC treatment, which was swapped at the following day. Whereas 86 % of VHC treated HAB mice emitted at least one sonic call (Fig. 3.5g) during a 5 min TST (Fig. 3.5g, *cartoon*), none of the MUSC treated animals vocalized (Fischer's exact, p<0.0001). All calls were in the sonic range. Figure 3.5h shows the spectral analysis of sonic vocalizing HAB mice (two mice have been excluded due to their low disposition of only short calls). Evidently, HAB mice vocalize at a dominant frequency of 4090 Hz with a strong 1^{st} harmonic at 8180 Hz. All recordings were carried out using a USV transducer and were scored online using the heterodyne headphone output, thereby we can exclude that MUSC treated animals vocalized in the ultrasonic range only. Figure 3.5i shows an exemplary sonic call with the dominant frequency in the 4 kHz range, and formant harmonics up to approx. 16 kHz. In some calls (white asterisks) we can see that these harmonics even range up to 40-50 kHz, however these signal do not resemble any typical rodent ultrasonic call. These results indicate an increased tonic activation of the PAG in HAB mice, which precipitates as an exaggerated anxiety-like behavior phenotype accompanied by a strong disposition to emit sonic calls, which could be reverted by low doses of muscimol.

3.6 Assessment of Fear Coping Strategies in HAB, NAB and LAB Mice using the *Moving Wall Box* (MWB) Task

In order to further investigate the relationship between extremes in anxiety-like behavior and fear expression, another cohort of HAB (N=23), NAB (N=19) and LAB (N=17) animals were subjected to the *Moving Wall Box* (MWB) task (*see submitted manuscript* 'Differential involvement of the endocannabinoid system in the regulation of behavioral inhibition.', Appendix 5.4.3). In brief, during the MWB task the animals were forced by a slowly (2.3 mm/s, maximal for 60 seconds) moving wall to repeatedly (10× per session, 1 minute in between each trial) jump over a small ice-filled container (W14×H3×D10 cm). Two measures for the level of behavioral inhibition are determined: (1) the latency

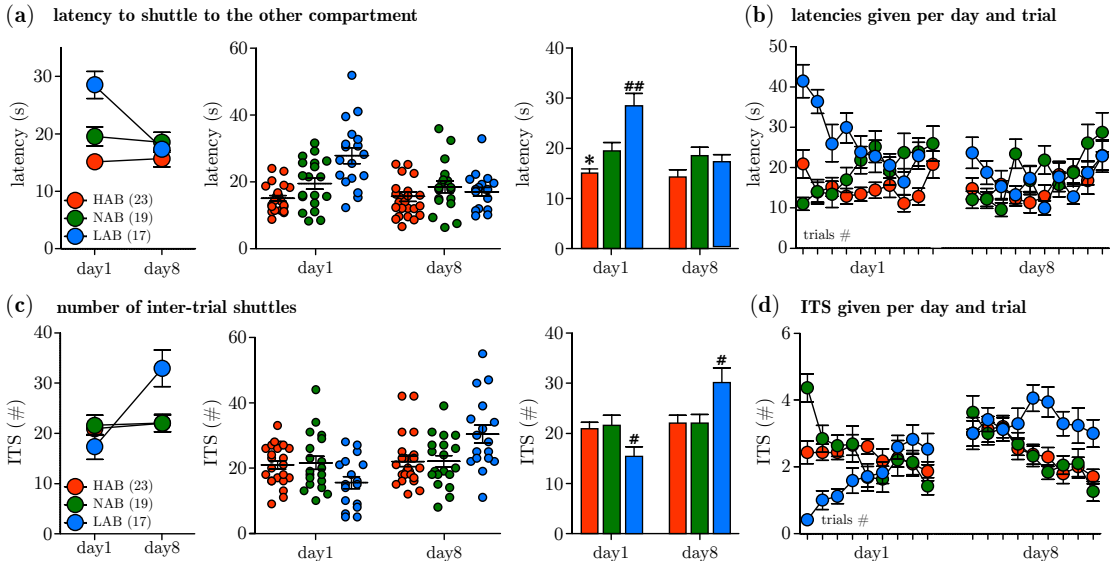

Figure 3.6 | Assessment of Fear Coping Strategies in HAB, NAB and LAB Mice using the *Moving Wall Box* (MWB) Task
(**a**) Latencies determined during the MWB task for HAB (N=23), NAB (N=19) and LAB (N=17) animals given per testing day. (**b**) Latencies given per testing day and trial. (**c**) Inter-trial shuttles given per testing day. (**d**) Inter-trial shuttles given per testing day and trial. Significance values, obtained by two-tailed, unpaired t-tests, are given by asterisks for HAB vs. NAB comparisons and hashes for LAB vs. NAB comparisons. * p<0.05, # p<0.05, ## p<0.01. Values are given as mean±SEM.

to shuttle to the other compartment and (2) the number of inter-trial shuttles. To assess possible habitual components the MWB task was conducted two times with one week between the sessions. Figure 3.6a shows the latencies for all three lines per testing day. On the first testing day NAB animals needed 19.5±1.7 s, while HAB animals needed less time (15.1±0.5 s, t-test, t_{40}=2.482, p=0.017), LAB animals shuttled after 28.6±2.4 s (t-test, t_{34}=3.196, p=0.003). These differences were not observed at the second testing day. A fast learning effect was present in LAB animals (Fig. 3.6b) on day 1 during the first 3 trials. Looking at the inter-trial shuttles (ITS) shown in figure 3.6c, it is evident that while HAB and NAB animals showed comparable behavioral responses on both testing days (HAB day 1: 21.0±1.3 #; HAB day 2: 22.0±1.8 #; NAB day 1: 21.6±2.0 #; NAB day 2: 22.0±1.8 #), LAB animals shuttled less on day 1 (15.6±1.8

#, t-test, t_{34}=2.196, p=0.035, compared to NAB) but the level of ITS was strongly increased on day 8 (30.4±2.7 #, t-test, t_{34}=2.59, p=0.014, compared to NAB). Figure 3.6d shows the temporal development of ITS during the sessions. On day 1 LAB animals showed strongly increased levels of behavioral inhibition, indicated by minimal numbers of inter-trial shuttles during the first 3 trials.

3.7 Contributions

Here I want to emphasize that parts of the before mentioned results, namely the EPM and IndyMaze data, has been included in similar form in the unpublished master thesis of Nina Scheithauer (Scheithauer, 2016). Ms. Scheithauer conducted those experiments under my supervision and with my help, whereas cannula implantations, muscimol and virus intracerebral injections were performed only by myself. Intraperitoneal CNO injections were performed either by Dr. Andreea Bura-Simona or myself. The idea for the IndyMaze (also called Mouse Anxiety Fear Inhibitory Avoidance Task, MAFIA) is based on the Moving Wall Box and was therefore conceived by PD. Dr. Carsten T. Wotjak and myself. Histological analysis of HAB and LAB animals was performed by Daniel E. Heinz under my supervision and with my help during his laboratory internship. Animal behavior was scored by Paul M. Kaplick who was hired as a student assistant to aid unbiased offline behavioral analysis. The MEMRI data has been generated and analyzed by Dr. Benedikt T. Bedenk and Dr. Michael Czisch. The Robocat paradigm was conceived by PD. Dr. Carsten T. Wotjak, Caitlin J. Riebe and Dr. Sebastian F. Kaltwasser and experiments were conducted by Ms. Riebe and Dr. Kaltwasser. Further help with setting up the EPM test and especially the ANY-maze behavioral tracking software was provided by Markus Nussbaumer. In addition Ms. Scheithauer also performed the MWB experiments with HAB, NAB, LAB animals.

Keep thy tongue from evil, and thy lips from speaking guile.

Psalm 34:13 (KJV)

Chapter 4

Discussion

The main hypothesis of this study was that complex behavioral readouts which apparently involve the interplay of higher brain regions are modulated to a substantial degree by midbrain structures. More specifically, the question was whether different levels of anxiety-like behavior in mice can be explained by altered neuronal activity within brain areas, which mediate innate fear responses and are typically considered to act as mere behavioral output regions.

In this study I have shown that there is indeed a causal link between the anxiety-like phenotypes of two mouse-lines, which have been selectively bred for extremes in trait anxiety (HAB and LAB mice) and their respective midbrain (PAG and SC) neuronal activity. Further, two novel ethologically inspired testing paradigms (Robocat, IndyMaze) for the study of fear in mice have been developed. In combination with the additionally developed Moving Wall Box task, these tests allow for the first time a conclusive analysis of the fear reactions of HAB and LAB animals. Using optomotor response analysis, electroretinographic recordings as well as home-cage activity monitoring in combination with photoentrainment, I could demonstrate that LAB animals have a profound visual deficit (complete retinal blindness) which precipitates as a deficit to avoid an impeding threatening stimulus. But on top of this, these animals also have a decreased fear responsivity to e.g. tactile stimuli which could be reverted by pharmacogenetical activation of the SC. HAB mice, on the other hand, show strong fear responses in general, which is maladaptive in certain respects. A pharmacological inactivation of the dl/lPAG reverted these overshooting fear responses. I could further show, that while the level of fear in HAB mice is pathologically altered, the fear coping strategies are not affected and these animals are able to display the appropriate fear behavior towards different stimuli (flight vs. freezing). In order to foster paralleled extracellular in-vivo electrophysiological recordings combined with optogenetic inquiries in freely moving and behaving animals, I have further developed a low-cost motorized combined electrical and fiber-optic rotary joint which reduces the asset costs from €5000 for a commercially available solution (Doric Lenses Inc. AHRJ-OE_FC) to less than €600 for the proposed design.

4.1 HAB and LAB Mice are Model Organism for the Study of Anxiety

For this project it was important that a model organism or mouse model was used where both, increased and decreased levels of anxiety can be assessed. Moreover, both extremes should be compared to a common control and the level of anxiety must be constant over time to allow for repeated testing. With respect to pharmacological induced models, only systemic treatments would be reasonable, considering the question. In general pharmacologically induced models for anxiogenesis and anxiolysis, allow to titrate the dose towards the desired behavioral phenotype. Probably one of the most widely studied pharmacological anxiolytic treatments is the systemic administration of benzodiazepines like alprazolam, diazepam and chlordiazepoxide, and their anxiolytic effects in mice have been shown numerous times using behavioral assays like the EPM (Calzavara et al., 2005), open-field test (Siemiątkowski et al., 2000) and the DLB (Crawley, 1981). Using ethobehaviorally inspired testing paradigms like the mouse defense test battery (MDTB), even chronic administration of alprazolam has been shown to effectively ameliorate anxiety-like responses (Griebel et al., 1995). Benzodiazepines have been found to act as positive allosteric modulators of $GABA_A$ receptors through their high affinity towards a specific benzodiazepine binding site, located at interface between α/γ $GABA_A$ receptor subunits (*for review see* Rudolph and Knoflach, 2011 and Sigel and Steinmann, 2012). Where in the brain benzodiazepines exert their anxiolytic potential, is still a matter of debate. $GABA_A$ receptor subunits necessary for the binding of benzodiazepines ($\alpha1$, $\alpha2$, $\alpha3$, $\alpha5$ and $\gamma2$) have been found to be expressed also within subcortical areas (amygdala) and midbrain structures (PAG, SC) (Heldt and Ressler, 2007). However, it was suggested by Löw et al. (2000) that especially $\alpha2$ containing $GABA_A$ receptors mediate the anxiolytic properties of benzodiazepines, and the immunohistochemical detection of this protein only revealed weak to moderate expression within the PAG and SC, while in the amygdalar nuclei moderate to intense expression could be observed (Fritschy and Mohler, 1995).

A comparable anxiogenic effect could be achieved with the use of negative allosteric modulators (sometimes also referred to as inverse agonists) of the benzodiazepine binding site, like methyl β-carboline-3-carboxylate (β-CCM). β-CCM was shown to decrease the number of head-dippings in a hole-board task (Takeda et al., 1998) and increases the time spend in the dark compartment in a DLB task (Belzung et al., 1987) indicating an anxiogenic effect. However, there is no data about the chronic administration of β-CCM in mice. Another pharmacological model to induce both, anxiolysis and anxiogenesis which involves the endocannabinoid system was proposed by Rey et al. (2012). Here, the authors have used the CB_1 agonist CP-55,940 and found a dose-dependent shift from anxiolysis to anxiogenesis as demonstrated by a differential modulation of open-arm entries and active risk assessment within the EPM, as well as differentially changed values of head-dipping frequency in a holeboard task. However, several studies on the chronic administration of CP-55,940 in rats, reported changes in cannabinoid receptor mRNA levels (Rubino et al., 1994), a marked reduction in G-protein α-subunit

expression (Rubino et al., 1997) and increased CRH levels within the paraventricular and arcuate nucleus of the hypothalamus (Corchero et al., 1999). These side effects were observed with doses which were 8-20× higher than the maximal dosage used by Rey et al. (2012). Despite these interesting models, it is likely that pharmacologically altered states of anxiety are less stable over time and secondary effects would complicate the interpretation of the observed behavioral phenotypes. Therefore the use of different mouse strains which show an a priori altered level of anxiety or selective breeding lines seem to be the obvious choice. Despite the availability of genetically modified mutant mouse strains or conditional knock-outs, those models were excluded beforehand. As those models originate usually from mono-genetic manipulations, they are certainly interesting to study facets of anxiety, but cannot reflect the multi-genetic nature of anxiety disorders. Among the commonly used commercially available mouse strains (*for review see* Sartori et al., 2011a) most consistently A/J, BALB/c and DBA/J2 mice (Crawley et al., 1997; Bouwknecht and Paylor, 2002; Lad et al., 2010) have been shown to exhibit the strongest anxiety-related phenotype compared to C57BL/6 mice. Four mouse lines which have been associated with moderate to low levels of anxiety-related behavior, based on EPM and DLB measures, are the C3H (Griebel et al., 2000), C3H/HeJ (Bouwknecht and Paylor, 2002), CBA/J (Ducottet and Belzung, 2005) and FVB/N (Võikar et al., 2001; Bouwknecht and Paylor, 2002; Ducottet and Belzung, 2005). However, all four lines have been found to suffer from complete retinal degeneration and their low avoidance of brightly lid areas most likely arises from the inability to perceive luminance differences (Cook et al., 2001).
As visually impaired animals would not be suitable for most innate fear tasks, the use of selective breeding lines was favored. These lines typically originate from an outbred mouse strain, and mating pairs are selected from this heterogeneous population based on their behavior in a specific behavioral task which assesses the desired behavior. Among the small number of available selective breeding mouse lines for trait anxiety (*for review see* Sartori et al., 2011a) the by far most studied models are high anxiety-related behaving (HAB) and low anxiety-related behaving (LAB) mouse lines (Krömer et al., 2005). HAB and LAB lines were generated from the CD1 outbred strain, and the mating pairs were selected based on extreme behavior on the elevated plus maze (low open arm time vs. high open arm time). Unselected CD1 mice, which represent the mean of HAB and LAB and serve as a common control, have been bred in parallel and are therefore termed NAB (normal anxiety-related behaving) mice. This approach led after more than 50 generations to two very distinct and robust behavioral phenotypes, whereby HAB mice show a strongly reduced, and LAB mice a marked increased open arm time compared to NAB (Krömer et al., 2005; Bunck et al., 2009; Erhardt et al., 2011; Avrabos et al., 2013; Yen et al., 2013; Füchsl et al., 2014).

Based on these findings, the HAB, NAB and LAB mouse lines were selected for the purpose of this study. In order to reassess the anxiety-related phenotype of HAB, NAB and LAB mice, the EPM task was employed, but the testing duration was extended to 30 minutes. This approach even further unveiled the strong anxiety-related phenotype of

HAB mice as more than 45% of these animals did not enter the open arm at all, whereas LAB mice readily explored the open-arm with low latency, and NAB mice displayed an intermediate response with high variability. This bidirectionally altered anxiety phenotype was also present in all other EPM measures as well in the levels of active risk assessment. Interestingly, the treatment of HAB mice with diazepam (DZP, 1 mg/kg) did not show any anxiolytic effects in the classic EPM measures, but strongly affected the levels of active risk assessment. More specifically the pathologically non-habituating response profile of HAB mice treated with DZP resembled the habituating response of NAB animals. While there is evidence that DZP decreases ultrasonic vocalizations in HAB pups (Krömer et al., 2005), this is the first study which shows an anxiolytic effect in adults. It has to be noted that some studies report a consistent dose-dependent anxiolytic effect of benzodiazepines in inbred mouse strains in the EPM task (Rodgers et al., 1992; Cole and Rodgers, 1995; Holmes and Rodgers, 1999; Griebel et al., 2000). Others, however, fail to do so (Rodgers et al., 2002) and especially highly anxious mouse strains like A/J and BALB/c which might be comparable to HAB mice in certain aspects, seem to generally exhibit decreased benzodiazepine sensitivity in similar emergence-based behavioral tasks (Crawley et al., 1997). Taken together, based on the performance in the EPM task, the HAB and LAB animals can be considered to represent a valid model of extremes in anxiety-related behavior.

4.2 Assessing Fear Responses in HAB and LAB Mice

Next, the goal was to assess the innate fear responses of HAB, NAB and LAB animals. There is evidence that the changes in anxiety-related behavior are also accompanied by differences in conditioned fear responsivity indicated by an increase in cued and contextual fear in HAB mice, whereas LAB show the opposite response (Sartori et al., 2011b; Yen et al., 2012). However, only one study so far demonstrated increased levels of innate fear in HAB mice, using the 2,5-dihydro-2,4,5-trimethylthiazoline (TMT) odor avoidance task, whereby LAB animals showed no altered behavior (Sotnikov et al., 2011).
Behavioral assays which aim to query innate fear responses in rodents are typically employed in the field of panic research. Here, in contrast to fear & anxiety research, the important role of the brainstem areas, most prominently the PAG, is well accepted, not least due to the long history of electrical stimulation within the PAG, which can induce strong defensive reactions in cats (Spiegel et al., 1954; Hunsperger, 1956) and the feeling of imminent horror of death in humans (Nashold et al., 1969). Recent findings, however, have demonstrated that unconditioned avoidance responses evoked by electrical stimulation of the dPAG in rats are abolished if the BLA is lesioned or inactivated by muscimol (Kim et al., 2013). This indicates that the BLA is also a downstream target of the dPAG and there is evidence from retrograde tracing studies that the PAG sends direct projections towards the CeA (Ottersen, 1981; Rizvi et al., 1991). Therefore, it is justified to consider certain behavioral tasks for panic responses suitable to investigate innate fear responses in general. One of the

most frequently applied innate fear tasks is the elevated T-maze (Viana et al., 1994; Graeff et al., 1998), which simply consists of a regular EPM, whereby the entrance to one closed arm is sealed. By placing the animals either into the closed arm or the open arm one could assess inhibitory avoidance (a measure of anxiety-like behavior) or escape latency (a measure of panic-like behavior). The test has been shown to be repeatable and allows the assessment of inhibitory avoidance learning. Pharmacological validation of the involvement of important innate fear regulatory centers have been demonstrated by Bertoglio and Zangrossi (2005). Using local injections of the known panicogenic tetrapeptide cholecystokinin-4 (CCK) and the selective CCK_2 receptor antagonist LY-225910 into the dlPAG of rats, the authors could bidirectionally modulate the escape latency (Bertoglio and Zangrossi, 2005). While this task is certainly an invaluable paradigm for the validation of panicolytic drugs in rats and mice (Carvalho-Netto and Nunes-de Souza, 2004), due to its simplicity, it is insufficient to assess innate fear responses HAB mice, as those animals would simply choose to freeze on the open arm instead of seeking shelter immediately. Another more ethobehaviorally inspired task which avoids the shortcomings of the elevated T-maze, by reducing the controllability, is the mouse defensive test battery (Blanchard et al., 2003). In this test, mice are repeatedly confronted with a hand-held deeply anesthetized or freshly killed rat, and avoidance, flight or defensive aggression towards the rat are scored. Due to ethical reasons this task is not considered to be suitable, just as the exposure to life predators like snakes (Almada and Coimbra, 2015). Alternatives are tasks which utilize the exposure to a living rat, but limit direct contact and therefore prevent biting wounds (the rat exposure task Yang et al., 2004; Ribeiro-Barbosa et al., 2005). However, those tasks assess active-risk assessment, approach-avoidance conflicts and only undirected flight responses without the predator being present and therefore still exert a high degree of controllability. In order to equally expose high and low anxious animals to a threatening situation, the animals should not be allowed to control the encounter. Moreover, in order to cover auditory, tactile and visual sensory modalities the test should incorporate a direct confrontation with an approaching threatening stimulus. Choi and Kim (2010) have implemented such a behavioral paradigm by placing a Lego Mindstorms robot (what they termed the Robogator), equipped with movement detectors within a large arena, behind a food pellet. Food deprived rats than were asked to forage the *guarded* food pellet. Once the rats approached the food pellet, the robot was automatically activated and moved towards the animal which subsequently displayed a pronounced flight response. Further, Choi and Kim (2010) could show that this flight response is completely abolished once the amygdala was inactivated. This behavioral paradigm seemed ideal for the purpose of this study. As the natural exploratory drive of mice is sufficient to motivate them to enter the arena, food-depriving the animals prior to the experiment was unnecessary. In order to render our behavioral paradigm distinguishable from the original description, it was termed the Robocat task. Using this task, the strongly increased fear responses of HAB mice were evident, as they always retrieved upon the activation of the Robocat. Further, HAB mice were unable to bypass the activated Robocat and therefore their fear response can be termed maladaptive, as in this case they would be unable to evade an

impeding threat. On the contrary LAB animals never showed any fear responses towards the Robocat at all, but were highly tolerant to its movements. In addition, almost all LAB animals collided at least once with the moving robot. The common comparator strain NAB showed intermediate levels of flight and collision but high levels of tolerance as theses animals simply bypassed the robot. The possibility to bypass the moving threat, however, brings the difficulty about to differentiate between the inability to perceive the threat and the inability to express an appropriate fear response. In order to overcome this shortcoming the IndyMaze task was developed. This task demonstrated that all HAB and NAB animals are able to either show a preemptive flight response or retrieve to the home compartment once they came in contact with the ball, but the minority of LAB animals were able to do so.
As a third task to evaluate the different fear coping strategies of HAB, NAB and LAB animals, the Moving Wall Box task was applied. In this paradigm it could be observed that HAB animals have slightly decreased latencies to shuttle to the other compartment but unaltered levels of inter-trial shuttles. This leads to the conclusion that besides their generally increased levels of fear, assayed by the various fear & anxiety paradigms, HAB animals do not differ in their fear coping style. HAB animals rather respond with extreme levels of fear but display the appropriate fear behavior, e.g. they do not freeze in front of the Robocat but have an increased preposition to flee. Regarding the fear behavior in HAB mice, no study so far looked at active fear coping styles. The results in this thesis obtained by the Robocat, IndyMaze, MWB task as well as the recently published observations that HAB mice have a high disposition to actively avoid an erratic moving robo-beetle (Heinz et al., 2017), show for the first time that HAB animals possess an intact fear response selection, but show a pathologically altered level of fear. This renders these animals an ideal model organism for the study of fear.

The behavior of LAB animals assessed in the MWB task, however, gave inconclusive results. It was expected that these animals have decreased latencies to shuttle and increased numbers of inter-trials shuttles. But especially on the first testing day, LAB animals behaved in the opposite way and one could interpret this as a strongly increased level of behavioral inhibition or a shift towards passivity. This observation stands in steep contrast with the results obtained in the Robocat and IndyMaze task and also contradict previous reports of the LAB animals hyperactive phenotype (Yen et al., 2013)(*see also manuscript in press* 'A simplified microwave-based motion detector for home cage activity monitoring in mice', Appendix 5.4.1, figure 5.5d). However, at the second testing days, the formerly increased latencies normalized to control level, but the number of inter-trial shuttles increased, which indicates that either adaptation or learning processes took place. The inconclusive results of LAB animal behavior in the MWB task are most certainly explained by the visual deficits of these animals (*see* next section). Using the Robocat and IndyMaze task it was shown for the first time that differences in anxiety-like behavior are accompanied by differences in fear responsivity in HAB and LAB mice. Whether altered levels of fear account for the changes in anxiety-like behavior in a causative manner, cannot be reasoned from these observations.

4.3 Visual Deficits of LAB Mice

Before the causal link between fear and anxiety was investigated, the deficit of LAB mice to avoid an impeding threatening stimulus posed the question whether these animals can perceive moving objects adequately. A suitable task to measure the ability to translate moving visual stimuli into motor behavior, seemed to be the *rotating drum* which assesses the optomotor response. First, the results of this behavioral paradigm showed that the pigmented C57BL/6 mice outperformed all albino mice by far, but whether this performance deficit of the non-pigmented animals is due to decreased visual acuity or simply an altered disposition to show the motor behavior cannot be deduced from only one visual grating. Second, among the albino mice, LAB animals failed to respond to the moving stripes. This visual deficit was further analyzed using flash-evoked electroretinographic analysis. The fERG measures showed a complete absence of any retinal response in LAB mice, whereas C57BL/6, CD1, HAB and NAB displayed normal ERGs, indicating that LAB animals lack a functional retina. Indeed the histological investigation of the retinal sections revealed the absence of the photoreceptor layer in LAB mice, and PCR analysis confirmed that LAB mice are positive for a mutation within the rod cGMP-specific 3',5'-cyclic phosphodiesterase subunit beta ($Pde6b^{rd1}$) indicative of the eye disease called *retinal degeneration 1*. The fact that LAB mice are blind, most likely accounts for the decreased aversion of the open arm, and it was shown previously that if the EPM task is carried out in complete darkness, rats spend more time on the open arm compared to 2 lux background illumination (Garcia et al., 2005). The retinal degeneration in LAB animals also accounts for the inconclusive results obtained in the MWB task. Further, it explains the high average latency observed in LAB mice to exit the home compartment in the IndyMaze task.

Similar observations in the elevated zero-maze have been reported for C3H/HeJ, CBA/J and FVB/NJ mice which all suffer from retinal degeneration (Cook et al., 2001). While the levels of conditioned fear (auditory fear conditioning) of C3H/HeJ, CBA/J and FVB/NJ mice are within the normal range (Bolivar et al., 2001), LAB mice show a strongly decreased response (Sartori et al., 2011b; Yen et al., 2012). The decreased freezing levels of LAB mice might be explained by altered hearing capabilities, but acoustic startle measure in fact showed an increased startle response in LAB mice (Yen et al., 2012; Yen et al., 2013). Alternatively, LAB mice might exhibit an elevated pain threshold which renders them insensitive to tactile stimuli. However, repeated tone-footshock pairings (20 s, 9 kHz, 80 dB tone co-terminated with 1 s, 0.7 mA electric footshock, not to be confused with startle pulses) with paralleled movement measurements (Yen et al., 2012) showed a clear perception of the noxious stimuli. This suggests that LAB mice, despite being blind, have in addition a deficit to respond adequately to fearful stimuli. This notion is further substantiated by their behavior in the IndyMaze task, as even after the ball had physical contact with the animals, the majority of LAB mice failed to show a flight response. Therefore it is likely that LAB mice exhibit a deficit in the central processing of tactile fear evoking stimuli.

4.4 Midbrain Areas of HAB and LAB Mice Exhibit Altered Neuronal Activity

The differences in trait anxiety among HAB, NAB and LAB animals might be reflected by tonic changes in brain activity during basal conditions. So far only a single study attempted to map neuronal activity markers in HAB, NAB and LAB mice (Muigg et al., 2009). But the authors challenged the animals by forcing them to reside on the open arm of the EPM, and therefore focused on the expression of the immediate early gene *cFos* which typically integrates phasic neuronal changes. However, all three lines showed significantly increased cFos levels in limbic structures compared to baseline conditions, whereby HAB animals generally exhibited higher expression than NAB animals (except dentate gyrus, PVN, anterior hypothalamic area, vlPAG). LAB animals showed decreased expression within the PVN, anterior hypothalamic area and medial preoptic area compared to NAB. In order to asses the tonic activity changes, MEMRI measurements were employed similar to a study by (McGuire et al., 2013) where the authors identified differentially regulated regions within the limbic system in a selective breeding mouse line for susceptibility and resistance to contextual fear expression.
Using the MEMRI approach a significantly increased manganese accumulation was found in the dl/lPAG/vlPAG of HAB mice and a decreased accumulation within the the motor related areas of the SC of LAB mice. The vlPAG has been implicated in the generation of conditioned and unconditioned freezing behavior as well as in the regulation of cardiovascular tone (Zhang et al., 1990; Kim et al., 1993; De Oca et al., 1998; Morgan and Carrive, 2001; Vianna et al., 2001; Walker and Carrive, 2003; Tovote et al., 2016) in cats, rats and mice. So far it has been only shown that altered activity in the dl/dmPAG relates to altered anxiety-related behavior, assessed by the EPM task (Guimarães et al., 1991; Graeff et al., 1993; Kincheski and Carobrez, 2010).
The PAG, in general, is the most critical brain structure for gating vocal control in squirrel monkeys (*for review see* Jürgens, 2009), and electrical stimulation studies in guinea pigs (Kyuhou and Gemba, 1998; Sugiyama et al., 2010) confirmed that also in rodents especially the lPAG mediates sonic vocalization.

The SC integrates visual, auditory and somatosensory (tactile) information (Meredith and Stein, 1986) in order to guide visual attention and control reflexive visually-guided saccades (Pierrot-Deseilligny et al., 1991), and ultimately mediates predatory pursuit and hunting (Furigo et al., 2010). Further, a recent study (Wei et al., 2015) has reported a CaMKIIα-positive population of neurons within the intermediate layers of the SC in mice, which when activated elicits freezing. Therefore the SC is ideally suited to process threatening visual (Shang et al., 2015) and tactile stimuli in order to generate an immediate behavioral response.

4.5 Increased Neuronal Activity within the SC of LAB Normalizes Anxiety and Fear Responses

For the purpose of establishing a causal link between the hypoactive SC in LAB mice and their fear response deficit, the recently established *designer receptors exclusively activated by designer drugs* (DREADD) approach (*for review see* Sternson and Roth, 2014; Urban and Roth, 2015; Roth, 2016) was utilized. The application of DREADDs for the modulation of brain stem targets has been successfully demonstrated earlier (Silva et al., 2013; Silva et al., 2016; Franklin et al., 2017). However, here the authors have used local injections of the DREADD-specific ligand clozapine-*N*-oxide (CNO) within the PAG to accomplish projection-specificity. Recent findings heavily question the biological activity of CNO (Gomez et al., 2017). It was observed that DREADDs do not bind CNO and the activation of DREADDs is explained by the bio-conversion of CNO to the atypical antipsychotic clozapine, which has been found to bind to the DREADDs with high affinity. In oder to exclude any non-specific behavioral effects due to clozapine, it is therefore necessary to include CNO/clozapine treated controls in every DREADD experiment. This has been done in this thesis.

In this study, increasing the neuronal activity in CaMKII$^+$ neurons within the SC, resulted in an increased anxiety-like behavior as assessed by the EPM task and a marked increase in fear responsivity as shown by the IndyMaze paradigm. The anxiogenic nature of the SC stimulation did not only cause the animals to be simply more passive in the EPM task but also increased the amount of active risk assessment. Similar observations have been made in rats using the elevated zero-maze and systemic administration of the known anxiogenic substance *m*-chlorophenyl-piperazine (mCPP) (Shepherd et al., 1994). A role of the SC in modulating anxiety-like behavior (elevated T-maze, avoidance) has been already suggested by de Almeida et al. (2006), as electrical stimulation of the SC, 5 minutes prior to testing, resulted in an increased latency to access the open arm. In summary it was shown that the pharmacogenetical modulation of a multisensory integration center within the brain stem alters complex behavioral responses and even has the potential to revert extreme and pathological behavioral phenotypes.

4.6 Decreased Neuronal Activity within the PAG of HAB Normalizes Anxiety and Fear Responses

For the purpose of establishing a causal link between the hyperactive PAG in HAB mice and their maladaptively increased levels of fear, local injections of muscimol (MUSC) and fluorescently labeled muscimol (fMUSC) at doses of 10 ng per hemisphere into the dl/lPAG were applied. Histological analysis revealed that the MUSC also diffused slightly into neighboring brain areas like the dPAG, the deep layers of the SC as well as parts of the vlPAG. Muscimol is a selective $GABA_A$ agonist and when locally infused into the brain, effectively suppresses neuronal activity (Morin et al., 2001;

Holahan and White, 2004) by mimicking increased GABAergic signaling. Muscimol infusion into the dl/lPAG of HAB animals caused strong anxiolytic effects as assessed by the EPM, but also increased locomotor activity. In addition the levels of active fear coping behavior were markedly decreased, showing again a reduction in anxiety-like behavior. Further, fMUSC treatment completely abolished sonic vocalization in HAB animals. The strong increase in locomotor activity upon MUSC treatment (17.6±2.2 m vs. 8.0±1.2 m VEH), which was even higher than the basal activity of naïve LAB mice (14.0.0±1.7 m), might suggest a non-specific panicogenic effect which is commonly associated with d/dlPAG stimulation by excitatory amino acids (EAA) (da Silva et al., 2006). But it has to be noted that the electrical stimulation of the d/dlPAG, first induces alertness and immobility followed by panic-like behavior in a gradual manner. Therefore an inhibition of the d/dlPAG immobility circuits might precipitate in an increased locomotor activity. However, de Menezes et al. (2006) used muscimol injections of similar concentrations into the d/dlPAG of naïve rats and reported no change in locomotor activity and Bueno et al. (2005) even demonstrated panicolytic effects in the elevated T-maze upon dPAG MUSC infusion. But further, the inhibition of the dPAG by MUSC was shown to reduce conditioned freezing and inhibit the expression of fear-potentiated startle (FPS) responses (Reimer et al., 2008). Also MUSC injections into neighboring brain structures like the SC in naïve rats, do not cause an increased locomotor activity (Imperato and Di Chiara, 1981) but reduce the levels of FPS (Meloni and Davis, 1999). Using local infusions of the benzodiazepine midazolam or muscimol into the dmPAG Bueno et al. (2005), reported no change in avoidance in the elevated T-maze task, while Motta and Brandão (1993) showed a decreased aversion of the open arms in the EPM task upon local infusion of muscimol into the dlPAG.

Interestingly, Walker and Carrive (2003) found that rats which underwent an auditory fear-conditioning paradigm and received muscimol injections into the vlPAG showed an unusual high amount of activity during the re-exposure to the shock-context but also once the animals have returned to their home cage. Further they observed a complete absence of the otherwise typical 22-kHz distress calls during the re-exposure to the shock-context. The authors explain the increased locomotor activity with an inhibition of the vlPAG immobility circuit (*see* Tovote et al., 2016). However, they cannot explain the inhibition of the ultrasonic vocalization as they exclude a possible diffusion from the vlPAG to the lPAG, a region which is considered to gate vocalization in mammals. Also Tovote et al. (2016) could demonstrate, using optogenetic inhibition of glutamatergic vlPAG→medulla projecting neurons, that this circuit does not generate activity in naïve animals, but effectively reduces immobility if the animals are confronted with an imminent threat or a conditioned context. In addition, De Luca-Vinhas et al. (2006) showed, using local infusion of midazolam, that increasing the GABAergic drive within the vlPAG increases locomotor activity on the EPM, but does not affect avoidance behavior (unaltered entries to the open arm). The vlPAG immobility circuit is typically associated with total quiescence, tonic immobility or freezing (e.g. during conditioned fear responses) while the d/dlPAG is considered to mediate predominantly sensory and affective aspects of unconditioned immobility (e.g. during an approach-avoidance conflict)

as well as active defensive responses (Brandão et al., 2008). Despite the fact that HAB mice show strongly increased levels of fear, the mechanisms to select the appropriate fear coping strategies (but not the level) are intact. Given the evidence shown above, it is therefore concluded, that the anxiolytic effects (decreased open arm avoidance) of MUSC infusion in the PAG of HAB mice can be attributed to the inhibition of the d/dl-PAG fear promoting circuits. As naïve HAB mice possess heightened fear responsivity, a strongly increased arousal level can be inferred in the context of the EPM or innate fear paradigms mentioned before. The marked increase in locomotor activity upon MUSC treatment might therefore be due to an inhibition of the immobility promoting circuits within the d/dlPAG which seem to be disproportionately recruited in HAB animals. Alternatively the increase in locomotor activity can be explained by a diffusion of MUSC into the vlPAG, which however, given the extent of the fluorescently labeled MUSC, seems unlikely. The absence of vocalization during the tail-suspension test is most likely due to an inhibition of the dl/lPAG vocalization areas (Jürgens, 2002) which mediate forebrain induced vocalization (Siebert and Jürgens, 2003). However, the absence of vocalization as a secondary effect due to an inhibition of the active fear response promoting areas in the d/dlPAG, can not be excluded.

4.7 Summary

In this thesis it was shown, using semi-naturalistic and ethobehaviorally inspired testing paradigms, that anxiety and fear are closely related in the HAB-NAB-LAB mouse model. Further, it was demonstrated that apparent complex behavioral phenotypes (anxiety) are governed, or at least modulated to a very large extent, by developmentally ancient brain structures. The experimental manipulation of neuronal activity within the PAG and SC was sufficient to revert the extremes in anxiety-like behavior in HAB and LAB animals. It can be argued that the induced anxiogenesis in LAB mice and the anxiolysis in HAB mice are simply the product of a changed locomotor activity. But the opposite change in active risk assessment (SAP) in both cases, strongly contradicts this notion. These unequivocal findings can be explained by two possible scenarios: modulating the neuronal activity within SC and PAG (a) changes the valence/imminence of the sensory cues or (b) directly affects fear response circuits.

In the case of LAB animals, an altered value of sensory cues would change the aversiveness of the longitudinal arena and the styrofoam ball in the IndyMaze task as well as the aversiveness of the open arms in the EPM. As mentioned earlier, the electrical stimulation of the SC (similar to the pharmacogenetic activation of the SC in LAB) elicits defensive responses (Sahibzada et al., 1986; Dean et al., 1988) but also cardiovascular changes (Dampney, 2015) which resemble the bodily changes in states of high fear. However, to my knowledge there are no studies on the direct inhibition of the SC (which would mimic the situation in naïve LAB animals) in the context of fear responses and/or cardiovascular control, which could serve as an indirect measure of autonomic

arousal. Another indirect measure measure of autonomic arousal is the acoustic startle amplitude (Kokkinidis and Anisman, 1977). But it was shown that an excitotoxic lesion of the superficial layers of the SC or enucleation (removal of the eyes) does not affect the baseline startle amplitude in rats (Tischler and Davis, 1983; Fendt et al., 1994) while a lesion to the deep layers of th SC slightly increases baseline startle responses (Tischler and Davis, 1983). Interestingly, fear potentiated startle was strongly increased after a lesion to the superficial layers of the superior colliculus (Tischler and Davis, 1983). In the context of the acoustic startle response, the strong hypo-activity within the inferior colliculus (IC) of LAB animals (*see* Appendix 5.3 'MEMRI Data set', Fig. 5.1) as well as the area ventral to the SC and lateral to the PAG (sometimes referred to as 'lateral tegmental group', 'lateral tegmental tract' or 'midbrain reticular nucleus') has to be noted. While lesions to the IC only slightly increase ASR levels, electrolytic but not excitotoxic (NMDA) lesions to the lateral tegmental group (LTG) strongly increase ASR levels and in addition decrease conditioned freezing responses (Leaton and Brucato, 2001; Leaton, 2003). This suggests a possible involvement of the IC (projecting towards the SC) in the generation of the startle phenotype of LAB mice. Further, the electrolytic lesions of the fibers within LTG in this study also affected the ventral parts of the motor related deep layers of the SC which is known to project towards the pedunculopontine tegmental nucleus (PPT) − the major site of prepulse inhibition (Steininger et al., 1992; Koch and Schnitzler, 1997). A lesion of the PPT is associated with a potentiation of the baseline startle amplitude (Swerdlow and Geyer, 1993). The fact that LAB mice show a decreased manganese accumulation in all brain areas which mediated prepulse inhibition of the startle response (IC, SC and LTG) might explain the increase in baseline startle amplitude observed in these animals.
With respect to fear responses mediated by the SC it was demonstrated that upon the optogenetic activation of the inhibitory GABAergic nigrotectal pathway (SNr→SC), innate fear responses are attenuated as evident by a decreased threat detection (*see submitted manuscript* 'Nigrotectal pathway controls threat detection at the level of the superior colliculus', Appendix 5.4.4). LAB animals show decreased fear & anxiety responses in general, whereas the level of acoustic startle responses (Yen et al., 2012; Yen et al., 2013) are elevated. This phenotype can be explained well with the above-mentioned observations, and therefore it is concluded that the pharmacogenetical manipulation of the SC in LAB mice most likely reversed the hypo-functionality in naïve animals via changing the valence of the multisensory afferents. Whether the reduced activity within the SC is a direct result of the selective breeding for low open-arm avoidance in the EPM task and to which extent the complete retinal blindness accounts for this neurological condition, cannot be conclusively assessed at this point. But the retinal degeneration is a confounding factor for further experiments, which is the reason why the breeding of the LAB mouse line has been stopped and to my knowledge there are no other breedings of this line.

HAB animals on the other side consistently display the appropriate behavioral response (e.g. freezing vs. flight) if confronted with a specific stimulus (e.g. conditioned

tone vs. Robocat), but in an exaggerated manner. Further, a general non-specific hyper-reactivity towards fear provoking stimuli or an altered pain perception can be excluded as these animals do not show abnormal freezing levels during the acquisition of an auditory conditioned fear memory (five repetitive CS-US pairings) (Sartori et al., 2011b). Even if the animals are placed 24h after the conditioning in a different context, the baseline freezing levels (in the absence of the CS/tone) are indistinguishable from NAB controls (Sartori et al., 2011b; Yen et al., 2012). HAB animals do not suffer from any visual/auditory sensory deficit. Therefore it is assumed that in naïve HAB animals, the direct (e.g. retina→SC and spinal cord→PAG) or indirect (SC/IC→PAG) neuronal pathways which convey sensory information to the midbrain defensive circuits are functional. Consequently, abnormal sensory perception or its first-order evaluation (IC and SC) can be excluded to constitute the cause of the HAB phenotype. Much more likely and also indicated by the increased manganese accumulation, is an increased recruitment of the periaqueductal gray. This study aimed on purpose to investigate the role of the dorso-lateral and lateral parts of the PAG as it would have been technically challenging to pharmacologically modulate the vlPAG without affecting superficial structures. The local infusion of MUSC completely reversed the anxious phenotype observed in the EPM in naïve HAB animals. Further, MUSC infusion abolished sonic vocalization during the TST. These effects are mediated via an inhibition of the local defensive (Brandão et al., 2008) and vocalization (Kirzinger and Jürgens, 1991) circuits found within the d/dlPAG and dl/lPAG. But based on these findings, the question whether the observed hyperactivity of the PAG is due to an increased *fear state signaling input* or due to an intrinsic dysregulation at the level of the PAG cannot be answered. However, it can be argued that, while in the anxiety parameters *latency to enter the open arm/arena* HAB animals have extremely high levels, they still enter these compartments eventually, which indicates a certain level of plasticity. Whether the PAG is the site of this adaptive process is unknown, but there are reports which demonstrated that the endocannabinoid (eCB) system, a major regulator of neuronal plasticity, is directly involved at the level of the dlPAG in the context of stress-induced analgesia (Hohmann et al., 2005). Further, the local infusion into the dlPAG of the CB_1-selective agonist arachidonyl-2-chloro-ethylamide (ACEA) at low doses increased the threshold for for panic-like response induced by electrical stimulation within the dlPAG (Casarotto et al., 2012).

Alternatively, afferent projections towards the PAG can undergo different forms of plasticity which has been described in the case of central amygdala(CEA)→vlPAG projection for long-term potentiation(LTP)-like processes (Adamec et al., 2005). Among the many afferents to the dl/lPAG (Dujardin and Jürgens, 2005), I will only briefly discuss the possible involvement of the anterior cingulate area (ACA) and the lateral septum (LS) in the specific phenotype of HAB animals. In the context of vocalization, the anterior cingulate cortex and its strong glutamatergic (Beitz, 1989) projections towards the dlPAG (Bandler and Shipley, 1994) is of great importance. While the ACA is commonly associated with the affective component of pain (Johansen et al., 2001), several studies have shown that the electrical stimulation of the ACA in squirrel monkeys and guinea pigs results in vocalization (Jürgens and Müller-Preuss, 1976;

Kyuhou and Gemba, 1999). But is has to be noted that lesions to the ACA in monkeys only abolish the expression of learned vocal calls but leave spontaneous calls unaffected Kirzinger and Jürgens (1982), which suggests that the ACA in monkeys mediates the volitional control of vocalization. Zugaib et al. (2014), however, demonstrated that combined local infusion of the NMDA receptor antagonist MK-801 and MUSC within the ACA transiently abolishes shock-induced vocalizations in restraint guinea pigs. Further, MacLean (1985) noted that after the ablation of the anterior cingulate cortex in young monkeys, the typical 'cry'-like calls were abolished when the animals were separated from their mothers. This close relation between distress vocalizations and the affective state of pain was comprehensively conceptualized by Panksepp (2010) to form the GRIEF/PANIC-separation-distress primary-process emotional system. So far the exact function of the ACA→PAG projection has not been assessed, and to which extent this projection accounts for the HAB phenotype remains speculative. However, the results obtained from the MEMRI measures do not suggest an increased neuronal activity within the ACA of HAB mice. But it is important to remember that the MEMRI approach holds a certain bias towards projection terminals.

The lateral septal region (LS), on the other hand, shows marked manganese accumulation in HAB animals (*see* Appendix 5.3 'MEMRI Data set', Fig. 5.1) and is known to project towards the PAG (Blume et al., 1982; Marchand and Hagino, 1983; Staiger and Nürnberger, 1991). Further, immediate early gene expression studies, revealed an increased activation of the ventral and intermediate LS in HAB mice compared to NAB if the animals are forced to stay on the open arm of the EPM (Muigg et al., 2009). In the context of vocalization, the LS does not seem to have a predominant role, however, Jürgens et al. (1967) noted the occurrence of *peep* calls in squirrel monkey upon electrical LS stimulation. The LS receives strong projections from the ventral part of the hippocampus and these projection have been found to act in a serial manner to promote open-arm avoidance in the EPM task in rats (Trent and Menard, 2010). What effect a stimulation of the LS→PAG projection has on animal behavior has not been assessed so far. Inactivation studies of the LS using MUSC, however, revealed a decreased fear response towards TMT, the repelling ingredient in fox-odor (Endres and Fendt, 2008), which fits well to the increased response to TMT in HAB animals (Sotnikov et al., 2011).

Another important neural circuit controlling the expression of defensive responses is the medial hypothalamic defensive system (MHDS) (Canteras, 2002; Gross and Canteras, 2012), which is comprised by the anterior hypothalamic nucleus (AHN), the ventromedial hypothalamic nucleus (VMH), the medial preoptic nucleus (MPN) as well as the dorsal premammillary nucleus (PMD). The AHN, VMH and dorsal PMD (PMDd) send strong projections towards the dlPAG, while the PMDd and AHN in addition innervate the dmPAG, lPAG and vlPAG (Vianna and Brandão, 2003). Various kinds of defensive responses can be elicited from all of these structures. For example, the electrical stimulation within the medial hypothalamus induces vocalization in guinea pigs (Kyuhou and Gemba, 1998). In HAB animals, the AHN and VMH have been found to show increased c-Fos expression upon forced open-arm exposure (Muigg et al., 2009). Most brain areas

within the MHDS exhibit recurrent connections which poses a high level of complexity, and discussing the possible involvement of all of these areas in the context of the HAB phenotype is beyond the scope of this thesis.

4.8 Outlook

In the following I will suggest several experiments which are necessary to complement the main findings of this thesis, and further, should lead to a better understanding of the HAB high-anxiety phenotype.

(1) Transient inactivation of the dl/lPAG in the context of innate fear responses
So far MUSC treatment was only shown to be effective in the EPM task and the TST. But it is necessary to show in addition its effect on innate fear responses evoked in the IndyMaze task. Moreover, it is important to include a NAB control group, to see whether the increased locomotor activity observed in HAB animals is specific.

(2) Combined retrograde tracing from the dl/lPAG and c-Fos immunohistochemistry in the context of the TST
In order to identify the afferents towards the dl/lPAG and investigate their responsiveness to the TST, fluorogold injections into the dl/lPAG followed by a TST (after five days) and the subsequent immunohistochemical analysis of c-Fos (immediate early gene) expression, will be carried out. This allows to answer the following questions: Which brain areas projects towards the dl/lPAG? How strong is the projection? What is the percentage of c-Fos$^+$ cells projecting towards the dl/lPAG?

(3) In-vivo electrophysiological assessment of the dl/lPAG and dl/lPAG afferents during vocalization
The high disposition to vocalize, which was shown to be decreased by anxiolytic treatment, poses a promising readout to investigate the involvement of different brain structures in the precipitation of the HAB phenotype. In-vivo extracellular electrophysiological recordings within the dl/lPAG or in afferent brain structures during the TST, allow the correlation with neuronal activity to the temporally precise vocalization onsets. The activity from direct mono-synaptic projections towards the dl/lPAG from remote areas (ACA, LS) will be investigated by optogenetically evoked antidromic action potentials and collisions. For these experiments, 350 nl of a neuron-specific viral vector encoding for channelrhodopsin (AAV5-hSyn-ChR2-EYFP) will be injected bilaterally into the afferent structure. After 3 weeks, an optrode (consisting of 15 single tungsten wire electrodes, one reference and one GND electrode as well as an optic fiber) will be implanted unilaterally into the afferent structure and in addition two optic fibers will be implanted into the dl/lPAG. This allows (a) to investigate whether the projection transverses to the other hemisphere (antidromic action potentials) and (b) to activate these projections

and analyze their potential involvement in evoking vocalizations.

(4) In-vivo electrophysiological assessment of the dl/lPAG and dl/lPAG afferents during innate fear

In recent work (Heinz DE & Genewsky A & Wotjak CT, 2017, *in press*) it was observed that HAB mice show an increased avoidance towards an erratically moving robot-beetle. During a 10 minute robo-beetle task (BEETLEMANIA) the animal is confronted up to 50× with the semi-naturalistic threat and displays flight and approach behavior. A modified version of this task (*see* Appendix 5.4.2, Fig 5.9) in combination with a custom-built motorized combined electrical and fiber-optic rotary joint (*see* manuscript in preparation, Appendix 5.4.2, 'A low-cost motorized combined electrical and fiber-optic rotary joint for physiological recordings.') allows to analyze correlated neuronal activity within the dl/lPAG as well as in afferent brain structures during escape (accelerometer on head-mounted preamplifier/headstage) and approach behavior as well as neuronal activity with respect to the distance to the robo-beetle. The experimental approach is identical to experiment 3.

(5) Optogenetic inhibition of afferents do the dl/lPAG originating from the MHDS during innate fear and vocalization

In their seminal publication Wang et al. (2015) could demonstrate that neurons within the VMH send collateral projections towards the PAG as well as to the AHN, which when activated separately mediate different aspects of defensive responses (immobility vs. avoidance). Therefore an optogenetic activation of the terminals of PMD→PAG projecting neurons without prior knowledge of the circuitry is prohibited. Circuit analysis will be undertaken by multiple injections of different retrograde tracers (Fluorogold and FastBlue in combination with a red nuclear counterstain e.g propidium iodide + RNAse or TOTO-3). But before this extensive circuit tracing will be carried out, the potential involvement of these projections in the precipitation of the HAB phenotype shall be tested first. Therefore 350 nl of a neuron-specific viral vector encoding for halorhodopsin (AAV5-hSyn-eNpHR-EYFP) will be injected into the AHN, VMH (combined dorsal, central and ventral subdivisions) as well as the PMD (combined dorsal and ventral subdivisions). After 3 weeks of incubation time, two fibers will implanted in the dl/lPAG. Using the EPM, IndyMaze and modified robo-beetle task, the potential involvement of these projections in the modulation of innate fear shall be studied. A similar approach for the afferents to the PAG arising from the ACA and LS is necessary.

These experiments will demonstrate if the increased anxiety-like behavior and fear-responsivity in HAB mice is the result of a collective change in brain activity in several brain areas, or allows the identification of a specific anxiety-promoting region. In the latter case, this could ultimately lead to targeted systemic pharmacological treatment, once the neurotransmitter receptor profile of those cells are known, for example via a Cre-dependent RiboTag approach (Sanz et al., 2009) in combination with retrograde AAVs expressing Cre-recombinase.

4.9 Conclusion

In this thesis I have demonstrated that midbrain structures which mediate the valence of sensory stimuli as well as the expression of fear responses, heavily influence the phenotype in a mouse model of anxiety-like behavior. The fact that HAB and LAB mice are termed an anxiety-model, stems from the sole reason that the selection criterion for the selective breeding approach which lead to the generation of these lines, was their performance on the EPM. This task is considered to reveal differences in anxiety. As we cannot assess the subjective feeling of anxiety, which is elicited by constant ruminating thoughts about distant, potentially threatening situation, it is highly questionable if the term 'anxiety' or its slightly disguised form 'anxiety-like' should be used at all in animal research. The imprudent conventionalism to stick to these human psychiatric terms in order to imply a translational value *per se* rather derogates the credibility of preclinical research and may even lead to faulty conclusions. The phenotype of HAB and LAB animals is described as either high or low *anxiety-like* behaving, which is in fact simply sum of differentially expressed fear reactions.

This suggests that the complex facets of fear cannot be conclusively analyzed with unimodal tasks like the EPM. It is in fact necessary to use multimodal tests in order to measure not only the level of expression of one particular behavior (e.g. freezing) but also to determine its relative expression compared to other fear coping styles (e.g. active flight). A simple example should explain this circumstance: Rodents which underwent auditory fear conditioning, are typically retested on the following day in another context to assess their fear memory. In this retention test the animals are free to explore the new context for several minutes until, out of the sudden, the previously negatively conditioned tone sounds. If the fear memory formation was successful, the sound has been associated with a noxious stimulus. In anticipation of pain the animals display a profound freezing behavior. But within the first seconds after the onset of the tone, most animals show in fact a strong escape behavior (jumping). As a result those animals which jumped do not freeze, and all to often this would be interpreted as a decreased expression of fear which is obviously not true. The simplest solution to this problem might seem to add additional tests in order to capture the full spectrum of fear responses. But retesting e.g. stress sensitive or highly anxious strains is not possible using this approach as the repeated testing might exaggerate fear responsivity in an unpredictable manner. This would mean to use new cohorts of animals for every test. The best alternative is to use ethobehaviorally inspired testing paradigms like the IndyMaze or the robo-beetle task (Heinz et al., 2017) in oder to sample the natural expression of active and passive fear responses at once.

The complete retinal blindness of LAB animals, demonstrated for the first time in this thesis, affects the significance of several prior studies which have incorporated LAB mice. This is most important for studies which compared LAB directly to HAB as in this case this would affect the results obtained from both strains. Future genotyping

experiments of frozen samples from different labs will clarify when during the selective breeding process, LAB animals lost their vision. Judging from spatial navigation tasks in which LAB animals showed a profound deficit (Yen et al., 2013) it seems that these animals were blind already 2011.

In this thesis I have tried to highlight the limitations of behavioral experiments for the study of negative affect. Whether LAB animals whose SC is activated or HAB mice with inactivated PAG 'feel' differently cannot be assessed from behavioral measures. It is also not certain to which level diazepam treatment in HAB animals changes the valence of the EPM. Despite the fact that midbrain structures control the activity of the ANS, I think it is of the uttermost importance to incorporate neurophysiological (e.g. vHPC-mPFC theta synchrony, Padilla-Coreano et al., 2016) as well as physiological (electrocardiographic, electromyographic, electrogastrographic, pupillometric, sympathetic/parasympathetic nerve activity) and electrochemical (voltammetric, amperometric) measures in behavioral experiments in freely moving animals aiming to measure changes in negative affect. Only with this approach it is possible (e.g. in real time) to distinguish different behavioral states which might phenotypically look similar (e.g. immobility and freezing) and trigger acute e.g. optogenetic manipulations. In order to comply to the often massively paralleled behavioral experiments, the use of low-cost open-source electrophysiological equipment (e.g. OpenEphys, Siegle et al., 2017) is necessary. Up to now there is no available open-source alternative which allows a mouse to be recorded from 64 channels and in addition offers optogenetic manipulation. Therefore I have designed and constructed a low-cost motorized combined electrical and fiber-optic rotary joint and validated it with electrocardiographic recordings and an auditory fear conditioning task as well together with a modified robo-beetle task. This setup allows in the future the controlled electrophysiological inquiry of the neural correlates of the defensive distance.

Rejoicing in hope; patient in tribulation; continuing instant in prayer.

Romans. 12:12 (KJB)

Chapter 5

Appendix

5.1 List of Materials

Item	Manufacturer	P/N	Lot/Serial №
Surgery			
syringe 75RN w/o NDL (ga/mm/pst) 5 μl	Hamilton	7634-01/00	1373565
RN needle 6/pk (33/38/pst3/tapN)	Hamilton	7803-05/00	249654
Stereotaxic Instrument Angle Two	Leica	39464676	110901
Micropump Controller UMC4	WPI	SYS-MICRO4	144201 WO7B
Ultra Micro Pump	WPI	UMP3	144777
Animal Temperature Controller	WPI	ATC2000	166186 E1026
Gas Anesthesia Mask, Mice	Stoelting	51609	n.a.
Kallocryl Af Cold-Curing	Speiko	1609	10628
Kallocryl A/c	Apeiko	1615	10169
Natriumchlorid-Infusionslösung 154	Berlin-Chemie	23357508	V041916101
Iodine Braunol®2000	Braun	3864154	0145M11
Verdünnte H_2O_2 Lösung	KH Apotheke	271211	11.103
Metcam 5 mg/ml, 10 ml	Böhringer I.	n.a.	H-20802A-13
Vetalgin 500 mg/ml Metamizol-Natrium·H_2O	Intervet	n.a.	A155A01
Isofluran CP® 1ml/ml	CP-pharma	n.a.	B49G15A
Paladur®	Heraeus	0197	023091
Lidocain 10% in EtOH, topical	Sigma-Aldrich	L-5647	50K0201
Sugi absorbant swabs	Kettenbach	30601	151531
Panthenol eye cream	Jenapharm®	n.a.	04226-0605
*fast*PGLA 13 mm, reverse-cut	vetsuture	FPGLA1CN	n.a.
Histochemistry			
Roti®-Histol	Carl-Roth	6646.1	505237333
Roti®-Histokit	Carl-Roth	6638.1	36239661
2-Methylbutane	Carl-Roth	3927.1	1096240917
Paraformaldehyde	Carl-Roth	0335.3	973203007
Vectaschield® HardSet™ w. D.	Vector	H-1500	ZC1221
Xylene	VWR	UN1308	0404464
DePeX mounting medium	Gurr® BDH Chem.	36125	7741550G
cover slips 24x60 mm	Carl-Roth	H878	n.a.
in-*vivo* electrophysiology			
Fiber Optic Cannula, ø1.25 mm	Thorlabs	CFMLC12U-20	n.a.
Ceramic Split Mating Sleeve	Thorlabs	ADAL1-5	n.a.
ø200 μm multimode fiber 0.39NA 2 m length, ferrules and FC/PC	Thorlabs	FG200UCC	n.a.
Micro Capillary Polyimide AWG25-E	Detakta	n.a.	n.a.
Stainless steel wire	Science Products	SS-3T/FH	n.a.
Thin Profile Long Reach Plier	Xcelite	378M	n.a.
Tweezer Carbon Fiber	Ideal-Tek	259CFR.SA	n.a.
MWA wire, .001 Tungsten+SML 2020 pcs	Wire Tronic Inc.	#Tung-001SML-7CM-cut	5818

Item	Manufacturer	P/N	Lot/Serial №
Electrode scissors	Fine Science Tools	14558-11	n.a.
NPD-36-VV-GS	Omnetics	A79026-001	n.a.
NSD-36-AA-GS	Omnetics	A79025-001	n.a.
PZN-12-AA	Omnetics	A79623-001	n.a.
MWA connector	Mill-Max	853-93-100-10-001000	n.a.
Other Chemicals			
Dimethyl sulfoxide ACS	Sigma-Aldrich	472301-500ML	SZBDI790V
Acetic Acid	Carl-Roth	3738.1	212187331
Hydrochloric Acid 37%	VWR	20252.290	12K210509
2-Propanol	Carl-Roth	9866.1	233201091
Citric Acid	Sigma-Aldrich	C0759-1KG	SLBJ7376V
Sodium Chloride	Carl-Roth	9265.2	229104522
di-Sodium hydrogenphosphate·$2H_2O$	Carl-Roth	4984.3	390162658
Potassium dihydrogen phosphate	Carl-Roth	3904.1	490165427
Methylcellulose	Carl-Roth	8421.1	066232493
Cresyl violet acetate	Merck	5235	K20587835
Sodium dihydrogenphosphate·$2H_2O$	Carl-Roth	T879.1	475234796
Sodium hydrogen carbonate	Carl-Roth	HN01.1	146235373
Potassium chloride	Carl-Roth	P017.2	105219596
DPBS(1x)	Gibco	14190-094	1644393
Muscimol, Bodipy®TMR-X conj. 1 mg in 1.878 ml aCSF	Thermo Fisher Sc.	M23400	1722988
Clozapine *N*-oxide 50 mg stock 75 mM DMSO	Tocris	4936	4A/1771/54
Replisil 22N Comp. A/B	dent-e-com	241122701	34181
Eosin Y solution aq.	Sigma-Aldrich	HT110-2-32	040K4359
Hematoxylin	Serva	24420	16041
Chloralhydrate	Merck	1.02425.1000	K24127724 728
Potassium aluminium sulphate·$12H_2$	Carl-Roth	8896.1	24045241
Sodium iodate	Fluka	71705	301964/1 13996
EEG High Conductive Gel	dermedics	L082301	15A13-410009

Table 5.1 | List of Materials

5.2 Statistical Checklist

In order to avoid overloading the *Results* section with tedious details regarding every statistical test which has been performed within the respective figure, I decided to place part of this information in the following section. Thereby the reading fluency is not unnecessarily disturbed, but also no important information is left out. Much like the www.nature.com checklist (Biol., 2014), the minor details which might be necessary to evaluate the quality of each experiment will be reported.

Table 5.2 | Experiment 1, Figure 3.1

Data Set	Sample Size	Comparison	Stat. Test	Test Result
3.1a 'latency'	♂HAB (N=11), NAB (N=7), LAB (N=7)	HAB vs. NAB	KW, D	dd rank sum 2.444, ns
—"—	—"—	HAB vs. NAB vs. LAB	1wA, NK	$F_{2,22}$=15.07, p<0.0001
3.1a 'OA time'	—"—	—"—	—"—	$F_{2,22}$=26.25, p<0.0001
3.1a 'time in center'	—"—	—"—	—"—	$F_{2,22}$=12.96, p=0.002
3.1a 'CA time'	—"—	—"—	—"—	$F_{2,22}$=28.98, p<0.0001
3.1a 'locomotion'	—"—	—"—	—"—	$F_{2,22}$=22.49, p<0.0001
3.1b 'no. of SAPs'	♂HAB (N=11), NAB (N=5), LAB (N=6) (*excluded animals did not show SAP's*)	—"—	—"—	$F_{2,19}$=29.84, p<0.0001
3.1b 'SAP duration'	—"—	—"—	—"—	$F_{2,19}$=32.74, p<0.0001
3.1b 'SAP dur. over time'	—"—	HAB vs. NAB	2wA, RM, group x time, BF	Interaction $F_{2,28}$=3.587, p=0.0410 Group $F_{1,14}$=5.60, p=0.0329
3.1b 'SAP dur. over time'	—"—	LAB vs. NAB	2wA, RM, group x time, BF	Interaction $F_{2,26}$=2.368, p=0.1136 Group $F_{1,13}$=13.32, p=0.0029
3.1c 'defecation'	♂HAB (N=11), NAB (N=7), LAB (N=7) (*1 a. excluded as sign. outlier, Grubb's*)	HAB vs. NAB vs. LAB	1wA, NK	$F_{2,21}$=4.779, p<0.0195
3.1d 'vocalization'	♂HAB (N=15), NAB (N=13), LAB (N=15)	HAB vs. NAB vs. LAB	χ^2	(2,N=43)=15.61, p=0.0004
3.1e 'HAB DZP OA visits'	HAB (VHC N=13, DZP N=13)	VHC vs. DZP	Fisher's exact, TT	p=0.48
3.1e 'locomotion'	—"—	—"—	UP, TT, t-test	t(24)=2.174, p=0.0398
3.1f 'HAB DZP SAP dur. over time'	—"—	—"—	2wA, RM, group x time, BF	Interaction $F_{2,24}$=3.085, p=0.0549 Time $F_{2,24}$=6.468, p=0.0033
3.1g 'HAB DZP defecation'	—"—	—"—	UP, TT, t-test	t(24)=3.344, p=0.0027
3.1h 'HAB DZP vocalization'	—"—	—"—	Fisher's exact, TT	p=0.0472

1wA one-way analysis of variance (ANOVA); 2wA two-way ANOVA; NK Newman-Keuls Multiple Comparison; RM repeated measures; KW Kruskal-Wallis rank sum test; BF Bonferroni post-hoc test; D Dunn's post test; χ^2 chi square; ns not significant; DZP diazepam 1 mg/kg, VHC vehicle; OA open arm, CA closed arm; UP unpaired; TT two-tailed, dd difference.

Table 5.3 | Experiment 2, Figure 3.2

Data Set	Sample Size	Comparison	Stat. Test	Test Result
3.2b 'flight'	♂HAB (N=7), NAB (N=6), LAB (N=9)	HAB vs. NAB	Fisher's exact, TT	p=0.021
3.2b 'bypass'	—"—	HAB vs. NAB	Fisher's exact, TT	p=0.0047
3.2b 'collision'	—"—	LAB vs. NAB	Fisher's exact, TT	p=0.011
3.2d 'latency 1st'	♂HAB (N=17), NAB (N=19), LAB (N=17)	HAB vs. NAB vs. LAB	1wA, NK	$F_{2,50}$=12.64, p<0.0001
3.2e 'exploration'	♂HAB (N=24), NAB (N=19), LAB (N=19)	HAB vs. NAB vs. LAB	χ^2	(2,N=62)=6.671, p=0.0356
3.2g 'fear responses'	♂HAB (N=8), NAB (N=9), LAB (N=10)	HAB vs. NAB vs. LAB	χ^2	(2,N=27)=13.11, p=0.0014
3.2h 'latency 1st'	HAB (VHC N=12, DZP N=13) (*1 a. excluded as sign. outlier, Grubb's*)	VHC vs. DZP	MW, TT	$U_{\mathrm{n1=208,\ n2=117}}$=39.00, p<0.0361

1wA one-way analysis of variance (ANOVA); 2wA two-way ANOVA; NK Newman-Keuls Multiple Comparison; RM repeated measures; KW Kruskal-Wallis rank sum test; BF Bonferroni post-hoc test; D Dunn's post test; χ^2 chi square; ns not significant; DZP diazepam 1 mg/kg, VHC vehicle; OA open arm, CA closed arm; UP unpaired; TT two-tailed, dd difference, MW Mann-Wihtney test.

Table 5.4 | Experiment 3, Figure 3.3

Data Set	Sample Size	Comparison	Stat. Test	Test Result
3.3a 'OMR'	♂BL6, CD1, HAB, NAB, LAB à N=12	multiple comparison	1wA, BF	$F_{4,54}$=93.13, p<0.0001
3.3d 'scotopic fERG'	♂BL6, CD1, HAB, NAB, LAB à N=6	—"—	2wA, RR, BF, group×time	Interaction $F_{8,50}$=4.69, p=0.0003 Group $F_{4,25}$=14.38, p<0.0001 Time $F_{2,50}$=38.73, p<0.0001
3.3d 'photopic fERG'	♂BL6, CD1, HAB, NAB, LAB à N=6	—"—	2wA, RR, BF, group×time	Interaction $F_{8,50}$=3.39, p=0.0035 Time $F_{2,50}$=42.65, p<0.0001

1wA one-way analysis of variance (ANOVA); 2wA two-way ANOVA; NK Newman-Keuls Multiple Comparison; RM repeated measures; KW Kruskal-Wallis rank sum test; BF Bonferroni post-hoc test; D Dunn's post test; χ^2 chi square; ns not significant; DZP diazepam 1 mg/kg, VHC vehicle; OA open arm, CA closed arm; UP unpaired; TT two-tailed, dd difference, MW Mann-Wiltney test.

Table 5.5 | Experiment 4, Figure 3.4

Data Set	Sample Size	Comparison	Stat. Test	Test Result
3.4d 'latency'	♂LAB (mCherry/control N=12, hM3Dq N=11)	mCherry vs. hM3Dq	MW, TT	$U_{n1=94,\ n2=182}$=16.00, p=0.0023
3.4e 'exploration'	—"—	—"—	Fisher's exact, TT	p=0.0373
3.4f 'lat. end. expl.'	♂LAB (mCherry/control N=12, hM3Dq N=7) (*four hM3Dq a. did not leave the start compartment*)	—"—	MW, TT	$U_{n1=86,\ n2=104}$=8.00, p=0.0046
3.4g 'fear resp.'	—"—	—"—	Fisher's exact, TT	p=0.0095
3.4h 'latency'	♂LAB (mCherry/control N=11, hM3Dq N=11) (*1 a. excluded as sign. outlier, Grubb's*)	—"—	MW, TT	$U_{n1=69.5,\ n2=183.5}$=3.500, p=0.0002
3.4h 'OA time'	♂LAB (mCherry/control N=12, hM3Dq N=11)	—"—	MW, TT	$U_{n1=183,\ n2=93}$=27.00, p=0.0178
3.4h 'CA time'	—"—	—"—	MW, TT	$U_{n1=100.5,\ n2=175.5}$=22.50, p=0.0081
3.4h 'locomotion'	—"—	—"—	MW, TT	$U_{n1=179,\ n2=97}$=31.00, p=0.0337
3.4i 'no. of SAPs'	♂LAB (mCherry/control N=10, hM3Dq N=11) (*1 a. excluded as sign. outlier, Grubb's*) (*1 a. excluded as it didn't show any SAP*)	—"—	MW, TT	$U_{n1=56.5,\ n2=174.5}$=1.5, p=0.0002
3.4i 'SAP dur. over time'	—"—	—"—	2wA, RR, BF, group×time	Interaction $F_{2,38}$=3.59, p=0.0375 Group $F_{1,29}$=15.76, p=0.0008 Time $F_{2,38}$=8.48, p=0.0009

1wA one-way analysis of variance (ANOVA); 2wA two-way ANOVA; NK Newman-Keuls Multiple Comparison; RM repeated measures; KW Kruskal-Wallis rank sum test; BF Bonferroni post-hoc test; D Dunn's post test; χ^2 chi square; ns not significant; DZP diazepam 1 mg/kg, VHC vehicle; OA open arm, CA closed arm; UP unpaired; TT two-tailed, dd difference, MW Mann-Wihtney test.

Table 5.6 | Experiment 5, Figure 3.5

Data Set	Sample Size	Comparison	Stat. Test	Test Result
3.5e 'OA visiting'	HAB (VHC N=5, MUSC N=6) (3 animals were excluded due to initially too high MUSC concentrations)	VHC vs. MUSC	Fisher's exact, TT	p=0.0152
3.5e 'OA time'	—"—	—"—	MW, TT	$U_{\mathrm{n1=16,\ n2=50}}$=1.000, p=0.0116
3.5e 'CA time'	—"—	—"—	MW, TT	$U_{\mathrm{n1=44,\ n2=22}}$=1.000, p=0.0087
3.5e 'locomotion'	—"—	—"—	MW, TT	$U_{\mathrm{n1=15,\ n2=61}}$=0.0, p=0.0043
3.5f 'no. of SAPs'	—"—	—"—	MW, TT	$U_{\mathrm{n1=45,\ n2=21}}$=0.0, p=0.008
3.5f 'SAP dur. over time'	—"—	—"—	2wA, RR, BF, group×time	Interaction $F_{2,18}$=3.11, p=0.0692 Group $F_{1,9}$=13.71, p=0.0049 Time $F_{2,18}$=9.87, p=0.0013
3.5g 'vocalization'	HAB N=14 in tot., crossover VHC N=14, MUSC N=13 half of the group was treated first with MUSC the other half with VHC, on the next day the treatment was switched. 1 a. lost its implants and was excluded	—"—	Fischer's exact, TT	p<0.0001

1wA one-way analysis of variance (ANOVA); 2wA two-way ANOVA; NK Newman-Keuls Multiple Comparison; RM repeated measures; KW Kruskal-Wallis rank sum test; BF Bonferroni post-hoc test; D Dunn's post test; χ^2 chi square; ns not significant; DZP diazepam 1 mg/kg, VHC vehicle; OA open arm, CA closed arm; UP unpaired; TT two-tailed, dd difference, MW Mann-Wihtney test, MUSC muscimol.

5.3 MEMRI Data Set

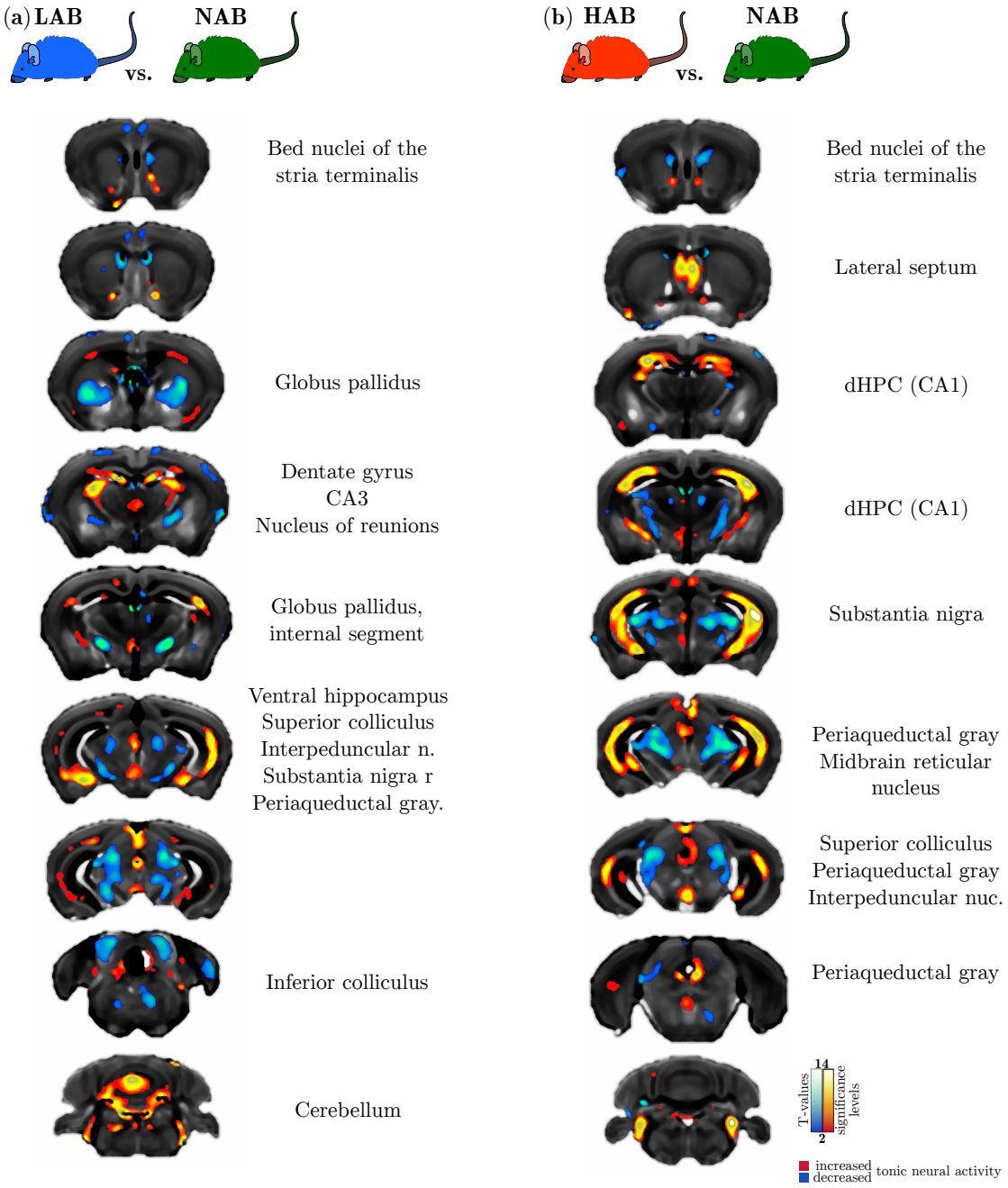

Figure 5.1 | Complete MEMRI Data Set for LAB vs. NAB and HAB vs. NAB
Significantly altered manganese accumulation in (**a**) LAB (N=30) vs. NAB (N=26) and (**b**) HAB (N=31) vs. NAB. Analysis parameters: FDR p<0.001, cluster extent >20, 3-level full-factorial design based on a voxel-wise analysis.

5.4 Manuscripts

5.4.1 Microwave-based Motion Detector

A simplified microwave-based motion detector for home cage activity monitoring in mice

(*in press* Journal of Biological Engineering)

Genewsky A, Heinz D, Kaplick PM, Kilonzo K, Wotjak CT
Research Group 'Neuronal Plasticity'
Department 'Stress Neurobiology and Neurogenetics'
Max Planck Institute of Psychiatry, Kraepelinstr. 2-10, D-80804 Munich, Germany

Background Locomotor activity of rodents is an important readout to assess well-being and physical health, and is pivotal for behavioral phenotyping. Measuring homecage-activity with standard and cost-effective optical methods in mice has become difficult, as modern housing conditions (e.g. individually ventilated cages, cage enrichment) do not allow constant, unobstructed, visual access. Resolving this issue either makes greater investments necessary, especially if several experiments will be run in parallel, or is at the animals' expense. The purpose of this study is to provide an easy, yet satisfying solution for the behavioral biologist at novice makers level.

Results We show the design, construction and validation of a simplified radar-based motion detector for home cage activity monitoring in mice. In addition we demonstrate that mice which have been selectively bred for low levels of anxiety-related behavior (LAB) have deficits in circadian photoentrainment compared to CD1 control animals.

Conclusion In this study we have demonstrated that our proposed low-cost microwave-based motion detector is well-suited for the study of circadian rhythms in mice.

Introduction

The monitoring of circadian rhythms in laboratory mice is essential in biomedical research and goes far beyond the issues of chronobiology. Numerous psychiatric illnesses are comorbid with sleep/circadian disturbances (McClung, 2013) rendering the assessment of rodent locomotor activity an important measure in pre-clinical psychiatric research. Mouse models of psychiatric disorders have been found to be ethological valid (Belzung and Lemoine, 2011) with respect to changes in circadian rhythms e.g. trait-anxiety (Griesauer et al., 2014) and also social-stress induced depression-like behavior (Bartlang et al., 2015). However, the trend to replace conventional open-top with individually-ventilated cages as well as increasing use of environmental enrichment (e.g. wooden tunnels), hinder the function of the well-proven optical based methods as visual access is obstructed. Disproportional financial expenditure for special cages and apparatuses are necessary to implement this formerly rather simple behavioral phenotyping test. Therefore it is not surprising, that the normalized numbers of publications using the term 'locomotor activity', 'home cage activity' or 'circadian rhythm' are regressive (Palidwor and Andrade-Navarro, 2010). Conventional methods to measure home cage ac-

tivity in small rodents are typically based on vibration/tilt sensing (Parreño et al., 1985; Megens et al., 1987; Ganea et al., 2007), infrared light beam crossings (Clarke et al., 1985), resistance changes (Tarpy and Murcek, 1984), capacitive sensing (Stoff et al., 1983), video tracking (Morrel-Samuels and Krauss, 1990), wheel-running (Banks and Nolan, 2011), passive infrared emission (Tamborini et al., 1989), ultrasound transducers (Young et al., 1996) but also microwave-based Doppler-shift radar systems (Marsden and King, 1979; Vanuytven et al., 1979; Martin and Unwin, 1980; Rose et al., 1985; Pasquali et al., 2006). Since each of these methods has its own advantages and disadvantages, we wanted our hardware to meet the following criteria: (a) flexible usage with various cage types, (b) simple, standalone operation and fast access to raw data, (c) motion detection without visual contact to the animal, (d) fast detection <1 Hz sampling rate, (e) open-source, and cost-effective, (f) easy to build with readily available tools. Here we present the design, construction and validation of a simplified microwave-based Doppler shift motion detector, with emphasis on detailed and comprehensive building instructions. Further, we have applied the proposed system to assay circadian rhythmicity and photoentrainment in a mouse model which was initially established to resemble a low anxiety-related behavior (LAB) phenotype (Krömer et al., 2005). However, those animals have been found in addition to mimic certain characteristics of attention deficit hyperactivity disorder (ADHD) (Yen et al., 2013), including increased locomotor activity in emotionally challenging behavioral tasks as well as a slightly disturbed sleeping pattern (Jakubcakova et al., 2012). We could demonstrated that LAB animals show a drastically increased homecage locomotor activity and additionally suffer from deficits in photoentrainment.

Methods

Animals In this study only male LAB (Krömer et al., 2005)(N=3) and CD1 (N=3) mice have been used. Both strains were bred in the animal facilities of the Max-Planck Institute of Psychiatry, Munich, Germany. The selective breeding of LAB animals has been described extensively elsewhere (Krömer et al., 2005; Yen et al., 2013). All animals have been single-housed >1 week prior to the experiments in Makrolon type II cages (23 x 16.5 x 14 cm) equipped with wood chop bedding and nesting material (wood wool). The animals were kept under standard housing conditions: 12h/12h inverted light-dark cycle (light off at 8 AM), temperature 24°C, food and water *ad libitum*. Experimental procedures were approved (AZ 188-12) by the Committee on Animal Health and Welfare of the State of Bavaria (Regierung von Oberbayern, Munich, Germany). Animal care taking and experiments were performed in compliance with the European Economic Community (EEC) recommendations for the care and use of laboratory animals (2010/63/EU). We have kept the number of animals at the absolute minimum, sufficient to reveal group significant group differences.

PCB Design & Manufacturing The printed circuit boards (PCBs) have been designed using the cross-platform open-source electronic design automation suite KiCAD (http://kicad-pcb.org/). All design files are available online (https://github.com/

AGenews/MDS) or on request. The PCBs have been manufactured by the community printed circuit board service OSH Park (https://oshpark.com/) using the standard manufacturing parameters: two-layered FR4, 1.6 mm thickness, electroless nickel immersion gold finish, clearance >160 μm, trace width >160 μm, >254 μm drill size. The circuit board however, is rather simple (e.g. stray capacitances can be largely neglected) and a DIY solution using presensitized PCBs, UV exposure, fixation and etchants like iron(III) chloride or hydrogen peroxide/hydrochloric acid give very good results. An entire assembly using perfboard likely requires wired components, instead of the surface-mounted devices (SMD).

Software Design The cross-platform software to write and upload the Arduino code (*see* listing 5.1) is freely available online (https://www.arduino.cc/en/main/software). All files are available online (https://github.com/AGenews/MDS) or on request. The Python analysis script (*see* listing 5.2) was written using Anaconda Python 2.7 (Continuum Analytics,). Porting this script to Octave, MATLAB or C++ is possible with only little effort.

Statistical Analysis All data is presented as mean values ± standard error. Statistical analysis has been performed using GraphPad Prism 5.03. One-way and two-way analysis of variance was followed by *Dunnett's Multiple Comparison Test* or *Bonferroni* post-hoc analysis.

Results

Operating Principle and Circuit Design The overview of the operating principle of microwave-based homecage-activity monitoring system is depicted in figure 5.2. The X-Band Motion Detector module (Parallax Inc, #32213) emits electromagnetic waves at a frequency of 10.525 GHz (Parallax Inc., 2009), pulsed at 1.34 kHz with 25 μs pulse duration (measured). These microwaves penetrate through the cage walls, bedding and housing material but are partly reflected by the animal. The frequency of the reflected waves is modulated due to the Doppler shift which allows the X-Band Motion Detector module to capture movement and output logic +5 volt signals as a function of the animals velocity. In order to reliably detect movement across up to six inputs, another interface board, the Motion Detector Shield (MDS) is necessary. Each logic output from up to six X-Band Motion Detectors is fed into three dual, monostable, retriggerable multivibrators (SN74LS423), which transform the short pulses in the microsecond range, to pulses of at least 1 second. This is sufficient for the Arduino microcontroller board to poll the digital inputs for the state. Additionally the Motion Detector Shield possesses an onboard ambient light sensor (TEMT6009) which allows to capture the light intensity. Present on the shield are three additional general purpose input/outputs pins (GPIO) or 10-bit analog-to-digital converters (ADC) in a convenient (+5V-GND-SIGNAL) three-pin configuration, which allows the easy connection of other sensors (e.g. an electret microphone) or switches. After every detected movement a short latency <5 μs interrupt is generated which initiates the polling and data handling routines. After the data

has been written to the SD card via the Data Logger Shield (Adafruit Industries, LLC, #1141) the multivibrators are reset, allowing the circuit to react again to new incoming movement events. The data is stored as standard comma-separated values (*.csv*) and easily accessible with various open-source spreadsheet programs like Gnumeric or LibreOffice Calc rendering our system cross-platform capable. However, simple scripts written in Python 3.5 (Continuum Analytics,) allow a quick and flexible standardized high quality analysis. The outputs from the X-Band Motion Detector modules are connected to

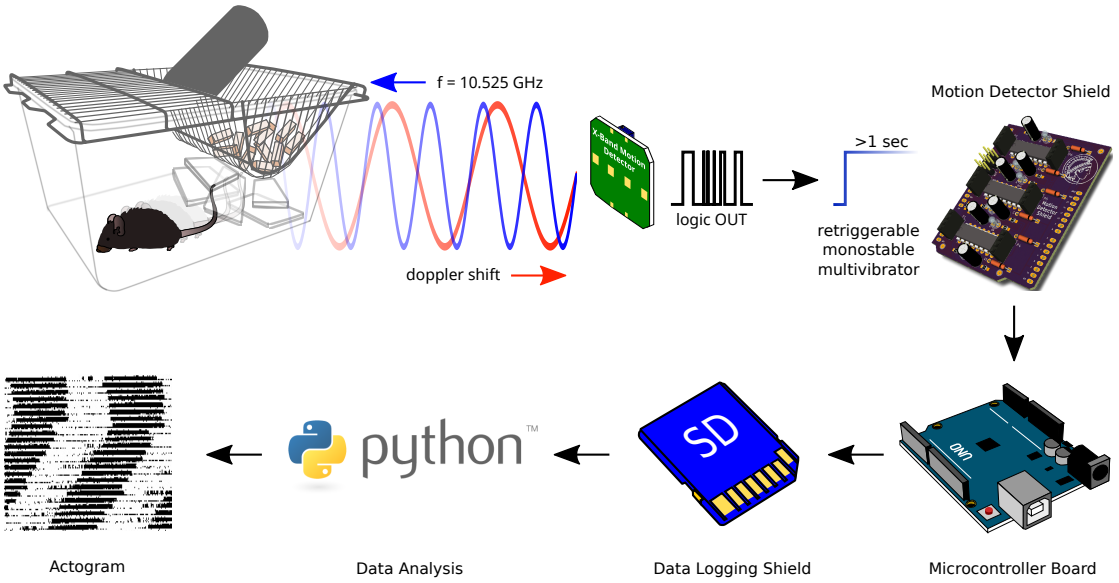

Figure 5.2 | Operating Principle of the Homecage Activity Detection System.
Movements of a small animal modulate and reflect the emitted 10.525 GHz radar waves via Doppler shift. This deviation from the emission frequency is sensed by the X-Band Motion Detector and an internal circuitry generates logic +5V signals according to the velocity of the animals motion. These multiple pulses of short and variable duration are transformed by the Motion Detector Shield to >1 seconds retriggerable pulses, and allows a downstream Arduino microcontroller board to reliably poll its I/O ports. Detected movement activity will be written to a SD card in *.csv* format with a timestamp from the realtime clock and Python scripts allow the analysis and generation of actograms.

the MDS via the pin headers P1-P6 and are summed first altogether through the diodes D1-D6 and routed to one of the Arduino's interrupt pin. Additionally, the sensor outputs are routed to the multivibrators (IC1-IC3) where the RC circuits consisting of C1-C6 and R4-R7, R11, R12 generate >1 second pulses. These pulses are available at the Arduino's digital inputs pin after an interrupt has been sensed by the interrupt function *detected()* (*see* listing 5.1), all inputs flopA-flopF will be polled, the result will be written to the sensors[ ] array and the state variable changes (to HIGH). In the subsequent loop, the main function will see the if() condition fulfilled and writes the sensor[ ] array together with the timestamp from the RTC to the SD card. Afterwards flopRST will be pulled down briefly whereby all multivibrators are reset. Every motion event is signaled with a red (>640 nm) LED, which is only barely visible to mice and rats (Lucas et al., 2001; Jacobs et al., 2001; Imai et al., 2007). In order to completely exclude any disturbances due to the red light flashes, we recommend to cover the motion detector shield during

recording (e.g. with a cardboard box) or alternatively place it outside of the recording setup. The MDS is stacked together with the Data Logger Shield onto an Arduino Uno Rev.3 microcontroller board (*see* Fig. 5.3b). The components used in this design are readily available (see table 5.7) and easy to hand-solder. All diodes, capacitors, connectors and integrated circuits are through-hole components, whereas the resistors are easy to handle SMD 0805 packages. The printed circuit boards were manufactured by OSH Park (https://oshpark.com). The design files for the MDS (*see* Fig. 5.3c & e) can be directly accessed online (https://github.com/AGenews/MDS/tree/v0.4) or are available upon request. The last step is to upload the code from listing 5.1 (*motion.ino*) in the

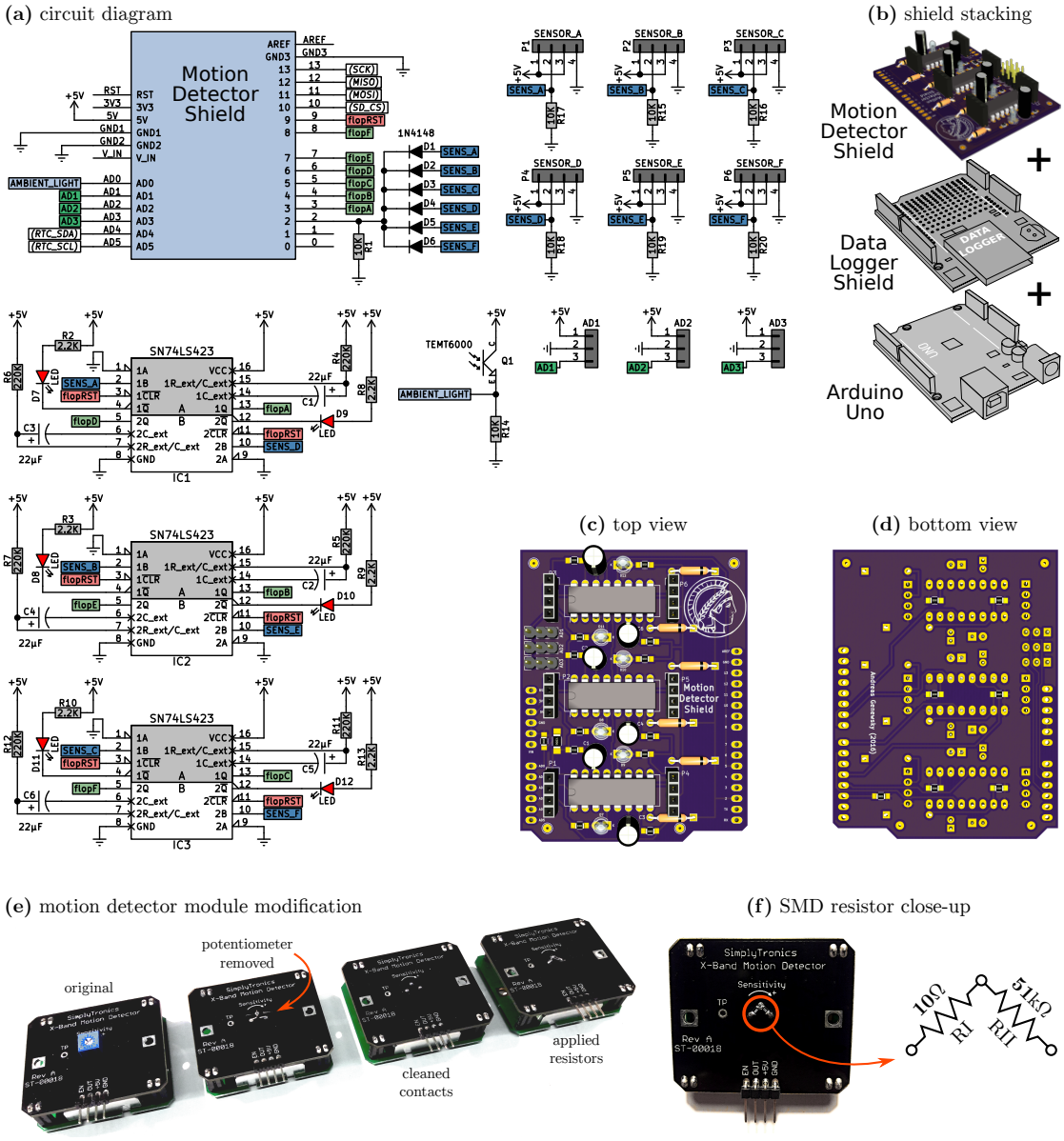

Figure 5.3 | Circuit Diagram and Assembly of the Motion Detector Shield
(**a**) Circuit Diagram of the Motion Detector Shield (MDS). (**b**) The MDS is stacked onto the Data Logger Shield and ultimately both are plugged into an Arduino Uno Rev3. (**c**) Top view of MDS. (**d**) Bottom view of MDS. (**e**) Replacement of onboard potentiometer with SMD0805 resistor pair. (**f**) Detailed depiction of SMD0805 resistor placement.

standard way described here (https://www.arduino.cc/en/Guide/HomePage). In order to compile the code the libraries 'SD.h', 'RTClib.h' and 'Wire.h' need to be installed using the Arduino IDE Library Manager. In order to use the motion detector modules in close range (e.g. type II mouse cages), we need to replace the original potentiometer with at least 50-100 kΩ as suggested previously (Pasquali et al., 2006). The potentiometer is removed with rather 'brute force' using a large enough wire cutter (*see* Fig 5.3e). After cleaning the solder points with fresh solder the SMD resistors RI and RII can be applied as seen in figure 5.3f. This leads to a rather sensitive setup and electrical shielding using aluminum foil in between the cages is necessary. Optionally the resistor RII can be replaced with 100 kΩ. The current consumption of the entire system (six sensors attached, all LEDs lighting up, writing data to the SD card) was maximally 180 mA and typically 135 mA, while being powered from a 12 V, 500 mA wall-wart type linear DC power supply. The current consumption of a single enabled X-Band Motion Detector module was 6.3 mA at 5.00 V. For applications were high levels of locomotor activity are expected, we therefore recommend to operate the purposed design using mains power. Another important issue is the potentially hazardous exposure to microwave radiation. According to data sheet (Parallax Inc., 2009) the X-Band Motion Detector modules are designed to meet the FCC rules for use within a building (Federal Communications Commission, 2011) and it is further stated that the microwave emissions are below established safety standards for general public environments (Institute of Electrical and Electronic Engineers, 1991).

Validation of the Simplified Microwave-based Motion Detector System

Besides the easy assembly and simple usage, the most important hallmark of our design is the good temporal precision. We have used an analog clock (Pasquali et al., 2006) with a piece (2 x 2 cm) of aluminum foil attached to the second clock hand (*see* Fig. 5.4a). The motion detector was placed 30 cm away from the clock and allowed to record the clock-hand movements for 30 minutes (1800 s). During the recording session the system detected 1758 events with a median value of 1.000 s and an average of 1.02407 s (*see* Fig. 5.4a right panel). Figure 5.4b shows the intervals in between the detected motion events and notably, besides high overall accuracy, there are several intervals which fall well outside the 1 second range. These events cannot be attributed to a potential malfunction of the MDS but stem from the certainly amendable measurement setup. A quantification of the events (Fig. 5.4c) reveals that 85.38 % of all intervals fall into the 950-1050 ms range. A closer look at the the intervals between 990-1010 ms (Fig. 5.4d) shows the normally distributed nature of the measured data. In order to test, whether our movement detection approach is qualified and sufficiently sensitive to detect rhythmic changes, we utilized the rather poor quality of the analog clockwork. An auto-correlation (Fig. 5.4e) of the interval data shows the rhythmic modulation of the data every minute. This is most likely due to the additional weight on the clock-hand in combination with the slackness in the clockwork which causes the aluminum foil to shake (*see* Fig. 5.4e inset).

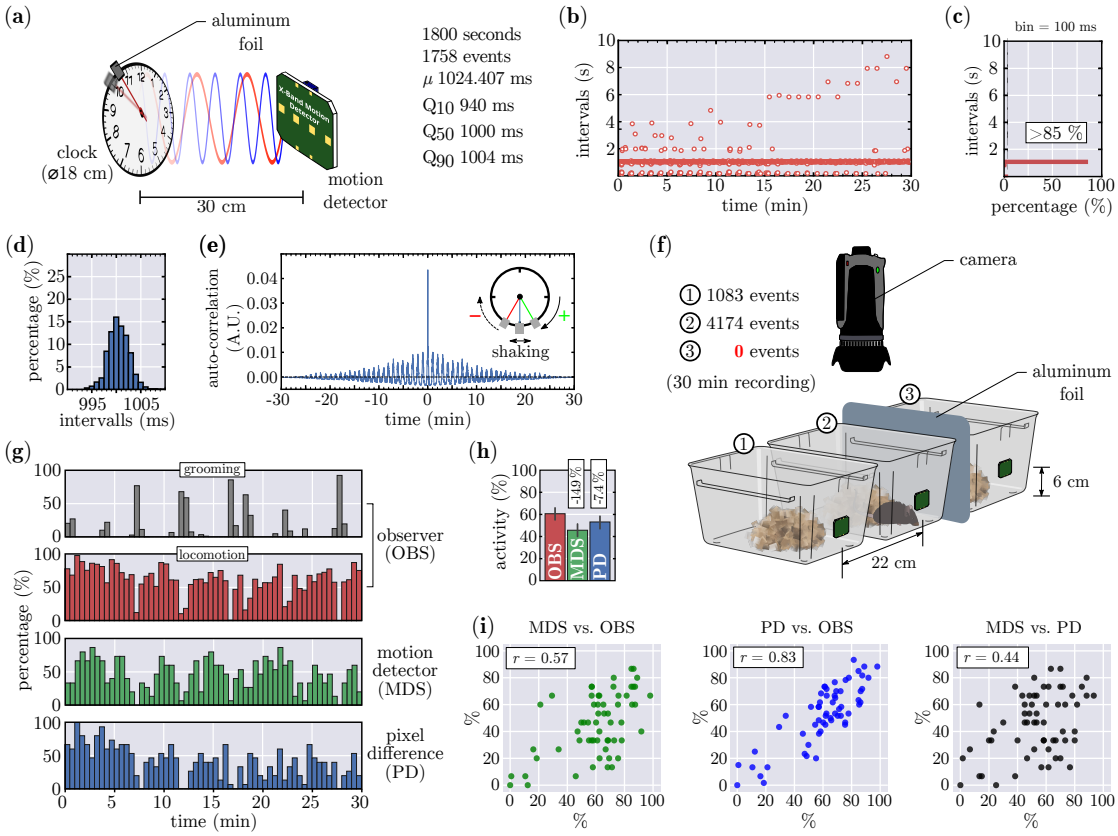

Figure 5.4 | Validation of the Simplified Microwave-base Motion Detector System
a) (*left panel*) Setup for assessing the precision of the motion detector. A small piece (2 x 2 cm) of aluminum foil is mounted on the large clock-hand of an analog clock. The motion detector is placed 30 cm away from the analog clock and was allowed to capture the movements of the clock-hand for 30 minutes. (*right panel* Basic summary of the clock experiment; total number of detected events, mean value of event intervals and the respective percentiles are given. (**b**) Intervals of detected events over time. Note the occurrence of long intervals (>2 s) which indicate slight detection problems due to blind spots in the recording setup. (**c**) Histogram (bin = 100 ms) of all intervals demonstrating, that 85.38 % of the detected events are in the range of 950 ms to 1050 ms. (**d**) A magnified view of the range of 990 ms to 1010 ms shows the normally distributed nature of the recorded data. (**e**) The auto-correlation of the recorded interval data demonstrates a prominent rhythmicity with a frequency of 1 minute, which is most likely due to the additional weight on the clock-hand in combination with the slackness of the low quality gear used in the ordinary analog clock, which causes the aluminum foil to vibrate (*see inset*). (**f**) In oder to asses the crosstalk between simultaneously recorded, neighboring cages and the effect of shielding we have conducted another experiment (<18 lux), where one CD1 mouse was introduced to cage 2 while cages 1 & 3 where unpopulated. Further, we have placed an A4-sized sheet of aluminum foil (floating, not connected to GND) between cage 2 & 3. The experiment was conducted for 30 minutes and in addition the behavior of the animals was video-taped. The green rectangles at the cage front show the placement of the motion detector modules. While in the unshielded cage, the detector picked up 26 % of the neighboring cage, the detector of cage 3 did not detect a single event. (**g**) Performance comparison of the 30 minutes behavior (30 s bins) in cage 2 between three different locomotion detection approaches: a) an experienced observer (OBS) manually scored either the occurrence grooming (grey bars) behavior or locomotor (red bars) activity (ambulatory activity, digging and rearing); b) locomotor activity measured by the motion detector shield (MDS) (green bars); c) frame-by-frame pixel difference (PD) as an unbiased measure of movement in the video file. The pixel noise was found to generate 5.5 % differences between the frames and we used a rather liberal threshold of 8.5 % to determined locomotor activity. MDS and PD datasets were initially binned at 2 second bins in a binary manner (motion = 1, no motion = 0). OBS data was also binned initially at 2 seconds but the data was already given in percentages due to the two different variables. Further, all data set where binned to 30 second bins and the percent presence locomotion/grooming determined. (**h**) Averaged overall locomotor activity for OBS, MDS, PD; numbers indicate the difference to OBS. (**i**) Pearson correlation analysis of MDS vs. OBS, PD vs. OBS and MDS vs. PD.

To determine the amount of shielding necessary to eliminate any crosstalk between to neighboring cages which are simultaneously measured with the MDS, we have conducted the experiment outlined in figure 5.4f. Three cages (with bedding and nesting material) were placed close to each other, and every cage was equipped with a motion detector module (green rectangles) using double-sided tape. Between cage 2 & 3 we have introduced an A4-sized piece of aluminum foil (floating, not connected to GND) and only cage 2 contained a CD1 animal, whose activity was monitored for 30 minutes at dim illumination (<180 lux). While in the unshielded but unpopulated cage the motion detector picked up 26 % of the neighboring cage, the aluminum foil effectively eliminated any crosstalk. In the same experiment we have in addition used a video camera to record the animals motion and an experienced observer manually scored the occurrence of grooming behavior as well as locomotion, which we defined as ambulatory activity, digging and rearing. From the video file we further deduced the frame-by-frame absolute pixel difference and used the number of changed pixels as an unbiased measure of motion in the video. This allowed a performance comparison of the three different approaches shown in figure 5.4g. Notably both, the motion detector (MDS) and the pixel difference (PD) approach, equally reliably detect the absence of locomotor activity during high levels of grooming as well as high levels of locomotion. However, differences in the total amount of detected locomotor activity exist between the three methods (Fig. 5.4h), where the PD approach resulted in 7.4 % less activity compared to the human observer, the MDS approach detected 14.9 % less than OBS. Pearson correlation analysis (Fig. 5.4i) revealed a moderate positive correlation between the MDS and OBS (Pearsons's r=0.57), a high positive correlation between PD and OBS (Pearsons's r=0.83) and a low positive correlation between MDS and PD (Pearsons's r=0.44).

Altered Circadian Photoentrainment and Locomotor Activity in LAB Mice
In order to test whether our system is able to detect the activity changes in two different mouse lines, we have made use of the low-anxiety related behaving animals (LAB mice) which were also described as a model for attention deficit hyperactivity disorder (ADHD) and were shown previously to display increased activity in emotionally challenging behavioral tasks (Krömer et al., 2005; Yen et al., 2013). Before the onset of the experiment, the animals were kept at an inverted 12h/12h light-dark cycle (8:00PM light ON, 8:00AM light OFF) for 1 week, which was shifted minus 6h (advance) at day 3. The photoentrainment of the circadian rhythm allows the animals to adjust slowly to the new light cycle. Figures 5.5a & 5.5db shows the actograms as averaged and binned (bin = 1h) homecage activity of CD1 and LAB animals. Figure 5.5c depicts the overlaid activity of CD1 and LAB animals over entire course of the experiment. CD1 animals showed a pronounced circadian rhythmicity in their locomotor activity during baseline (days 1 & 2). By far the greatest portion of activity is observed during the dark phase. With the onset of the light phase this activity ceased. LAB animals on the contrary showed a less contrasted activity profile with high activity at the beginning of the light phase.

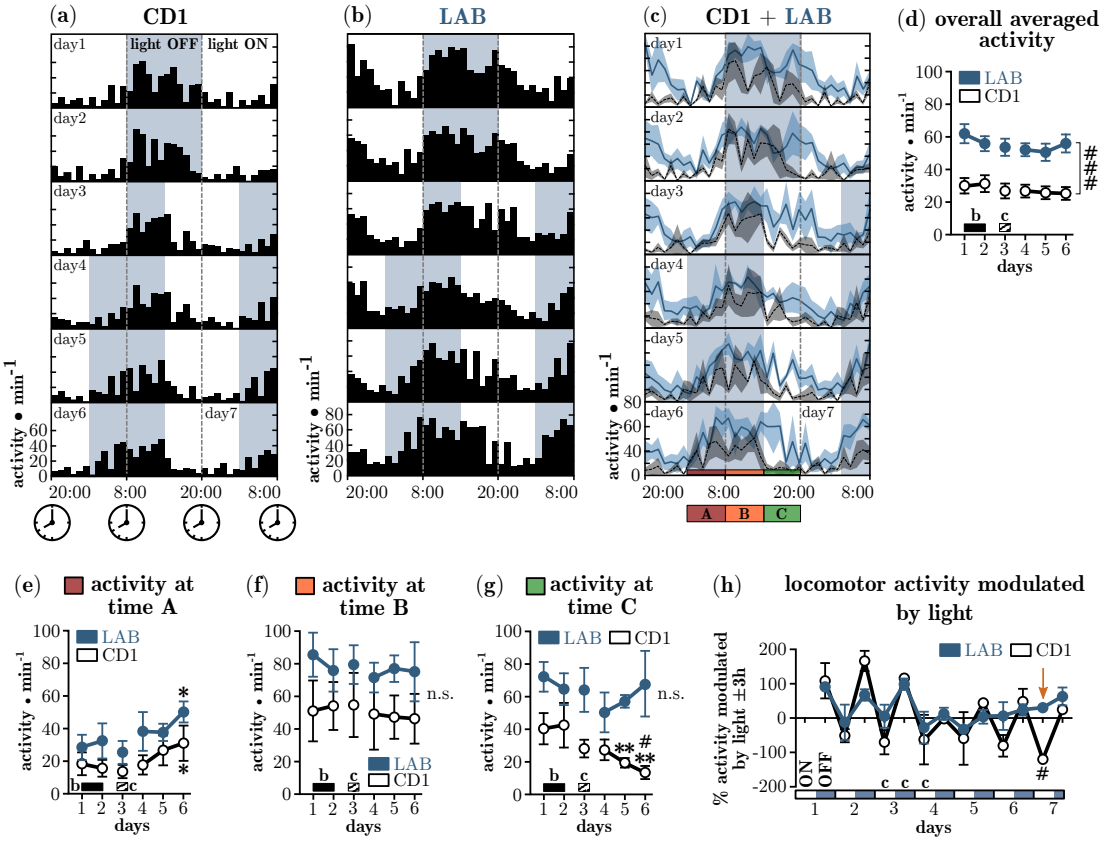

Figure 5.5 | Deficient Photoentrainment & Increased Basal Locomotor Activity in LAB Mice

(**a**) Actogram of CD1 animals (mean values only, 1h bin). White background indicates housing lights ON; gray background indicates housing lights OFF. On day 3 the light cycle was shifted -6 hours, by shortening the dark period. (**b**) Actogram of LAB animals. (**c**) Overlaid actograms of CD1 (black, dashed line) and LAB (blue , solid line) with the respective SEM ranges. Colored boxes (bottom) A red, B orange, C green, indicate the three different time points which have been analyzed separately (*see* e-g). (**d**) Overall averaged activity of CD1 (black) and LAB (blue) mice. Inset *b* indicates the baseline recording; *c* indicates the light cycle change. (**e**) Activity at time point A (2 am - 8 am), part of the dark period after day 3. (**f**) Activity at time point B (8 AM - 2 PM). (**g**) Activity at time point C (2 PM - 8 PM), part of the light period after day 3. (**h**) Modulation of locomotor activity by changes in light cycle. The individual activity of the first 3h after a light cycle change, was normalized to the activity 3h before the change in order to dissect the % modulation. The arrow indicates the absence of any modulation in LAB animals. Asterisks (*) indicates 1-way ANOVA, Dunnett's Multiple Comparison Test compared to averaged baseline: ** p=<0.01. Hash (#) indicates 2-way ANOVA significance values as either strain (bracket) or time differences with Bonferroni post-hoc: # p=<0.05, ### p=<0.0001. Day 3 (light cycle change, indicated by 'c') has been excluded from statistical analysis.

The overall averaged activity per day (Fig. 5.5d) of LAB animals was approx. two-times increased compared to CD1 controls and different throughout the experiment ($F_{1,184}$=24.95, p<0.0001), confirming the hyperactivity phenotype of LAB animals. The light cycle shift (LCS) on day 3 forced the animals to adapt their activity pattern to the new onset of the dark phase. Over the course of days 4-6, both CD1 and LAB animals significantly increased their locomotor activity during the first 6h of the dark phase (Fig. 5.53) compared to baseline (CD1: $F_{2,6}$=5.469, p=0.0375; LAB: $F_{2,6}$=5.92, p=0.0317), indicating that both strains were able to adjust their circadian locomotor activity. Between 8:00AM and 2:00PM (time point B, unaltered light condition) both

strains showed equal amounts of activity ($F_{1,20}$=1.845, p=0.2459), which was also unaffected by the LCS (Fig. 5.5f). The locomotor activity at time point C (2:00PM to 8:00PM, now light phase) of CD1 animals at days 5+6 decreased strongly ($F_{2,6}$=13.21, p=0.0047) indicating a robust photoentraining effect (Fig. 5.5g). LAB animals on the other hand did not react to the altered light cycle. The modulation of locomotion by light cycle changes became evident when the individual, averaged activity of 3h after a change, was normalized to 3h before and was plotted for every change in cycle (Fig. 5.5h). During days 1-3 this modulation was prominent for CD1 and LAB mice. After the light cycle shift the modulation was severely disturbed in both strains. While LAB animals seemed to be unable to establish normal rhythmicity in the observed time window, CD1 animals could recover quickly. A strong time effect was revealed by 2-way ANOVA ($F_{9,40}$=50.45, p<0.0001) with moderate interaction ($F_{9,40}$=2.530, p<0.0212). This indicates that LAB animals are impaired in using photoentraining signals to adjust their circadian rhythm compared to CD1 controls.

Discussion

Here we have described the design, construction and validation of a simplified microwave-based motion detector for home cage activity monitoring in mice. We have emphasized all necessary steps to copy and built the proposed project. Particular care was taken to use readily available parts in order to ease the straightforward adoption and 'jump-start' the application in the laboratory. We have demonstrated the high detection accuracy and temporal resolution. Moreover, we could show for the first time that animals which were selectively bred for low-anxiety behavior (LAB), a model organism for extremely low levels of trait anxiety (Krömer et al., 2005) and attention-deficit hyperactivity disorder (Yen et al., 2013), have strong deficits in photoentrainment.

Deficient Photoentrainment in LAB Mice

Photoentraining signals reach the retinal ganglion cells (RGC), which constitute the optic tract, and in turn send the photic information from the retina via the retinohypothalamic tract (RHT) to the two primary targets of the circadian regulatory system, namely the suprachiasmatic nucleus (SCN) and the intergeniculate leaflet of the the thalamus (IGL) (Provencio et al., 1998). However, the SCN is considered to act as the 'master clock' (Moore et al., 1995). Only the photic signals perceived via the eyes carry entraining information, as binocular enucleation completely abolishes photoentrainment (Nelson and Zucker, 1981). Theories about extraocular photoreception (Campbell and Murphy, 1998) e.g. humoral phototransduction have not been substantiated nor accepted so far (Foster, 1998). Despite the photoreceptor cells within the retina (rods & cones) also as special form of RGCs have been found to be intrinsically photosensitive (ipRGC) through their photopigment melanopsin. Genetic ablation of theses cells was found to abolish photoentrainment (Güler et al., 2008; Hatori et al., 2008) and indicates that visual information via rods and cones is not necessary for functional circadian photoentrainment. This is further substantiated by studies with mice which carry a homozygous mutation in the gene *Pde6b* encoding for the rod-specific phosphodiesterase

6b. These *rd1* mice (retinal degeneration 1) loose their rod photoreceptors within the first weeks after birth, followed by a secondary, slower degeneration of the cone photoreceptor cells (Farber et al., 1994), leading to complete retinal blindness while RGC function is unaffected. These animals, however, have been shown to exhibit normal circadian rhythms (Foster et al., 1991). The LAB mouse line descended from the commonly used outbred strain CD1 which has been described of possessing high incidences of retinal degeneration (Serfilippi et al., 2004). Whether LAB animals carry the *rd1* mutation is currently not known, but would otherwise also not explain their deficient circadian photoentrainment. Interestingly there is growing evidence that links ADHD with disturbed sleeping patterns and distorted circadian rhythms (Walters et al., 2008; Baird et al., 2012). The underlying neurophysiological changes in LAB animals, impairing the ability to entrain their circadian rhythm to photic stimuli, cannot be resolved at this stage. But a potentially altered functionality of the SCN in LAB animals could explain the hyperactivity as well as the previously described altered sleeping patterns (Jakubcakova et al., 2012) and possibly also the impairment in photoentrainment.

Significance of the Current Design

Several studies so far have proposed elegant ways to monitor activity in small animals like mice and invertebrates. The by far most widely applied methods usually utilize some sort of optical readout, be it (active) infrared light beam crossings (Clarke et al., 1985; Pasquali et al., 2016; Pasquali et al., 2017) or motion detection using passive infrared (PIR) sensors (Tamborini et al., 1989), which detect black body radiation in the mid infrared ($\approx 3\ \mu$m) range. These methods are readily applied as their operating principles are easy to comprehend and their technical implementation is rather simple. However, all optical based approaches have in common that a constant, unobstructed, visual access must be guaranteed throughout the experiment, and those typically last several days up to weeks. It is therefore desirable to house the animals in their accustomed environment also during home cage activity monitoring in order to minimize distress and long acclimatization periods. With the sanitary and technical advances in animal husbandry, the conventional grid top cages are progressively replaced by individually ventilated cages (IVCs), which are typically operated in specific high-density racks. These systems provide only little space around the cages and obscure most sides especially the top side (filter top). Therefore the usage of microwave based radar systems, which have been beautifully described previously (Pasquali and Renzi, 2005; Pasquali et al., 2006; Pasquali et al., 2010), is advisable. However, none of the previously published studies give detailed building instructions which would be necessary to enable an electronics novice to copy and apply the method. Our design is simple to implement and involves the crucial basic building blocks, like the popular Arduino microcontroller platform and the powerful scientific programming language Python, which form the core of many open-source research equipment projects (Pearce, 2012; Teikari et al., 2012; Sheinin et al., 2015). The decision to favor the Arduino Uno microcontroller board over other devices like the single-board computers Raspberry Pi or the BeagleBone (for a

comparison of the different systems see Leccese et al. 2014 (Leccese et al., 2014)) was motivated by the fact that the Arduino platform is an ideal candidate for beginners due to the plethora of available online documentation, while offering more than sufficient peripherals, on-board connectivity features and computing power to fulfill the respective tasks.

There are some additional features which might be desirable to implement in the future which will be briefly mentioned: (**1**) The measured output is given as activity per minute which is simply the detector activation per minute and an ongoing locomotion triggers the detector several times. For our purpose, this measure was sufficient, but more biologically relevant measures like percent activity over time can be implemented in the Python script. (**2**) More advanced analysis parameters like period, phase and phase-shift can be obtained from the acquired data and the reader is advised to follow the excellent protocols and guidelines for analyzing locomotor activity rhythms published by Rosato et al. (2006) (Rosato and Kyriacou, 2006) and Jud et al. (2005) (Jud et al., 2005). (**3**) Instead of storing the data onto a SD card, it is rather simply possible to use an additional WiFi or Ethernet shield to send the data directly to a central network storage or cloud service. Thereby, also the parallel use of several motion detectors at once is realized best. (**4**) In addition one could equip the microwave based motion detector system with one or several small serial cameras. Thereby, the entire system can be used to e.g. study wildlife animal densities in the field. The Doppler shift sensors consume very little amount of current (6.3 mA) while providing large spatial coverage. A detected motion could be used to wake up the Arduino board from deep sleep, whereby the overall power consumption is minimized enabling even battery powered operation in a reasonable manner.

Potentially Hazardous Effects of Microwave Radiation

The FCC rules for the use of radio frequency devices within a building (Federal Communications Commission, 2011) and the established safety standards for general public environments (Institute of Electrical and Electronic Engineers, 1991) are only valid with respect to the human physiology. It is therefore an important question whether our device, emitting 10.525 Ghz, might exert any biological effects on mice. First we try to estimate the emitted power of the microwave radiation. In the data sheet (Parallax Inc., 2009) we find the maximal effective isotropic radiated power (EIRP) of 14 dBm which is equivalent to 25.12 mW radiated power during continuous wave (CW) operation. Therefore we can predict the power density S ($\frac{W}{m^2}$) using the formula $S = \frac{EIRP(W)}{4\pi R^2}$ (Federal Communications Commission, 1997), where R is the distance in meter. This formula over-predicts the power densities in the near-field (Federal Communications Commission, 1997), but can be used to for making a 'worst-case' or conservative prediction. A mouse is exposed most to the microwaves, if it would build its nest directly in front of the sensor. In our experiments we have mounted the sensor modules 6 cm above the cage floor with double-sided tape directly at the outside of the cages. Considering bedding material and the approximate size of the murine body we therefore assume a minimal

distance of 2 cm to the sensor. Given this distance we can estimate a power density of ≈ 0.5 mW/cm^2. However, our module does not emit this power constantly but only at less than 4 % of the time, giving an approximate averaged power density of < 0.02 mW/cm^2.
However, there is compelling evidence (Sharma et al., 2017) that microwave (10 Ghz) exposure to infant mice (postnatal day) at a power density of 0.25 mW/cm^2 for 2 h/day (CW), for 15 consecutive days stresses the animals, as shown by a decreased weight gain and ultimately leads to a decreased performance in a spatial memory task (Morris water maze) later in their live (>6 weeks). Further, 10 Ghz exposure to adolescent (>6 weeks) animals with the same intensity and exposure regime, but for 30 consecutive days also leads to decreased performance in the Morris water maze (Sharma et al., 2014). However, another study showed that constant 10 Ghz exposure in adolescent mice (>4 weeks) at 13 dBm (20 mW) for 6 consecutive days modulated at 8 Hz (within the theta-alpha EEG frequency band) but not at 2 Hz (within the delta EEG frequency band) decreased the spontaneous locomotor behavior in an open-field test. Despite the modulation (assuming 100 % amplitude modulation), the effective microwave power (based on the root man square) used in this study and those mentioned in the studies before, are >12× higher (taking the low duty cycle of our sensors into account). Therefore we consider the microwave radiation emitted from the sensor modules used in our design to be nonhazardous for mice.

Conclusion

We have successfully developed a simple, yet powerful open-source project which aids laboratory practice while reducing costs. It is suitable for the beginner (e.g undergraduate behavioral neuroscience course) but holds enough expandability to satisfy the advanced. Do-it-yourself (DIY) solutions have been considered all to often as a compromise and inferior in performance compared to commercial products. However, knowing the limitations of an own design allows the careful and responsible interpretation of the obtained data, which might sometimes be better than simply relying entirely on the output of an expensive setup.

Table 5.7 | List of Materials for the Motion Detector Shield

Reference	Qty.	Item	Part No.	Mfr.	RS No.
AD1, AD2, AD3	3	3-pole, 2.54 mm, header	M20-9990346	Harwin	745-7068
C1, C2, C3, C4, C5, C6	6	electrolytic capacitor 22μF, 25V	ECE-A1EKA220	Panasonic	807-3554
D1, D2, D3, D4, D5, D6	6	1N4148, 100V, 300mA	1N4148	Fairchild Semi	843-1562
D7, D8, D9, D10, D11, D12	6	LED, 3 mm, 1.85V, red	L-7104SRC-D	Kingbright	619-4886
IC1, IC2, IC3	3	SN74LS423N	SN74LS423N	Texas Instr.	809-5661
P1, P2, P3, P4, P5, P6	6	4-pole, 2.54 mm, socket	M20-7820446	Harwin	681-6814
Q1	1	TEMT6000 Light Sensor	TEMT6000X01	Vishay	768-9354
R1, R14, R15, R16, R17, R18, R19, R20	8	10 kΩ, SMD 0805	CRG0805F10K	TE Connect.	223-0562
R2, R3, R8, R9, R10, R13	6	2.2 kΩ, SMD 0805	CRG0805F2K2	TE Connect.	223-0477
R4, R5, R6, R7, R11, R12	6	220 kΩ, SMD 0805	CRG0805F220K	TE Connect.	223-0742
–	6	X-Band Motion Detector SimplyTronics	32213	Parallax Inc.	781-3074
–	6	4-pole, female, 2.54 mm	5-103960-3	TE Connect.	842-8021
–	6	4-pole, male, 2.54 mm	5-103944-3	TE Connect.	842-8093
–	1	PTFE Cable	–	RS Pro	877-5443
–	2	Arduino Stackable Header Kit - R3	PRT-11417	Sparkfun	–
–	1	Data Logger Shield	1141	Adafruit	–
–	1	Arduino Uno Rev3	A000073	Arduino	769-7409
RI	6	10 Ω, SMD 0805	CRG0805F10R	TE Connect.	223-0152
RII	6	51 kΩ, SMD 0805	CRCW080551K0FKEA	Vishay	679-1525
–	1	DC power supply	8154014	RS Pro	737-8149

Listing 5.1 | Arduino Code for the Motion Detection Shield

```
// MIT License
// Copyright (c) [2017] [Andreas Genewsky]
// Permission is hereby granted, free of charge, to any person obtaining a
// copy of this software and associated documentation files (the "Software"),
// to deal in the Software without restriction, including without limitation
// the rights to use, copy, modify, merge, publish, distribute, sublicense,
// and/or sell copies of the Software, and to permit persons to whom the
// Software is furnished to do so, subject to the following conditions:
// The above copyright notice and this permission notice shall be included
// in all copies or substantial portions of the Software.
// THE SOFTWARE IS PROVIDED "AS IS", WITHOUT WARRANTY OF ANY KIND, EXPRESS OR
// IMPLIED, INCLUDING BUT NOT LIMITED TO THE WARRANTIES OF MERCHANTABILITY,
// FITNESS FOR A PARTICULAR PURPOSE AND NONINFRINGEMENT. IN NO EVENT SHALL
// THE AUTHORS OR COPYRIGHT HOLDERS BE LIABLE FOR ANY CLAIM, DAMAGES OR OTHER
// LIABILITY, WHETHER IN AN ACTION OF CONTRACT, TORT OR OTHERWISE, ARISING
// FROM, OUT OF OR IN CONNECTION WITH THE SOFTWARE OR THE USE OR OTHER
// DEALINGS IN THE SOFTWARE.

#include <SD.h>
#include "RTClib.h"
// echo data to serial port
#define ECHO_TO_SERIAL   1
// initialize SD and write data
#define WRITE_TO_SD   1
int flopRST = 9;  // SN74LS423 RESET Pin
int SENS_A = 3;   // channel A
int SENS_B = 4;   // channel B
int SENS_C = 5;   // channel C
int SENS_D = 6;   // channel D
int SENS_E = 7;   // channel Esingle-housed
int SENS_F = 8;   // channel F
int AMBIENT = 14; // TEMT6000 lightsensor
int AD1 = 15;     // optional analog input
int AD2 = 16;     // optional analog input
int AD3 = 17;     // optional analothat g input
float lux = 0.0;  // value necessary for lux
float lplux = 0.0;  //necessary for lux
int sensors[6];   // motion sensor array
//changes if motion was detected
volatile byte state = LOW;  single-housed
int ledPin = 13;  // the Arduino onboard LED
int bootup = 0; // stores ms at bootup
unsigned int ms = 0;  // ms between seconds
RTC_DS1307 RTC; // define the Real Time Clock
const int chipSelect = 10;
// the logging file
File logfile;

void error(char *str) //error function
{that
  Serial.print("error: ");
  Serial.println(str);
  while(1);
}

//here we set the date- and timestamp
//for the logging file
void dateTime(uint16_t* date, uint16_t* time)
{
  DateTime now = RTC.now();
  *date = FAT_DATE(now.year(), now.month(), now.day());
  *time = FAT_TIME(now.hour(), now.minute(), now.second());
}

void setup() {  //the setup function begins
  Serial.begin(57600); //debugging that purpose
   if (! RTC.begin()) { //starting the RTC
    Serial.println("Couldn't find RTC");of the programing PC
    while (1);
  }
//Here we set the clock according
//to the CPU Time
  RTC.adjust(DateTime(F(__DATE__), F(__TIME__)));
//elapsed ms since bootup
  bootup = millis();

//no we set the INPUT & OUTPUT Pins
  pinMode(flopRST, OUTPUT);
  pinMode(SENS_A, INPUT);
  pinMode(SENS_B, INPUT);
  pinMode(SENS_C, INPUT);
  pinMode(SENS_D, INPUT);
  pinMode(SENS_E, INPUT);
```

```
  pinMode(SENS_F, INPUT);
  pinMode(AMBIENT, INPUT);
  pinMode(AD1, INPUT);
  pinMode(AD2, INPUT);
  pinMode(AD3, INPUT);

  attachInterrupt(0, detected, FALLING);
//this links a +5V voltage level at pin 2
//(Arduino Interrupt Pin = pinnumber 0)
//to the function detected()
  digitalWrite(flopRST, HIGH);
#if WRITE_TO_SD
//we initialize the SD card, and check
//if we can write
  Serial.print("Initializing SD card...");
  pinMode(chipSelect, OUTPUT);
  if (!SD.begin(chipSelect)) {
    error("Card failed, or not present");
  }
  Serial.println("card initialized.");

//this function generates filenames
  char filename[] = "MOTION00.CSV";
  for (uint8_t i = 0; i < 100; i++) {
    filename[6] = i/10 + '0';
    filename[7] = i%10 + '0';
    if (! SD.exists(filename)) {
      SdFile::dateTimeCallback(dateTime);
      logfile = SD.open(filename, FILE_WRITE);
      break;  //leave the loop!
    }
  }
  if (! logfile) {error("couldnt create file");}
  Serial.print("Logging to: ");
  Serial.println(filename);
//the next line writes the column
//descriptors to the file
  logfile.println("MONTH,DAY,YEAR,HH,MM,SS,mmm,CH1,CH2,CH3,CH4,CH5,CH6,LUX");
#endif WRITE_TO_SD

//in order to blank any strange behavior
//we RESET all the flops before we log
digitalWrite(flopRST, LOW);
digitalWrite(ledPin, HIGH);
delay(50);
digitalWrite(ledPin, that LOW);
digitalWrite(flopRST, HIGH);
delay(50);
} //end of SETUP

//the loop routine runs over and over again forever:
void loop() {
  DateTime now; // here we get the time every loop
//we calculate the light intensity in lux
//the conversion from voltage to microamps to lux can be
//found in the datasheet of the TEMT6000
  lux = (analogRead(AMBIENT) * 0.9765625) * 0.1 + lplux * 0.9;
  lplux = lux;
  now = RTC.now();
  ms = (millis()-bootup)%1000; //here we calculate the ms

//we enter this loop if motion event has happend
  if (state == HIGH) {
    detachInterrupt(0);         // ('detected function has run)
    digitalWrite(flopRST, LOW); // we detach the interrupts
    digitalWrite(ledPin, HIGH);

    #if ECHO_TO_SERIAL
//we will print CommaSeparatedValues (CSV)
//to the Serial Monitor for:
//MONTH,DAY,YEAR,HOUR,MINUTES,SECONDS,
//MILLISECONDS,CH1,CH2,CH3,CH4,CH5,CH6,LUX
      if(now.month()<10){Serial.print(0);}
      Serial.print(now.month(), DEC);
      Serial.print(","that );
      if(now.day()<10){Serial.print(0);}
      Serial.print(now.day(),DEC);
      Serial.print(",");
      Serial.print(now.year(),DEC);
      Serial.print(",");
      if(now.hour()<10){Serial.print(0);}
      Serial.print(now.hour(),DEC);
      Serial.print(",");
      if(now.minute()<10){Serial.print(0);}
      Serial.print(now.minute(),DEC);
      Serial.print(",");
      if(now.second()<10){Serial.print(0);}
```

```
171       Serial.print(now.second(),DEC);
172       Serial.print(",");
173       if(ms<10){Serial.print("00");}
174       if((ms >= 10)&&(ms<100)){Serial.print(0);}
175       Serial.print(ms,DEC);
176       for(int i=0; i<6; i++){
177         Serial.print(",");
178         Serial.print(sensors[i]);
179       }
180       Serial.print(',');
181       Serial.println(lux,1);
182     #endif ECHO_TO_SERIAL
183       #if WRITE_TO_SD
184 //we will write some CommaSeparatedValues (CSV)
185 //to the logfile for:
186 //MONTH,DAY,YEAR,HH,MM,SS,mmm,CH1,CH2,CH3,CH4,CH5,CH6,LUX
187       if (now.month() < 10) {logfile.print(0);}
188       logfile.print(now.month(), DEC);
189       logfile.print(",");
190       if(now.day()<10){logfile.print(0);}
191       logfile.print(now.day(),DEC);
192       logfile.print(",");
193       logfile.print(now.year(),DEC);
194       logfile.print(",");
195       if(now.hour()<10){logfile.print(0);}
196       logfile.print(now.hour(), DEC);
197       logfile.print(",");
198       if(now.minute()<10){logfile.print(0);}
199       logfile.print(now.minute(), DEC);
200       logfile.print(",");
201       if(now.second()<10){logfile.print(0);}
202       logfile.print(now.second(),DEC);
203       logfile.print(",");
204       if(ms<10){logfile.print("00");}
205       if((ms >= 10)&&(ms%1000<100)){logfile.print(0);}
206       logfile.print(ms, DEC);
207       for(int i=0; i<6; i++){
208         logfile.print(",");
209         logfile.print(sensors[i]);
210         sensors[i] = 0;
211       }
212       logfile.print(',');
213       logfile.println(lux,1);
214 //flush() actually writes the data to the SD card
215       logfile.flush();
216     #endif WRITE_TO_SD
217 
218 //here we basically write 0's in our sensor array
219 //to be able to store new events
220     sensors[6];
221 
222 //than we RESET the SN74LS423 IC's
223     delay(10);
224     digitalWrite(ledPin, LOW);
225     digitalWrite(flopRST, HIGH);
226     delay(10);
227 //now we arm our interrupt routine again
228     state = LOW;
229     attachInterrupt(0, detected, FALLING);
230   }
231 }
232 
233 void detected() {
234 //the interrupt routine simply checks all the
235 //sensor ports if something happend (0-5V)
236   if (state == LOW) {
237     detachInterrupt(0);
238     sensors[0] = digithat talRead(SENS_A);
239     sensors[1] = digitalRead(SENS_B);
240     sensors[2] = digitalRead(SENS_C);
241     sensors[3] = digitalRead(SENS_D);
242     sensors[4] = digitalRead(SENS_E);
243     sensors[5] = digitalRead(SENS_F);
244     state = HIGH;
245 
246     int sum = 0;
247     for (int i = 0; i < 6; i++) {
248       sum = sum + sensors[i];
249     }
250     if (sum == 0) {
251       state = LOW;
252       attachInterrupt(0, detected, FALLING);
253     }
254   }
255 }
```

Listing 5.2 | Python Script to analyze Motion Data

```
#!/usr/bin/env python
# -*- coding: utf-8 -*-

#////////////////////////////////////////////////////////////////////////////
#/ MIT License                                                             //
#/                                                                         //
#/ Copyright (c) [2017] [Andreas Genewsky]                                 //
#/                                                                         //
#/ Permission is hereby granted, free of charge, to any person obtaining a //
#/ copy of this software and associated documentation files (the "Software"), //
#/ to deal in the Software without restriction, including without limitation //
#/ the rights to use, copy, modify, merge, publish, distribute, sublicense, //
#/ and/or sell copies of the Software, and to permit persons to whom the   //
#/ Software is furnished to do so, subject to the following conditions:    //
#/                                                                         //
#/ The above copyright notice and this permission notice shall be included //
#/ in all copies or substantial portions of the Software.                  //
#/                                                                         //
#/ THE SOFTWARE IS PROVIDED "AS IS", WITHOUT WARRANTY OF ANY KIND, EXPRESS OR //
#/ IMPLIED, INCLUDING BUT NOT LIMITED TO THE WARRANTIES OF MERCHANTABILITY, //
#/ FITNESS FOR A PARTICULAR PURPOSE AND NONINFRINGEMENT. IN NO EVENT SHALL  //
#/ THE AUTHORS OR COPYRIGHT HOLDERS BE LIABLE FOR ANY CLAIM, DAMAGES OR OTHER //
#/ LIABILITY, WHETHER IN AN ACTION OF CONTRACT, TORT OR OTHERWISE, ARISING  //
#/ FROM, OUT OF OR IN CONNECTION WITH THE SOFTWARE OR THE USE OR OTHER      //
#/ DEALINGS IN THE SOFTWARE.                                               //
#////////////////////////////////////////////////////////////////////////////

__author__ = 'Andreas Genewsky (2017)'
import argparse
import numpy as np
import matplotlib.mlab as mlab
import matplotlib.pyplot as plt
from datetime import datetime
import math
np.seterr(all='ignore')

parser = argparse.ArgumentParser(description="**** Motion Detector Analysis Script ****",
                                 epilog="<<< Andreas Genewsky (2017) - Max-Planck Institute
    for Psychiatry >>>")

parser.add_argument('-i','--input', help='Input file name',required=True)
parser.add_argument('-o','--output',help='Output file name', required=True)
parser.add_argument('-b','--bin',help='Bin Width in Milliseconds', required=True)
args = parser.parse_args()
inputfile = args.input
outputfile = args.output
binwidth = int(args.bin)
data = np.genfromtxt(inputfile, delimiter=',',skip_header=1)
timestamps = []
dtime = []
abstime = []
# MONTH, DAY, YEAR, HH, MM, SS, mmm
for x in range(0,data.shape[0]):
    YYYY = int(data[x,2])
    MM = int(data[x,0])
    DD = int(data[x,1])
    HH = int(data[x,3])
    mm = int(data[x,4])
    SS = int(data[x,5])
    ms = int(data[x,6])*1000
    timestamps.append(datetime(YYYY,MM,DD,HH,mm,SS,ms))

for x in range(0,len(timestamps)):
    abst = ((timestamps[x]-timestamps[0]).total_seconds())*1000
    abstime.append(abst)

mod = data[:,7:14]
abstime=np.array([abstime], dtype='float64').T
condata = np.concatenate((abstime,mod),axis=1)

maxBin = round(max(abstime[:,0]))
bincount = int(maxBin/(binwidth*1.0))
lastBin = maxBin-(maxBin%bincount)
bincount = int(lastBin/(binwidth*1.0))
bins = np.linspace(0,lastBin+binwidth,bincount+1,dtype='int',endpoint=False)
bins = np.array([bins]).T
bindata = np.zeros((bins.shape[0],condata.shape[1]),dtype='float64')
for x in range(0,bins.shape[0]):
    eventcounter = 0.0
    index = 0
    for y in range(0,condata.shape[0]):
        if( (condata[y,0]>=bins[x,0]) and (condata[y,0]<(bins[x,0]+binwidth)) ):
            bindata[x,:]=bindata[x,:]+condata[y,:]
            eventcounter += 1.0
```

```
84              index = y
85      condata = condata[index:condata.shape[0],:]
86      bindata[x,7]=bindata[x,7]/eventcounter
87      bindata[x,0]=bins[x,0]
88      print (str( round(((float(bins[x,0])/float(bins.max()))*100),2) )+" %")
89
90  np.savetxt(outputfile, bindata, delimiter=',',fmt='%10.3f')
```

5.4.2 Combined Electrical and Fiber-optic Rotary Joint

A low-cost motorized combined electrical and fiber-optic rotary joint for physiological recordings

(*in preparation*)

Genewsky A, Wotjak CT
Research Group 'Neuronal Plasticity'
Department 'Stress Neurobiology and Neurogenetics'
Max Planck Institute of Psychiatry, Kraepelinstr. 2-10, D-80804 Munich, Germany

Background The tethered acquisition of electrophysiological measures in freely moving and behaving rodents requires a system which permits the rotation of the animal, while ensuring constant electrical contact to the preamplifier. Electrical swivels, used for this purpose, should allow small animals (e.g. mice or zebra finches) to operate the rotary joint easily, but should also incorporate a fiber-optic rotary joint for optogenetic experiments. Commercially available combined electrical and fiber-optic rotary joints are disproportionately expensive compared to the asset costs of popular open-source electrophysiology systems. Therefore we aim to provide an affordable open-source solution.

Results We show the design, construction and validation of a low-cost motorized combined electrical and fiber-optic rotary joint (MEFRJ) for physiological recordings. We demonstrate first its applicability by non-invasive electrocardiographic (ECG) recordings during signaled auditory fear-conditioning memory recall, and secondly combine ECG measurements with single-unit neuronal recordings of optogenetically identified glutamatergic neurons within the murine motor cortex using a novel innate fear paradigm.

Conclusion This study features for the first time the entire process for the successful construction of a motorized combined electrical and fiber-optic rotary joint, with an emphasis on detailed building instructions and careful material selection in order to aid reproducibility. We further highlight its usefulness in combining electrocardiographic measurements with behavioral paradigms, and hope that our design fosters the pursuit of such an approach in preclinical affective & behavioral neuroscience to ultimately substantiate behavioral readouts of fear and anxiety with physiological data.

Introduction

The recording of electrical signals in freely moving and behaving animals equipped with sensors, transducers or amplifiers, is a fundamental approach to link physiology

and behavior. Thereby the electrophysiological measurement of biological & chemical potentials (single-units, EEG, ECG, EMG, voltammetry, amperometry) plays an equally important role as the recording of core body temperature, blood-pressure, acceleration or breathing (inhalation & exhalation) in conjunction. However, the low-noise, multi-channel acquisition of these modalities at high sampling rates is challenging especially if large arenas (e.g. EPM) are required. A typical setup consists of a signal transducer (e.g. an electrode or a sensor) followed by a preamplifier which contains passive input filters, most commonly differential or buffer amplifiers (Buzsàki et al., 1989) and some active signal conditioning. The amplified channels are conveyed via individual wires (e.g. litz wire) to the main amplifier where the final amplification, filtering and digitization takes place. All analog signal lines have to be shielded from electrical interference using either shielded wires or possibly quite large faraday cages. If the animal is allowed to move freely and rotate, the recording wires will ultimately end up being twisted and will interfere with the animals behavior. Therefore it is necessary to interpose electrical swivels or commutators typically between the preamplifier (headstage) and the main amplifier/data acquisition (DAQ) device. Battery powered, wireless systems offer a straightforward solution to this problem. However, those systems typically consist, besides the preamplifier-transmitter combination, of the entire DAQ system in combination with specialized software, and therefore do rarely permit the use of open-source soft- or hardware. The proposed system does not aim to compete with wireless solutions in any respect.

An electrical swivel has two major characteristics: the electrical and the mechanical resistance. In analog systems the electrical resistance and mostly its unpredictable change over time can be a major source of noise. Enclosed and shielded slip-ring assemblies with gold-plated contacts have acceptable electrical noise characteristics, but the torque force which is necessary to actuate them is high and already at low channel counts (<12), mice are unable to rotate them even with rigid wires. In order to minimize electrical and mechanical resistance Sutton and Miller (1963) developed a 'mercury swivel' in 'pancake' configuration (Fig. 5.6a m*left panel*) where each channel was attached to a contact which was immersed in concentric mercury filled pools. These swivels are excellent for small animals, but also expensive. Fee and Leonardo (2001) took a different approach and motorized the more cost-effective slip-ring assemblies using a rotation sensing circuitry which controls small geared motors to carefully counterbalance any rotation introduced by the animal. Thereby the necessary force to actuate the whole apparatus was elegantly reduced to the torque of a small, degreased ball bearing (<100 μNm). As optical stimulation techniques are nowadays part of the standard in-vivo electrophysiologists methods repertoire, a combined electrical and fiber-optic rotary joint is crucial. However, the costs of commercially available electrical and fiber-optic rotary joints stand in steep contrast with popular open-source recordings systems like Open-Ephys (Siegle et al., 2017). To address disproportional expenditure, we have designed a low-cost motorized combined electrical and fiber-optic rotary joint (MEFRJ) for physiological recordings.

Methods

Animals In this study only male, single-housed C57BL/6N (N=10) and C57BL/6$^{\text{NEX-ChR2}}$ (N=1) mice have been used. Both strains were bred in the animal facilities of the Max Planck Institute of Biochemistry, Martinsried, Germany. The animals were kept under standard housing conditions: 12h/12h inverted light-dark cycle (light off at 8 AM), temperature 24°C, food and water *ad libitum*. Experimental procedures were approved (AZ 142-12) by the Committee on Animal Health and Welfare of the State of Bavaria (Regierung von Oberbayern, Munich, Germany). Animal care taking and experiments were performed in compliance with the European Economic Community (EEC) recommendations for the care and use of laboratory animals (2010/63/EU). We have kept the number of animals to the absolute minimum, sufficient to reveal significant group differences.

Surgical Procedure & Electrode Design The optrode consisted of 12-channel micro-wire (25 μm formvar-coated tungsten wire) array, one ground and reference electrode (stainless steel skull screws), a 200 μm optic fiber, and one ECG electrode. While the ECG electrode was placed behind the animals right foreleg between the fat tissue and the skin, the optrode was implanted to target the border between the right primary and secondary motor cortex (AP +1.0 mm, ML +0.5 mm, DV -0.5 mm) of a NEX-ChR2 animal, using a stereotaxic frame (Leica Biosystems, AngleTwo). The animal received pre-surgical analgesic treatment (200 mg/kg Novalgin/Metamizol in saline, s.c.) and was anesthetized using isoflurane (2-2.5 % in oxygenated air), while the animals body temperature was kept constant (37.5°C) using a heating pad, a rodent rectal probe and an animal temperature controller. The optrode was attached to the skull and screws using dental cement (Paladur®, Heraeus-Kulzer). After the surgery the animal received post-surgical analgesic treatment (1 mg/kg Metacam in saline, s.c.) for 5 consecutive days. The animal was allowed to recover for 2 weeks in total.

PCB Design & Manufacturing The printed circuit boards (PCBs) have been designed using the cross-platform open-source electronic design automation suite KiCAD (http://kicad-pcb.org/). All design files are available online (https://github.com/AGenews/MEFRJ) or on request. The PCBs have been manufactured by the community printed circuit board service OSH Park (https://oshpark.com/) using the standard manufacturing parameters: two-layered FR4, 1.6 mm thickness, electroless nickel immersion gold finish, clearance >160 μm, trace width >160 μm, >254 μm drill size. Most electronic components are of the through-hole type and are therefore very easy to hand-solder.

Software Design The cross-platform software to write and upload the Arduino code (*see* additional files, Listing 5.3) is freely available online (https://www.arduino.cc/en/main/software). All files are available online

(https://github.com/AGenews/MEFRJ) or on request.

Statistical Analysis All data is presented as mean values ± standard error. Statistical analysis has been performed using GraphPad Prism 5.03. One-way and two-way analysis of variance was followed by *Dunnett's Multiple Comparison Test* or *Bonferroni* post-hoc analysis.

Results

Design and Construction of the MEFRJ The combination of commercially available fiber-optic rotary joints with through-bore slip-ring (SR) assemblies are a possible solution for large animals like rats, which can tolerate the substantial torque forces necessary to operate the swivel (Fig. 5.6a *middle panel*). For smaller animals like mice, a motorization of the SR is necessary. We have taken the initial idea suggested by Fee and Leonardo (2001), replaced the analog sensing and motor driving circuitry with a microprocessor prototyping board and also exchanged magnet and Hall effect sensor with optical sensors. Further, we did not incorporate a special ball bearing for the translation of the animals movements to the rotation sensing circuit, but utilized the in-built bearing of the integrated fiber-optic rotary joint. In addition this allowed the use of an optical fiber, instead of entangling prone wires, to translate rotational torques. This resulted in a rather simple and easily comprehensible system (Fig. 5.6a *right panel*). In order to aid the smooth integration into existing open-source based electrophysiology rigs, we have designed our MEFRJ with the Open Ephys system* in mind. As the mechanical implementation of a device consisting of moving parts, gears and electronics, requires a basic knowledge of electrical and mechanical engineering, we sought to provide in addition all supporting construction material. The most user-friendly and cost-effective solution seemed to devise the entire MEFRJ as being constructed of printed circuit board (PCB) material. PCBs are fabricated of glass-reinforced epoxy laminate, and therefore offer high rigidity and torsional stiffness. Using this approach we could design all parts with the cross-platform open-source electronic design automation suite KiCAD† in a manner that they fulfill both, mechanical and electrical functions. This resulted in a panelized PCB (Fig. 5.6b) featuring all necessary elements (besides electronic and a small number of other components) in a kit-like manner to build the MEFRJ, which is easily obtainable via e.g. the community printed circuit board service OSH Park‡. Figure 2.4c provides multiply views on an assembled and populated MEFRJ. In detail (Fig. 5.6d) the MEFRJ consists of a main board (board 1) which houses most necessary electronic components (microprocessor prototyping board, motor driving circuit, voltage regulators, supply voltage buffer capacitors, indicator LEDs, switches, potentiometer, etc.), the movable motor fixture (board 2), the slip-ring assembly, and

*http://www.open-ephys.org/
†http://kicad-pcb.org/
‡https://oshpark.com/

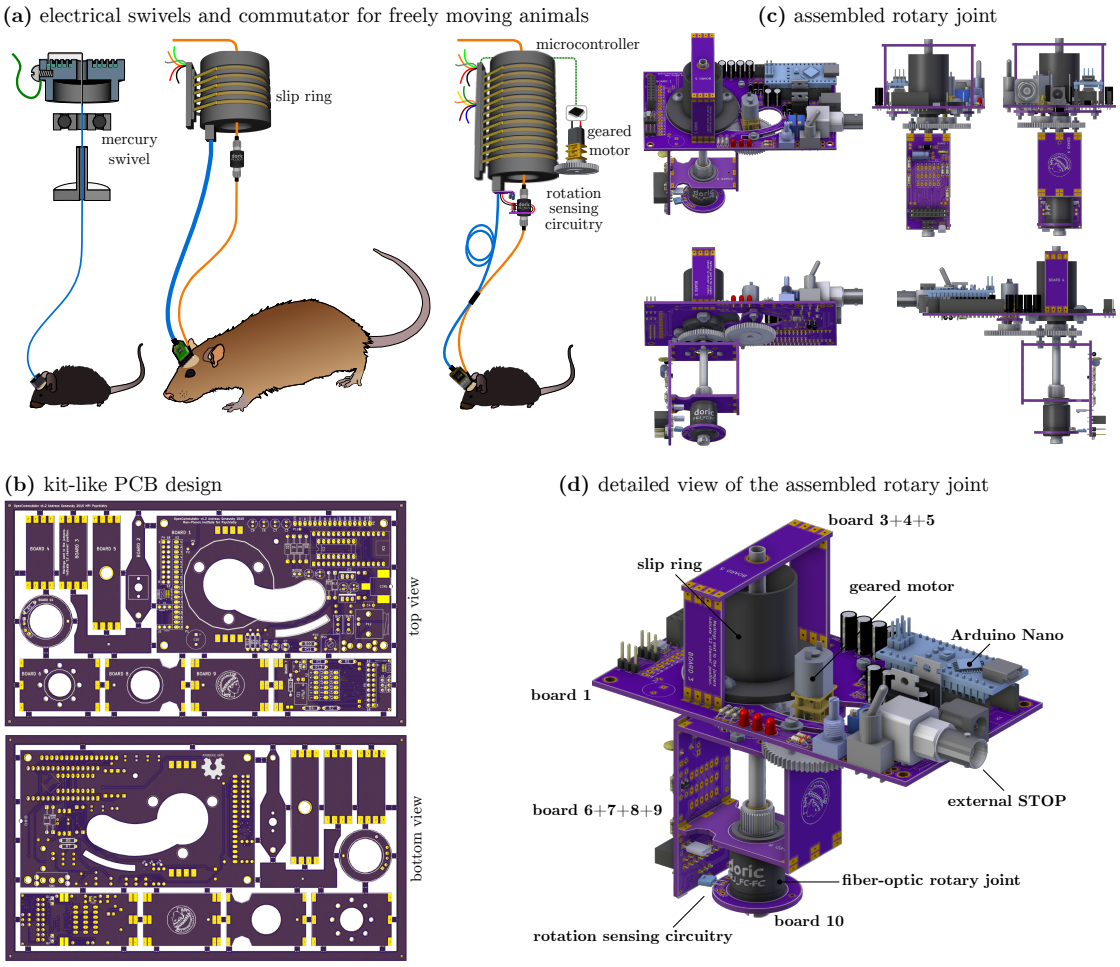

Figure 5.6 | Design and Construction of the Low-cost Motorized Combined Electrical and Fiber-optic Rotary Joint (MEFRJ)
(**a**) Overview of the different types of commonly used swivels for experiments with freely-moving animals. *Left*: mercury swivel; *middle*: commercially available through-bore slip-ring assembly used for rats; *right*: motorized combined electrical fiber-optic rotary joint. (**b**) A notable highlight of the current design is that its body parts are entirely constructed out of printed circuit board (PCB) material (60$ per board). (**c**) Different views at the proposed MEFRJ design. (**d**) Detailed and annotated view of the proposed MEFRJ design.

the fiber-optic support frame (board 3+4+5) to which the fiber-optic rotary joint is attached via a piece of silicone tubing. Subjacent to the main board is the rotating element, attached to a gear-wheel (via board 6), which is in turn glued to the rotor of the swivel. The rotating element consists of board 7, which houses part of the sensing circuitry, the IR photodiodes, connectors and a panel to solder the wires coming from the slip-ring onto. Board 8 holds a large bore for a flanged ball bearing which supports the fiber-optic rotary joint. Board 9 simply provides more stability. The IR emitter which allows the two photodiodes to detect a rotation, is mounted on the circular board 10, which in turn is glued to the rotating part of the fiber-optic rotary joint. The electrical connection towards board 10 is made via 0.1 mm enameled magnet wire. All mechanical connections between the PCB are made via solder bridges. A list with all necessary parts for the construction of the MEFRJ is shown in table 5.8. A detailed step-by-step instruction for the assembly and operation can be found online*.

*https://github.com/AGenews/MEFRJ

Table 5.8 | List of Materials for the MEFRJ

Reference	Qty.	Item	Part No.	Mfr.	RS No.
Electronic Parts					
C1, C2, C5, C8, C9	5	electrolytic capacitor, 10 μF, 35V	UPW1V100MDD	Nichicon	715-2713
C3, C6, C7	3	electrolytic capacitor, 22 μF, 35V	UPW1V220MDDD	Nichicon	715-2729
C4, C12	2	ceramic capacitor, 100 nF, 50V	RPER71H104K2M1A03A	Murata	653-0153
C10	1	*user defined*	*n.a.*	*n.a.*	*n.a.*
C11	1	electrolytic capacitor, 470 μF, 6.3V	ECA0JHG471	Panasonic	715-2713
D1	1	IR emitter	IRL 81 A	OSRAM	654-9179
D2, D7, D8	3	red indicator LEDs	L-934ID	Kingbright	228-5916
D3, D4, D5. D6	4	ultrafast switching diode	STTH102	STMicroelectronics	486-2896
D9, D10, D11, D12	4	general purpose rectifier diode	1N4002-E3/54	Vishay	708-7966
D13	1	Schottky diode	1N5818RLG	ON Semiconductor	625-5212
CON1	1	DC barrel jack	*n.a.*	RS Pro	476-157
IC1	1	Arduino Nano V3.1	Arduino Nano	Arduino	696-1667
IC2	1	high-current half-H bridge driver	L293NE	Texas Instruments	526-274
IC3, IC4	2	adjustable voltage regulator	LM317TG	ON Semiconductor	113-8596
IC5	1	low power operational amp.	LT6220IS5#TRMPBF	Linear Technology	761-8891
J2, J3, J4, J5	4	jumper	M20-9990346	Harwin	745-7068
K1, K4	2	connectors for Open Ephys	PZN-12-AA	Omnetics	*n.a.*
K2, K3	*n.a.*	slip ring solder connections	*n.a.*	*n.a.*	*n.a.*
P1, P2, P3, P8. P9, P10, P11, P13	*n.a.*	test pins	*n.a.*	*n.a.*	*n.a.*
P4, P5	2	9-pin female header 2,54 mm	SSW-109-01-G-D	Samtec	765-5717
P6	3	16-pin female header RM2.54, also used to reversibly mount the Arduino Nano	SSW-116-02-G-S	Samtec	765-5795
P7	*n.a.*	solder connections to the motor	*n.a.*	*n.a.*	*n.a.*
P12	1	BNC connector	1-1337542-0	TE Connectivity	512-1203
P14, P15	*n.a.*	solder connections for magnet wire	*n.a.*	*n.a.*	*n.a.*
Q1, Q2	2	IR receiver	LPT 80 A	OSRAM	654-7993
R1, R2	2	resistor 100 kΩ	MRS25000C1003FCT00	Vishay	683-2923
R3, R4	2	resistor 430 Ω	MRS25000C4300FCT00	Vishay	683-4225
R5, R14	2	resistor 1 kΩ	MRS25000C1001FCT00	Vishay	683-3165
R6, R7, R8, R9, R12	5	resistor 560 Ω	MRS25000C5600FCT00	Vishay	683-3837
R10, R11	2	resistor 220 Ω	MRS25000C2200FCT00	Vishay	683-3314
R13	1	resistor 100 Ω	MBB02070C1000FCT00	Vishay	477-7681
RV1	1	potentiometer 1 kΩ	3310Y-001-103L	Bourns	522-0625
RV2	1	trimmer 500 Ω	3296W-1-501LF	Bourns	521-9782
RV3	1	trimmer 2.2 kΩ	3296W-1-222LF	Bourns	785-9736
SW1	1	toggle switch	1MS1T1B4VS2QES	RS Pro	734-7084

List of Materials for the MEFRJ (continued)

Reference	Qty.	Item	Part No.	Mfr.	RS No.
Accessories					
n.a.	1	miniature geared motor 50 RPM@6V	951D2981/6V	Como Drills	752-2005
n.a.	1	spur gear-wheel, 0.5 MOD 50 teeth	DS05-50B	RS Pro	521-7146
n.a.	1	spur gear-wheel, 0.5 MOD 60 teeth	DS05-60B	RS Pro	521-7174
n.a.	1	silicone tubing	760320	Saint-Gobain	492-4578
n.a.	1	bore adapter, Ø6.35 mm×6.6 mm, shaft Ø3 mm	253.14	Huco	689-108
n.a.	2	screws to mount the motor, 0-80x1/4 in.	*n.a.*	*n.a.*	*n.a.*
n.a.	6	jumper	AKSCT/Z BLACK	ASSMANN WSW	674-2397
n.a.	1	ball bearing, F6700 ZZ = FL61700 2Z 10×15×4 mm	*n.a.*	*n.a.*	*n.a.*
Other					
n.a.	1	through bore slipring assembly 12-rings	rotarX RX-HS-12	b-command.com	*n.a.*
n.a.	1	FC/PC fiber-optic rotary joint patch cable	RJPFL2	Thorlabs	*n.a.*
n.a.	1	1×1 Fiber-optic rotary joint	FRJ_1x1_FC-FC	doric	*n.a.*
n.a.	1	power adapter	8154014	RS Pro	737-8149

Operating Principle of the MEFRJ A detailed circuit schematic of the MEFRJ is given in figure 5.7, whereby sub-circuits are indicated with different background color. Depicted with white background is the the main board 1. The board is powered via a 7.5-12 V DC stabilized voltage supply which can be implemented using typical 'wall-wart' type external power adapters. The voltage input is buffered slightly by C3 and C5 and subsequently relayed to the two adjustable linear voltage regulator (LM317) circuits around IC3 and IC4. IC3 is used to generate an output voltage in the range of 4.4-7.3 volts, in order to power the Arduino Nano microprocessor prototyping board (IC1) and the motor driver (IC2, L293NE). The adjustable voltage regulator accounts for the possibility to use a custom microprocessor plug-in board (e.g. built around an Atmel ATiny85), using a similar form factor, which might incorporate none or another 5V voltage regulator (different drop-out voltage). If the suggested Arduino Nano is used, the output voltage of IC3 should be set via the trimmer RV2 in a way that the voltage output (5 V) of the Arduino Nano reads stable +5.00 V (all voltages are accessible via P6, *not shown*). The other regulator (IC4) generates the voltage (4.4-17 V, *limited by the power supply*) which is used to drive the geared motor. Using the proposed miniature geared motor (951D2981/6V), the output should read +6.00 V (adjusted via trimmer RV3). The motor supply output is subsequently buffered by C3, C6, C7 in order to provide the necessary current to drive the motor. In addition C1 offers the possibility to use another larger electrolytic capacitor, if necessary. Indicator LEDs D7 and D8 show the correct functionality of the power supply, but more importantly provide a minimal load ($\approx$ 10 mA) to a allow stable voltage regulation by IC3 and IC4. Indicator LED D2 is used to signal failure malfunctions (LED blinking, motor output is disabled). The Arduino Nano microprocessor prototyping board (IC1) is used to power and simultaneously read the rotation sensing circuitry and control the direction and speed of the miniature geared-motor. The potentiometer RV1 allows to adjust the maximal motor speed manually. The BNC input P12 offers the possibility to externally suppress an activation of the motor, e.g. during noise sensitive tasks, by pulling this input to ground. Alternatively the toggle switch SW1 can be used. The motor is controlled via the half-H bridge driver L293NE (IC2) in combination with four high-speed output diodes (D3, D4, D5, D6) for inductive transient suppression. The MEFRJ interfaces with the OpenEphys system via the Omnetics connectors K4 (to the acquisition board) and K4 (on rotating element with the preamplifier headstage). Otherwise, connectors P4 and P5 can be used for custom interfacing solutions to other DAQ and recording system. The MEFRJ is designed to be used with either 12-ring or 18-ring slip-ring (SR) assemblies. Whereas a 18-ring SR allows the use of up to 64 recording channels (via the use of two headstages)*, we have focused on the use of the far better available and inexpensive 12-ring SRs, which however, permit only the use of one single headstage (32 channels). The combination of all signal lines for the operation of one headstage and the rotation sensing circuitry into 12 rings, opposed a design challenge. However, by omitting the second pair of serial peripheral interface

*https://open-ephys.atlassian.net/wiki/display/OEW/Multiple+headstages+on+one+cable

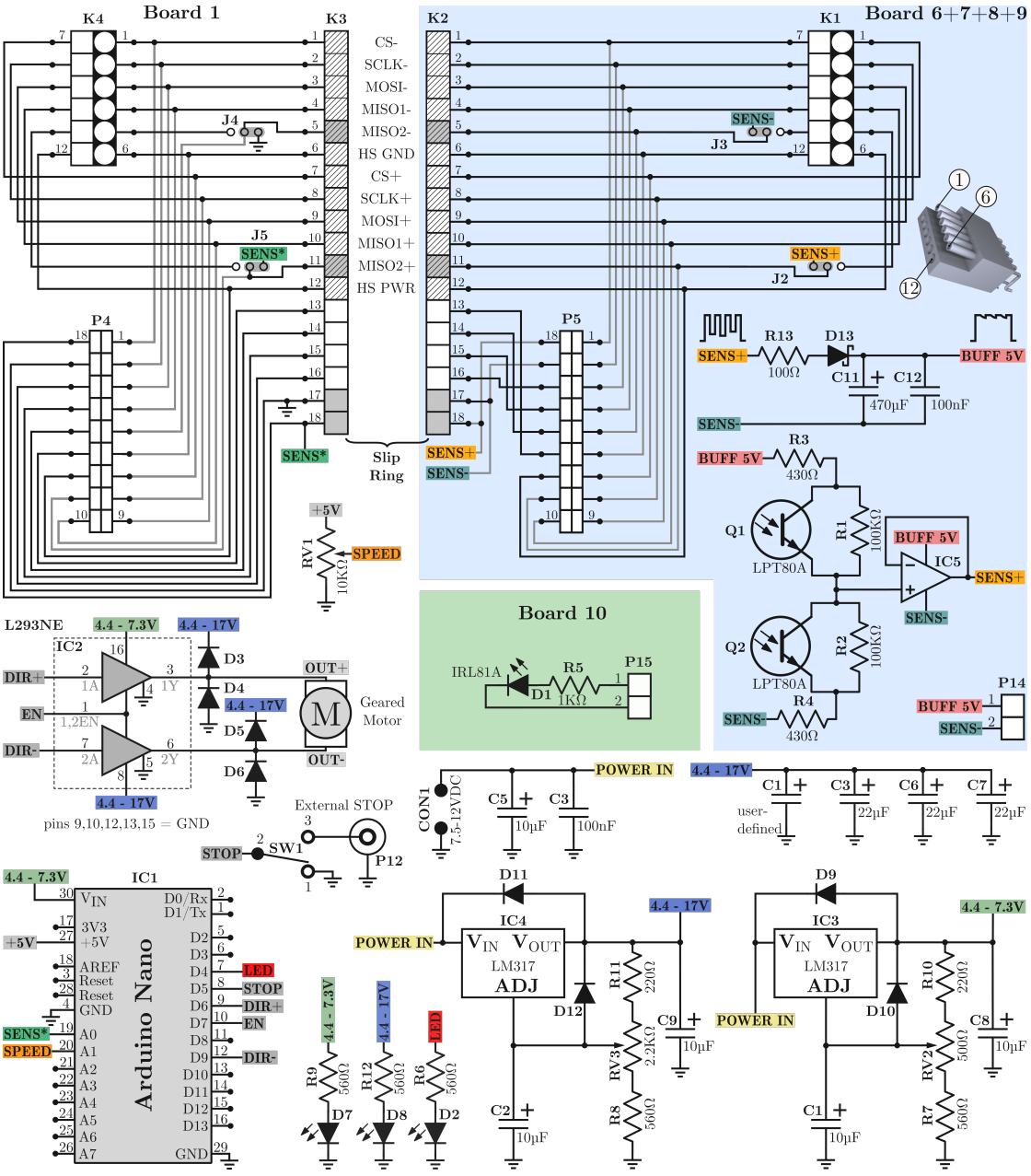

Figure 5.7 | Schematic Drawing of the MEFRJ
This figure shows the very simple working principle of the design and allows to populate the PCBs. Subcircuits are shown according to their respective place on the boards.

(SPI) master input slave output (MISO) logic signal lines (MISO2+, MISO2-), only 10 rings were necessary to operate one headstage. In order to implement the rotation sensing circuitry with only two available rings, while keeping the power supply separate from the headstage, we have developed a simple 1-Wire bus inspired solution. The Arduino Nano's analog input (A0) can be set to low impedance output mode and provides +5 V (SENS*). This is sufficient to charge a large electrolytic capacitor (C11) on the rotating element side (*blue background*, boards 6,7,8,9), via a current limiting resistor R13 and the rectifying Schottky diode D13, generating a 5 V (BUFF 5V) power supply, which is additionally buffered by C12. This voltage is used to power the infrared

emitter on board 10, connected via P14 and P15 (enameled magnet wire). Moreover the buffered supply voltage powers the two photodiodes (Q1, Q2) in voltage divider configuration, and the resulting sensor voltage is relayed via a buffer amplifier (IC5), which imposes the measured signal onto the power line (SENSE+). Once the analog input A0 is configured to high impedance input mode, the resulting voltage corresponds to the voltage between the photodiodes and thus can be used to sense a displacement of the infrared emitter. This reconfiguration occurs every 20 ms, yielding a rotaion sampling rate of >40 Hz which is sufficient for smooth operation. Once a rotation has been detected, the motor is activated to counteract this displacement. The main loop of the Arduino code (listing 2.3) is set up to allow parallel processes. Therefore the Arduino Nano could even be used to carry out simple data acquisition tasks e.g. body temperature monitoring at low sampling rates (<10 Hz), autonomously.

Noise Characterization and Functional Validation of the MEFRJ In order to asses the possible noise levels, imposed by the low-cost slip-ring assembly used in this study, we have measured (Keithley 2110, Digital Multimeter) the average, minimal and maximal DC resistance of one ring, before and during 10 consecutive rotations of 5 seconds length (Fig. 5.8a). The only significant parameter suggested by one-way ANOVA ($F_{5,9}$=87.50, p<0.0001) was the increased maximal resistance (Rmax 203±4 mΩ vs. $R\bar{X}$ 163±2 mΩ) during rotation. This is explained by the construction technique of the slip-ring assembly itself, where minute irregularities in thickness between the sliding contacts generate short spikes in resistance. These resistance spikes do certainly not affect digital or amplified and conditioned analog signals to a larger extent, but might distort merely impedance buffered signals in the microvolt range. Therefore we henceforward assessed the noise characteristics of the complete MEFRJ only with the Open-Ephys miniature headstage attached, whereby one channel and the reference, were connected to ground via two 150 kΩ unshielded, axial, metaloxide resistors (Fig. 5.8b), without the use of a Faraday cage, in order to obtain realistic levels of electrical noise. The rotation was induced manually by rotating the connected optic fiber and limited to maximal 5 seconds by the Arduino firmware, while the headstage was swinging freely (Fig. 5.8f), for 3 different channels. The root mean square levels of noise during rotation were 7.2±0.6 μV in the low LFP (0-300 Hz), and 3.1±0.3 μV in the high single-unit (0.3-6 kHz) frequency band, both well acceptable values for high quality in-*vivo* electrophysiological recordings of various kinds (Fig. 5.8c). Further, no detectable signal deflection was observed upon the onset or offset of rotation, neither in the low, nor the high frequency band (Fig. 5.8d). In addition, there was no observable frequency specific signal deterioration, analyzed by fast Fourier transform (NumPy v1.12 *numpy.fft.rfft*), due to the rotation of the MEFRJ (Fig. 5.8e). In order to demonstrate the applicability of the proposed system, we aimed to conduct non-invasive electrocardiographic (ECG) recordings in unrestrained mice. Therefore we first designed a simple two-lead, AC-coupled ECG amplifier shown in figure 5.8g.

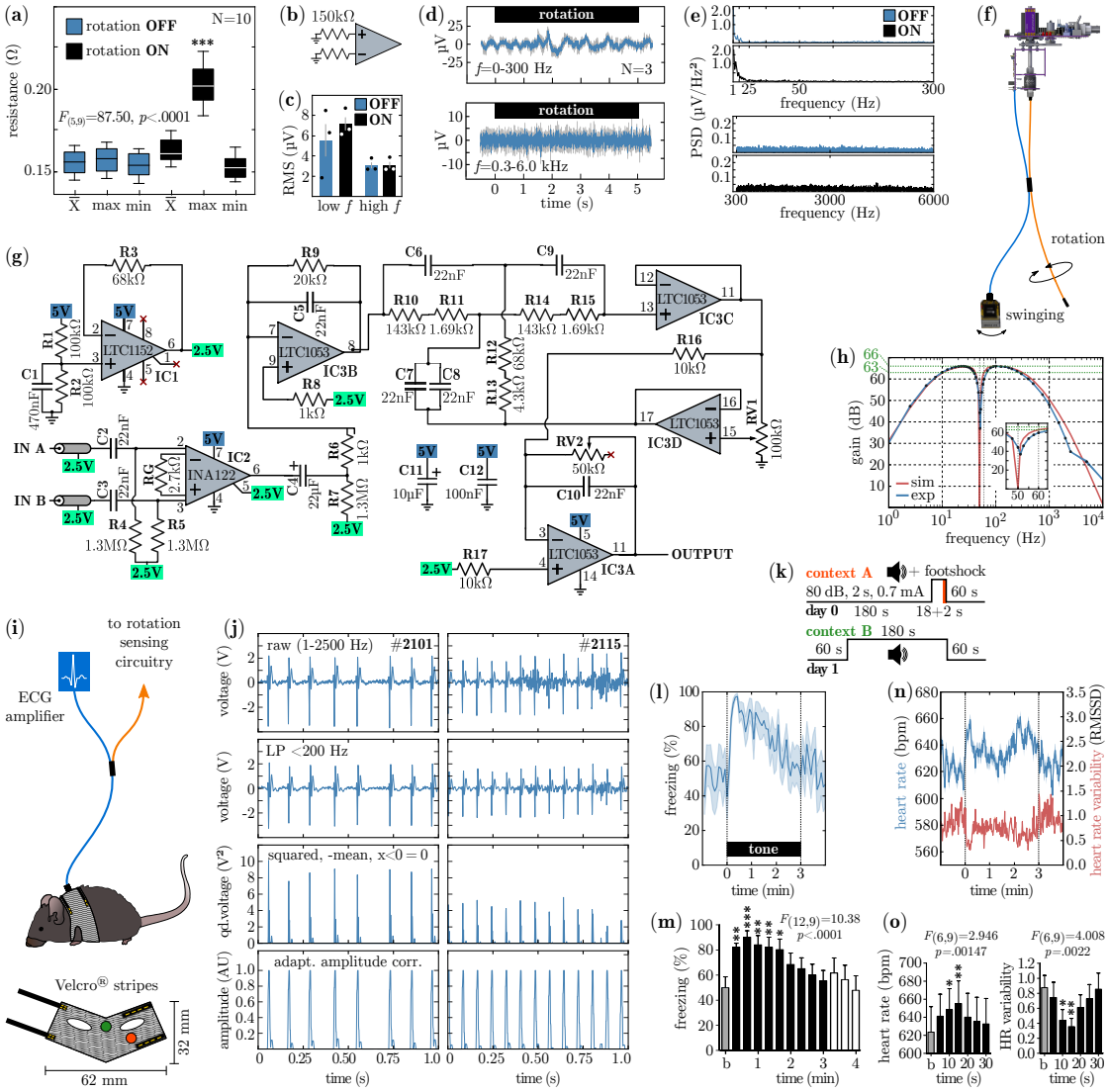

Figure 5.8 | Noise Characterization and Functional Validation of the MEFRJ
(**a**) Resistance measurements of the slip-ring assembly during rotation OFF and ON states. (**b**) Measurement setup. The active recording channel and the reference input were connected to GND via 150 kΩ metal-oxide resistors. (**c**) Quantification of RMS noise level before and during rotation. (**d**) Onset and offset of rotation does not introduce any detectable noise. (**e**) Spectral noise characteristics. (**f**) Recording setup. The headstage was allowed to swing freely, while the necessary torque to engage the feedback circuitry was applied via a fiber-optic cable. (**g**) Simple AC-coupled two-lead ECG amplifier circuit design, with 50 Hz notch filter. (**h**) Simulated (sim) and measured (exp) amplification characteristics of the ECG amplifier circuitry. (**i**) Upper panel: ECG recording setup using a custom mouse vest. Lower panel: to-scale depiction of the mouse vest. (**j**) Detailed ECG signal analysis procedure of clean (left) and noisy (right) exemplary data sets. (**k**) Auditory fear-conditioning and recall protocol. (**l**) Freezing response of C57BL/6N (N=10) animals towards a previously conditioned tone. (**m**) Quantification of dataset seen in l. One-way ANOVA with Dunnett's Multiple Comparison post-hoc test compared to baseline (b, 1 min before tone presentation). (**n**) Changes in heart-rate and heart-rate variability during fear expression. (**o**) Quantification of dataset seen in o. Same statistical analysis as in m. Significance values for one-way analysis of variance (ANOVA) followed by Dunnett's Multiple Comparison post-hoc test are given as: * $p < 0.05$, ** $p < 0.01$, *** $p < 0.001$.

The circuit consists of a precision instrumentation amplifier (INA122, IC2), an inverting amplification stage (IC3B), an active twin-T 50 Hz notch filter* with adjustable Q (RV1) and a final inverting output stage with variable gain (IC3A, RV2 set to $\approx$ 13 kΩ). The measured frequency characteristics fitted well to the simulated† results, and a peak amplification of 66 dB with corner frequencies (-3 dB) at 10 Hz and 250 Hz (Fig. 5.8h), ideal for murine ECGs, was achieved. To non-invasively record ECGs in freely moving mice, we have adopted a previously designed (Pereira-Junior et al., 2010) elastic cotton vest for rats and adjusted the dimension to fit a mouse (Fig. 5.8i). The vest contained two smooth nickel-plated brass buttons (Ø5mm, easy to solder) which served as electrodes. Each mouse was shaved at the electrode sites, and in addition small amounts of ECG conductive gel ensured low-noise recordings. The raw ECG amplifier output (relayed via the MEFRJ) was bandpass filtered (1-2500 Hz) and sampled at 10 kHz using the Open-Ephys acquisition board (analog inputs). Offline ECG analysis involved additional low-pass filtering (<200 Hz), squaring, subtraction of the mean and subsequently negative values were substituted with zero. Finally, the signals were normalized using an adaptive amplitude correction and peaks were identified using the automatic multiscale-based peak detection (AMPD) method (Scholkmann et al., 2012). Figure 5.8j illustrates the various steps of ECG analysis for a clean (*left panel*) and a noisy (*right panel*) signal. It has to be noted that this recording setup and analysis procedure is suitable to detect R-R intervals only, therefore no other parameters than heart rate and heart rate variability can be extracted. In order to assess whether the proposed setup is suited to detect physiological changes in heart rate and heart rate variability in situations with increased fear, we employed the auditory fear conditioning paradigm. Therefore we acclimatized a cohort of single-housed mice (C57BL/6N, N=10) to dummy vests for 2 consecutive days. On the conditioning day, each animal was placed in a chamber with an electrifiable grid-floor wiped with 70% ethanol (context A, Fig 5.8k *upper panel*) for 3 minutes, followed by 20 seconds presentation of a 9 kHz sine tone (80 dB SPL) which was co-terminated with a 0.7 mA aversive footshock 2 seconds in length. One minute after the shock the animal were returned to their home cage. Next day, the animals were equipped with the recording vest under light isoflurane anesthesia and 30 minutes later were placed into a new cage (wiped with 1% acetic acid) filled with bedding (context B, Fig 5.8k *lower panel*). After 1 minute of acclimatization, the animals were presented with the previously conditioned tone for 3 minutes. The successful auditory fear memory formation was evident, as the animals showed a strongly increased freezing response during the tone presentation (Fig. 5.8l) was significantly different from baseline (1 min before) within the first 100 seconds (Fig. 5.8m) after the onset of the tone (repeated measures one-way ANOVA, $F_{12,9}$=10.38, p<0.0001).

*http://www.changpuak.ch/electronics/Active_Notch_Filter.php
†http://www.linear.com/designtools/software/#LTspice

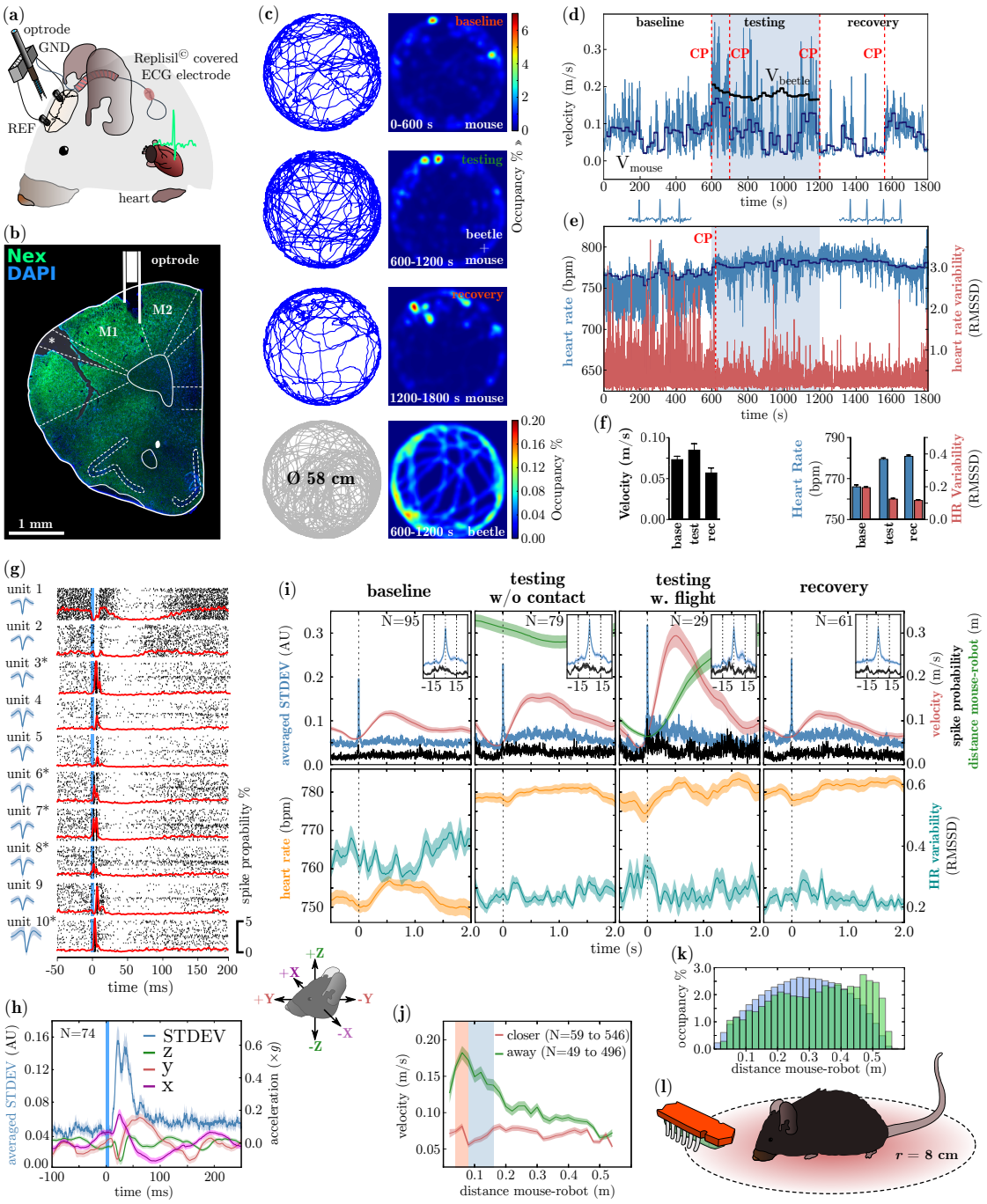

Figure 5.9 | Neurophysiological Recordings During a Novel Innate Fear Paradigm Using the MEFRJ

(**a**) Depiction of implanted electrodes. (**b**) Histological verification of electrode placement. (**c**) Movements of mouse and robot in the arena during the different phases of the paradigm. (**d**) Velocity of mouse and robot over time. (**e**) Changes in heart rate and heart-rate variability over time. (**f**) Quantification of datasets seen in d & e. (**g**) Optogenetic identification of glutamatergic neurons in the motor cortex. (**h**) Strong optogenetic activation of the recording site lead to robust motor output in the form of headshakes which could be detected in the accelerometer data. (**i**) Isolation of movement bouts during baseline, testing and recovery phase. Alignment was carried out with respect to accelerometer output. Movements bouts in close proximity to the robot were classified as flight responses. Changes of heart-rate and heart-rate variability occurred with respect to the movements. (**j**) Setting the distance between mouse and robot in relation with the animals speed with respect of the robots direction yields the defensive distance. (**k**) The animals overall distance towards the robots is right shifted compared to the theoretical distance distribution, indicating an active avoidance reaction. (**l**) Cartoon displaying the defensive distance.

The maximal changes in behavior were accompanied by a steep but transient increase in heart rate (beats per minute, bpm) and a resulting reduction in heart rate variability, which is expressed as the root mean square of successive R-R interval differences. These changes were shown to be significantly different from baseline only 10 and 15 seconds after the onset of the tone (Fig. 5.8o), by repeated measures one-way ANOVA (heart rate, $F_{6,9}$=2.946, p=0.00147; heart rate variability, $F_{6,9}$=4.008, p=0.0022).

Neurophysiological Recordings During a Novel Innate Fear Paradigm Using the MEFRJ In order to show the applicability of our proposed MEFRJ system in a more challenging situation, we combined the electrophysiological recording of optogenetically identified glutamatergic neurons and parallel ECG recordings with a novel innate fear paradigm. Therefore we have implanted an optrode (Fig. 5.9a), consisting of a 12-channel micro-wire array, one ground and reference electrode, a 200 μm optic fiber, and one ECG electrode, over the right primary/secondary motor cortex of a Nex-ChR2 animal, expressing channelrhodopsin and the reporter EGFP under the control of the murine NEX locus (Goebbels et al., 2006) in glutamatergic principal neurons. The ECG electrode consisted of a 100 μm Teflon-insulated stainless steel wire, which was routed over the neck muscle to the animals right flank. To ensure high flexibility and good recording conditions, one part of the electrode was spiral wound and covered with dental duplicating silicone, while the end of the electrode was striped and formed to a loop. A representative section showing the micro-wire electrode position and EGFP fluorescence is shown in figure 5.9b. For the innate fear paradigm we connected the animals to the headstage and placed it in a circular arena (Ø58 cm) and measured baseline activity for 10 minutes. Subsequently we added an autonomously moving bristle bot (HEXBUG Nano*), henceforward called beetle, for 10 minutes. Afterwards the animal was allowed to recover for additional 10 minutes. The entire experiments was captured using a GigE camera (PointGrey Blackfly s, BFS-PGE-13Y3C-C) at 30 frames per second (fps) and the position of the mouse and the orange painted beetle was determined via a custom C++ script utilizing the Open Source Computer Vision Library (OpenCV†). Figure 2.7c *left panel* shows the tracked movements of the mouse (blue) and the beetle (gray), which was used to generate occupancy plots (Fig. 5.9c *right panel*). At the occupancy plots one can seen the increased amounts of immobility of the animals (indicated by higher occupancy levels) while the beetle covered the entire arena with a tendency to move along the wall. Knowing the position of the mouse and the beetle, allowed us to calculate the velocity for both (Fig. 5.9d). In order to detect significant changes in the binned (20 seconds) velocity over time in a single measurement, we applied nonparametric multiple change point analysis (CPA) (James and Matteson, 2015). With the introduction of the beetle ($\approx$ 20 cm/s) the animals velocity (Fig. 5.9d) increased (p<0.005) and normalized after 100 seconds (p<0.001). With the removal of the beetle, the mouse showed increased immobility ((p<0.001), which lasted for

*https://www.hexbug.com/nano/glows-in-the-dark-hexbug-nano.html
†http://opencv.org/

360 seconds ($p<0.001$). The presence of the beetle, further, led 20 seconds after the introduction to a significant ($p<0.001$) increase in heart-rate, which was accompanied by a reduction in heart rate variability. Even after the removal of the beetle, when the animal showed a reduced locomotion and no increased cardiorespiratory need due to motor activity seemed necessary, the heart rate stayed unchanged. High levels of immobility and increased heart rate indicate an emotional challenging situation − in this case most likely a strong fear response. The quantification of these observations, based on binned (20 seconds, N=30 per time point) data, is shown in figure 5.9f. Every 10 seconds, during the entire task, we have applied a single 1 ms 460 nm light pulse (1 mW at fiber tip) in order to optogenetically identify NEX$^+$ glutamatergic principal neurons (Fig. 5.9g). Of the 10 isolated single units, we have taken only those for further analysis which showed a low-latency action potential (N=5) upon optogenetic activation. The Open-Ephys headstage is equipped with three-axis accelerometer and in order to prove whether M1/M2 optogenetic stimulation induced a detectable motor behavior we have increased the laser output power to 10 mW, set the pulse width to 5 ms (this experiment was conducted after the behavioral task) and stimulated (N=74) every 10 seconds. The stimulation of the right motor cortex led to a visible head shake towards the animals right side with additional deflection down- and backwards. This was also reflected by the accelerometer output (Fig. 5.9h) which showed low-latency responses in the range of 20-25 ms similar to previously published results (Silasi et al., 2013). The averaged standard deviation over a window of 3 samples was found to constitute a robust measure of acceleration. This value was taken also to align the neural, cardiac and behavioral responses during the innate fear task. Movement bouts were detected by taking the first derivative of the velocity obtained from video data, while focusing only on positively accelerating movement bouts which lasted longer than 8 frames (240 ms) and were not in close proximity of optogenetic stimulation (±250 ms). These temporally imprecise (30 fps) onsets of movements were used to find peaks in the accelerometer (30 kHz, LP 1.6 kHz) data (±150 ms). All episodes which showed a velocity greater than 15 cm/s within 500 ms before the onset, or a velocity smaller than 5 cm/s within 500 ms after the onset of the movement, were removed from the corrected movement bout onsets. Figure 5.9i shows the neural, locomotor and cardiac responses with respect to the onset of movement, either without or with the beetle. Further, we have subdivided the testing phase into episodes were the distance between the beetle and mouse was large, or minimal. The latter was considered to constitute a flight response (low distance and movement bout). The baseline movement bouts were characterized by a modest increase in velocity and a transient increase in heart rate which was expected due to the physical effort. The single unit responses were marginally increased at 20 to 5 ms prior to the onset of movement. The presence of the beetle (without contact) increased the peak velocity slightly (besides increased cardiac output). When the distance between the mouse and the beetle was less than 10 cm, the movements bouts were characterized by high peak velocity 29 cm/s, indicative of flight responses. Further, the neural activity was of the motor cortex was increased. After

the removal of the beetle, the locomotor profile, as well as the neural resembled the baseline condition, but as mentioned before, the heart rate remained elevated, while the heart rate variability was minimal. Whether the depicted temporal changes in heart rate and heart rate variability during flight responses, have any biological meaning cannot be deduced from one single animal, but we want to highlight the slight drop in heart rate around the onset of movement, seen in all four conditions. Figure 5.9j set the velocity of the mouse in relation to the distance between the mouse and the beetle. Further, we have distinguished between the two conditions, namely whether the beetle is coming closer and approaching or when the distance between the mouse and the beetle is increasing. When the distance in increasing (e.g. during a flight response) the velocity is maximal between 5 to 10 cm and slowly decays over the whole size of the arena. On the contrary, if the beetle is approaching the mouse, the velocity is always low, and has its minimum at 8 cm, indicative of high levels of immobility/freezing. In order to asses whether the mouse is avoiding the beetle in general, we have looked at the mouses' occupancy over the binned (2 cm) range of possible distance, and found a clear right shift of the distribution (green), compared to the theoretical occupancy (blue), suggesting an avoidance behavior. Knowing that the mouse avoided the beetle and reacted to it with increased flight responses and elevated heart rate, indicated that at a distance of 16 cm, when the mouse progressively showed increased levels of immobility, paralleling the approaching beetle, the defensive distance was entered. The switch from passive to active fear at 8 cm (Fig. 5.9l) further underlines the notion that this behavioral task is a promising model for the electrophysiological study of midbrain defensive circuits.

Discussion

In this study we have demonstrated the design, construction operation and functional validation of a low-cost motorized combined electrical and fiber-optic rotary joint (MEFRJ). We have shown the simple application of the MEFRJ combined with a custom amplifier to record non-invasively electrocardiographic signals during conditioned fear memory recall. Further, we have demonstrated the combined electrophysiological recording of optogenetically identified glutamatergic principal neurons in the murine motor cortex with electrocardiocardiographic recordings in a novel innate fear paradigm. This setup allowed us to find define a procedure to measure two essential markers within the defensive distance model proposed by Blanchard and Blanchard (1990) and refined by McNaughton and Corr (2004), namely the onset of immobility (high defensive distance) and the switch from passive to active fear coping strategies (low defensive distance).

Non-invasive ECG recordings We have labeled our ECG recording procedure, using a small jacket, *non-invasive*. This however, holds only true in a sense that we did not implant electrodes. Looking at the animals behavior, especially at the high levels of freezing ($\approx 50\%$), before the onset of the tone, it becomes obvious that the vest had clear restraining properties, which is accompanied by an elevated heart rate, an indicator of increased stress levels. Therefore we conclude, that the vest might be a useful approach

if sufficient (>2 days) time to acclimatize is allowed. But the aim of this experiment was to demonstrate how physiological parameters in the moving animal can be easily measured using a custom-built amplifier in combination with the MEFRJ. Possible other measures, which could be acquired in a similar manner are changes in body temperature using e.g. an IR thermometer (Melexis MLX90614), or respiratory rate using a contact microphone or a pressure sensor, or 3D-acceleration if no headstage is used. For ECG recording in freely moving animals we favor implanted electrodes especially if large arenas are used where typical telemetric devices cannot transmit data anymore. In addition this is also by far the most cost-effective solution.

Beetle-based innate fear paradigm Using the autonomously moving beetle in combination with video tracking of both objects, we have developed a promising paradigm to study neuronal circuits involved in the generation and regulation of fear responses and the accompanying changes in cardiorespiratory parameters. The most prominent feature of this test is the high number of threat-encounters, which is an important factor especially for neurophysiological studies, where the acquired neural signal can only be interpreted if precise time points are known for alignment. We aim to equip the small-sized beetle with an IR based remote control, in order to activate it only for short periods of time. This will hopefully enable us to titrate the aversiveness of the situation to a level were a recovery (seen by a drop in the heart rate) can be seen in reasonable time. In addition this would also allow us to asses approach behavior, which likely occurs once the robot stops.

Listing 5.3 | Arduino Code for the MEFRJ

```
// MEFRJ Control Software
// Copyright (C) 2015 Andreas Genewsky
//
#include <math.h>
// ------------------------------ //
//    SOFTWARE VERSION NUMBER:
int ver[2] = {
  1, 2};
// ------------------------------ //
//    PCB VERSION NUMBER:
int verPCB = 2;
// ------------------------------ //
//    DEBUG MODE?
boolean debugMode = true;
boolean fullspeed_noise_test = false;
// ------------------------------ //

// ARDUINO CONNECTIONS:
//
// DIGITAL I/O
// D2 External Stop
// D4 Indicator LED
// D6 DIRECTION +
// D7 ENABLE
// D9 DIRECTION -
// D12  goes HIGH if Motor is on!
// D13  on-board LED
//
// ANALOG I/O
// A0 SENS_VAL
// A1 SPEED_VAL

// ARDUINO DEFINITIONS:
int extstop = 2;
int indled = 4;
int dirpos = 6;
int dirneg = 9;
int enable = 7;
int motoron = 12;
int obled = 13;
int senspin = A0;
int speedpin = A1;
volatile int extstate = LOW;
float sensval = 0.0;
int minspeed = 30;
int maxspeed = 0;
int speed = 0;
int step = 5;
int direction = 0;
unsigned long task0 = 0;
unsigned long task1 = 0;
unsigned long task2 = 0;
unsigned long  turning_start = 0;
volatile boolean turning = false;
boolean fail = false;
int ledstate1 = HIGH;
// BEGIN ACTUAL CODE:
void setup()
{
  pinMode(extstop, INPUT_PULLUP);
  pinMode(indled, OUTPUT);
  pinMode(dirpos, OUTPUT);
  pinMode(dirneg, OUTPUT);
  pinMode(enable, OUTPUT);
  pinMode(obled, OUTPUT);
  pinMode(motoron, OUTPUT);
  pinMode(A0,OUTPUT);
  digitalWrite(A0,HIGH);
  if (debugMode) {
      Serial.begin(9600);
    }
  extstate = digitalRead(extstop);
  if(extstate == LOW){
    attachInterrupt(0,start,RISING);
  }
  if(extstate == HIGH){
    attachInterrupt(0,stop,LOW);
  }
  digitalWrite(indled, extstate);
```

```
}
void loop()
{
  if(fullspeed_noise_test){
    turn(-255);
    delay(1000);
    turn(0);
    delay(2000);
    turn(255);
    delay(1000);
    turn(0);
    delay(2000);
  }
  if((millis()-task0)>20){
    pinMode(A0,INPUT);
    if((millis()-task0)>25){
      sensval = analogRead(senspin);
      sensval = map(sensval,12,478,0,100);
      pinMode(A0,OUTPUT);
      digitalWrite(A0,HIGH);
      task0 = millis();
      Serial.println(sensval);
    }
  }
  if(!fullspeed_noise_test){
    if(!turning){turning_start = millis();}
    if( ((millis()-turning_start)>5000)&&
     extstate==HIGH ){
      fail=true;
    }
    maxspeed = get_speed();
    if( ((millis()-task1)>20)&&(!fail) ){
      if(sensval<3.0){
        speed += step;
        direction = 1;
      }
      if(sensval>97.0){
        speed += step;
        direction = -1;
      }\mbox{}\\
      if( (sensval>5.0) && (sensval<95.0) ){
        speed = minspeed;
        direction = 0;
      }
      speed = constrain(speed,minspeed,
     maxspeed);
      turn(speed*direction);
      task1 = millis();
    }
    if(fail){
      turn(0);
      if((millis()-task2)>150){
        ledstate1 = !ledstate1;
        digitalWrite(indled, ledstate1);
        task2 = millis();
      }
    }
  }
}
void start(){
  extstate = HIGH;
  attachInterrupt(0,stop,LOW);
  digitalWrite(indled, extstate);
}
void stop(){
  extstate = LOW;
  attachInterrupt(0,start,RISING);
  digitalWrite(indled, extstate);
  digitalWrite(enable, LOW);
  digitalWrite(dirpos, LOW);
  digitalWrite(dirneg, LOW);
  fail=false;
}
void turn(int speed){
  int val = 0;
  if(speed<0){
    val = abs(speed);
    digitalWrite(enable, extstate);
    analogWrite(dirpos, 0);
    analogWrite(dirneg, val);
    digitalWrite(obled,HIGH);
    digitalWrite(motoron,HIGH);
    turning = true;
  }
  if(speed==0){
    digitalWrite(enable, LOW);
    analogWrite(dirpos, 0);
    analogWrite(dirneg, 0);
    digitalWrite(obled, LOW);
    digitalWrite(motoron,LOW);
    turning = false;
  }
  if(speed>0){
    val = abs(speed);
    digitalWrite(enable, extstate);
    analogWrite(dirpos, val);
    analogWrite(dirneg, 0);
    digitalWrite(obled,HIGH);
    digitalWrite(motoron,HIGH);
    turning = true;
  }
}
int get_speed(){
  int val = 0;
  val = analogRead(speedpin);
  val = map(val,0,1023,0,255);
  return val;
}
```

5.4.3 The Moving Wall Box: A Novel Strategy For Assessing Active and Passive Fear

Differential involvement of the endocannabinoid system in the regulation of behavioral inhibition

(*submitted to Frontiers in Behavioral Neuroscience*)

Genewsky A, Wotjak CT
Research Group 'Neuronal Plasticity'
Department 'Stress Neurobiology and Neurogenetics'
Max Planck Institute of Psychiatry, Kraepelinstr. 2-10, D-80804 Munich, Germany

Among the *hardwired* behaviors, fear or survival responses certainly belong to the most evolutionary conserved ones. However, higher animals possess the ability to adapt to certain environments (e.g. novel foraging grounds), and, therefore, those responses need to be plastic. Previous studies revealed a cell-type specific role of the endocannabinoid system in novelty fear, conditioned fear and active vs. passive avoidance in a shuttle box paradigm. In this study we aim to investigate, whether knocking-out the cannabinoid receptor type-1 (CB1) on cortical glutamatergic (Glu-CB1$^{-/-}$) or GABAergic (GABA-CB1$^{-/-}$) neurons differentially affects the level of behavioral inhibition, which could ultimately lead to differences in escape behavior. In this context, we developed a novel behavioral paradigm, the *Moving Wall Box* (MWB). Using the MWB task we could show that Glu-CB1$^{-/-}$ mice have higher levels of behavioral inhibition over the course of repeated testing, GABA-CB1$^{-/-}$ mice in contrast showed significantly lower levels of behavioral inhibition compared to wild-type controls and more escape behavior. These changes in behavioral inhibition and escape behavior cannot be explained by altered levels of arousal, as repeated startle measurements revealed general habituation irrespective of the genotype of the animals. Taken together, we could show that CB1 on cortical glutamatergic terminals is important for the acquisition of active avoidance, as the absence of CB1 on these neurons creates a bias towards inhibitory avoidance. This is the case in situations without punishment such as electric footshocks. On the contrary CB1 receptors on GABAergic neurons mediate the acquisition of passive avoidance, as the absence of CB1 on those neurons establishes a strong bias towards escape behavior.

Introduction

The endocannabinoid system (eCB) is a phylogenetically ancient neuromodulatory system, and genes encoding for the cannabinoid receptors CB_1 and/or CB_2 can be found most likely in all chordates (Elphick, 2012). Its endogenous ligands (endocannabinoides) are synthesized and released on demand from postsynaptic sites. They travel to presynaptically localized CB1 receptors, where they cause a decrease in transmitter release in a auto- and heterosynaptic manner. This feedback mechanism has been found to function as an important regulator in the balance of excitatory and inhibitory neurotransmission (Kano et al., 2003) and, hence, is a major system which mediates adaptation at the synaptic level. As evolutionary conserved as the eCB itself, are also behavioral responses

(i.e. stress & fear responses) which allow an individual to remove itself from dangerous situations. Higher vertebrates, like mammals, have a complex behavioral repertoire and are able to adapt the expression of defensive responses to certain environmental cues. This allows hemerophile species, like mice and rats to explore foraging grounds and habitats which are inaccessible to other species. The role of the eCB in the regulation of emotion, stress & fear responses has been implicated numerous times (Wotjak, 2005; Lutz, 2009; Hill et al., 2010; Riebe et al., 2012; Ruehle et al., 2012) which is substantiated by the reports of euphoria upon the recreational drug use of marijuana and cannabis extracts. Special attention received the bimodal role of eCB signaling on glutamatergic vs. GABAergic neurons in the adoption of active and passive fear coping strategies in shuttle box training using electric footshocks (Metna-Laurent et al., 2012) in mice: whereas the cell-type specific knock-out of CB_1 on glutamatergic cortical neurons (Glu-CB1$^{-/-}$) increased performance in a passive avoidance task and impaired active avoidance, the opposite was observed when CB_1 was absent on GABAergic (GABA-CB1$^{-/-}$) forebrain neurons (decreased freezing, increased performance in an active avoidance task, impaired passive avoidance). A similar differential involvement of CB1 on glutamatergic vs. GABAergic neurons has been observed also in conditioned fear (Dubreucq et al., 2012; Llorente-Berzal et al., 2015), novel object exploration (single-housed animals) (Lafenêtre et al., 2009) and fasting-induced food intake (Bellocchio et al., 2010)(*for review see* Lutz et al., 2015). It has been suggested, that the eCB is activated on demand (Di Marzo et al., 1998) upon the strong activation of presynaptic input, and the effects of Glu-CB1$^{-/-}$ and GABA-CB1$^{-/-}$ might therefore only precipitate after a strong stimulus combined with sufficient incubation time. Experimental paradigms which involve repeated physical punishments or painful stimuli (e.g. electric footshock) may activate the eCB beforehand. In consequence the observed behavioral differences in conditional CB1 knock-out animals may relate to altered processing of the unconditioned stimulus, rather than to cognitive processes. Such a scenario is supported by the implication of eCB in pain perception (Woodhams et al., 2017). Thus, for the study of the eCB's role in modulating a particular behavior, the use of experimental paradigms which do not involve painful stimuli and offer repeated testing are of considerable importance.

Here we describe a novel behavioral assay − the *Moving Wall Box* (MWB) task, which allows the repeated assessment of fear coping strategies without the need of preceding aversive conditioning or any other form of operant training involving footshocks, food or water deprivation. Using the MWB task we demonstrate the time-dependent involvement of the eCB in the generation of active vs. passive coping strategies depending on the neuronal cell-type affected.

Material & Methods

Animals We used adult (4-8 months), male, group-housed CB1$^{f/f;NEX\text{-}Cre}$(Monory et al., 2006), henceforward called Glu-CB1$^{-/-}$)(N=9) and CB1$^{f/f;Dlx5/6\text{-}Cre}$(Monory et al., 2006), henceforward called GABA-CB1$^{-/-}$)(N=9) and their corresponding wild-type litter mate controls, Glu-CB1$^{+/+}$(N=9) and GABA-CB1$^{+/+}$(N=10). All animals were bred in the animal facilities of the Max Planck Institute of Biochemistry, Martinsried, Germany. The animals were group-housed (2-4 animals per cage) under standard housing conditions: 12h/12h inverted light-dark cycle (light off at 8 AM), temperature 24°C, food and water *ad libitum*. Experimental procedures were approved (AZ 44-09) by the State of Bavaria (Regierung von Oberbayern, Munich, Germany). Animal husbandry and experiments were performed in strict compliance with the European Economic Community (EEC) recommendations for the care and use of laboratory animals (2010/63/EU). On the basis of prior power analysis, we have kept the number of animals at the absolute minimum, sufficient to reveal significant group differences.

Apparatus & Behavioral Paradigm In order to repeatedly assess the development of behavioral inhibition in an emotional challenging situation without footshocks, food or water deprivation, we devised a novel testing strategy, henceforward called the Moving Wall Box (MWB) task. In short, during the MWB task a mouse is repeatedly forced to jump over a small ice-filled box (10 trials, 1 min inter-trial intervals ITI), by slowly moving walls (2.3 mm/s, over 60 s) , whereby the presence of the animal is automatically sensed via balances and analyzed by a microcontroller board which in turn controls the movements of the walls. The behavioral readouts are (1) the latency to reach the other compartment (high levels of behavioral inhibition lead to high latencies) and (2) the number of inter-trial shuttles per trial (low level of behavioral inhibition lead to high levels of shuttles during the ITI). The MWB, depicted in figure 5.10a, consists of two separate compartments, connected via two red transparent acrylic glass plates (W160×H340×D4 mm) which are outfitted with strong neodymium magnets at their corners. The magnets in turn allow to adjust the space between the two compartments as they can be attached along the top and bottom metal bands on each compartment. The compartments hold further, a window at their front panels for unrestricted visual access to the animal inside, at all times. Each compartment possesses one servo motor (Bluebird or Turnigy 620DMG+HS) which is connected via an articulated joint (Fig. 5.10b), consisting of an arm (8 cm), mounted to the servo motor and a rod (14 cm) connecting to the sliding carriage. The sliding carriage can freely travel along the entire width of one compartment, while being supported by a pair of rails mounted at the inner faces of the rear and front panels. Supported by the sliding carriage is the eponymous moving wall, which is further hanging via two long slotted mounts from a short rod (mounted upper-midways between the rear and front panel of each compartment). Once the sliding carriage is pushed towards the mid, the resting wall simply moves up- and forwards. The presence of the mouse is sensed via load cell units (details *see below*, surface W160×D100 mm) and its output is amplified and filtered with a dedicated

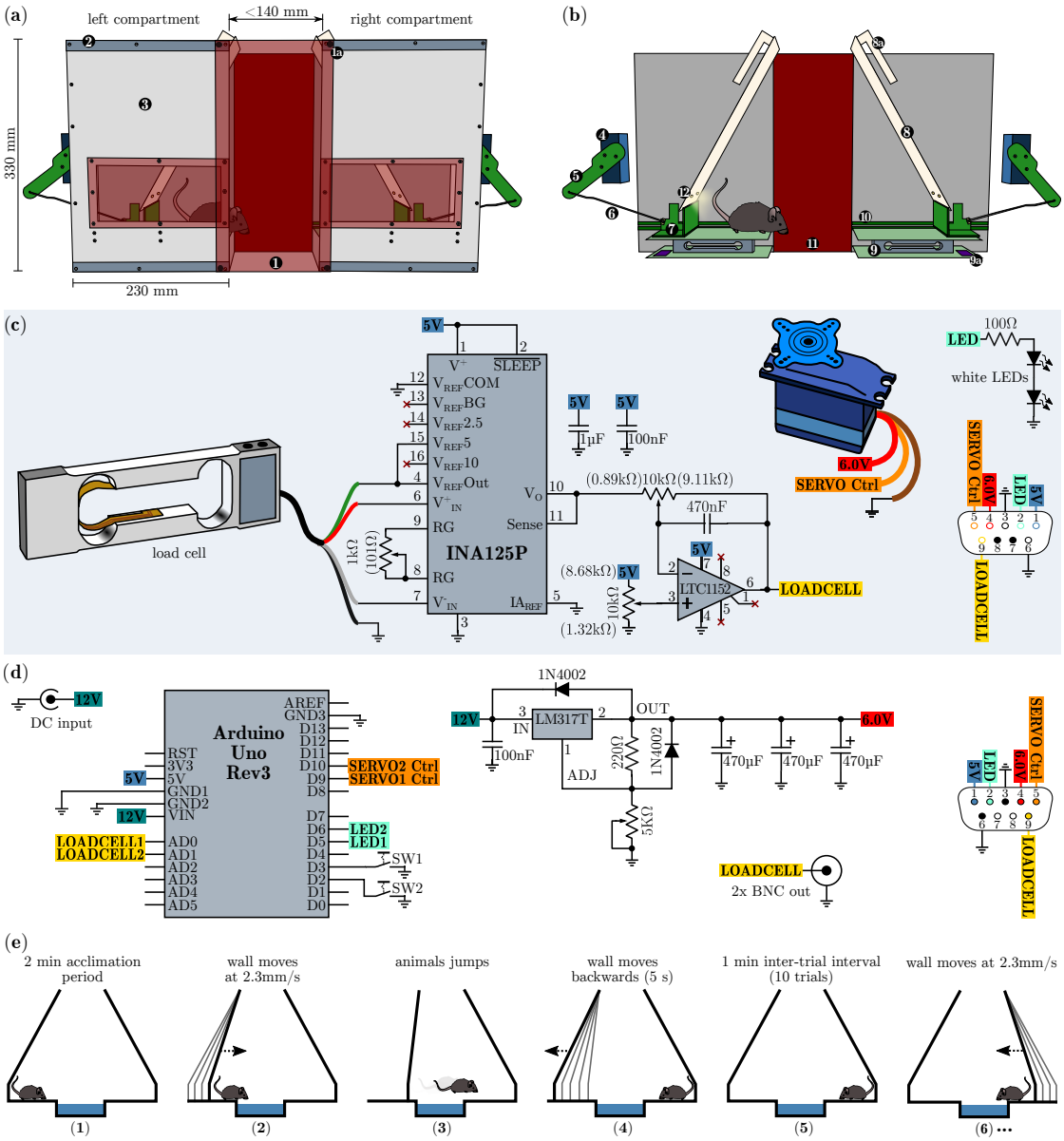

Figure 5.10 | Design, Schematics and Operational Procedure of the Moving Wall Box (MWB)

(**a**) Overview of the MWB. (1) Red transparent front cover which is equipped with four strong neodymium magnets at its corners (1a) and allows to adjust the distance between the left and the right compartment via metal bands (2). The front cover of the compartments (3) is equipped with a red transparent window, allowing to observe the animal at all times. (**b**) Inner workings of the MWB. Servo motor (4); articulated joint, consisting of an arm (5) and a rod (6); sliding carriage (7) supporting the moving wall (8), which itself is equipped with slotted mounts (8a); balance (9), consisting of two opposite plates and the load cell signal conditioning circuit (9a); rails (10) for the sliding carriage; red transparent back cover (11); two white LEDs per wall (12). (**c**) Schematic depiction of the circuitry of one compartment. Potentiometer settings which gave best results are given in brackets. (**d**) MWB controller circuity. (**e**) Schematic representation of the MWB task procedure. (1) acclimatization for 2 minutes; (2) the wall of the compartment in which the mouse resides starts to move with constant speed of 2.3 mm/s, maximal for 60 seconds (138 mm); (3) the wall stops to move once the animal has shuttled to the opposite compartment; (4 & 5) during a 1 minute inter-trial interval the first wall move quickly back to its default position; (6) subsequently the wall of the compartment in which the mouse resides starts to move and the second trial has started. This cycle is repeated 10×.

amplifier circuit (Fig. 5.10c) and fed towards a microcontroller board with little auxiliary circuitry (Fig. 5.10d) which in turn controls the servo motors as well as a pair of LED per wall which illuminate the active compartment.
The load cell (Tedea Huntleigh 1004-00.3-JW00-RS, 0.3 kg, Fig. 5.10c) is connected to an INA125P instrumentation amplifier (Texas Instruments) which is configured to provide a gain of 600×. The output of the instrumentation amplifier is further fed towards a high performance Rail-to-Rail I/O zero-drift operational amplifier LTC1152 (Linear Technology) which is configured as an inverting stage with a gain of 10× and includes a low-pass filter (-3 dB at 35 Hz). The load cell circuit, the servo motor and the white LEDs (e.g. Cree XLamp XM-L2 or Osram Oslon SSL 80) of one compartment are connected via a female D-sub-miniature 9-pin (DB9) receptacle and the wiring diagram is shown in figure 1c at the lower right side. The MWB controller (Fig. 5.10d) is powered via an external stabilized 12 V power supply (>750 mA) and houses an Arduino Uno Rev3 microcontroller prototyping platform which interfaces to a PC via USB, running the MWB graphical user interface, and controls the movements of the servo motors. The servo motor voltage supply is implemented using the adjustable voltage regulator LM317T (TO-220) set to provide stable 6.0 V voltage supply. The LM317T should be protected from overheat using a standard TO-220 heat sink with a thermal resistance of 7.5-10°C/W. The outputs of the MWB controller interfaces with the compartments via male DB9 connectors, whose wiring diagram is depicted in figure 1d at the lower right side. In addition the MWB controller provides the filtered output of the load cell circuits via two BNC connectors. This is useful if, at later stages, in *vivo* electrophysiological recordings are attempted in order to align neural responses to the time of jump. However, given the low frequency response of the low-pass filter, one should consider to tap the INA125P output directly and route it via the remaining free pins of the DB9 connectors, in order to obtain fast load cell voltage outputs. All circuits can be built using perfboard, but in order to interface with the Arduino Uno directly, specific Arduino Proto Shields (e.g. Adafruit PID: 2077 or SparkFun DEV-07914) have been found very useful. The behavioral paradigm using the MWB is simple and straightforward (Fig. 5.10e). Before each session (consisting of 10 trials) a small container (W14×H3×D10 cm) is filled with crushed ice and placed in between the two compartments. In addition the apparatus should be wiped with water and detergent. The mouse is placed at compartment A and left 2 minutes to acclimatize. Subsequently the left wall starts to move slowly and forces the animals to walk/jump over the ice. The time from the onset of the movement of the wall to the time when the animal is reaching the other compartment is the latency. During the inter-trial interval (ITI) of one minute, the left wall is moving back to the default position, and the animal can perform a certain number of inter-trial shuttles between the compartments. The compartment in which the animal resides after ITI expiration, will become active next.

Acoustic Startle Reflex In order to assess the animals general arousal level in a non-invasive manner with minimal stress, we have employed acoustic startle measurements

using a modified version of a commercially available startle apparatus (SR-LAB™, San Diego Instruments), which allowed unrestrained movements of the animals. The modification involved the replacement of the restraining startle chamber with a customized version, based on a Makrolon type II cage (27 × 16 × 12 cm) where all walls were cut to a height of 5 cm and the floor plate was allowed to translate the animals movements by placing long 3 mm wide slits along the bottom edges (leaving 1 cm fillets at the corners). A Ø5 cm piezoelectric transducer was glued (Pattex Stabilit Express) to the center from outside and its output was fed via a 6.3 mm audio jack towards the startle apparatus input. In addition we have placed four black walls (3 mm, PROTEX, rigid PFC foam plate) 5 mm above the floor plate, inside this modified cage, to force the animal to reside roughly above the sensor. This resulted in sufficient space (W15×H16×D9 cm) for the animals to move freely while receiving startle pulses. Rubber feet at the corners, isolated the startle chamber from unwanted vibrational signals. To account for the animals inter-individual difference in startle responsivity, we have first (7 days before MWB task) determined an individual input-output (I/O) response using a startle protocol which involved the display of 15 white noise startle pulses (50 ms) per sound pressure level (SPL) ranging from 70 dB to 120 dB in increments of 10 dB with variable inter-pulse intervals of 7 s to 15 s in a pseudo-randomized manner. In addition each animal received 10 startle pulses (5×70 dB + 5×100 dB) before the I/O session (acclimatization), whose responses have been discarded, giving a total number of 100 startle pulses. Based on these individual I/O curves, we have selected the SPL which was closest to the half-maximal response (SPL_{50}). After each MWB session on the same day, the animals have been subjected to a startle session which involved 50 startle pulse at the individual SPL_{50} with variable inter-pulse intervals of 7 s to 15 s.

Software Design The cross-platform software to write and upload the Arduino code used in this study is freely available online*. In addition all files (Arduino firmware and Python GUI for controlling the MWB) are available online† or on request.

Statistical Analysis All data are presented as mean values ± standard error (SEM). Statistical analysis has been performed using GraphPad Prism 5.03. Two-way analysis of variance (ANOVA for repeated measures) was followed by *Bonferroni* post-hoc analysis. A $p<0.05$ was considered statistically significant.

Results

In order to investigate whether the cell-type specific knock-out of the CB1 receptor on glutamatergic vs. GABAergic neurons affects the level of behavioral inhibition, we subjected Glu-CB1$^{-/-}$, GABA-CB1$^{-/-}$ and their respective litter mate controls (Glu-CB1$^{+/+}$, GABA-CB1$^{+/+}$) to the MWB task. Once the walls start to move, the animals can stay for maximally 60 seconds within the initial compartment before they

*https://www.arduino.cc/en/main/software
†https://github.com/AGenews/MWB

are forced to enter the ice and ultimately reach the opposite compartment. Figure 5.11a depicts the latencies to reach the opposite compartment for Glu-CB1 animals per trial. Within the first session, all animals adapt to the task, as seen by the decreasing latencies from the first to the last trial. These within-session dynamics could not be observed on day 6, nor on day 13. The individual data per day (Fig. 5.11a, *mid panel*), visualizes the increasing variation among Glu-CB1$^{+/+}$ mice with time, while the knock-out mice show a very robust response. The grouped data per day (Fig. 5.11a, *right panel*) reveals the time-dependent development of a profound group difference, between Glu-CB1$^{+/+}$ and Glu-CB1$^{-/-}$ animals with significant group×time interaction ($F_{2,34}$=8.66, p=0.0009). The difference was strongest on day 13 when Glu-CB1$^{+/+}$ mice spent on average 30.3±3.7 s before they shuttled while Glu-CB1$^{-/-}$ needed 45.7±1.3 s. In other words, while the wild type animals controlled the situation and responded preemptively before the wall was pushing them (≈ 6.8 cm), the knock-out remained until there was only ≈ 3.3 cm between the wall and the ice. The high latencies were accompanied by a low disposition to show active escape attempts reflected by decreased number of inter-trial shuttles (ITS, Fig. 5.11b *left panel*). Statistical analysis between groups per day (non-parametric, two-tailed Mann-Whitney U-test) revealed a significant lower ITS values (Fig. 5.11b *left panel*) for Glu-CB1$^{-/-}$ mice at day 13 (0.01±0.01 ITS vs. 0.27±0.10 ITS, $U_{\mathrm{n1=129,\ n2=61}}$=16.00, p=0.0094). The percentage of Glu-CB1$^{+/+}$ animals which performed one or more ITS slightly increased from day 1 (50 %) to day 13 (70 %) but the values for Glu-CB1$^{-/-}$ decreased from day 1 (30 %) to day 13 (0 %). The analysis of the contingency tables using Fisher's exact test revealed a significant difference between Glu-CB1$^{+/+}$ and Glu-CB1$^{-/-}$ for ITS values on day 13 (p=0.0198).

Similar to the Glu-CB1, also GABA-CB1 animals showed an initial adaptation to the MWB task within the first session (Fig. 5.11c *left panel*), whereby especially GABA-CB1$^{-/-}$ mice seemed to show quicker preemptive responses. These within-session dynamics could not be observed in subsequent sessions. The variance among the groups was similar throughout the experiment, except that GABA-CB1$^{+/+}$ mice showed less variable responses on day 13 (Fig. 5.11c *left panel*). Looking at the average latencies per group and day revealed an overall lower latency for GABA-CB1$^{-/-}$ mice ($F_{1,17}$=4.6, p=0.0466). Whereas GABA-CB1$^{-/-}$ animals already transitioned to the other compartment after 29.1±5.7 s (≈ 7.1 cm between wall and ice), GABA-CB1$^{+/+}$ needed 38.1±2.0 s, which corresponds to ≈ 5.0 cm before the wall would have pushed them.

In the first session the number of ITS for both groups was comparable, but starting at day 6, both groups separated almost completely (Fig. 5.11d *left panel*). Statistical analysis between groups per day (non-parametric, two-tailed Mann-Whitney U-test) revealed on average a significant higher number of ITS per trial for GABA-CB1$^{-/-}$ on day 6 (0.56±0.05 ITS vs. 0.17±0.05 ITS, $U_{\mathrm{n1=58,\ n2=132}}$=3.00, p=0.0006), and the difference was even more pronounced on day 13 (0.69±0.05 ITS vs. 0.17±0.05 ITS, $U_{\mathrm{n1=58,\ n2=132}}$=3.00, p=0.0006). Looking at the percentage of GABA-CB1$^{+/+}$ animals which performed at least one ITS per trial, a clear increase from day 1 (20 %) to day

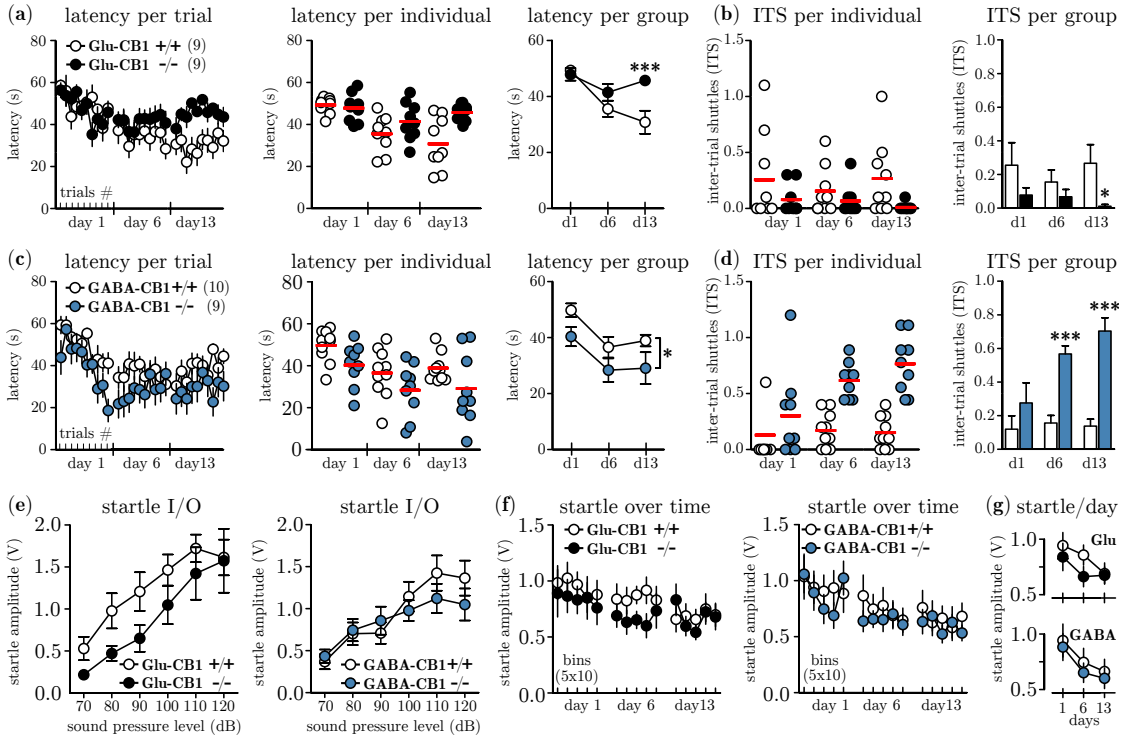

Figure 5.11 | The Knock-out of CB1 on Glutamatergic vs. GABAergic Neurons Differentially Affects Behavioral Inhibition
(**a**) Latencies to shuttle to the opposite compartment during the MWB task, given per trial (*left panel*), per individual + per day (*mid panel*) and per group + per day (*right panel*) for Glu-CB1$^{+/+}$(N=9) and Glu-CB1$^{-/-}$(N=9). (**b**) Inter-trial shuttles per individual + per day (*left panel*) and per group + per day (*right panel*) for Glu-CB1$^{+/+}$ and Glu-CB1$^{-/-}$. (**c**) Latencies to shuttle to the opposite compartment during the MWB task, given per trial (*left panel*), per individual + per day (*mid panel*) and per group + per day (*right panel*) for GABA-CB1$^{+/+}$(N=10) and GABA-CB1$^{-/-}$(N=9). (**d**) Inter-trial shuttles per individual + per day (*left panel*) and per group + per day (*right panel*) for GABA-CB1$^{+/+}$ and GABA-CB1$^{-/-}$. (**e**) Startle input-output (I/O) curved for Glu-CB1 and GABA-CB1 animals. (**f**) Startle response at SPL_{50} development over time depicted in bins of 10 trials. (**g**) Same data as in f but shown as average startle amplitude at SPL_{50} per day for the individual groups for (*upper panel* Glu-CB1$^{+/+}$ (empty circles) and Glu-CB1$^{-/-}$ (filled circles) animals and (*lower panel* GABA-CB1$^{+/+}$ (empty circles) and GABA-CB1$^{-/-}$ (filled circles) animals. Asterisks indicate significance values (*see* text for the specific statistical tests): * = p<0.05, ** = p<0.01, *** = p<0.001. All values are given as mean±SEM. Red bars in individual data represent the mean value.

13 (70 %) was noted. Also the number of ITS for GABA-CB1$^{+/+}$ animals increased from day 1 (67 %) to day 13 (100 %). Statistical analysis using Fisher's exact, however, revealed no difference on day 13 (p=0.2105).

In order to monitor the arousal level of Glu-CB1 and GABA-CB1 animals throughout the experiment we have applied acoustic startle measurements along the MWB task. To account for inter-individual differences in startle response, we first subjected all animals 7 days before the first MWB session to a startle input-output (I/O) protocol, which allowed us to determine the sound pressure level which yielded a half-maximal response (SPL_{50}) for each individual. The results of the startle I/O experiments for Glu-CB1 mice are shown in figure 5.11e (*left panel*); no significant group difference was found (repeated measures two-way ANOVA, group $F_{1,16}$=2.48, p=0.1352). For GABA-CB1 mice, the results of the startle I/O experiment are shown in 2e (*right panel*), and

also here no group difference was observed (repeated measures two-way ANOVA, group $F_{1,17}$=0.28, p=0.6068). Based on the I/O measurements the average SPL_{50} were determined for Glu-CB1 (WT 85.6±2.4 dB, KO 92.2±3.2 dB) and GABA-CB1 (WT 86.0±2.2 dB, KO 83.3±2.4 dB) mice. A non-parametric Kruskal-Wallis analysis revealed no significant difference among the groups ($p \geq 0.127$). These individual SPL_{50} values were used to asses the general arousal on each experimental day after MWB session. Figure 5.11f shows the startle responses (one bin represents the average of 10 startle responses) of Glu-CB1 and GABA-CB1 animals. The habituation, reflected by decreasing startle amplitudes over time per testing day (Fig. 5.11g), was significant revealed two-way ANOVA (Glu-CB1 $F_{2,32}$=6.76, p=0.0036; GABA-CB1 $F_{2,34}$=15.47, p<0.0001), with no effect of genotype (Glu-CB1 $F_{1,16}$=0.68, p=0.4212; GABA-CB1 $F_{1,17}$=0.21, p=0.6514) or genotype×day interaction (Glu-CB1 $F_{2,32}$=1.23, p=0.3062; GABA-CB1 $F_{2,34}$=0.07, p=0.9341).

Discussion

The prior activation of the eCB with noxious stimuli, water restriction or food deprivation is a confounding factor in many experiments aiming to investigate the involvement of endocannabinoid signaling in a certain behavior. Therefore different behavioral assays need to be employed to overcome this limitation. In this context, we have developed the Moving Wall Box task, which allows the repeated assessment of escape behavior in mice, without the use of painful stimuli. Further, the MWB offers the possibility to conduct simultaneous in *vivo* electrophysiological recordings, which could be later aligned to the behavioral responses (escapes). Therefore the MWB task promotes the study of activity patterns in e.g. optogenetically identified neurons with respect to escape responses in a controlled setup.

Using this new behavioral paradigm, we could demonstrate that the level of behavioral inhibition, i.e. the balance between active and passive fear coping strategies, is differentially affected by the absence of CB1 on glutamatergic vs. GABAergic neurons in a gradual, time-dependent manner. While GABA-$CB1^{-/-}$ animals show a strong disposition to actively evade impeding danger, Glu-$CB1^{-/-}$ animals are behaviorally inhibited and behave much more passively. The latencies to escape could possibly depend on the general arousal levels of these animals, and their genetic disposition might render them differentially sensitive to stress. The parallel assessment of startle amplitudes over the course of the experiment, however, showed no sensitization of a specific group, but revealed an overall tendency to habituate to the experimental procedures, as the startle amplitudes declined within 3 testing days. This excludes a general deficit of Glu-$CB1^{-/-}$ in long-term habituation of defensive responses.

The role of CB1 in the regulation of coping styles has been highlighted by (Metna-Laurent et al., 2012), however in this study the authors observed different levels of freezing upon a previously aversively conditioned tone. The noxious quality of the unconditioned stimulus (US) activated the eCB beforehand, and the authors observed a bimodal modulation of fear coping strategies already at the first tone-fear memory recall

session. Another confounding factor in this behavioral task is the high degree of freedom to display different active behaviors like sniffing, rearing, digging, which all have to be scored by an experienced experimenter, blind to the conditions. In the MWB, the analysis is based on two simple parameters and the animals do have only little opportunity, except in the desired way, to control the situation. The question, whether the observable changes in the latency and number of ITS in the MWB are attributable to a differential recruitment of higher fear-regulatory brain areas (e.g. amygdala) and therefore reflect indeed a different behavioral state, cannot be answered currently. But it was shown before that a local re-expression of CB1 within the amygdalar complex (mainly basolateral amygdala and central amygdala in part) in CB1$^{-/-}$ animals was sufficient to restore active fear-coping styles (Metna-Laurent et al., 2012). Taken together our study adds a new facet to our picture about implications of CB1 glutamatergic vs. GABAergic neurons in controlling escape behavior (i.e. active vs. passive coping strategies; Lutz et al., 2015).

5.4.4 Nigrotectal Pathway, SC and Threat Detection

Nigrotectal pathway controls threat detection at the level of the superior colliculus

(*submitted to Scientific Reports*)

Almada R C[a,b,c*], **Genewsky A**[a*], Heinz D E[a,e], Kaplick P M[a], Coimbra N C[b,c,d], Wotjak C T[a]

* equal contribution

[a]Research Group 'Neuronal Plasticity'
Department 'Stress Neurobiology and Neurogenetics'
Max Planck Institute of Psychiatry, Kraepelinstr. 2-10, D-80804 Munich, Germany
[b]Laboratory of Neuroanatomy and Neuropsychobiology, Department of Pharmacology, Ribeirão Preto Medical School of the University of São Paulo (FMRP-USP), Ribeirão Preto, 14049-900, São Paulo, Brazil.
[c]Behavioural Neurosciences Institute (INeC), São Paulo, Av. do Café, 2450, Ribeirão Preto, 14050-220, São Paulo, Brazil.
[d]NAP-USP-Neurobiology of Emotions Research Centre (NuPNE), Ribeirão Preto Medical School of the University of São Paulo (FMRP-USP), Ribeirão Preto, 14049-900, São Paulo, Brazil.
[e]Neuroscience Master's Program, Interdisciplinary Center for Neurosciences (IZN), Heidelberg University, Im Neuenheimer Feld 504, 69120 Heidelberg, Germany.

Abstract

Defensive behavioral responses are essential for survival in threating situations. The superior colliculus (SC) has been implicated in the generation of defensive behaviors elicited by visual, tactile, and auditory stimuli. Furthermore, substantia nigra pars reticulata (SNr) neurons are known to exert a modulatory effect on midbrain tectum neural substrates. However, the functional role of this nigrotectal pathway in threating situations is still poorly understood. Using optogenetics in mice, we activated SNr projections at the level of the SC, and assessed consequences on behavioral performance in an open field test (OFT) and the beetle mania task (BMT). The latter confronts a

mouse with an erratic moving object. Channelrhodopsin-2 (ChR2)-mediated activation of the nigrotectal pathway did not affect anxiety-like and exploratory behavior in the OFT, yet increased the number of contacts between robo-beetle and test animal in the BMT. Active avoidance responses remained unaffected, whereas tolerance was significantly increased in the BMT. Taken together, we demonstrate that the nigrotectal pathway plays an important role in modulating innate fear primarily by attenuating threat detection.

Introduction

The ability to sense and predict threatening or stressful events is essential for survival. Accordingly, the brain has developed distinct pathways to control and process different types of fear (Gross and Canteras, 2012). While the hippocampus, the amygdala, and the prefrontal cortex play a fundamental role in conditioned fear (Tovote et al., 2015; Sotres-Bayon et al., 2012), mesencephalic structures, such as the superior colliculus (SC) and the periaqueductal gray (PAG), are part of a complex neuronal circuit underlying innate defensive responses (Coimbra and Brandão, 1993; Brandão et al., 1999). For instance, electrical activation of the SC was found to cause an increase in defensive behavior, such as alertness, freezing, and escape, along with autonomic responses (Brandão et al., 1994). More recently, it could be demonstrated that optogenetic activation of parvalbumin-positive SC neurons triggers both active (avoidance) and passive (freezing) fear responses depending on stimulus properties and sex of the mice (Shang et al., 2015). The SC receives multiple sensory inputs - of visual (Feinberg and Meister, 2014; Shi et al., 2017), auditory (King, 2004), and tactile (Favaro et al., 2011) nature − which predisposes it as a central hub for translating sensory information into innate defensive responses (Wei et al., 2015). SC activity is tightly controlled by GABAergic signaling (Brandão et al., 1994). For instance, local infusion of the GABA-A receptor antagonist was observed to cause patterns of defensive responses, as from electrical stimulation (Brandão et al., 2005). Even though we cannot entirely rule out the involvement of local GABAergic interneurons, there is evidence for a significant contribution of GABAergic afferences from the substantia nigra pars reticulata (SNr) (Castellan-Baldan et al., 2006): First, anterograde tracing revealed a dense projection from the SNr to deep layers of the SC (dlSC) (Ribeiro et al., 2005), the so-called nigrotectal pathway, which additionally innervates the dorsal PAG. Second, this nigrotectal pathway is primarily comprised by GABAergic neurons (Ribeiro et al., 2005), and GABAergic cells in the SNr tonically inhibit neural firing of dlSC (Hormigo et al., 2016; Grillner and Robertson, 2016). Third, inactivation of neuronal somata of the SNr increased escape behavior which was elicited by microinjections of the GABA-A receptor antagonist bicuculline in the dlSC (Almada and Coimbra, 2015). Moreover, chemogenetic and optogenetic manipulations of GABAergic neurons at the level of the SNr have promoted (in case of inhibited neuronal activity) respectively attenuated (in case of enhanced neuronal activity) active avoidance in an auditory-cued conditioning

paradigm (Hormigo et al., 2016). Despite compelling evidence for anatomical, physiological, and functional interactions between the SNr and dlSC, direct demonstration of an involvement of nigrotectal projections in modulation of defensive responses is still missing. Therefore, the present study aims to investigate consequences of activating afferences from the SNr at the level of the dlSC upon confrontation with an approaching threat, using optogenetics and the recently validated beetle mania task (BMT).

Methods

Animals Experiments were performed with male C57BL/6N mice purchased from Charles River (Bad Sulzfeld, Germany) aged eight to 15 weeks. All mice were naïve before surgery and maintained on a 12:12 inverted light cycle (lights off: 08:00 h) under standard housing conditions (23°C ± 4°C, 50% humidity ± 10%) in type 2 Macrolon cages with ad libitum access to food (1314, Altromin Spezialfutter GmbH & Co. KG, Lage, Germany) and water. All behavioral tests were carried out in the dark phase between 09:00 and 17:00 h. Experimental procedures were performed according to the European Community Council Directive 2010/63/EEC and approved by the local government of Upper Bavaria (55.2.1.54-2532-142-12, 55.2.1.54-2532-188-12 and 55.2.1.54-2532-08-12). Efforts were made to minimize animal suffering and to reduce the number of animals used in the present work.

Viral Injections and Optogenetics For optogenetics experiments, mice were treated with an analgesic (Novalgin, 200 mg/kg), anesthetized with isoflurane (Forene®, Abbott, Germany, under induction at 4%, maintained at 1.5%), and headfixed in a stereotaxic frame (Leica Biosystems, Nussloch, Germany, AngleTwo). Craniotomies were made bilaterally above the lateral SNr and mice were randomly assigned to ChR2 or mCherry groups. For SNr→SC stimulation, 350 nl of AAV5-hSyn-ChR2(H134R)-mCherry (ChR2; N=10) or the control vector AAV5-hSyn-mCherry (mCherry; N=8) was injected using a micro-syringe (80 nl/min) into the SNr with the following stereotaxic coordinates: AP -3.2 mm, ML ±1.5 mm, DV -4.2 mm, from the skull surface. All viral aliquots were obtained from the University of North Carolina Vector Core (Chapel Hill, NC, USA). For optical manipulation, fiber optic cannulas (Thorlabs, Dachau/Munich, Germany, CFML12L10, Ø200 μm, NA 0.39, cut to 3 mm length) were implanted targeting the dlSC (AP: -3.9 mm, ML: ±1.1 mm, DV: -2.0 mm) 5-6 weeks after the virus injections. The fiber tip was lowered at an angle of 12° to 250 μm above the injection site in the dlSC. The mice were allowed to recover for 2 weeks after the fiber implantation. For optical stimulation of ChR2, pulsed (5 ms at 20 Hz) laser light (Omicron-Laserage, Rodgau-Dudenhofen, Germany, LightHUB-4) of 460 nm was applied. The laser output power was set to measure 7.5 mW at the single fiber tip. Bilateral optical stimulation was achieved using a fiber-optic rotary joint with two output ports (Doric Lenses Inc., Quebec, Canada, FRJ_1×2i_FC-2FC).

Behavioral Tests

Open field test (OFT) The open field arena consisted of a gray Plexiglas cube (50×50×53 cm), which was divided into a center zone (25×25 cm) and an outer peripheral zone. Mice were connected to the patch cables, placed in the center, and allowed three minutes to recover from handling before assessment for nine minutes. The OFT session was divided into three minute epochs with alternating laser manipulation (OFF-ON-OFF) (Felix-Ortiz et al., 2016). Video tracking (Stoelting, Dublin, Ireland) was employed to track the location of the mouse in the open field. All measurements were quantified relative to the mouse center. The setup was illuminated with 50 Lux white light.

Beetle Mania Task (BMT) The BMT has been developed and validated to enable the assessment of both passive and active innate fear (Heinz & Genewsky et al., submitted). In experiment one, the BMT consisted of a gray polyethylene arena (L150×W25×H37 cm) with curved end walls. The floor of the arena was divided into six equal spaced sectors and illuminated with 50 Lux white light. In experiment two, the BMT arena was shortened to two sectors (50×25×37 cm). The robo-beetles (4×1×1 cm) weighting 7.2 g, made out of plastic and rubber with 12 rubber legs. They were equipped with a powerful vibrating motor that causes them to travel over any smooth surface in an unpredictable manner (Hexbug Micro Robotic Creatures, Greenville, USA). The test comprised two successive five-minute sessions: during habituation, mice were familiarized with the test arena, immediately followed by the test session with the robo-beetle. Behavioral performance was scored online by a highly experienced observer blind to the treatment. The following measures were considered: horizontal (number of segment crossings) and vertical (number of rearings) exploration during habituation; chasing contacts (number direct contacts between robo-beetle and mouse), tolerance (ignorance of the approaching/ bypassing beetle, i.e., no evidence of freezing or avoidance behavior; expressed as a percentage of chasing contacts), close following (number of sectors the mouse is following the bypassing beetle), avoidance behavior [sum of flight (i.e., movement in direction of the moving beetle with accelerating speed) and escape behavior (i.e., running in opposite direction of the moving beetle)], and freezing during the test session. Laser stimulation was performed only in test sessions. In experiment one, the laser was activated only when the beetle was in the same sector as that as the mouse or in the sector adjacent to it, while in experiment two, the laser was activated during the whole test session.

Anatomical Tracing

To identify the origin of SNr inputs to SC, we injected 350 nl of the retrogradely transported fluorescent latex beads (Lumafluor) into the SC (AP: -3.5 mm; ML: ±1.0; DV: -2.2 mm) in C57BL/6N mice. Four days after injection, mice were sacrificed, transcardially perfused with 4% paraformaldehyde in PBS, and brains were extracted and processed for histology as described below. Brains were sliced into 40 μm coronal

sections by cryostat (Leica CM 3000, Wetzlar, Germany) and after co-staining with DAPI. Histology Following completion of experiments, mice were sacrificed with an overdose of isoflurane, immediately transcardially perfused with ice cold PBS followed by 4% paraformaldehyde. Brains were post-fixed overnight at 4°C in paraformaldehyde and then cryoprotected with 30% sucrose in PBS. For optogenetics experiments, brains were sliced at 40 μm with a cryostat. The locations of electrodes, fibers, and injection sites were compared with the atlas of Paxinos and Franklin (Keith and Paxinos, 2008).

Statistical Analysis Data are presented as mean ±standard error of the mean (S.E.M.) or as box-whisker plots with medians, interquartile range, and 5^{th}-95^{th} percentiles. Statistical analyses were performed as indicated in the results section using GraphPad Prism (version 6.0; GraphPad Software Inc.; San Diego, CA, USA). Significance was accepted if $P \leq 0.05$; significance levels are indicated as follows: (*) $P<0.05$; (**) $P<0.01$.

Results

Nigrotectal projections: retrograde tracing

To visualize the origin of the nigrotectal pathway, we injected retrogradely transported green fluorescent latex beads into the dlSC (Fig. 5.12a). Retrobeads were found throughout the SNr (Fig. 5.12b), showing that SNr neurons, which project to the dlSC, are homogeneously distributed throughout the SNr.

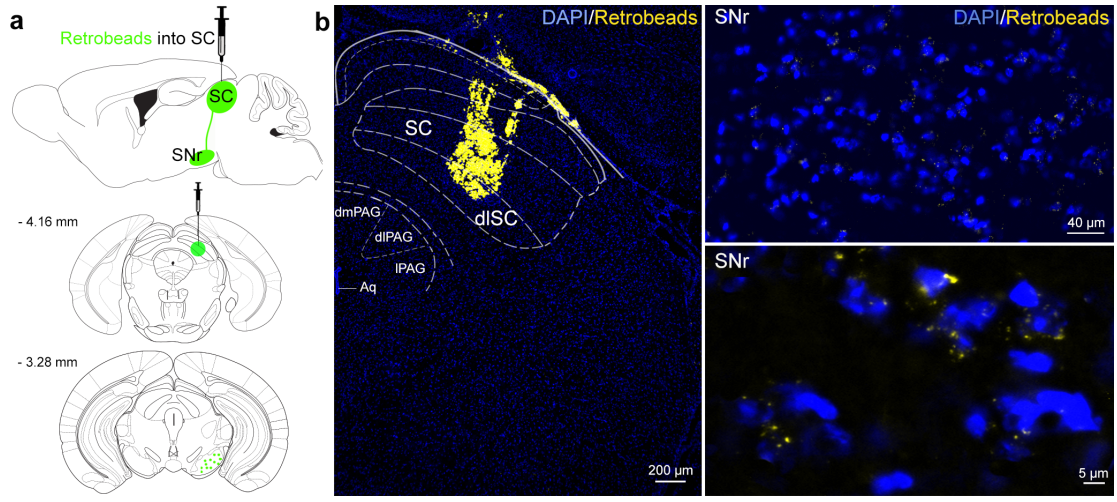

Figure 5.12 | Neural Connections from SNr to SC.
(**a**) Schematic representation of anatomical tracing strategy. Retrobeads were unilaterally injected into the SC (n = 4). (**b**) The fluorescent latex beads injected into the SC (left panel) were retrogradely transported to SNr neurons (right panel).

Stimulation of SNr Projections at the Level of the SC did not Produce Anxiolytic Effects

The SNr was bilaterally transfected with viral vectors encoding the expression of ChR2-mCherry or mCherry (controls) under control of the hSyn promoter (Fig. 5.13a).

Six weeks later, light fibers were implanted right above the projection terminals of the nigrotectal pathway in the dlSC (Fig. 5.13a), followed by two weeks of recovery before the start of experiments. Placement of injection and implantation sites (for representative photographs see Fig. 5.13b) were verified in the end of the study (Fig. 5.14). In the open field test (OFT), photostimulation of the nigrotectal pathway failed to affect center time (Fig. 5.15c; 2-way ANOVA for repeated measures; group: $F_{1,15}$ = 0.02, P = 0.95; laser: $F_{1,15}$ = 0.09, P = 0.91; interaction: $F_{1,15}$ = 0.39, p = 0.68) and distance traveled (Fig. 5.15d; group: $F_{1,15}$ = 0.02, P = 0.96; laser: $F_{1,15}$ = 0.65, P = 0.59; interaction: $F_{1,15}$ = 0.38, P = 0.67). In sum, these findings indicate that activation of SNr→SC projections at the level of the SC did not alter anxiety-like behavior and locomotor activity.

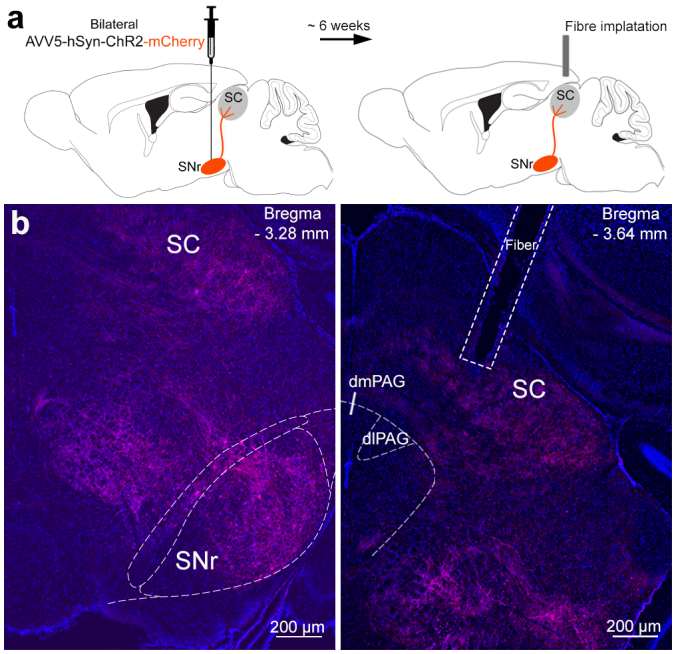

Figure 5.13 | Infusion of Viral Vectors into the SNr.
(**a**) Viral vectors were injected into the SNr, resulting in the expression of either ChR2-mCherry (n = 10) or mCherry (n = 8) in the nigrotectal pathway. The optical fibers were placed over the SC. (**b**) Coronal photomicrographs showing expression of ChR2-tdtomato in SNr somata, as well as in SNr terminals within the periaqueductal grey matter (PAG) and superior colliculus (SC) (blue, DAPI; red, tdTomato).

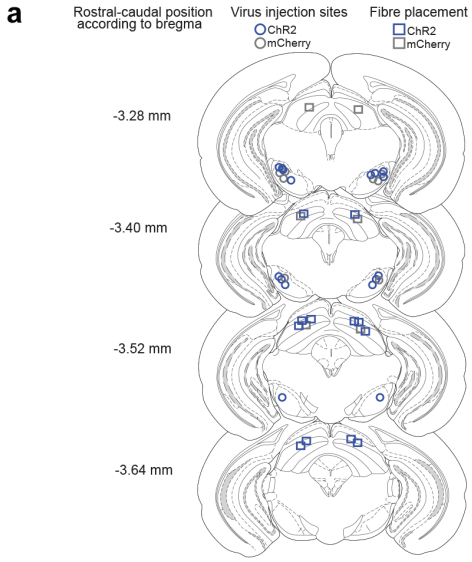

Figure 5.14 | Histological Verification of Injection and Implantation Sites.
(**a**) Coronal drawings across rostro-caudal extensions of the SNr and SC, depicting the center of viral infusions in the SNr (ChR2-mice: blue circles, mCherry-mice: gray circles) and fiber placements in the SC (ChR2-mice: blue squares, mCherry-mice: gray squares).

Activation of SNr Afferences at the Level of the SC Decreases Threat Detection and Promotes Tolerance in the Beetle Mania Task (BMT)

To study consequences of increased activity in SNr→SC projections (Fig. 5.16a) on defensive behavior, we tested animals in the BMT. In this test mice are confronted with an erratic-moving, potentially threatening beetle (Heinz & Genewsky et al., submitted). During habituation to the setup, during which no laser stimulation was employed (Fig. 5.16b), both groups of mice showed the same exploratory behavioral activity (Fig. 5.16c; $t_{16} = 0.173$, P = 0.86; Fig. 5.16d; $t_{16} = 0.354$, P = 0.77). In the subsequent test session, mice were confronted with the beetle, and laser stimulation was activated when the beetle was in the same segment as the mouse or the adjacent segments (Fig. 5.16b). Stimulation of SNr→SC projections at the level of the SC selectively increased the number of contacts between the beetle and the mouse (Fig. 5.16f; $t_{16} = 5.77$, P = 0.003), whereas no significant differences were observed on close following (Fig. 5.16g; $t_{16} = 0.92$, P = 0.37), tolerance (Fig. 5.16h; $t_{16} = 0.37$, P = 0.71), avoidance (Fig. 5.16i; $t_{16} = 1.94$, P = 0.08), and freezing behavior (Fig. 5.16j; $t_{16} = 1.55$, P = 0.86, respectively). Further, we tested how the activation of the SNr-SC pathway affects the interaction between the mouse and the beetle in a smaller arena with laser stimulation throughout the entire five-min test session (Fig. 5.17b). Again, stimulation of the SNr-SC pathway increased the number of chasing contacts (Fig. 5.17c; $t_{16} = 2.92$, P = 0.012) without affecting avoidance behavior (Fig. 5.17f; $t_{16} = 1.67$, P = 0.11). This time, however, we additionally observed an increase in tolerance (Fig. 5.17e; t = 3.28, P = 0.006) and close following behaviour (Fig. 5.17d; $t_{16} = 2.09$, P = 0.05).

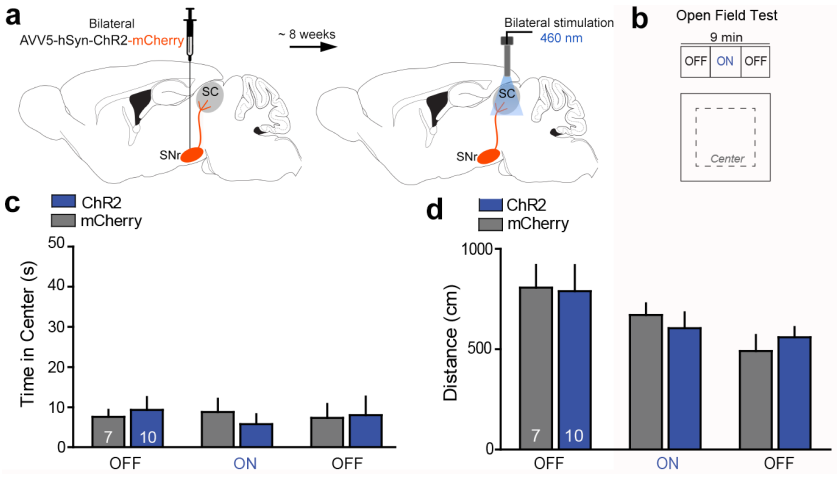

Figure 5.15 | Photostimulation of SNr→SC Projections at the Level of the SC did not Alter Anxiety-like and Locomotor Behavior.

(**a**) Design of the optogenetic approach with transfection of the SNr either with ChR2-mCherry (n = 10) or mCherry (n = 8) and placement of the optical fibers over projection terminals of the nigrotectal pathway at the level of the SC. (**b**) The open field test (OFT) consisted of three-minute epochs with alternating laser treatment (OFF-ON-OFF). (**c**) Average time spent in exploring the center of the OFT arena. ChR2-mice did not show significant differences regarding the time spent in the center of the arena during the ON epoch, relative to mCherry-mice and the OFF epochs. (**d**) No significant effects were detected for the total distance traveled in the OFT. Data are shown as mean ±S.E.M. Numbers within bars indicate the number of rodents per group.

Discussion

Using optogenetics in combination with a recently established ethobehavioral task, we provide first direct evidence that stimulation of the nigrotectal pathway at the level of the SC reduces threat detection and increases tolerance to an approaching robo-beetle without affecting anxiety, locomotion, freezing, and escape responses. Our results confirm and extend previous reports about the important role of nigrotectal pathways in the control of innate defensive behaviors (Hormigo et al., 2016; Ribeiro et al., 2005; Coimbra and Brandão, 1993). The SNr sends projections not exclusively to the SC, but to a variety of brain structures (Grillner and Robertson, 2016). Therefore, manipulations of the SNr (Hormigo et al., 2016) (even with simultaneous manipulations of the SC Hormigo et al., 2016; Almada and Coimbra, 2015) cannot unequivocally validate an involvement of SNr→SC projections in fear regulation. This can only be achieved by direct manipulations of projection terminals at the level of the SC. We used viral vectors to drive the expression of the light-activate cation channel ChR2 in SNr neurons, while stimulating axon terminals in the SC. Behavioral consequences of the stimulation were surprisingly distinct, given previous reports about an involvement of the SC in several defensive behavioral responses, such active avoidance, panic-like behavior, escape, and freezing. We observed an increase in a number of contacts between the approaching beetle and the test animal and, depending on stimulation duration and the size of the test arena, also an increase in tolerance of the encounter (i.e., mice lead the beetle bypass without showing freezing or avoidance responses). These behavioral alterations could not be explained by general changes in locomotor activity.

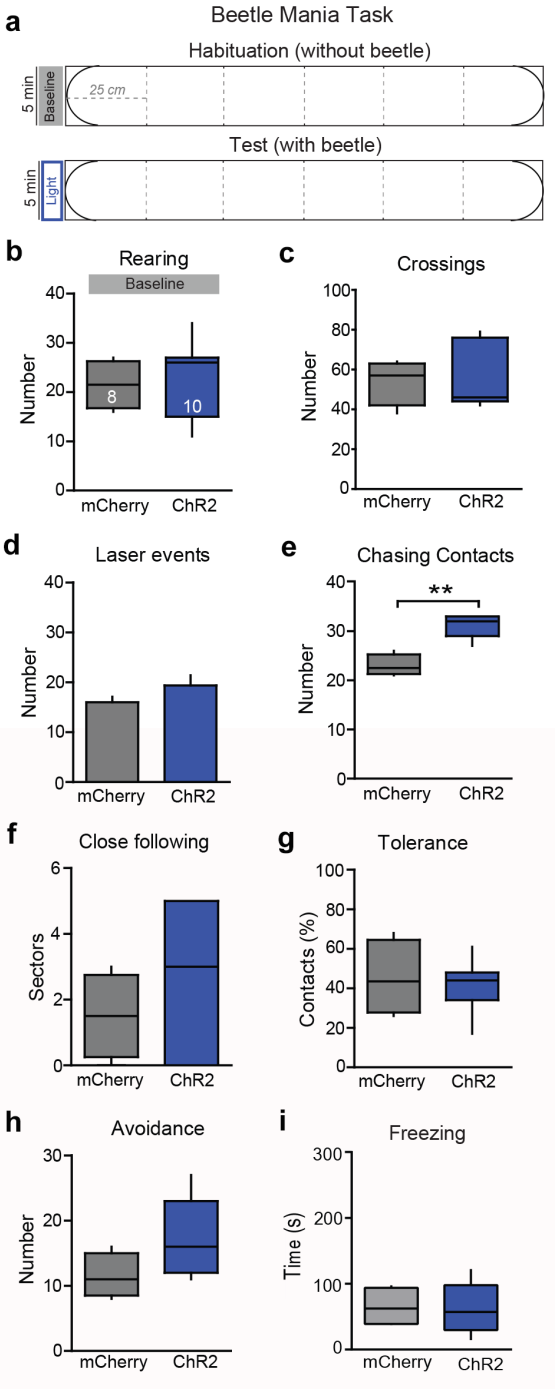

Figure 5.16 | Photostimulation of SNr→ SC Projections at the Level of the SC Decreases Threat Detection in the Beetle Mania Task.
(**a**) The Beetle mania task (BMT) consisted of two consecutive five-minute sessions in an arena (length: 150 cm). Initially, mice were allowed to habituate to the arena without beetle and optical stimulation, followed by confrontation with an erratic moving robo-beetle and laser stimulation. The laser was activated after the beetle had entered the sector adjacent to the mouse or the mouse sector. No significant effects were detected in (**b**) vertical (rearings) and (**c**) horizontal (crossings) exploration during habituation to the arena. In the test session, no significant differences were observed in (**d**) number of laser events, but (**e**) number of chasing contacts. No significant effects were detected in (**f**) close following, (**g**) tolerance, (**h**) avoidance and (**i**) freezing. Numbers within bars indicate the number of rodents per group. ** $P < 0.01$.

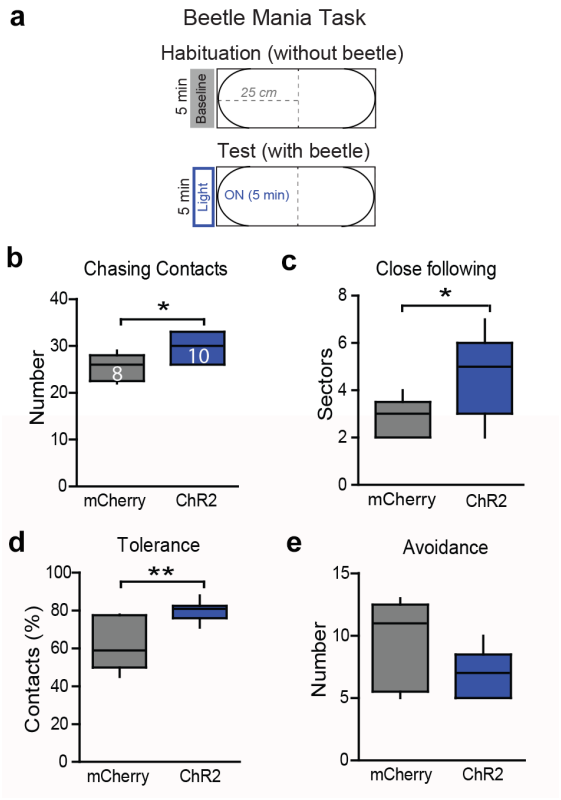

Figure 5.17 | Consequences of Photostimulation of SNr→SC Projections at the Level of the SC on Threat Detection in a Smaller Arena.
(**a**) The Beetle mania task (BMT) was repeated in a smaller arena (length: 50 cm), again with five minutes of habituation without beetle and light stimulation, followed by the five-minutes test session with the robo-beetle and laser stimulation being present throughout the entire session. Stimulation of axon terminals of SNr neurons at the level of the SC increased (**b**) the number of chasing contacts, (**c**) close following, and (**d**) tolerance behavior. No significant effects were detected for (**e**) avoidance behavior. Numbers within bars indicate the number of rodents per group. * $P < 0.05$, ** $P < 0.01$.

The absence of effects on avoidance responses or freezing was unexpected, given the prominent role of the SC in initiating such defensive responses (Shang et al., 2015). If one assumes a modulatory rather than instructive role for nigrotectal projections, it is conceivable that the behavioral task was insufficient in triggering panic-like behavior in regular C57BL/6 mice. Compared to other ethobehavioral tasks, which are based on only a few confrontations with large robogators (Choi and Kim, 2010) , the BMT allows the analysis of multiple encounters with an ambiguous, only potentially-threatening object. Moreover, the dimension of the robo-beetle enables the assessment of both defensive and offensive responses. This is of particular interest for studies of the nigrotectal pathway, given the involvement of the SC in predatory hunting (Furigo et al., 2010; Comoli et al., 2012). Indeed, we could observe an increase in close following of the beetle upon stimulation of the nigrotectal pathway. However, inactivation of the SC was shown to reduce predatory hunting (Furigo et al., 2010), and activation of the nigrotectal pathway inhibits neuronal activity at the level of the SC (Hormigo et al., 2016). Therefore, we conclude that the increase in close following observed in the present

study most likely results from a devaluation of the threat associated with the bypassing beetle rather than an initiation of hunting. The SC is a multimodal sensory motor structure that receives inputs from the retina and somatosensory cortex (King, 2004; Shi et al., 2017). Thus, arguably, stimulation of the nigrotectal pathway, which results in inhibition of SC neurons, may obscure sensory perceptions. In this context we have to consider that the SC is separated into superficial, intermediate, and deep layers (Shi et al., 2017; Redgrave et al., 1993). Although the superficial layers are involved in diverse visual response properties (Shi et al., 2017), including detection of moving stimuli changes (Savage et al., 2017), the deep layers are highly associated with defensive behaviors (Brandão et al., 1994). In this scenario, intrinsic connections from the superficial layers to the dlSC appear to provide a rapid route for orienting movements of the head and eyes (Shang et al., 2015; Redgrave et al., 1993) towards a given stimulus. It is known that the position of the head in space is crucial during a variety of tasks, including defensive behaviors (Dean et al., 1989), among others (Furigo et al., 2010; Wang and Redgrave, 1997). This suggests that the SC acts as a crucial structure which is strongly implicated in initial behavioral responses to visual sensory events (Comoli et al., 2012), such as those related to threatening stimuli. Histological verification of the transfections could localize projection terminals of SNr neurons in the dlSC, where the optical fibers were aimed at. Therefore, stimulation of the nigrotectal pathway highly likely affected the integration of primary sensory perception into defensive responses. Given the multisensory nature of the beetle (i.e., its movement produces noise and vibrations in addition to its visual appearance), it is highly likely that the observed behavioral phenotype results from interference not only with visual, but also tactile and auditory signals. Taken together, we demonstrate that the nigrotectal pathway bears the potential to control defensive responses to threatening stimuli. Specifically, projections from the SNr to deep layers of the SC appear to selectively dampen threat detection.

Bibliography

Abdeljalil J, Hamid M, Abdel-mouttalib O, Stéphane R, Raymond R, Johan A, José S, Pierre C, Serge P (2005) The optomotor response: A robust first-line visual screening method for mice. *Vis Res* 45(11):1439–1446.

Adamec RE, Blundell J, Burton P (2005) Neural circuit changes mediating lasting brain and behavioral response to predator stress. *Neurosci Biobehav Rev* 8(29):1225–41.

Adametz J, O'Leary JL (1959) Experimental mutism resulting from periaqueductal lesions in cats. *Neurology* 9:636–42.

Adelman S, Taylor CR, Heglund NC (1975) Sweating on paws and palms: what is its function? *Am J Physiol* 229(5):1400–2.

Adolphs R, Tranel D, Damasio H, Damasio A (1994) Impaired recognition of emotion in facial expressions following bilateral damage to the human amygdala. *Nature* 372(6507):669–672.

Alerstam T (1987) Radar observations of the stoop of the Peregrine Falcon Falco peregrinus and the Goshawk Accipiter gentilis. *Ibis* 129(S1):267–273.

Alexander GM, Rogan SC, Abbas AI, Armbruster BN, Pei Y, Allen JA, Nonneman RJ, Hartmann J, Moy SS, Nicolelis MA, McNamara JO, Roth BL (2009) Remote control of neuronal activity in transgenic mice expressing evolved G protein-coupled receptors. *Neuron* 63(1):27–39.

Almada RC, Coimbra NC (2015) Recruitment of striatonigral disinhibitory and nigrotectal inhibitory GABAergic pathways during the organization of defensive behavior by mice in a dangerous environment with the venomous snake Bothrops alternatus (Reptilia, Viperidae). . *Synapse* 69(6):299–313.

Alsene KM, Carasso BS, Connors EE, Bakshi VP (2006) Disruption of Prepulse Inhibition after Stimulation of Central but not Peripheral α-1 Adrenergic Receptors. *Neuropsychopharmacol* 31(10):2150–61.

Alvestad S, Goa PE, Qu H, Risa Ø, Brekken C, Sonnewald U, Haraldseth O, Hammer J, Ottersen OP, Håberg A (2007) In vivo mapping of temporospatial changes in manganese enhancement in rat brain during epileptogenesis. *NeuroImage* 38(1):57–66.

Ambroggi F, Ishikawa A, Fields HL, Nicola SM (2008) Basolateral amygdala neurons facilitate reward-seeking behavior by exciting nucleus accumbens neurons. *Neuron* 59(4):648–661.

American Psychiatric Association (1994) *Diagnostic and statistical manual of mental disorders (DSM).*

Amir A, Lee SC, Headley DB, Herzallah MM, Paré D (2015) Amygdala Signaling during Foraging in a Hazardous Envirnoment. *J Neurosci* 35(38):12994–13005.

Andreini C, Bertini I, Cavallaro G, Holliday GL, Thornton JM (2008) Metal ions in biological catalysis: from enzyme databases to general principles. *J Biol Inorg Chem* 13(8):1205–1218.

Apfelbach R, Blanchard CD, Blanchard RJ, Hayes RA, McGregor IS (2005) The effects of predator odors in mammalian prey species: A review of field and laboratory studies. *Neurosci Biobehav Rev* 29(8):1123–1144.

Aravanis AM, Wang LP, Zhang F, Meltzer LA, Mogri MZ, Schneider MB, Deisseroth K (2007) An optical neural interface: in vivo control of rodent motor cortex with integrated fiberoptic and optogenetic technology. *J Neural Eng* 4(3):S143–S156.

Armbruster BN, Li X, Pausch MH, Herlitze S, Roth BL (2007) Evolving the lock to fit the key to create a family of G protein-coupled receptors potently activated by an inert ligand. *PNAS* 104(12):5163–8.

Arriaga G, Zhou EP, Jarvis ED (2012) Of mice, birds, and men: the mouse ultrasonic song system has some features similar to humans and song-learning birds. *PloS one* 7(10):e46610.

Asahina M, Poudel A, Hirano S (2015) Sweating on the palm and sole: physiological and clinical relevance. *Clinical Autonomic Research* 25(3):153–159.

Auffenberg E, Jurik A, Mattusch C, Stoffel R, Genewsky A, Namendorf C, Schmid RM, Rammes G, Biel M, Uhr M, Moosmang S, Michalakis S, Wotjak CT, Thoeringer CK (2016) Remote and reversible inhibition of neurons and circuits by small molecule induced potassium channel stabilization. *Sci Rep* 6:19293.

Austin AW, Wissmann T, von Kanel R (2013) Stress and hemostasis: an update. *Semin Thromb Hemost* 39(8):902–12.

Avrabos C, Sotnikov SV, Dine J, Markt PO, Holsboer F, Landgraf R, Eder M (2013) Real-Time Imaging of Amygdalar Network Dynamics In Vitro Reveals a Neurophysiological Link to Behavior in a Mouse Model of Extremes in Trait Anxiety. *J Neurosci* 33(41).

Ayers LW, Asok A, Heyward FD, Rosen JB (2013) Freezing to the predator odor 2,4,5 dihydro 2,5 trimethylthiazoline (TMT) is disrupted by olfactory bulb removal but not trigeminal deafferentation. *Behav Brain Res* 253:54–59.

Azzopardi E, Typlt M, Jenkins B, Schmid S (2013) Sensorimotor gating and spatial learning in α7-nicotinic receptor knockout mice. *Genes Brain Behav* 12(4):414–423.

Baarendse PJ, van Grootheest G, Jansen RF, Pieneman AW, Ogren SO, Verhage M, Stiedl O (2008) Differential

involvement of the dorsal hippocampus in passive avoidance in C57bl/6J and DBA/2J mice. *Hippocampus* 18(1):11–19.

Bailey KR, Crawley JN (2009) *Anxiety-Related Behaviors in Mice* CRC Press/Taylor & Francis.

Baird AL, Coogan AN, Siddiqui A, Donev RM, Thome J (2012) Adult attention-deficit hyperactivity disorder is associated with alterations in circadian rhythms at the behavioural, endocrine and molecular levels. *Mol Psychiatr* 17(10):988–995.

Bale TL, Chen A (2012) Minireview: CRF and Wylie Vale: a story of 41 amino acids and a Texan with grit. *Endocrinology* 153(6):2556–61.

Bale TL, Picetti R, Contarino A, Koob GF, Vale WW, Lee KF (2002) Mice deficient for both corticotropin-releasing factor receptor 1 (CRFR1) and CRFR2 have an impaired stress response and display sexually dichotomous anxiety-like behavior. *J Neurosci* 22(1):193–9.

Bandler R, Shipley MT (1994) Columnar organization in the midbrain periaqueductal gray: modules for emotional expression? *Trends Neurosci* 17(9):379–89.

Bandler R, Carrive P (1988) Integrated defence reaction elicited by excitatory amino acid microinjection in the midbrain periaqueductal grey region of the unrestrained cat. *Brain Res* 439(1):95–106.

Bandler R, Carrive P, Depaulis A (1991) Emerging Principles of Organization of the Midbrain Periaqueductal Gray Matter In *The Midbrain Periaqueductal Gray Matter*, pp. 1–8. Springer US, Boston, MA.

Banghart M, Borges K, Isacoff E, Trauner D, Kramer RH (2004) Light-activated ion channels for remote control of neuronal firing. *Nat Neurosci* 7(12):1381–1386.

Banks GT, Nolan PM (2011) Assessment of Circadian and Light-Entrainable Parameters in Mice Using Wheel-Running Activity. *Curr Protoc Mouse Biol* 1(3):369–81.

Barrington FJF (1925) The effects of lesions of the hind and midbrain on micturition in the cat. *Q J Exp Physiol* 15(1):81–102.

Bartelle BB, Szulc KU, Suero-Abreu GA, Rodriguez JJ, Turnbull DH (2013) Divalent metal transporter, DMT1: a novel MRI reporter protein. *Magn Reson Med* 70(3):842–50.

Bartlang M, Oster H, Helfrich-Förster C (2015) Repeated psychosocial stress at night affects the circadian activity rhythm of male mice. *J Biol Rhythms* 30(3):228–41.

Basbaum AI, Fields HL (1984) ENDOGENOUS PAIN CONTROL SYSTEMS: Brainstem Spinal Pathways and Endorphin Circuitry. *Ann Rev Neurosci* 7:309–38.

Battelli F, Stern L (1912) Die Oxydationsfermente. *Ergebnisse der Physiologie* 12(1):96–268.

Bearer EL, Falzone TL, Zhang X, Biris O, Rasin A, Jacobs RE (2007) Role of neuronal activity and kinesin on tract tracing by manganese-enhanced MRI (MEMRI). *NeuroImage* 37 Suppl 1(Suppl 1):S37–46.

Beitz AJ (1982) The organization of afferent projections to the midbrain periaqueductal gray of the rat. *Neuroscience* 7(1):133–59.

Beitz AJ (1989) Possible origin of glutamatergic projections to the midbrain periaqueductal gray and deep layer of the superior colliculus of the rat. *Brain Res Bull* 23(1-2):25–25.

Bekoff M (2000) Animal Emotions: Exploring Passionate Natures. *Bioscience Washington* 50(10):861–870.

Bell C (1806) *The Anatomy and Philosophy of Expression as Sons, Connected with the Fine Arts* George Bell and Sons, London.

Bellocchio L, Lafenêtre P, Cannich A, Cota D, Puente N, Grandes P, Chaouloff F, Piazza P, Marsicano G (2010) Bimodal control of stimulated food intake by the endocannabinoid system. *Nat Neurosci* 13(3):281–283.

Belzung C, Lemoine M (2011) Criteria of validity for animal models of psychiatric disorders: focus on anxiety disorders and depression. *Biol Mood Anxiety Disord* 1(1):9.

Belzung C, Misslin R, Vogel E, Dodd RH, Chapouthier G (1987) Anxiogenic effects of methyl-β-carboline-3-carboxylate in a light/dark choice situation. *Pharmacol Biochem Behav* 28(1):29–33.

Benedykcinska A, Ferreira A, Lau J, Broni J, Richard-Loendt A, Henriquez NV, Brandner S (2016) Generation of brain tumours in mice by Cre-mediated recombination of neural progenitors in situ with the tamoxifen metabolite endoxifen. *Dis Model Mech* 9(2):211–220.

Bennet-Clark HC, Ewing AW (1968) The Courtship Songs of Drosophila. *Behaviour* 31(3):288–301.

Berényi A, Somogyvári Z, Nagy AJ, Roux L, Long JD, Fujisawa S, Stark E, Leonardo A, Harris TD, Buzsáki G (2014) Large-scale, high-density (up to 512 channels) recording of local circuits in behaving animals. *J Neurophysiol* 111(5).

Berridge MJ (1998) Neuronal calcium signaling. *Neuron* 21(1):13–26.

Berridge MJ (1993) Inositol trisphosphate and calcium signalling. *Nature* 361(6410):315–325.

Bertoglio LJ, Zangrossi H (2005) Involvement of dorsolateral periaqueductal gray cholecystokinin-2 receptors in the regulation of a panic-related behavior in rats. *Brain Res* 1059(1):46–51.

Betley JN, Xu S, Cao ZFH, Gong R, Magnus CJ, Yu Y, Sternson SM (2015) Neurons for hunger and thirst transmit a negative-valence teaching signal. *Nature* 521(7551):180–5.

Bi A, Cui J, Ma YP, Olshevskaya E, Pu M, Dizhoor AM, Pan ZH (2006) Ectopic expression of a microbial-type rhodopsin restores visual responses in mice with photoreceptor degeneration. *Neuron* 50(1):23–33.

Biol. ENC (2014) An update on data reporting standards. *Nature Cell Biology* 16(5):385–385.

Blain S, Mihailidis A, Chau T (2006) Conf Proc IEEE Eng Med Biol Soc. *Conference proceedings : ... Annual International Conference of the IEEE Engineering in Medicine and Biology Society. IEEE Engineering in Medicine and Biology Society. Annual Conference* Suppl:6561–4.

Blanchard DC, Griebel G, Blanchard RJ (2003) The Mouse Defense Test Battery: pharmacological and behavioral assays for anxiety and panic. *Eur J Pharmacol* 463(1-3):97–116.

Blanchard DC, Li CI, Hubbard D, Markham CM, Yang M, Takahashi LK, Blanchard RJ (2003) Dorsal premammillary nucleus differentially modulates defensive behaviors induced by different threat stimuli in rats. *Neurosci Lett* 345(3):145–8.

Blanchard RJ, Blanchard DC (1969) Crouching as an index of fear. *J Comp Physiol Psych* 67(3):370–5.

Blanchard RJ, Blanchard DC, Weiss SM, Meyer S (1990) The effects of ethanol and diazepam on reactions to predatory odors. *Pharmacol Biochem Behav* 35(4):775–80.

Blanchard RJ, Blanchard DC (1990) An ethoexperimental analysis of defense, fear, and anxiety. In *Anxiety*, pp. 124–133. University of Otago Press.

Blessing WW (2003) Lower Brainstem Pathways Regulating Sympathetically Mediated Changes in Cutaneous Blood Flow. *Cell Mol Neurobiol* 23(4/5):527–538.

Blume Hw, Pittman QJ, Lafontaine s, Renaud LP (1982) Lateral septum-medial hypothalamic connections: An electrophysiological study in the rat. *Neuroscience* 7(11):2783–92.

Boehm S, Kubista H (2002) Fine tuning of sympathetic transmitter release via ionotropic and metabotropic presynaptic receptors. *Pharmacol Rev* 54(1):43–99.

Bolivar VJ, Pooler O, Flaherty L (2001) Inbred strain variation in contextual and cued fear conditioning behavior. *Mamm Genome* 12(8):651–656.

Bolles RC (1970) Species-specific defense reactions and avoidance learning. *Psychol Rev* 77(1):32–48.

Bouron A, Kiselyov K, Oberwinkler J (2015) Permeation, regulation and control of expression of TRP channels by trace metal ions. *Pflugers Arch* 467(6):1143–64.

Bouwknecht JA, Paylor R (2002) Behavioral and physiological mouse assays for anxiety: a survey in nine mouse strains. *Behav Brain Res* 136(2):489–501.

Bovet D, Bovet-Nitti F, Oliverio A (1969) Genetic Aspects of Learning and Memory in Mice. *Science* 163(3863).

Boyden ES (2011) A history of optogenetics: the development of tools for controlling brain circuits with light. *F1000 Biol Rep* 3:11.

Boyden ES, Zhang F, Bamberg E, Nagel G, Deisseroth K (2005) Millisecond-timescale, genetically targeted optical control of neural activity. *Nat Neurosci* 8(9):1263–8.

Brand G (2006) Olfactory/trigeminal interactions in nasal chemoreception. *Neurosci Biobehav Rev* 30(7):908–917.

Brandão ML, Borelli K, Nobre MJ, Santos JM, Albrecht-Souza L, Oliveira AR, Martinez R (2005) Gabaergic regulation of the neural organization of fear in the midbrain tectum. *Neurosci Biobehav Rev* 29(8):1299–311.

Brandão ML, Cardoso SH, Melo LL, Motta V, Coimbra NC (1994) Neural substrate of defensive behavior in the midbrain tectum. *Neurosci Biobhav Rev* 18(3):339–46.

Brandão ML, Zanoveli JM, Ruiz-Martinez RC, Oliveira LC, Landeira-Fernandez J (2008) Different patterns of freezing behavior organized in the periaqueductal gray of rats: Association with different types of anxiety. *Behav Brain Res* 188(1):1–13.

Brandão M, Anseloni V, Pandóssio J, De Araújo J, Castilho V (1999) Neurochemical mechanisms of the defensive behavior in the dorsal midbrain. *Neurosci Biobehav Rev* 23(6):863–875.

Brouillet E, Shinobu L, McGarvey U, Hochberg F, Beal MF (1993) Manganese Injection into the Rat Striatum Produces Excitotoxic Lesions by Impairing Energy Metabolism. *Exp Neurol* 120(1):89–94.

Brown DA, Sihra TS (2008) Presynaptic Signaling by Heterotrimeric G-Proteins In *Handbook of experimental pharmacology*, number 184, pp. 207–260. Springer.

Brown JS, Kalish HI, Farber IE (1951) Conditioned fear as revealed by magnitude of startle response to an auditory stimulus. *J Exp Psychol* 41(5):317–328.

Brücke FT (1935) Über die Wirkung von Acetylcholin auf die Pilomotoren. *Klin Wochenschr* 14(1):7–9.

Brudzynski SM, Bihari F, Ociepa D, Xiao-Wen F (1993) Analysis of 22 kHz ultrasonic vocalization in laboratory rats: Long and short calls. *Physiol Behav* 54(2):215–21.

Bueno CH, Zangrossi Jr H, Nogueira RL, Soares VP, Viana MB (2005) Panicolytic-like effect induced by the stimulation of GABAA and GABAB receptors in the dorsal periaqueductal grey of rats. *Eur J Pharmacol* 516(3):239–46.

Bukalo O, Pinard CR, Silverstein S, Brehm C, Hartley ND, Whittle N, Colacicco G, Busch E, Patel S, Singewald N, Holmes A (2015) Prefrontal inputs to the amygdala instruct fear extinction memory formation. *Science Advances* 1(6).

Bulwer J (1644) *Chirologia, or the Natural Language of the Hand* Harper, London.

Bunck M, Czibere L, Horvath C, Graf C, Frank E, Keßler MS, Murgatroyd C, Müller-Myhsok B, Gonik M, Weber P, Pütz B, Muigg P, Panhuysen M, Singewald N, Bettecken T, Deussing JM, Holsboer F, Spengler D, Landgraf R (2009) A Hypomorphic Vasopressin Allele Prevents Anxiety-Related Behavior. *PLoS ONE* 4(4):e5129.

Burdach CF (1822) *Vom Baue und Leben des Gehirns. Zweyter Band.* Dyk'sche Buchhandlung, Leipzig.

Burn JH, Leach EH, Rand MJ, Thompson JW (1959) Peripheral effects of nicotine and acetylcholine resembling those of sympathetic stimulation. *J Physiol* 148:332–52.

Burn JH, Rand MJ (1965) Acetylcholine in adrenergic transmission. *Annu Rev Pharmacol* 5:163–82.

Burstone MS (1959) NEW HISTOCHEMICAL TECHNIQUES FOR THE DEMONSTRATION OF TISSUE OXIDASE (CYTOCHROME OXIDASE). *J Hist Cytochem* 7(2):112–122.

Butler RK, Finn DP (2009) Stress-induced analgesia. *Prog Neurobiol* 88(3):184–202.

Buzsàki G, Bickford RG, Ryan LJ, Young S, Prohaska O, Mandel RJ, Gage FH (1989) Multisite recording of brain field potentials and unit activity in freely moving rats. *J Neurosci Meth* 28(3):209–17.

Cai H, Haubensak W, Anthony TE, Anderson DJ (2014) Central amygdala PKC-δ(+) neurons mediate the

influence of multiple anorexigenic signals. *Nat Neurosci* 17(9):1240–8.

Calhoon GG, Tye KM (2015) Resolving the neural circuits of anxiety. *Nat Neurosci* 18(10):1394–1404.

Callaway EM, Yuste R (2002) Stimulating neurons with light. *CCurr Opin Neurobiol* 12(5):587–92.

Calzavara M, Patti C, Lopez G, Abílio V, Silva R, Frussa-Filho R (2005) Role of learning of open arm avoidance in the phenomenon of one-trial tolerance to the anxiolytic effect of chlordiazepoxide in mice. *Life Sci* 76(19):2235–2246.

Cameron AA, Khan IA, Westlund KN, Cliffer KD, Willis WD (1995a) The efferent projections of the periaqueductal gray in the rat: APhaseolus vulgaris-leucoagglutinin study. I. Ascending projections. *J Comp Neurol* 351(4):568–584.

Cameron AA, Khan IA, Westlund KN, Willis WD (1995b) The efferent projections of the periaqueductal gray in the rat: APhaseolus vulgaris-leucoagglutinin study. II. Descending projections. *J Comp Neurol* 351(4):585–601.

Campbell SS, Murphy PJ (1998) Extraocular Circadian Phototransduction in Humans. *Science* 279(5349).

Campos AC, Fogaca MV, Aguiar DC, Guimaraes FS, Campos AC, Fogaca MV, Aguiar DC, Guimaraes FS (2013) Animal models of anxiety disorders and stress. *Rev Bras Psiquiatr* 35:S101–S111.

Cannon WB (1929) *Bodily Changes in Pain, Hunger, Fear and Rage* D. Appelton and Company, New York and London, second edi edition.

Canteras NS (2002) The medial hypothalamic defensive system: hodological organization and functional implications. *Pharmacol Biochem Behav* 71(3):481–91.

Canteras NS, Goto M (1999) Fos-like immunoreactivity in the periaqueductal gray of rats exposed to a natural predator. *Neuroreport* 10(2):413–8.

Canteras NS, Simerly RB, Swanson LW (1994) Organization of projections from the ventromedial nucleus of the hypothalamus: APhaseolus vulgaris-Leucoagglutinin study in the rat. *J Comp Neurol* 348(1):41–79.

Capecchi MR (1989) Altering the genome by homologous recombination. *Science* 244(4910):1288–92.

Carlé N M, Meletis K, Siegle J, Cardin J, Futai K, Vierling-Claassen D, Rü Hlmann C, Jones S, Deisseroth K, Sheng M, Moore C, Tsai LH (2011) A critical role for NMDA receptors in parvalbumin interneurons for gamma rhythm induction and behavior. *Mol Psychiatr* 17:537–548.

Carobrez A, Bertoglio L (2005) Ethological and temporal analyses of anxiety-like behavior: The elevated plus-maze model 20 years on. *Neurosci Biobehav Rev* 29(8):1193–1205.

Carrive P (2006) Dual activation of cardiac sympathetic and parasympathetic components during conditioned fear to context in the rat. *Clin Exp Pharmacol Physiol* 33(12):1251–4.

Carvalho-Netto EF, Nunes-de Souza RL (2004) Use of the elevated t-maze to study anxiety in mice. *Behav Brain Res* 148:119–132.

Casarotto PC, Terzian AL, Aguiar DC, Zangrossi H, Guimarães FS, Wotjak CT, Moreira FA (2012) Opposing roles for cannabinoid receptor type-1 (CBâĆĄ) and transient receptor potential vanilloid type-1 channel (TRPV1) on the modulation of panic-like responses in rats. *Neuropsychopharmacol* 2(37):478–86.

Castellan-Baldan L, da Costa Kawasaki M, Ribeiro S, Calvo F, Corrêa VM, Coimbra NC (2006) Topographic and functional neuroanatomical study of GABAergic disinhibitory striatum-nigral inputs and inhibitory nigrocollicular pathways: neural hodology recruiting the substantia nigra, pars reticulata, for the modulation of the neural activity in the inferior colliculus involved with panic-like emotions. *J Chem Neuroanat* 32(1):1–27.

Castro M, Elias LL, Elias PCL, Moreira AC (2010) Physiology and Pathophysiology of the HPA Axis In *Cushing's Syndrome*, pp. 1–20. Humana Press, Totowa, NJ.

Chan KC, Cheng JS, Fan S, Zhou IY, Yang J, Wu EX (2012) In vivo evaluation of retinal and callosal projections in early postnatal development and plasticity using manganese-enhanced MRI and diffusion tensor imaging. *NeuroImage* 59(3):2274–83.

Chan KC, Fan SJ, Chan RW, Cheng JS, Zhou IY, Wu EX (2014) In vivo visuotopic brain mapping with manganese-enhanced MRI and resting-state functional connectivity MRI. *NeuroImage* 90:235–45.

Chan KC, Li J, Kau P, Zhou IY, Cheung MM, Lau C, Yang J, So Kf, Wu EX (2011) In vivo retinotopic mapping of superior colliculus using manganese-enhanced magnetic resonance imaging. *NeuroImage* 54(1):389–95.

Chang B, Hurd R, Wang J, Nishina P (2013) Survey of common eye diseases in laboratory mouse strains. *Invest Ophthal Vis Sci* 54(7):4974–81.

Chang WH, Lin SK, Lane HY, Wei FC, Hu WH, Lam YW, Jann MW (1998) Reversible metabolism of clozapine and clozapine N-oxide in schizophrenic patients. *Prog Neuropsychopharmacol Biol Psychiatry* 22(5):723–39.

Chaouloff F, Durand M, Mormède P (1997) Anxiety- and activity-related effects of diazepam and chlordiazepoxide in the rat light/dark and dark/light tests. *Behav Brain Res* 85(1):27–35.

Chen D, Katdare A, Lucas N (2006) Chemosignals of fear enhance cognitive performance in humans. *Chem Senses* 31(5):415–23.

Chen S, Zhou H, Guo S, Zhang J, Qu Y, Feng Z, Xu K, Zheng X (2015) Optogenetics Based Rat-Robot Control: Optical Stimulation Encodes "Stop" and "Escape" Commands. *Ann Biomed Eng* 43(8):1851–64.

Chiken S, Nambu A (2016) Mechanism of Deep Brain Stimulation: Inhibition, Excitation, or Disruption? *Neuroscientist* 22(3):313–22.

Chinwalla AT, Cook LL, Delehaunty KD, Fewell GA, Fulton LA, Fulton RS, ..., Zody MC (2002) Initial sequencing and comparative analysis of the mouse genome. *Nature* 420(6915):520–562.

Chivukula S, Grandhi R, Friedlander RM (2014) A brief history of early neuroanesthesia. *Neurosurg Focus* 36(4):E2.

Choate JK, Danson EJ, Morris JF, Paterson DJ (2001) Peripheral vagal control of heart rate is impaired in

neuronal NOS knockout mice. *Am J Physiol-Heart C* 281(6):H2310–7.

Choi JS, Kim JJ (2010) Amygdala regulates risk of predation in rats foraging in a dynamic fear environment. *PNAS* 107(50):21773–21777.

Chow BY, Han X, Dobry AS, Qian X, Chuong AS, Li M, Henninger MA, Belfort GM, Lin Y, Monahan PE, Boyden ES (2010) High-performance genetically targetable optical neural silencing by light-driven proton pumps. *Nature* 463(7277):98–102.

Christmas AJ, Maxwell DR (1970) A comparison of the effects of some benzodiazepines and other drugs on aggressive and exploratory behaviour in mice and rats. *Neuropharmacology* 9(1):17–29.

Chuong AS, Miri ML, Busskamp V, Matthews GAC, Acker LC, Sørensen AT, Young A, Klapoetke NC, Henninger MA, Kodandaramaiah SB, Ogawa M, Ramanlal SB, Bandler RC, Allen BD, Forest CR, Chow BY, Han X, Lin Y, Tye KM, Roska B, Cardin JA, Boyden ES (2014) Noninvasive optical inhibition with a red-shifted microbial rhodopsin. *Nat Neurosci* 17(8):1123–9.

Ciocchi S, Herry C, Grenier F, Wolff SBE, Letzkus JJ, Vlachos I, Ehrlich I, Sprengel R, Deisseroth K, Stadler MB, Müller C, Lüthi A (2010) Encoding of conditioned fear in central amygdala inhibitory circuits. *Nature* 468(7321):277–282.

Clark KL, Armstrong KM, Moore T (2011) Probing neural circuitry and function with electrical microstimulation. *Proc Biol Sci* 278(1709):1121–30.

Clarke RL, Smith RF, Justesen DR (1985) An infrared device for detecting locomotor activity. *Behav Res Meth Ins C* 17(5):519–525.

Clement CI, Keay KA, Podzebenko K, Gordon BD, Bandler R (2000) Spinal sources of noxious visceral and noxious deep somatic afferent drive onto the ventrolateral periaqueductal gray of the rat. *J Comp Neuol* 425(3):323–44.

Coburn CA (1912) Singing mice. *J Anim Behav* 2(5):364–366.

Coimbra NC, Brandão ML (1993) GABAergic nigro-collicular pathways modulate the defensive behaviour elicited by midbrain tectum stimulation. *Behav Brain Res* 59(1-2):131–9.

Cole J, Rodgers R (1995) Ethological comparison of the effects of diazepam and acute/chronic imipramine on the behaviour of mice in the elevated plus-maze. *Pharmacol Biochem Behav* 52(3):473–478.

Comoli E, Das Neves Favaro P, Vautrelle N, Leriche M, Overton PG, Redgrave P (2012) Segregated anatomical input to sub-regions of the rodent superior colliculus associated with approach and defense. *Front Neuroanat* 6(9).

Conejo N, González-Pardo H, Gonzalez-Lima F, Arias J (2010) Spatial learning of the water maze: Progression of brain circuits mapped with cytochrome oxidase histochemistry. *Neurobiol Learn Mem* 93(3):362–371.

Connolly SJ, Sheldon R, Thorpe KE, Roberts RS, Ellenbogen KA, Wilkoff BL, Morillo C, Gent M, VPS II Investigators (2003) Pacemaker therapy for prevention of syncope in patients with recurrent severe vasovagal syncope: Second Vasovagal Pacemaker Study (VPS II): a randomized trial. *JAMA* 289(17):2224–9.

Continuum Analytics Anaconda software distribution (https://continuum.io/) Accessed: 2017-06-05.

Cook MN, Williams RW, Flaherty L (2001) Anxiety-related behaviors in the elevated zero-maze are affected by genetic factors and retinal degeneration. *Behav Neurosci* 115(2):468–76.

Coon JM, Rothman S (1940) The nature of the pilomotor response to acetyl choline; some observations on the pharmacodynamics of the skin. *J Pharmacol Exp Ther* 68(3):301–311.

Corchero J, Fuentes J, Manzanares J (1999) Chronic treatment with CP-55,940 regulates corticotropin releasing factor and proopiomelanocortin gene expression in the hypothalamus and pituitary gland of the rat. *Life Sci* 64(11):905–911.

Coulson SE, O'dwyer NJ, Adams RD, Croxson GR (2004) Expression of emotion and quality of life after facial nerve paralysis. *Otol Neurotol* 25(6):1014–9.

Craske MG, Stein MB, Eley TC, Milad MR, Holmes A, Rapee RM, Wittchen HU (2017) Anxiety disorders. *Nat Rev Dis Primers* 3:17024.

Crawley J, Goodwin FK (1980) Preliminary report of a simple animal behavior model for the anxiolytic effects of benzodiazepines. *Pharmacol Biochem Behav* 13(2):167–70.

Crawley JN (1981) Neuropharmacologic specificity of a simple animal model for the behavioral actions of benzodiazepines. *Pharmacol Biochem Behav* 15(5):695–9.

Crawley JN, Belknap JK, Collins A, Crabbe JC, Frankel W, Henderson N, Hitzemann RJ, Maxson SC, Miner LL, Silva AJ, Wehner JM, Wynshaw-Boris A, Paylor R (1997) Behavioral phenotypes of inbred mouse strains: implications and recommendations for molecular studies. *Psychopharmacology* 132(2):107–24.

Csicsvari J, Henze DA, Jamieson B, Harris KD, Sirota A, Barthó P, Wise KD, Buzsáki G (2003) Massively Parallel Recording of Unit and Local Field Potentials With Silicon-Based Electrodes. *J Neurophysiol* 90(2):1314–1323.

Currie S, Hoggard N, Craven IJ, Hadjivassiliou M, Wilkinson ID (2013) Understanding MRI: basic MR physics for physicians. *Postgrad Med J* 89(1050):209–223.

da Silva LGJ, de Menezes RC, Villela DC, Fontes MA (2006) Excitatory amino acid receptors in the periaqueductal gray mediate the cardiovascular response evoked by activation of dorsomedial hypothalamic neurons. *Neuroscience* 139(3):1129–39.

Dampney RAL (2015) Central mechanisms regulating coordinated cardiovascular and respiratory function during stress and arousal. *Am J Physiol* 309(5).

Darwin C (1872) *The expression of the emotions in man and animals* Oxford University Press, USA.

Davis M (1980) Neurochemical modulation of sensory-motor reactivity: acoustic and tactile startle reflexes. *Neurosci Biobehav Rev* 4(2):241–63.

Davis M, Astrachan D (1978) Conditioned fear and startle magnitude: effects of different footshock or backshock intensities used in training. *J Exp Psychol Anim B* 4(2):95–103.

Davis M (1984) The Mammalian Startle Response In *Neural Mechanisms of Startle Behavior*, pp. 287–351. Springer US, Boston, MA.

Davis M (2006) Neural systems involved in fear and anxiety measured with fear-potentiated startle. *Am Psychol* 61(8):741–756.

Davisson M (1996) Rules for nomenclature of inbred strains. In Lyon M, Rastan S, Brown S, editors, *Genetic Variants and Strains of the Laboratory Mouse*, pp. 1532–1536. Oxford University Press, oxford edition.

de Almeida LP, Ramos PL, Pandossio JE, Landeira-Fernandez J, Zangrossi H, Nogueira RL (2006) Prior electrical stimulation of dorsal periaqueductal grey matter or deep layers of the superior colliculus sensitizes rats to anxiety-like behaviors in the elevated T-maze test. *Behav Brain Res* 170(2):175–181.

de Barenne JGD (1933) THE MODE AND SITE OF ACTION OF STRYCHNINE IN THE NERVOUS SYSTEM. *Physiol Rev* 13(3):325–335.

de Gelder B (2006) Towards the neurobiology of emotional body language. *Nat Rev Neurosci* 7(3):242–249.

de Groot JHB, Semin GR, Smeets MAM (2014) Chemical communication of fear: A case of maleâĂŞfemale asymmetry. *J Exp Psychol* 143(4):1515–1525.

De Luca-Vinhas MCZ, Macedo CE, Brandão ML (2006) Pharmacological assessment of the freezing, antinociception, and exploratory behavior organized in the ventrolateral periaqueductal gray. *Pain* 121(1-2):94–104.

de Menezes RCA, Zaretsky DV, Fontes MAP, DiMicco JA (2006) Microinjection of muscimol into caudal periaqueductal gray lowers body temperature and attenuates increases in temperature and activity evoked from the dorsomedial hypothalamus. *Brain Res* 1092(1):129–37.

De Oca BM, DeCola JP, Maren S, Fanselow MS (1998) Distinct regions of the periaqueductal gray are involved in the acquisition and expression of defensive responses. *J Neurosci* 18(9):3426–32.

Dean P, Mitchell IJ, Redgrave P (1988) Responses resembling defensive behaviour produced by microinjection of glutamate into superior colliculus of rats. *Neuroscience* 24(2):501–10.

Dean P, Redgrave P, Westby GW (1989) Event or emergency? two response systems in the mammalian superior colliculus. *Trends Neurosci* 12(4):137–47.

Deisseroth K (2015) Optogenetics: 10 years of microbial opsins in neuroscience. *Nat Neurosci* 18(9):1213–1225.

Delgado JM (1977) Instrumentation, working hypotheses, and clinical aspects of neurostimulation. *Appl Neurophysiol* 40(2-4):88–110.

Deng H, Xiao X, Wang Z (2016) Periaqueductal Gray Neuronal Activities Underlie Different Aspects of Defensive Behaviors. *J Neurosci* 36(29):7580–7588.

Devinsky O, Morrell MJ, Vogt BA (1995) Contributions of anterior cingulate cortex to behaviour. *Brain* 118(Pt 1):279–306.

Di Marzo V, Melck D, Bisogno T, De Petrocellis L (1998) Endocannabinoids: endogenous cannabinoid receptor ligands with neuromodulatory action. *Trends Neurosci* 21(12):521–528.

Dilger S, Straube T, Mentzel HJ, Fitzek C, Reichenbach JR, Hecht H, Krieschel S, Gutberlet I, Miltner WHR (2003) Brain activation to phobia-related pictures in spider phobic humans: an event-related functional magnetic resonance imaging study. *Neurosci Lett* 348(1):29–32.

Dine J, Genewsky A, Hladky F, Wotjak CT, Deussing JM, Zieglgänsberger W, Chen A, Eder M (2016) Local Optogenetic Induction of Fast (20-40 Hz) Pyramidal-Interneuron Network Oscillations in the In Vitro and In Vivo CA1 Hippocampus: Modulation by CRF and Enforcement of Perirhinal Theta Activity. *Front Cell Neurosci* 10:108.

Do-Monte FH, Quiñones-Laracuente K, Quirk GJ (2015) A temporal shift in the circuits mediating retrieval of fear memory. *Nature* 519(7544):460–463.

Doherty NS, Hancock AA (1983) Role of alpha-2 adrenergic receptors in the control of diarrhea and intestinal motility. *J Pharmacol Exp Ther* 225(2):269–74.

Dolezal V, Tucek S (1998) The effects of brucine and alcuronium on the inhibition of [3H]acetylcholine release from rat striatum by muscarinic receptor agonists. *Brit J Pharmacol* 124(6):1213–8.

Donald J, Chambers W (1872) *Chambers's etymological dictionary of the English language* Chambers.

Drapeau P, Nachshen DA (1984) Manganese fluxes and manganese-dependent neurotransmitter release in presynaptic nerve endings isolated from rat brain. *J Physiol* 348:493–510.

Drummond PD (1997) The effect of adrenergic blockade on blushing and facial flushing. *Psychophysiology* 34(2):163–168.

Drummond PD (2003) Psychophysiology of the blush In Crozier RW, De Jong PJ, editors, *The Psychological Significance of the Blush*, chapter 2, pp. 15–38. Cambridge Universiyt Press, Cambridge.

Dubreucq S, Matias I, Cardinal P, Häring M, Lutz B, Marsicano G, Chaouloff F (2012) Genetic dissection of the role of cannabinoid type-1 receptors in the emotional consequences of repeated social stress in mice. *Neuropsychopharmacol* 37(8):1885–1900.

Duchene de Boulogne GB (1862) *Mécanismes de la Physionomie Humaine, ou Analyse Electrophysiologique de l'expression des Passions* (Baillière, Paris.

Ducottet C, Belzung C (2005) Correlations between behaviours in the elevated plus-maze and sensitivity to unpredictable subchronic mild stress: evidence from inbred strains of mice. *Behav Brain Res* 156(1):153–162.

Dudek M, Canals S, Sommer WH, Hyytiä P (2016) Modulation of nucleus accumbens connectivity by alcohol drinking and naltrexone in alcohol-preferring rats: A manganese-enhanced magnetic resonance imaging study. *Eur Neuropsychopharmacol* 26(3):445–55.

D'Udine B, Robinson DJ, Oliverio A (1982) An analysis of single-gene effects on audible and ultrasonic vocalizations in the mouse. *Behav Neural Biol* 36(2):197–203.

Dujardin E, Jürgens U (2005) Afferents of vocalization-controlling periaqueductal regions in the squirrel monkey. *Brain Res* 1034(1-2):114–31.

Edwards SB, Ginsburgh CL, Henkel CK, Stein BE (1979) Sources of subcortical projections to the superior colliculus in the cat. *J Comnp Neurol* 184(2):309–329.

Ehrlich P (1885) *Das Sauerstoff-Bedürfniss des Organismus, eine farbenanalytische Studie* A. Hirschwald.

Elfvin L, Lindh B, Hökfelt T (1993) The Chemical Neuroanatomy of Sympathetic Ganglia. *Annu Rev Neurosci* 16(1):471–507.

Elphick M (2012) The evolution and comparative neurobiology of endocannabinoid signalling. *Philos T Roy Soc B* 367(1607):3201–15.

Endres T, Fendt M (2008) Inactivation of the lateral septum blocks fox odor-induced fear behavior. *Neuroreport* 19(6):667–70.

Endres T, Fendt M (2009) Aversion- vs fear-inducing properties of 2,4,5-trimethyl-3-thiazoline, a component of fox odor, in comparison with those of butyric acid. *J Exp Biol* 212(15).

Ennis M, Xu S, Rizvi TA (1997) Discrete subregions of the rat midbrain periaqueductal gray project to nucleus ambiguus and the periambigual region. *Neuroscience* 80(3):829–845.

Eppig JT, Motenko H, Richardson JE, Richards-Smith B, Smith CL (2015) The International Mouse Strain Resource (IMSR): cataloging worldwide mouse and ES cell line resources. *Mammalian genome : official journal of the International Mammalian Genome Society* 26(9-10):448–55.

Erhardt A, Czibere L, Roeske D, Lucae S, Unschuld PG, Ripke S, ..., Binder EB (2011) TMEM132D, a new candidate for anxiety phenotypes: evidence from human and mouse studies. *Mol Psychiatr* 16(6):647–663.

Eschenko O, Canals S, Simanova I, Beyerlein M, Murayama Y, Logothetis N (2010) Mapping of functional brain activity in freely behaving rats during voluntary running using manganese-enhanced MRI: Implication for longitudinal studies. *NeuroImage* 49(3):2544–2555.

Espinosa-Medina I, Saha O, Boismoreau F, Chettouh Z, Rossi F, Richardson WD, Brunet JF (2016) The sacral autonomic outflow is sympathetic. *Science* 354(6314):893–897.

Etkin A (2010) Functional neuroanatomy of anxiety: a neural circuit perspective. *Curr Top Behav Neurosci* 2:251–77.

Everitt BJ, Cardinal RN, Parkinson JA, Robbins TW (2003) Appetitive behavior: impact of amygdala-dependent mechanisms of emotional learning. *Ann N Y Acad Sci* 985:233–50.

Everitt BJ, Parkinson JA, Olmstead MC, Arroyo M, Robledo P, Robbins TW (1999) Associative processes in addiction and reward. The role of amygdala-ventral striatal subsystems. *Annals of the New York Academy of Sciences* 877:412–38.

Fa Z, Zhang P, Wu W, Wang Z, Huang F, Yang L, Chang H, Xu R, Wen Z, Zhang J, Zeng Y, Jiang X (2011) Functional mapping of rat brain activation following rTMS using activity-induced manganese-dependent contrast. *Neurol Res* 33(6):563–71.

Fadok JP, Krabbe S, Markovic M, Courtin J, Xu C, Massi L, Botta P, Bylund K, Müller C, Kovacevic A, Tovote P, Lüthi A (2017) A competitive inhibitory circuit for selection of active and passive fear responses. *Nature* 542(7639):96–100.

Falk TH, Guirgis M, Power S, Blain S, Chau T (2010) On the use of peripheral autonomic signals for binary control of bodyâĂŞmachine interfaces. *Physiol Meas* 31(11):1411–1422.

Falkai P, Wittchen HU (2015) *Diagnostisches und Statistisches Manual Psychiatrischer Störungen DSM-5* Hogrefe, Göttingen.

Falls WA, Carlson S, Turner JG, Willott JF (1997) Fear-potentiated startle in two strains of inbred mice. *Behav Neurosci* 111(4):855–61.

Fanselow MS, Poulos AM (2005) THE NEUROSCIENCE OF MAMMALIAN ASSOCIATIVE LEARNING. *Annu Rev Psychol* 56:207–34.

Fanselow M, Lester L (1988) A functional behavioristic approach to aversively motivated behavior: Predatory imminence as a determinant of the topography of defensive behavior. In Bolles R, Beecher M, editors, *Evolution and Learning*, pp. 185–212. Lawrence Erlbaum Associates, Inc, Hillsdale, NJ, US.

Farber DB, Flannery JG, Bowes-Rickman C (1994) The rd mouse story: Seventy years of research on an animal model of inherited retinal degeneration. *Prog Ret Eye Res* 13(1):31–64.

Favaro PD, Gouvêa TS, Oliveira SR, Vautrelle N, Redgrave P, Comoli E (2011) The influence of vibrissal somatosensory processing in rat superior colliculus on prey capture. *Neurosci* 176:318–27.

Federal Communications Commission (1997) Evaluating Compliance with FCC Guidelines for Human Exposure to Radiofrequency Electromagnetic Fields. *OET Bull* 65.

Federal Communications Commission (2011) OPERATION WITHIN THE BANDS 902-928 MHZ, 2435-2465 MHZ, 5785-5815 MHZ, 10500-10550 MHZ, AND 24075-24175 MHZ. *47 CFR* 15.245.

Fee M, Leonardo A (2001) Miniature motorized microdrive and commutator system for chronic neural recording in small animals. *J Neurosci Meth* 112:83–94.

Feinberg EH, Meister M (2014) Orientation columns in the mouse superior colliculus. *Nature* 519(7542):229–232.

Feinstein JS, Adolphs R, Damasio A, Tranel D (2011) The Human Amygdala and the Induction and Experience of Fear. *Curr Biol* 21(1):34–38.

Felix-Ortiz AC, Burgos-Robles A, Bhagat ND, Leppla CA, Tye KM (2016) Bidirectional modulation of anxiety-related and social behaviors by amygdala projections to the medial prefrontal cortex. *Neuroscience* 321:197–209.

Fendt M, Koch M, Schnitzler HU (1994) Sensorimotor gating deficit after lesions of the superior colliculus. *Neuroreport* 5(14):1725–8.

Fendt M, Endres T, Lowry CA, Apfelbach R, McGregor IS (2005) TMT-induced autonomic and behavioral changes and the neural basis of its processing. *Neurosci Biobehav Rev* 29(8):1145–1156.

Fenno L, Yizhar O, Deisseroth K (2011) The Development and Application of Optogenetics. *Ann Rev Neruosci* 34(1):389–412.

Fernandez de Molina A, Hunsperger RW (1959) Central representation of affective reactions in forebrain and brain stem: electrical stimulation of amygdala, stria terminalis, and adjacent structures. *J Physiol* 145(2):251–65.

Fernández-Teruel A, Escorihuela R, Núñez J, Zapata A, Boix F, Salazar W, Tobeña A (1991) The early acquisition of two-way (shuttle-box) avoidance as an anxiety-mediated behavior: Psychopharmacological validation. *Brain Res Bull* 26(1):173–176.

File SE, Mabbutt PS, Hitchcott PK (1990) Characterisation of the phenomenon of "one-trial tolerance" to the anxiolytic effect of chlordiazepoxide in the elevated plus-maze. *Psychopharmacology* 102(1):98–101.

Ford CP, Mark GP, Williams JT (2006) Properties and opioid inhibition of mesolimbic dopamine neurons vary according to target location. *J Neurosci* 26(10):2788–97.

Fork RL (1971) Laser stimulation of nerve cells in Aplysia. *Science* 171(3974):907–8.

Foster RG, Provencio I, Hudson D, Fiske S, De Grip W, Menaker M (1991) Circadian photoreception in the retinally degenerate mouse (rd/rd). *J Comp Physiol A* 169(1):39–50.

Foster RG (1998) Shedding Light on the Biological Clock. *Neuron* 20(5):829–832.

Fowler CJ, Griffiths D, de Groat WC (2008) The neural control of micturition. *Nat Rev Neurosci* 9(6):453–66.

Frame MD, Milanick MA (1991) Mn and Cd transport by the Na-Ca exchanger of ferret red blood cells. *Am J Physiol* 261(3).

Franklin TB, Silva BA, Perova Z, Marrone L, Masferrer ME, Zhan Y, Kaplan A, Greetham L, Verrechia V, Halman A, Pagella S, Vyssotski AL, Illarionova A, Grinevich V, Branco T, Gross CT (2017) Prefrontal cortical control of a brainstem social behavior circuit. *Nat Neurosci* 20(2):260–270.

Fries W (1985) Inputs from motor and premotor cortex to the superior colliculus of the macaque monkey. *Behav Brain Res* 18(2):95–105.

Fritsch G, Hitzig E (1870) Über die elektrische Erregbarkeit des Grosshirns. *Arch. Anat. Physiol. Wissen. Med.* 37:300–332.

Fritsch G, Hitzig E (2009) Electric excitability of the cerebrum (Über die elektrische Erregbarkeit des Grosshirns). *Epilepsy Behav* 15(2):123–130.

Fritschy JM, Mohler H (1995) GABAA-receptor heterogeneity in the adult rat brain: Differential regional and cellular distribution of seven major subunits. *J Comp Neurol* 359(1):154–194.

Füchsl AM, Neumann ID, Reber SO (2014) Stress Resilience: A Low-Anxiety Genotype Protects Male Mice From the Consequences of Chronic Psychosocial Stress. *Endocrinology* 155(1):117–126.

Fullana MA, Harrison BJ, Soriano-Mas C, Vervliet B, Cardoner N, Àvila-Parcet A, Radua J (2016) Neural signatures of human fear conditioning: an updated and extended meta-analysis of fMRI studies. *Mol Psychiatry* 21(4):500–508.

Furigo I, de Oliveira W, de Oliveira A, Comoli E, Baldo M, Mota-Ortiz S, Canteras N (2010) The role of the superior colliculus in predatory hunting. *Neuroscience* 165(1):1–15.

Furshpan EJ, Landis SC, Matsumoto SG, Potter DD (1986) Synaptic functions in rat sympathetic neurons in microcultures. I. Secretion of norepinephrine and acetylcholine. *J Neurosci* 6(4):1061–79.

Fyhn M, Molden S, Witter MP, Moser EI, Moser MB (2004) Spatial representation in the entorhinal cortex. *Science (New York, N.Y.)* 305(5688):1258–64.

Gaburro S, Stiedl O, Giusti P, Sartori SB, Landgraf R, Singewald N (2011) A mouse model of high trait anxiety shows reduced heart rate variability that can be reversed by anxiolytic drug treatment. *Int J Neuropsychopharmacol* 14(10):1341–1355.

Gach MP, Cherednichenko G, Haarmann C, Lopez JR, Beam KG, Pessah IN, Franzini-Armstrong C, Allen PD (1986) a 2 d 1 Dihydropyridine Receptor Subunit Is a Critical Element for Excitation-Coupled Calcium Entry but Not for Formation of Tetrads in Skeletal Myotubes. *Biophys J* 116(1):135–141.

Ganea K, Liebl C, Sterlemann V, Müller MB, Schmidt MV (2007) Pharmacological validation of a novel home cage activity counter in mice. *J Neurosci Meth* 162(1-2):180–6.

Garcia AM, Cardenas FP, Morato S (2005) Effect of different illumination levels on rat behavior in the elevated plus-maze. *Physiol Behav* 85(3):265–70.

Geller I, Kulak JT, Seifter J (1962) The effects of chlordiazepoxide and chlorpromazine on a punishment discrimination. *Psychopharmacologia* 3(5):374–385.

Gibbins IL (1991) Vasomotor, pilomotor and secretomotor neurons distinguished by size and neuropeptide content in superior cervical ganglia of mice. *J Autonom Nerv Syst* 34(2-3):171–183.

Gildish I, Manor D, David O, Sharma V, Williams D, Agarwala U, Wang X, Kenney JW, Proud CG, Rosenblum K (2012) Impaired associative taste learning and abnormal brain activation in kinase-defective eEF2K mice. *Learn Mem* 19(3):116–125.

Goebbels S, Bormuth I, Bode U, Hermanson O, Schwab MH, Nave KA (2006) Genetic targeting of principal neurons in neocortex and hippocampus of NEX-Cre mice. *Genesis* 44(12):611–621.

Gomez JL, Bonaventura J, Lesniak W, Mathews WB, Sysa-Shah P, Rodriguez LA, Ellis RJ, Richie CT, Harvey BK, Dannals RF, Pomper MG, Nonci A, Michaelides M (2017) Chemogenetics revealed: DREADD occupancy and activation via converted clozapine. *Science* 357(6350):503–7.

Gonzalez-Lima F, Cada A (1994) Cytochrome oxidase activity in the auditory system of the mouse: a qualitative and quantitative histochemical study. *Neuroscience* 63(2):559–78.

Goodwin D (2007) Horse Behaviour: Evolution. Domestication and Feralisation In Waran N, editor, *The Welfare of Horses*, chapter 1, pp. 1–18. Springer Netherlands.

Goossens L, Schruers K, Peeters R, Griez E, Sunaert S (2007a) Visual presentation of phobic stimuli: amygdala activation via an extrageniculostriate pathway? *Psychiatry Res* 155(2):113–20.

Goossens L, Sunaert S, Peeters R, Griez EJL, Schruers KRJ (2007b) Amygdala hyperfunction in phobic fear normalizes after exposure. *Biol Psychiatry* 62(10):1119–25.

Gossen M, Bujard H (1992) Tight control of gene expression in mammalian cells by tetracycline-responsive promoters. *PNAS* 89(12):5547–51.

Gozzi A, Jain A, Giovanelli A, Bertollini C, Crestan V, Schwarz AJ, Tsetsenis T, Ragozzino D, Gross CT, Bifone A, Bifone A (2010) A Neural Switch for Active and Passive Fear. *Neuron* 67(4):656–666.

Gradinaru V, Zhang F, Ramakrishnan C, Mattis J, Prakash R, Diester I, Goshen I, Thompson KR, Deisseroth K (2010) Molecular and Cellular Approaches for Diversifying and Extending Optogenetics. *Cell* 141(1):154–165.

Graeff FG, Silveira MC, Nogueira RL, Audi EA, Oliveira RM (1993) Role of the amygdala and periaqueductal gray in anxiety and panic. *Behav Brain Res* 58(1-2):123–31.

Graeff FG, Ferreira Netto C, Zangrossi Jr H (1998) The elevated T-maze as an experimental model of anxiety. *Neurosci Biobehav Rev* 23(2):237–246.

Graham J (1977) An autoradiographic study of the efferent connections of the superior colliculus in the cat. *J Comp Neuol* 173(4):629–654.

Grant E, Mackintosh J (1963) A Comparison of the Social Postures of Some Common Laboratory Rodents. *Behaviour* 21(3):246–259.

Gratiolet LP (1854) *Mémoire sur les plis Cérébraux de l'homme et des Primates* A. Bertrand, Paris.

Gray CM, Maldonado PE, Wilson M, McNaughton B (1995) Tetrodes markedly improve the reliability and yield of multiple single-unit isolation from multi-unit recordings in cat striate cortex. *J Neurosci Meth* 63(1):43–54.

Graybiel AM (1975) Anatomical organization of retinotectal afferents in the cat: An autodiographic study. *Brain Res* 96(1):1–23.

Green DG, Kapousta-Bruneau NV, Hitchcock PF, Keller SA (1997) Electrophysiology and density of retinal neurons in mice with a mutation that includes the Pax2 locus. *Invest Ophthalmol Vis Sci* 38(5):919–29.

Grewal SS, Shepherd JK, Bill DJ, Fletcher A, Dourish CT (1997) Behavioural and pharmacological characterisation of the canopy stretched attend posture test as a model of anxiety in mice and rats. *Psychopharmacology* 133(1):29–38.

Griebel G, Belzung C, Perrault G, Sanger DJ (2000) Differences in anxiety-related behaviours and in sensitivity to diazepam in inbred and outbred strains of mice. *Psychopharmacology* 148(2):164–170.

Griebel G, Blanchard D, Jung A, Lee J, Masuda C, Blanchard R (1995) Further evidence that the mouse defense test battery is useful for screening anxiolytic and panicolytic drugs: Effects of acute and chronic treatment with alprazolam. *Neuropharmacology* 34(12):1625–1633.

Griebel G, Perrault G, Sanger DJ (1998) Characterization of the behavioral profile of the non-peptide CRF receptor antagonist CP-154,526 in anxiety models in rodents. Comparison with diazepam and buspirone. *Psychopharmacology* 138(1):55–66.

Griebel G, Beeské S (2011) The Mouse Defense Test Battery: A Model Measuring Different Facets of Anxiety-Related Behaviors In *Neuromethods Vol. 63: Mood and Anxiety Related Phenotypes in Mice*, pp. 97–106. Springer.

Griebel G, Sanger DJ, Perrault G (1997) Genetic differences in the mouse defense test battery. *Aggress Behav* 23(1):19–31.

Griesauer I, Diao W, Ronovsky M, Elbau I, Sartori S, Singewald N, Pollak DD (2014) Circadian abnormalities in a mouse model of high trait anxiety and depression. *Ann Med* 46(3):148–54.

Griffiths DJ, Fowler CJ (2013) The micturition switch and its forebrain influences. *Act Physiol* 207(1):93–109.

Grillner S, Robertson B (2016) The Basal Ganglia Over 500 Million Years. *Curr Biol* 26(20):R1088–1100.

Gröschel M, Götze R, Müller S, Ernst A, Basta D (2016) Central Nervous Activity upon Systemic Salicylate Application in Animals with Kanamycin-Induced Hearing Loss - A Manganese-Enhanced MRI (MEMRI) Study. *PLOS ONE* 11(4):e0153386.

Gröschel M, Müller S, Götze R, Ernst A, Basta D (2011) The possible impact of noise-induced Ca2+-dependent activity in the central auditory pathway: a manganese-enhanced MRI study. *NeuroImage* 57(1):190–7.

Gross CT, Canteras NS (2012) The many paths to fear. *Nat Rev Neurosci* 13(9):651–658.

Gruene TM, Flick K, Stefano A, Shea SD, Shansky RM, Lafenetre P, Marsicano G, Cain C, Gross C, Bifone A (2015) Sexually divergent expression of active and passive conditioned fear responses in rats. *eLife* 4:60–65.

Grünecker B, Kaltwasser SF, Peterse Y, Sämann PG, Schmidt MV, Wotjak CT, Czisch M (2010) Fractionated manganese injections: effects on MRI contrast enhancement and physiological measures in C57BL/6 mice. *NMR Biomed* 23(8):913–921.

Gu L, Uhelski ML, Anand S, Romero-Ortega M, Kim Yt, Fuchs PN, Mohanty SK (2015) Pain Inhibition by Optogenetic Activation of Specific Anterior Cingulate Cortical Neurons. *PLOS ONE* 10(2):e0117746.

Guimarães FS, Carobrez AP, De Aguiar JC, Graeff FG (1991) Anxiolytic effect in the elevated plus-maze of the NMDA receptor antagonist AP7 microinjected into the dorsal periaqueductal grey. *Psychopharmacology* 103(1):91–4.

Guina J, Rosetter SR, DeRhodes BJ, Nahhas RW, Welton RS (2015) Benzodiazepines for PTSD: A Systematic Review and Meta-Analysis. *J Psychiatr Pract* 21(4):281–303.

Güler AD, Ecker JL, Lall GS, Haq S, Altimus CM, Liao HW, Barnard AR, Cahill H, Badea TC, Zhao H, Hankins MW, Berson DM, Lucas RJ, Yau KW, Hattar S (2008) Melanopsin cells are the principal conduits for

rodâĂŞcone input to non-image-forming vision. *Nature* 453(7191):102–105.

Gunaydin LA, Yizhar O, Berndt A, Sohal VS, Deisseroth K, Hegemann P (2010) Ultrafast optogenetic control. *Nat Neurosci* 13(3):387–392.

Gunshin H, Mackenzie B, Berger UV, Gunshin Y, Romero MF, Boron WF, Nussberger S, Gollan JL, Hediger MA (1997) Cloning and characterization of a mammalian proton-coupled metal-ion transporter. *Nature* 388(6641):482–488.

Günther T, Vormann J, Cragoe EJ (1990) Species-specific Mn2+/Mg2+ antiport from Mg2(+)-loaded erythrocytes. *FEBS Lett* 261(1):47–51.

Haaker J, Gaburro S, Sah A, Gartmann N, Lonsdorf TB, Meier K, Singewald N, Pape HC, Morellini F, Kalisch R (2013) Single dose of L-dopa makes extinction memories context-independent and prevents the return of fear. *PNAS* 110(26):E2428–36.

Hacquemand R, Choffat N, Jacquot L, Brand G (2013) Comparison between low doses of TMT and cat odor exposure in anxiety- and fear-related behaviors in mice. *Behav Brain Res* 238:227–231.

Hall CS (1934) Emotional behavior in the rat. I. Defecation and urination as measures of individual differences in emotionality. *J Comp Psychol* 18(3):385–403.

Hall CS (1947) Genetic differences in fatal audiogenic seizures between two inbred strains of house mice. *J Hered* 38(1):2–6.

Hambsch B, Chen BG, Brenndörfer J, Meyer M, Avrabos C, Maccarrone G, Liu RH, Eder M, Turck CW, Landgraf R (2010) Methylglyoxal-mediated anxiolysis involves increased protein modification and elevated expression of glyoxalase 1 in the brain. *J Neurochem* 113(5):1240–51.

Han X, Chow BY, Zhou H, Klapoetke NC, Chuong A, Rajimehr R, Yang A, Baratta MV, Winkle J, Desimone R, Boyden ES (2011) A high-light sensitivity optical neural silencer: development and application to optogenetic control of non-human primate cortex. *Front Sys Neurosci* 5(18):18.

Hatori M, Le H, Vollmers C, Keding SR, Tanaka N, Schmedt C, Jegla T, Panda S, Jegla T, Panda S (2008) Inducible Ablation of Melanopsin-Expressing Retinal Ganglion Cells Reveals Their Central Role in Non-Image Forming Visual Responses. *PLoS ONE* 3(6):e2451.

Haubensak W, Kunwar PS, Cai H, Ciocchi S, Wall NR, Ponnusamy R, ..., Anderson DJ (2010) Genetic dissection of an amygdala microcircuit that gates conditioned fear. *Nature* 468(7321):270–276.

Hayashi T (1954) EFFECTS OF SODIUM GLUTAMATE ON THE NERVOUS SYSTEM. *Keio J Med* 3(4):183–192.

Heinz De, Genewsky A, Wotjak CT (2017) Enhanced anandamide signaling reduces flight behavior elicited by an approaching robo-beetle. *Neuropharmacology* S0028-3908(17):30427–6.

Helbing D, Mukerji P (2012) Crowd disasters as systemic failures: analysis of the Love Parade disaster. *EPJ Data Science* 1(1):7.

Heldt S, Ressler K (2007) Forebrain and midbrain distribution of major benzodiazepine-sensitive GABAA receptor subunits in the adult C57 mouse as assessed with in situ hybridization. *Neuroscience* 150(2):370–385.

Henes K, Wotjak C (2009) Traces of a trauma âĂŞ Long-lasting changes in brain activity in an animal model of PTSD. *Pharmacopsychiatry* 42(05):A58.

Herbert H, Saper CB (1992) Organization of medullary adrenergic and noradrenergic projections to the periaqueductal gray matter in the rat. *J Comp Neuol* 315(1):34–52.

Herrmann TF, Carran AB (1972) Heart Rate Conditioning in Mice. *Behav Genet* 2(4).

Hess WR (1954) *DAS ZWISCHENHIRN Syndrome, Lokalisationen, Funktionen.* Schwabe, Basel.

Hess WR, Brügger M (1943) Das subkortikale Zentrum der affektiven Abwehrreaktion. *Helvetica Physiologica et Pharmacologica Acta* .

Hettema JM, Neale MC, Kendler KS (2001) A Review and Meta-Analysis of the Genetic Epidemiology of Anxiety Disorders. *Am J Physiol* 158(10):1568–1578.

Hill M, Patel S, Campolongo P, Tasker J, Wotjak C, Bains J (2010) Functional interactions between stress and the endocannabinoid system: From synaptic signaling to behavioral output. *JNeurosci* 30(45):14980–6.

Hirling H, Scheller RH (1996) Phosphorylation of synaptic vesicle proteins: modulation of the alpha SNAP interaction with the core complex. *PNAS* 93(21):11945–9.

Hofer PA (1973) Urbach-Wiethe disease (lipoglycoproteinosis; lipoid proteinosis; hyalinosis cutis et mucosae). A review. *Acta Derm Venereol Suppl (Stockh)* 53:1–52.

Hohmann AG, L SR, Bolton NM, Neely MH, Fegley D, Mangieri R, Krey JF, Walker MJ, Holmes PV, Crystal JD, Duranti A, Tontini A, Mor M, Tarzia G, Piomelli D (2005) An endocannabinoid mechanism for stress-induced analgesia. *Nature* 435(7045):1108–12.

Holahan MR, White NM (2004) Intra-amygdala muscimol injections impair freezing and place avoidance in aversive contextual conditioning. *Learn Mem* 11(4):436–46.

Holmes A, Rodgers R (1999) Influence of spatial and temporal manipulations on the anxiolytic efficacy of chlordiazepoxide in mice previously exposed to the elevated plus-maze. *Neurosci Biobehav Rev* 23(7):971–980.

Holmes FL (1986) Claude Bernard, the milieu intérieur, and regulatory physiology. *Hist Philos Life Sci* 8(1):3–25.

Holstege G, Collewijn H (1982) The efferent connections of the nucleus of the optic tract and the superior colliculus in the rabbit. *J Comp Neurol* 209(2):139–175.

Hoover WB, Vertes RP (2007) Anatomical analysis of afferent projections to the medial prefrontal cortex in the rat. *Brain Struct Funct* 212(2):149–179.

Hormigo S, Vega-Flores G, Castro-Alamancos MA (2016) Basal Ganglia Output Controls Active Avoidance Behavior. *J Neurosci* 36(40):10274–84.

Horn J, Swanson L (2013) The Autonomic Motor System and the Hypothalamus In Kandel ER, Schwartz JH, Jessell MT, Siegelbaum SA, Hudspeth AJ, editors, *Principles of Neural Science*, chapter 47, pp. 1056–1078. McGraw-Hill, New York, fifth edit edition.

Hoskins RG, Gunning REL, Berry EL (1916) THE EFFECTS OF ADRENIN ON THE DISTRIBUTION OF THE BLOOD. *Am J Physiol* 41(4):513–528.

Hunsperger R (1956) Affektreaktionen auf elektrische Reizung im Hirnstamm der Katze. *Helv. physiol. pharmacol. Acta* 14:70–92.

Iijima M, Fukumoto K, Chaki S (2012) Acute and sustained effects of a metabotropic glutamate 5 receptor antagonist in the novelty-suppressed feeding test. *Behav Brain Res* 235:287–292.

Imai H, Kefalov V, Sakurai K, Chisaka O, Ueda Y, Onishi A, Morizumi T, Fu Y, Ichikawa K, Nakatani K, Honda Y, Chen J, Yau KW, Shichida Y (2007) Molecular properties of rhodopsin and rod function. *J Biol Chem* 282(9):6677–84.

Imperato A, Di Chiara G (1981) Behavioural effects of GABA-agonists and antagonists infused in the mesencephalic reticular formation - deep layers of superior colliculus. *Brain Res* 224(1):185–94.

Institute of Electrical and Electronic Engineers (1991) Standard for Safety Levels with Respect to Human Exposure to Radio Frequency Electromagnetic Fields, 3 kHz to 300 GHz. *Std* C95.1-1991.

Ishizuka T, Kakuda M, Araki R, Yawo H (2006) Kinetic evaluation of photosensitivity in genetically engineered neurons expressing green algae light-gated channels. *Neurosci Res* 54(2):85–94.

Ivanova E, Toychiev AH, Yee CW, Sagdullaev BT (2013) Optimized protocol for retinal wholemount preparation for imaging and immunohistochemistry. *JoVE* 82.

Iwata J, LeDoux JE (1988) Dissociation of associative and nonassociative concomitants of classical fear conditioning in the freely behaving rat. *Behav Neurosci* 102(1):66–76.

Jacobs GH, Fenwick JA, Williams GA (2001) Cone-based vision of rats for ultraviolet and visible lights. *J Exp Biol* 204(Pt 14):2439–46.

Jakubcakova V, Flachskamm C, Landgraf R, Kimura M, Quitkin F (2012) Sleep Phenotyping in a Mouse Model of Extreme Trait Anxiety. *PLoS ONE* 7(7):e40625.

James NA, Matteson DS (2015) ecp: An R Package for Nonparametric Multiple Change Point Analysis of Multivariate Data. *J Stat Soft* 62(7).

Janak P, Tye K (2015) From circuits to behaviour in the amygdala. *Nature* 517(7534):284–92.

Jänig W (2006) *The Integrative Action of the Autonomic Nervous System.* Cambridge University Press, Cambridge, UK.

Jänig W (2010) Vegetatives Nervensystem In Schmidt RF, Lang F, Heckmann M, editors, *Physiologie des Menschen*, chapter 20, pp. 403–434. Springer Medizin Verlag, Heidelberg, 31. auflag edition.

Janik VM, Sayigh LS, Wells RS (2006) Signature whistle shape conveys identity information to bottlenose dolphins. *PNAS* 103(21):8293–8297.

Jann MW, Lam YW, Chang WH (1994) Rapid formation of clozapine in guinea-pigs and man following clozapine-N-oxide administration. *Arch Int Pharmacodyn Ther* 328(2):243–50.

Jiang ZD, Moore DR, King AJ (1997) Sources of subcortical projections to the superior colliculus in the ferret. *Brain Res* 755(2):279–92.

Johansen JP, Fields HL, Manning BH (2001) The affective component of pain in rodents: direct evidence for a contribution of the anterior cingulate cortex. *PNAS* 98(14):8077–82.

Johnson AM, Ciucci MR, Russell JA, Hammer MJ, Connor NP (2010) Ultrasonic output from the excised rat larynx. *J Acoust Soc Am* 128(2):EL75.

Johnson PL, Shekhar A (2012) An animal model of panic vulnerability with chronic disinhibition of the dorsomedial/perifornical hypothalamus. *Physiol Behav* 107(5):686–698.

Jud C, Schmutz I, Hampp G, Oster H, Albrecht U (2005) A guideline for analyzing circadian wheel-running behavior in rodents under different lighting conditions. *Biol Proced Online* 7(1):101–16.

Jürgens U (2002) Neural pathways underlying vocal control. *Neurosci Biobehav Rev* 26(2):235–58.

Jürgens U (2009) The Neural Control of Vocalization in Mammals: A Review. *J Voice* 23(1):1–10.

Jürgens U, Maurus M, Ploog D, Winter P (1967) Vocalization in the Squirrel Monkey (Saimiri sciureus) Elicited by Brain Stimulation. *Exp Brain Res* 4(2):114–117.

Jürgens U, Müller-Preuss P (1976) Convergent projections of different limbic vocalization areas in the squirrel monkey. *Exp Brain Res* 29(1):75–83.

Jürgens U, Pratt R (1979) Role of the periaqueductal grey in vocal expression of emotion. *Brain Res* 167(2):367–78.

Kaesermann HP (1986) Stretched attend posture, a non-social form of ambivalence, is sensitive to a conflict-reducing drug action. *Psychopharmacology* 89(1):31–7.

Kano M, Ohno-Shosaku T, Maejima T, Yoshida T (2003) Endocannabinoid-mediated modulation of excitatory and inhibitory synaptic transmission In Hensch T, Fagiolini M, editors, *Excitatory-Inhibitory Balance*, pp. 99–109. Springer US, Boston, MA.

Karli P (1956) The Norway Rat's Killing Response To the White Mouse : an Experimental Analysis 1). *Behaviour* 10(1):81–102.

Keay KA, Feil K, Gordon BD, Herbert H, Bandler R (1997) Spinal afferents to functionally distinct periaqueductal gray columns in the rat: an anterograde and retrograde tracing study. *J Comp Neurol* 385(2):207–29.

Keay KA, Bandler R (2001) Parallel circuits mediating distinct emotional coping reactions to different types of stress. *Neurosci Biobehav Rev* 25(7):669–678.

Keifer OP, Hurt RC, Ressler KJ, Marvar PJ (2015) The Physiology of Fear: Reconceptualizing the Role of the

Central Amygdala in Fear Learning. *Physiology* 30(5):389–401.

Keilin D, Hartree E (1938) Cytochrome Oxidase. *P Roy Soc Lond B Bio* 125(838):171–186.

Keith F, Paxinos G (2008) *The Mouse Brain in Stereotaxic Coordinates, Compact, 3rd Edition.* Academic Press.

Keßler MS, Murgatroyd C, Bunck M, Czibere L, Frank E, Jacob W, Horvath C, Muigg P, Holsboer F, Singewald N, Spengler D, Landgraf R (2007a) Diabetes insipidus and, partially, low anxiety-related behaviour are linked to a SNP-associated vasopressin deficit in LAB mice. *Eur J Neurosci* 26(10):2857–2864.

Kessler RC, Angermeyer M, Anthony JC, DE Graaf R, Demyttenaere K, Gasquet I, ..., Ustün TB (2007b) Lifetime prevalence and age-of-onset distributions of mental disorders in the World Health Organization's World Mental Health Survey Initiative. *World Psychiatry* 6(3):168–76.

Kikuchi-Utsumi K, Ishizaka M, Matsumura N, Nakaki T (2013) Alpha1A-adrenergic control of piloerection and palpebral fissure width in rats. *Autonomic Neuroscience* 179(1):148–150.

Kim EJ, Horovitz O, Pellman BA, Tan LM, Li Q, Richter-Levin G, Kim JJ (2013) Dorsal periaqueductal gray-amygdala pathway conveys both innate and learned fear responses in rats. *PNAS* 110(36):14795–800.

Kim JJ, Rison RA, Fanselow MS (1993) Effects of amygdala, hippocampus, and periaqueductal gray lesions on short- and long-term contextual fear. *Behav Neurosci* 107(6):1093–8.

Kim JJ, Jung MW (2006) Neural circuits and mechanisms involved in Pavlovian fear conditioning: A critical review. *Neurosci Biobehav Rev* 30(2):188–202.

Kim SM, Eisner C, Faulhaber-Walter R, Mizel D, Wall SM, Briggs JP, Schnermann J (2008) Salt sensitivity of blood pressure in NKCC1-deficient mice. *Am J Physiol-Renal* 295(4):F1230–8.

Kincheski GC, Carobrez AP (2010) The dorsal periaqueductal gray modulates the increased fear-like behavior exhibited by experienced rats in the elevated plus-maze. *Behav Brain Res* 206(1):120–6.

King AJ (2004) The superior colliculus. *Cuur Biol* 14(9):R335–8.

Kirzinger A, Jürgens U (1982) Cortical lesion effects and vocalization in the squirrel monkey. *Brain Res* 233(2):299–315.

Kirzinger A, Jürgens U (1991) Vocalization-correlated single-unit activity in the brain stem of the squirrel monkey. *Exp Brain Res* 84(3):545–60.

Kita H, Narita K, Van der Kloot W (1981) Tetanic stimulation increases the frequency of miniature end-plate potentials at the frog neuromuscular junction in Mn2+-, CO2+-, and Ni2+-saline solutions. *Brain Res* 205(1):111–21.

Klapoetke NC, Murata Y, Kim SS, Pulver SR, Birdsey-Benson A, Cho YK, Morimoto TK, Chuong AS, Carpenter EJ, Tian Z, Wang J, Xie Y, Yan Z, Zhang Y, Chow BY, Surek B, Melkonian M, Jayaraman V, Constantine-Paton M, Wong GKS, Boyden ES (2014) Independent optical excitation of distinct neural populations. *Nat Meth* 11(3):338–46.

Koch M, Schnitzler HU (1997) The acoustic startle response in ratsâĂŤcircuits mediating evocation, inhibition and potentiation. *Behav Brain Res* 89(1):35–49.

Koelle GB (1986) Otto Loewi 1873-1961. *Trends Pharmacol Sci* 7:290–291.

Kokkinidis L, Anisman H (1977) Involvement of norepinephrine in startle arousal after acute and chronic d-amphetamine administration. *Psychopharmacology (Berl).* 59(3):285–292.

Komada M, Takao K, Miyakawa T (2008) Elevated plus maze for mice. *JoVE* 22.

Koutsikou S, Crook JJ, Earl EV, Leith JL, Watson TC, Lumb BM, Apps R (2014) Neural substrates underlying fear-evoked freezing: the periaqueductal grey-cerebellar link. *J Physiol* 592(10):2197–2213.

Krashes MJ, Koda S, Ye C, Rogan SC, Adams AC, Cusher DS, Maratos-Flier E, Roth BL, Lowell BB (2011) Rapid, reversible activation of AgRP neurons drives feeding behavior in mice. *J Clin Invest* 121(4):1424–1428.

Krebs HA (1935) Metabolism of amino-acids: Deamination of amino-acids. *Biochem J* 29(7):1620–44.

Krömer SA, Keßler MS, Milfay D, Birg IN, Bunck M, Czibere L, Panhuysen M, Pütz B, Deussing JM, Holsboer F, Landgraf R, Turck CW (2005) Identification of Glyoxalase-I as a Protein Marker in a Mouse Model of Extremes in Trait Anxiety. *J Neurosci* 25(17):4375–4384.

Kubista H, Boehm S (2006) Molecular mechanisms underlying the modulation of exocytotic noradrenaline release via presynaptic receptors. *Pharmacol Ther* 112(1):213–242.

Kunwar PS, Zelikowsky M, Remedios R, Cai H, Yilmaz M, Meister M, Anderson DJ (2015) Ventromedial hypothalamic neurons control a defensive emotion state. *eLife* 4(6).

Kyuhou S, Gemba H (1998) Two vocalization-related subregions in the midbrain periaqueductal gray of the guinea pig. *Neuroreport* 9(7):1607–10.

Kyuhou S, Gemba H (1999) Injection of orphanin fq/nociceptin into the periaqueductal gray suppresses the forebrain-elicited vocalization in the guinea pig. *Neurosci Lett* 260(2):113–6.

Lad HV, Liu L, Paya-Cano JL, Parsons MJ, Kember R, Fernandes C, Schalkwyk LC (2010) Behavioural battery testing: Evaluation and behavioural outcomes in 8 inbred mouse strains. *Physiol Behav* 99(3):301–316.

Lafenêtre P, Chaouloff F, Marsicano G (2009) Bidirectional regulation of novelty-induced behavioral inhibition by the endocannabinoid system. *Neuropharmacology* 57(7-8):715–721.

Lang F (2010) Hormone In Schmidt RF, Lang F, Heckmann M, editors, *Physiologie des Menschen*, chapter 21, pp. 435–461. Springer Medizin Verlag, Heidelberg, 31. auflag edition.

Langford DJ, Bailey AL, Chanda ML, Clarke SE, Drummond TE, Echols S, ..., Mogil JS (2010) Coding of facial expressions of pain in the laboratory mouse. *Nat Meth* 7(6):447–9.

Langley JN (1903) THE AUTONOMIC NERVOUS SYSTEM. *Brain* 26(1):1–26.

Langley J (1921) The autonomic nervous system (Pt. I).

Lanuza E, Moncho-Bogani J, LeDoux J (2008) Unconditioned stimulus pathways to the amygdala: Effects of lesions of the posterior intralaminar thalamus on foot-shock-induced c-Fos expression in the subdivisions of the lateral amygdala. *Neuroscience* 155(3):959–968.

Lauterbur P, Mendonca-Dias M, Rudin A (1978) Augmentation of tissue water proton spin-lattice relaxation rates by in vivo addition of paramagnetic ions. *Front Biol Energ* 1:752–759.

Leaton RN (2003) Electrolytic, but not neurotoxic, lesions to the lateral tegmental tract increase acoustic startle amplitude and reduce startle stimulus-induced freezing. *Neurobiol Learn Mem* 79(1):89–98.

Leaton RN, Brucato FH (2001) Startle amplitude and fear in an acoustic startle paradigm: lesions to the brachium of the inferior colliculus or the lateral tegmental tract. *Behav Neurosci* 2(115):477–92.

Lebow MA, Chen A (2016) Overshadowed by the amygdala: the bed nucleus of the stria terminalis emerges as key to psychiatric disorders. *Mol Psychiatr* 21(4):450–463.

Leccese F, Cagnetti M, Trinca DA (2014) A smart city application: A fully controlled street lighting isle based on Raspberry-Pi card, a ZigBee sensor network and WiMAX. *Sensors (Switzerland)* 12(14):24408–24.

LeDoux JE, Iwata J, Cicchetti P, Reis DJ (1988) Different projections of the central amygdaloid nucleus mediate autonomic and behavioral correlates of conditioned fear. *J Neurosci* 8(7):2517–29.

LeDoux J (1987) Emotion In Plum F, editor, *Handbook of Physiology-The Nervous System V*, pp. 419–459. Amerian Physiological Society, Bethesda, MD.

LeDoux J (2012) Rethinking the Emotional Brain. *Neuron* 73:653–676.

LeDoux JE (2000) EMOTION CIRCUITS IN THE BRAIN. *Annu Rev Neurosci* 23:155–184.

LeDoux JE (2014) Coming to terms with fear. *PNAS* 111(8):2871–8.

LeDoux JE, Farb Ca DA (1990) Topographic organization of neurons in the acoustic thalamus that project to the amygdala. *J Neurosci* 10(4):1043–54.

Lee IT, Chang AS, Manandhar M, Shan Y, Fan J, Izumo M, Ikeda Y, Motoike T, Dixon S, Seinfeld JE, Takahashi JS, Yanagisawa M (2015) Neuromedin s-producing neurons act as essential pacemakers in the suprachiasmatic nucleus to couple clock neurons and dictate circadian rhythms. *Neuron* 85(5):1086–1102.

Lee S, Ahmed T, Lee S, Kim H, Choi S, Kim DS, Kim SJ, Cho J, Shin HS (2011) Bidirectional modulation of fear extinction by mediodorsal thalamic firing in mice. *Nat Neurosci* 15(2):308–314.

Lee WH, Utomo AR, Nikitin AY (1999) Temporal, spatial, and cell type-specific control of Cre-mediated DNA recombination in transgenic mice. *Nat Biotech* 17(11):1091–1096.

Lein ES, Hawrylycz MJ, Ao N, Ayres M, Bensinger A, Bernard A, ..., Jones AR (2007) Genome-wide atlas of gene expression in the adult mouse brain. *Nature* 445(7124):168–176.

Lenz HJ, Burlage M, Raedler A, Greten H (1988a) Central nervous system effects of corticotropin-releasing factor on gastrointestinal transit in the rat. *Gastroenterology* 94(3):598–602.

Lenz HJ, Raedler A, Greten H, Vale WW, Rivier JE (1988b) Stress-induced gastrointestinal secretory and motor responses in rats are mediated by endogenous corticotropin-releasing factor. *Gastroenterology* 95(6):1510–7.

Leone M, Franzini A, Broggi G, May A, Bussone G (2004) Long-term follow-up of bilateral hypothalamic stimulation for intractable cluster headache. *Brain* 127(Pt 10):2259–64.

Lester HA, Nerbonne JM (1982) Physiological and Pharmacological Manipulations with Light Flashes. *Ann Rev Biophys Bioeng* 11(1):151–175.

Levey A, Edmunds S, Koliatsos V, Wiley R, Heilman C (1995) Expression of m1-m4 muscarinic acetylcholine receptor proteins in rat hippocampus and regulation by cholinergic innervation. *J Neurosci* 15(5).

Levine PA (1997) *Waking the tiger : healing trauma : the innate capacity to transform overwhelming experiences* North Atlantic Books.

Li X, Gutierrez DV, Hanson MG, Han J, Mark MD, Chiel H, Hegemann P, Landmesser LT, Herlitze S (2005) Fast noninvasive activation and inhibition of neural and network activity by vertebrate rhodopsin and green algae channelrhodopsin. *PNAS* 102(49):17816–21.

Limousin P, Krack P, Pollak P, Benazzouz A, Ardouin C, Hoffmann D, Benabid AL (1998) Electrical Stimulation of the Subthalamic Nucleus in Advanced Parkinson's Disease. *NEJM* 339(16):1105–1111.

Lin JY, Lin MZ, Steinbach P, Tsien RY (2009) Characterization of engineered channelrhodopsin variants with improved properties and kinetics. *Biophys J* 96(5):1803–14.

Lipka J, Hoffmann M, Miltner WH, Straube T (2014) Effects of Cognitive-Behavioral Therapy on Brain Responses to Subliminal and Supraliminal Threat and Their Functional Significance in Specific Phobia. *Biol Psychiatry* 76(11):869–877.

Llinás RR, Steriade M (2006) Bursting of thalamic neurons and states of vigilance. *J Neurophysiol* 95(6):3297–308.

Llorente-Berzal A, Terzian A, Di Marzo V, Micale V, Viveros M, Wotjak C (2015) 2-AG promotes the expression of conditioned fear via cannabinoid receptor type 1 on gabaergic neurons. *Psychopharmacology* 232(15):2811–2825.

Loffler S, Korber J, Nubbemeyer U, Fehsel K (2012) Comment on "Impaired Respiratory and Body Temperature Control Upon Acute Serotonergic Neuron Inhibition". *Science* 337(6095):646–646.

López AJ, Kramár E, Matheos DP, White AO, Kwapis J, Vogel-Ciernia A, Sakata K, Espinoza M, Wood MA (2016) Promoter-Specific Effects of DREADD Modulation on Hippocampal Synaptic Plasticity and Memory Formation. *J Neurosci* 36(12).

Lorenz KZ (1958) The evolution of behavior. *Scientific American* 199:67–78.

Lovick TA (1993) The periaqueductal gray-rostral medulla connection in the defence reaction: efferent pathways and descending control mechanisms. *Behav Brain Res* 58(1-2):19–25.

Löw K, Crestani F, Keist R, Benke D, Brünig I, Benson JA, Fritschy JM, Rülicke T, Bluethmann H, Möhler

H, Rudolph U (2000) Molecular and Neuronal Substrate for the Selective Attenuation of Anxiety. *Science* 290(5489).

Loyd DR, Murphy AZ (2009) The Role of the Periaqueductal Gray in the Modulation of Pain in Males and Females: Are the Anatomy and Physiology Really that Different? *Neural Plast* 2009(462879).

Lu H, Xi ZX, Gitajn L, Rea W, Yang Y, Stein EA (2007) Cocaine-induced brain activation detected by dynamic manganese-enhanced magnetic resonance imaging (MEMRI). *PNAS* 104(7):2489–94.

Lucas R, Douglas R, Foster R (2001) Characterization of an ocular photopigment capable of driving pupillary constriction in mice. *Nat Neurosci* 4(6):621–6.

Lutz B (2009) Endocannabinoid signals in the control of emotion. *Curr Opin Pharmacol* 9(1):46–52.

Lutz B, Marsicano G, Maldonado R, Hillard CJ (2015) The endocannabinoid system in guarding against fear, anxiety and stress. *Nat Rev Neurosci* 16:705–18.

MacLean P (1985) Brain evolution relating to family. play. and the separation call. *Arch gen Psychiatry* 42(4):405–17.

Mahrt E, Agarwal A, Perkel D, Portfors C, Elemans CPH (2016) Mice produce ultrasonic vocalizations by intra-laryngeal planar impinging jets. *Curr Biol* 26(19):R880–R881.

Malkova NV, Gallagher JJ, Yu CZ, Jacobs RE, Patterson PH (2014) Manganese-enhanced magnetic resonance imaging reveals increased DOI-induced brain activity in a mouse model of schizophrenia. *PNAS* 111(24):E2492–500.

Mantyh PW (1983) Connections of midbrain periaqueductal gray in the monkey. II. Descending efferent projections. *J Neurophysiol* 49(3):582–594.

Marchand JE, Hagino N (1983) Afferents to the periaqueductal gray in the rat. a horseradish peroxidase study. *Neuroscience* 9(1):95–106.

Maren S (2001) NEUROBIOLOGY OF PAVLOVIAN FEAR CONDITIONING. *Annu Rev Neurosci* 24(1):897–931.

Marsden C, King B (1979) The use of doppler shift radar to monitor physiological and drug induced activity patterns in the rat. *Pharmacol Biochem Behav* 10(5):631–635.

Martin PH, Unwin DM (1980) A microwave doppler radar activity monitor. *Behav Res Meth Ins C* 12(5):517–520.

Martínez V, Wang L, Rivier J, Grigoriadis D, Taché Y (2004) Central CRF, urocortins and stress increase colonic transit via CRF 1 receptors while activation of CRF 2 receptors delays gastric transit in mice. *J Physiol* 556(1):221–234.

Martinez-Finley EJ, Gavin CE, Aschner M, Gunter TE (2013) Manganese neurotoxicity and the role of reactive oxygen species. *Free Radic Biol Med* 62:65–75.

Mast M, Blanchard RJ, Blanchard DC (1982) The relationship of freezing and response suppression in a CER situation. *Psychol Rec* 32(2):151–167.

Mayberg HS, Lozano AM, Voon V, McNeely HE, Seminowicz D, Hamani C, Schwalb JM, Kennedy SH (2005) Deep brain stimulation for treatment-resistant depression. *Neuron* 45(5):651–60.

Mayer DJ, Wolfle TL, Akil H, Carder B, C LJ (1971) Analgesia from Electrical Stimulation in the Brainstem of the Rat. *Science* 174(4016):444–445.

McCaughran JA, Bell J, Hitzemann RJ (2000) Fear-Potentiated Startle Response in Mice: Genetic Analysis of the C57BL/6J and DBA/2J Intercross. *Pharmacol Biochem Behav* 65(2):301–312.

McClung CA (2013) How might circadian rhythms control mood? Let me count the ways... *Biol Psychiatry* 74(4):242–9.

McDonald AJ (1987) Organization of amygdaloid projections to the mediodorsal thalamus and prefrontal cortex: a fluorescence retrograde transport study in the rat. *J Comp Neurol* 262(1):46–58.

McDonald A, Mascagni F, Guo L (1996) Projections of the medial and lateral prefrontal cortices to the amygdala: a Phaseolus vulgaris leucoagglutinin study in the rat. *Neurosci* 71(1):55–75.

McDonald AJ, Jackson TR (1987) Amygdaloid connections with posterior insular and temporal cortical areas in the rat. *J Comp Neurol* 262(1):59–77.

McGuire JL, Bergstrom HC, Parker CC, Le T, Morgan M, Tang H, Selwyn RG, Silva AC, Choi K, Ursano RJ, Palmer AA, Johnson LR (2013) Traits of fear resistance and susceptibility in an advanced intercross line. *Eur J Neurosci* 38(9):3314–3324.

McKinney M, Miller JH, Aagaard PJ (1993) Pharmacological characterization of the rat hippocampal muscarinic autoreceptor. *J Pharmacol Exp Ther* 264(1).

McNaughton BL, O'Keefe J, Barnes CA (1983) The stereotrode: A new technique for simultaneous isolation of several single units in the central nervous system from multiple unit records. *J Neurosci Meth* 8(4):391–397.

McNaughton N, Corr PJ (2004) A two-dimensional neuropsychology of defense: fear/anxiety and defensive distance. *Neurosci Biobehav Rev* 28(3):285–305.

Mechias ML, Etkin A, Kalisch R (2010) A meta-analysis of instructed fear studies: Implications for conscious appraisal of threat. *NeuroImage* 49(2):1760–1768.

Megens AA, Voeten J, Rombouts J, Meert TF, Niemegeers CJ (1987) Behavioral activity of rats measured by a new method based on the piezo-electric principle. *Psychopharmacol* 93(3):382–8.

Melendez-Ferro M, Rice MW, Roberts RC, Perez-Costas E (2013) An accurate method for the quantification of cytochrome C oxidase in tissue sections. *J Neurosci Meth* 214(2):156–62.

Meller ST, Dennis BJ (1986) Afferent projections to the periaqueductal gray in the rabbit. *Neuroscience* 19(3):927–64.

Meller S, Dennis B (1991) Efferent projections of the periaqueductal gray in the rabbit. *Neuro-*

science 40(1):191–216.

Meloni EG, Davis M (1999) Muscimol in the deep layers of the superior colliculus/mesencephalic reticular formation blocks expression but not acquisition of fear-potentiated startle in rats. *Behav Neurosci* 113(6):1152–60.

Mendonça-Dias MH, Gaggelli E, Lauterbur PC (1983) Paramagnetic contrast agents in nuclear magnetic resonance medical imaging. *Semin Nucl Med* 13(4):364–76.

Meredith MA, Stein BE (1986) Visual, auditory, and somatosensory convergence on cells in superior colliculus results in multisensory integration. *J Neurophysiol* 56(3).

Merikangas KR, Swanson SA (2010) Comorbidity in Anxiety Disorders In Stein MB, Steckler T, editors, *Behavioral Neurobiology of Anxiety and Its Treatment*, pp. 37–59. Springer-Verlag Berlin Heidelberg.

Metna-Laurent M, Soria-Gómez E, Verrier D, Conforzi M, Jégo PL P, Marsicano G (2012) Bimodal control of fear-coping strategies by cb1 cannabinoid receptors. *JNeurosci* 32(21):7109–18.

Metzger D, Chambon P (2001) Site- and Time-Specific Gene Targeting in the Mouse. *Methods* 24(1):71–80.

Meuret AE, Rosenfield DW FH, Zhou E, Conrad A, Ritz T, Roth WT (2011) Do Unexpected Panic Attacks Occur Spontaneously? *Biol Psychiatry* 70(10):985–991.

Miampamba M, Maillot C, Million M, Taché Y (2002) Peripheral CRF activates myenteric neurons in the proximal colon through CRF(1) receptor in conscious rats. *Am J Physiol* 282(5):G857–65.

Miao C, Cao Q, Ito HT, Yamahachi H, Witter MP, Moser MB, Moser EI (2015) Hippocampal Remapping after Partial Inactivation of the Medial Entorhinal Cortex. *Neuron* 88(3):590–603.

Micale V, Stepan J, Jurik A, Pamplona FA, Marsch R, Drago F, Eder M, Wotjak CT (2017) Extinction of avoidance behavior by safety learning depends on endocannabinoid signaling in the hippocampus. *J Psych Res* 90:46–59.

Milad MR, Vidal-Gonzalez I, Quirk GJ (2004) Electrical stimulation of medial prefrontal cortex reduces conditioned fear in a temporally specific manner. *Behav Neurosci* 118(2):389–94.

Miller NE (1965) CHEMICAL CODING OF BEHAVIOR IN THE BRAIN. *Science* 148(3668):328–38.

Millhouse OE (1986) The intercalated cells of the amygdala. *The Journal of Comparative Neurology* 247(2):246–271.

Minett M, Falk S, Santana-Varela S, Bogdanov Y, Nassar M, Heegaard AM, Wood J (2014) Pain without Nociceptors? Nav1.7-Independent Pain Mechanisms. *Cell Rep* 6(2):301–312.

Mobbs D, Petrovic P, Marchant JL, Hassabis D, Weiskopf N, Seymour B, Dolan RJ, Frith CD (2007) When fear is near: threat imminence elicits prefrontal-periaqueductal gray shifts in humans. *Science (New York, N.Y.)* 317(5841):1079–83.

Monory K, Massa F, Egertová M, Eder M, Blaudzun H, Westenbroek R, Kelsch W, Jacob W, Marsch R, Ekker M, Long J, Rubenstein J, Goebbels S, Nave K, During M, Klugmann M, Wölfel B, Dodt HZ W, Wotjak C, Mackie K, Elphick MR, Marsicano G, Lutz B (2006) The endocannabinoid system controls key epileptogenic circuits in the hippocampus. *Neuron* 51(4):455–466.

Moore RY, Speh JC, Patrick Card J (1995) The retinohypothalamic tract originates from a distinct subset of retinal ganglion cells. *J Comp Neurol* 352(3):351–366.

Morgan MM, Carrive P (2001) Activation of the ventrolateral periaqueductal gray reduces locomotion but not mean arterial pressure in awake, freely moving rats. *Neuroscience* 102(4):905–10.

Morin SA, Stotz-Potter EH, Dimicco JA (2001) Injection of muscimol in dorsomedial hypothalamus and stress-induced Fos expression in paraventricular nucleus,. *Am J Physiol Regul Integr Comp Physiol* 280(5):R1276–84.

Morrel-Samuels P, Krauss RM (1990) Cartesian analysis: A computer-video interface for measuring motion without physical contact. *Behav Res Meth Ins C* 22(5):466–470.

Morris-Rosendahl DJ (2002) Are there anxious genes? *Dialogues Clin Neurosci* 4(3):251–60.

Motta SC, Carobrez AP, Canteras NS (2017) The periaqueductal gray and primal emotional processing critical to influence complex defensive responses, fear learning and reward seeking. *Neurosci Biobehav Rev* 76(Pt A):39–47.

Motta V, Brandão ML (1993) Aversive and antiaversive effects of morphine in the dorsal periaqueductal gray of rats submitted to the elevated plus-maze test. *Pharmacol Biochem Behav.* 44(1):119–25.

Muigg P, Scheiber S, Salchner P, Bunck M, Landgraf R, Singewald N (2009) Differential Stress-Induced Neuronal Activation Patterns in Mouse Lines Selectively Bred for High, Normal or Low Anxiety. *PLoS ONE* 4(4):e5346.

Nabeshima T, Tohyama K, Ichihara K, Kameyama T (1990) Effects of benzodiazepines on passive avoidance response and latent learning in mice: relationship to benzodiazepine receptors and the cholinergic neuronal system. *J Pharmacol Exp Ther* 255(2).

Nagel G, Ollig D, Fuhrmann M, Kateriya S, Musti AM, Bamberg E, Hegemann P (2002) Channelrhodopsin-1: A Light-Gated Proton Channel in Green Algae. *Science* 296(5577):2395–2398.

Nagel G, Brauner M, Liewald JF, Adeishvili N, Bamberg E, Gottschalk A (2005) Light activation of channelrhodopsin-2 in excitable cells of Caenorhabditis elegans triggers rapid behavioral responses. *Curr Biol* 15(24):2279–84.

Nagel G, Szellas T, Huhn W, Kateriya S, Adeishvili N, Berthold P, Ollig D, Hegemann P, Bamberg E (2003) Channelrhodopsin-2, a directly light-gated cation-selective membrane channel. *PNAS* 100(24):13940–5.

Nakashima M, Uemura M, Yasui K, Ozaki HS, Tabata S, Taen A (2000) An anterograde and retrograde tract-tracing study on the projections from the thalamic gustatory area in the rat: distribution of neurons projecting to the insular cortex and amygdaloid complex. *Neurosci Res* 36(4):297–309.

Nalivaiko E, Blessing WW (2001) Raphe region mediates changes in cutaneous vascular tone elicited by stimulation of amygdala and hypothalamus in rabbits. *Brain Res* 891(1):130–137.

Narita K, Kawasaki F, Kita H (1990) Mn and Mg influxes through Ca channels of motor nerve terminals are

prevented by verapamil in frogs. *Brain Res* 510(2):289–95.

Nashold BS, Wilson WP, Slaughter DG (1969) Sensations evoked by stimulation in the midbrain of man. *J Neurosurg* 30(1):14–24.

Nelson CP, Nahorski SR, Challiss RAJ (2005) Constitutive Activity and Inverse Agonism at the M2 Muscarinic Acetylcholine Receptor. *J Pharmacol Exp Ther* 316(1):279–288.

Nelson RJ, Zucker I (1981) Absence of extraocular photoreception in diurnal and nocturnal rodents exposed to direct sunlight. *Comp Biochem Phys A* 69(1):145–148.

Neuhuber W, Mclachlan E, Jänig W (2017) The sacral autonomic outflow is spinal, but not "sympathetic". *Anat Rec (Hoboken)* 300(8).

Neunuebel JP, Taylor AL, Arthur BJ, Egnor RSE (2015) Female mice ultrasonically interact with males during courtship displays. *eLife* 4:e06203.

Nikulina EM (1991) Neural control of predatory aggression in wild and domesticated animals. *Neurosci Biobehav Rev* 15(4):545–547.

Nordin M (1990) Sympathetic discharges in the human supraorbital nerve and their relation to sudo- and vasomotor responses. *J Physiol* 423(1):241–255.

Nosaka S, Murata K, Inui K, Murase S (1993) Arterial baroreflex inhibition by midbrain periaqueductal grey in anaesthetized rats. *Pflugers Arch* 424(3-4):266–75.

Nummenmaa L, Glerean E, Hari R, Hietanen JK (2014) Bodily maps of emotions. *PNAS* 111(2):646–51.

Nuttin BJ, Gabriëls LA, Cosyns PR, Meyerson BA, Andréewitch S, Sunaert SG, Maes AF, Dupont PJ, Gybels JM, Gielen F, Demeulemeester HG (2003) Long-term electrical capsular stimulation in patients with obsessive-compulsive disorder. *Neurosurgery* 52(6):1263–72; discussion 1272–4.

O'Keefe J, Dostrovsky J (1971) The hippocampus as a spatial map. Preliminary evidence from unit activity in the freely-moving rat. *Brain Res* 34(1):171–5.

Orsini CA, Kim JH, Knapska E, Maren S (2011) Hippocampal and prefrontal projections to the basal amygdala mediate contextual regulation of fear after extinction. *J Neurosci* 31(47):17269–77.

Otowa T, Hek K, Lee M, Byrne EM, Mirza SS, ..., Hettema JM (2016) Meta-analysis of genome-wide association studies of anxiety disorders. *Mol Psychieatry* 21(10):1391–9.

Ottersen OP (1981) Afferent connections to the amygdaloid complex of the rat with some observations in the cat. III. Afferents from the lower brain stem. *J Comp Neurol* 202(3):335–356.

Ottersen OP, Ben-Ari Y (1979) Afferent connections to the amygdaloid complex of the rat and cat. I. Projections from the thalamus. *J Comp Neurol* 187(2):401–424.

Pabba M (2013) Evolutionary development of the amygdaloid complex. *Front Neuroanat* 7:27.

Padilla-Coreano N, Bolkan SS, Pierce GM, Blackman DR, Hardin WD, Garcia-Garcia AL, Spellman TJ, Gordon JA (2016) Direct ventral hippocampal-prefrontal input is required for anxiety-related neural activity and behavior. *Neuron* 89(4):857–866.

Palidwor GA, Andrade-Navarro MA (2010) MLTrends: Graphing MEDLINE term usage over time. *J Biomed Discov Collab* 5:1–6.

Panksepp J (2010) Affective neuroscience of the emotional brainmind: evolutionary perspectives and implications for understanding depression. *Dialogues Clin Neurosci* 12(4):533–545.

Panksepp J, Biven L (2012) *The archaeology of mind : neuroevolutionary origins of human emotions.* W.W Norton, New York.

Panksepp J, Burgdorf J (2003) LaughingâĂİ rats and the evolutionary antecedents of human joy? *Physiol Behav* 79(3):533–47.

Panneton WM, Martin GF (1979) Midbrain projections to the trigeminal, facial and hypoglossal nuclei in the opossum. A study using axonal transport techniques. *Brain Res* 168(3):493–511.

Pape HC, Pare D (2010) Plastic Synaptic Networks of the Amygdala for the Acquisition, Expression, and Extinction of Conditioned Fear. *Physiol Rev* 90(2).

Parallax Inc. (2009) X-Band Motion Detector (#32213) v1.1, accessed: 2016-08-29 www.parallax.com/sites/default/files/downloads/32213-X-BandMotionDetector-v1.1_0.pdf.

Paré D, Quirk GJ (2017) When scientific paradigms lead to tunnel vision: lessons from the study of fear. *NPJ Sci Learn* 2(6).

Paré D, Quirk GJ, LeDoux JE (2004) New Vistas on Amygdala Networks in Conditioned Fear. *J Neurophysiol* 92:1–9.

Parreño A, Sarazá M, Subero C (1985) A new stabilimeter for small laboratory animals. *Physiol Behav* 34(3):475–478.

Pascual-Font A, Hernández-Morato I, McHanwell S, Vázquez T, Maranillo E, Sañudo J, Valderrama-Canales FJ (2011) The central projections of the laryngeal nerves in the rat. *J Anat* 219(2):217–228.

Pasquali V, Capasso A, Renzi P (2010) Circadian and ultradian rhythms in locomotory activity of inbred strains of mice. *Biol Rhythm Res* 41(1):63–74.

Pasquali V, D'Alessandro G, Gualtieri R, Leccese F (2017) A new Data Logger based on Raspberry-Pi for Arctic *Notostraca* Locomotion Investigations. *Measurement* 110:249–56.

Pasquali V, Gualtieri R, D'Alessandro G, Granberg M, Hazlerigg D, Cagnetti M, Leccese F (2016) Monitoring and Analyzing of Circadian and Ultradian Locomotor Activity Based on Raspberry-Pi. *Electronics (Switzerland)* 5(3) art. no. 58.

Pasquali V, Renzi P (2005) On the use of microwave radar devices in chronobiology studies: An application with *Periplaneta americana*. *Behav Res Meth* 37(3):522–27.

Pasquali V, Scannapieco E, Renzi P (2006) Validation of a microwave radar system for the monitoring of locomotor activity in mice. *J Circ Rhthms* 4(7).

Pavcovich LA, Yang MM RR, Valentino RJ (1998) Novel role for the pontine micturition center, Barrington's nucleus: evidence for coordination of colonic and forebrain activity. *Brain Res* 784(1):355–361.

Pavlov IP, Anrep GV (1927) *Conditioned reflexes; an investigation of the physiological activity of the cerebral cortex.* Oxford Univ. Press., London.

Pearce JM (2012) Materials science. Building research equipment with free, open-source hardware. *Science* 337(6100):1303–4.

Pellman B, Kim JJ (2016) What Can Ethobehavioral Studies Tell Us about the Brain's Fear System? *Trends Neurosci* 39(6):420–431.

Pellow S, Chopin P, File SE, Briley M (1985) Validation of open : closed arm entries in an elevated plus-maze as a measure of anxiety in the rat. *J Neurosci Meth* 14(3):149–167.

Pelosi GG, Corrêa FMA (2005) Cardiovascular effects of noradrenaline microinjected into the dorsal periaqueductal gray area of unanaesthetized rats. *Eur J Neurosci* 22(12):3188–3194.

Pelosi GG, Tavares RF, Antunes-Rodrigues J, Corrêa FMA (2008) Cardiovascular responses to noradrenaline microinjection in the ventrolateral periaqueductal gray of unanesthetized rats. *J Neurosci Res* 86(3):712–719.

Penfield W, Boldrey E (1937) Somatic motor and sensory representation in the cerebral cortex of man as studied by electrical stimulation. *Brain* 60(4):389–443.

Pereira-Junior PP, Marocolo M, Rodrigues FP, Medei E, Nascimento JH (2010) Noninvasive method for electrocardiogram recording in conscious rats: feasibility for heart rate variability analysis. *An Acad Bras Cienc* 82(2):431–437.

Perlmutter JS, Mink JW (2006) Deep Brain Stimulation. *Annu Rev Neurosci.* 29:229–257.

Pfleiderer B, Zinkirciran S, Arolt V, Heindel W, Deckert J, Domschke K (2007) fMRI amygdala activation during a spontaneous panic attack in a patient with panic disorder. *World J Biol Psychiatry* 8(4):269–72.

Pierrot-Deseilligny C, Rivaud S, Gaymard B, Agid Y (1991) Cortical Control of Reflexive Visually-Guided Saccades. *Brain* 114(3):1473–1485.

Pilz PKD, Arnold SW, Rischawy AT, Plappert CF, Schmid S, Preuss T (2014) Longterm-habituation of the startle response in mice is stimulus modality, but not context specific. *Front Integr Neurosci* 7(103).

Pinel JP, Mana MJ, Ward JA (1989) Stretched-approach sequences directed at a localized shock source by Rattus norvegicus. *J Comp Psychol* 103(2):140–148.

Pitkänen A, Pikkarainen M, Nurminen N, Ylinen A (2000) Reciprocal connections between the amygdala and the hippocampal formation, perirhinal cortex, and postrhinal cortex in rat. A review. *Ann N Y Acad Sci* 911:369–91.

Poole DS, Doorenweerd N, Plomp JJ, Mahfouz A, Reinders MJ, van der Weerd L (2017) Continuous infusion of manganese improves contrast and reduces side effects in manganese-enhanced magnetic resonance imaging studies. *NeuroImage* 147:1–9.

Poremba A, Jones D, Gonzalez-Lima F (1998) Classical conditioning modifies cytochrome oxidase activity in the auditory system. *Eur J Neurosci* 10(10):3035–43.

Porte D (1967) A receptor mechanism for the inhibition of insulin release by epinephrine in man. *J Clin Invest* 46(1):86–94.

Prast JM, Schardl A, Sartori SB, Singewald N, Saria A, Zernig G (2014) Increased conditioned place preference for cocaine in high anxiety related behavior (HAB) mice is associated with an increased activation in the accumbens corridor. *Front Behav Neurosci* 8:441.

Proctor GB, Carpenter GH (2007) Regulation of salivary gland function by autonomic nerves. *Auton Neurosci* 133(1):3–18.

Provencio I, Cooper HM, Foster RG (1998) Retinal projections in mice with inherited retinal degeneration: Implications for circadian photoentrainment. *J Comp Neurol* 395(4):417–439.

Prusky G, Alam N, Beekman S, RM D (2004) Rapid quantification of adult and developing mouse spatial vision using a virtual optomotor system. *Invest Ophthalmol Vis Sci.* 45(1):4611–6.

Puetz SL LT, Pfitzer G (2009) Regulation of smooth muscle contraction by small GTPases. *Physiology (Bethesda, Md.)* 24(6):342–56.

Pugh CR, Tremblay D, Fleshner M, Rudy JW (1997) A selective role for corticosterone in contextual-fear conditioning. *Behav Neurosci* 111(3):503–511.

Pugh EN, Falsini B, Lyubarsky AL (1998) The Origin of the Major Rod- and Cone-Driven Components of the Rodent Electroretinogram and the Effect of Age and Light-Rearing History on the Magnitude of These Components In *Photostasis and Related Phenomena*, pp. 93–128. Springer, Boston, MA.

Quattrini A, Lorenzetti I, Sciorati C, Corbo M, Previtali SC, Feltri M, Canal N, Wrabetz L, Nemni R, Clementi E (2001) Human IgM anti-GM1 autoantibodies modulate intracellular calcium homeostasis in neuroblastoma cells. *J Neuroimmunol* 114(1):213–219.

Quirk GJ (2002) Memory for extinction of conditioned fear is long-lasting and persists following spontaneous recovery. *Learn Mem* 9(6):402–7.

Ravindran LN, Stein MB (2010) The Pharmacologic Treatment of Anxiety Disorders. *J Clin Psychiat* 71(07):839–854.

Raz I, Katz A, Spencer MK (1991) Epinephrine inhibits insulin-mediated glycogenesis but enhances glycolysis in human skeletal muscle. *Am J Physiol* 260(3 Pt 1):E430–5.

Redgrave P, Westby GW, Dean P (1993) Functional architecture of rodent superior colliculus: relevance of multiple output channels. *Prog Brain Res* 95:69–77.

Redgrave P, Dean P (1991) Does the PAG Learn about Emergencies from the Superior Colliculus? In *The Midbrain Periaqueductal Gray Matter*, pp. 199–209. Springer US, Boston, MA.

Reimer AE, Oliveira AR, Brandão ML (2008) Selective involvement of GABAergic mechanisms of the dorsal periaqueductal gray and inferior colliculus on the memory of the contextual fear as assessed by the fear potentiated startle test. *Brain Res Bull* 76(5):545–50.

Rey A, Purrio M, Viveros M, Lutz B (2012) Biphasic Effects of Cannabinoids in Anxiety Responses: CB1 and GABAB Receptors in the Balance of GABAergic and Glutamatergic Neurotransmission. *Neuropsychopharmacol* 37(12):2624–2634.

Reynolds DV (1969) Surgery in the Rat during Electrical Analgesia Induced by Focal Brain Stimulation. *Science* 164(3878):444–445.

Ribeiro SJ, Ciscato JGJ, de Oliveira R, de Oliveira RC, D'Angelo-Dias R, Carvalho AD, Felippotti TT, Rebouças EC, Castellan-Baldan L, Hoffmann A, Corrêa SA, Moreira JE, Coimbra NC (2005) Functional and ultrastructural neuroanatomy of interactive intratectal/tectonigral mesencephalic opioid inhibitory links and nigrotectal GABAergic pathways: involvement of GABAA and mu1-opioid receptors in the modulation of panic-like reactions elicited by electrical stimulation of the dorsal midbrain. *J Chem Neuroanat* 30(4):184–200.

Ribeiro-Barbosa E, Canteras N, Cezário A, Blanchard R, Blanchard D (2005) An alternative experimental procedure for studying predator-related defensive responses. *Neurosci Biobehav Rev* 29(8):1255–1263.

Richter EA, Ruderman NB, Gavras H, Belur ER, Galbo H (1982) Muscle glycogenolysis during exercise: dual control by epinephrine and contractions. *Am J Physiol* 242(1):E25–32.

Ridgway JP (2010) Cardiovascular magnetic resonance physics for clinicians: part I. *J Cardiovasc Magn Reson* 12(1):71.

Riebe CJ, Pamplona FA, Kamprath K, Wotjak CT (2012) Fear relief-toward a new conceptual frame work and what endocannabinoids gotta do with it. *Neuroscience* 204:159–85.

Risbrough VB, Stein MB (2006) Role of corticotropin releasing factor in anxiety disorders: a translational research perspective. *Horm Behav* 50(4):550–61.

Rizvi TA, Ennis M, Behbehani MM, Shipley MT (1991) Connections between the central nucleus of the amygdala and the midbrain periaqueductal gray: topography and reciprocity. *J Comp Neurol* 303(1):121–31.

Roberts LH (1975a) Evidence for the laryngeal source of ultrasonic and audible cries of rodents. *J Zool* 175(2):243–257.

Roberts LH (1975b) The functional anatomy of the rodent larynx in relation to audible and ultrasonic cry production. *Zool J Linn Soc-Lond* 56(3):255–264.

Roberts LH (1975c) The rodent ultrasound production mechanism. *Ultrasonics* 13(2):83–88.

Roberts LH (2009) Correlation of respiration and ultrasound production in rodents and bats. *J Zool* 168(4):439–449.

Rodgers RJ, Davies B, Shore R (2002) Absence of anxiolytic response to chlordiazepoxide in two common background strains exposed to the elevated plus-maze: importance and implications of behavioural baseline. *Genes Brain Behav* 1(4):242–51.

Rodgers RJ, Lee C, Shepherd JK (1992) Effects of diazepam on behavioural and antinociceptive responses to the elevated plus-maze in male mice depend upon treatment regimen and prior maze experience. *Psychopharmacology* 106(1):102–110.

Roger M, Cadusseau J (1985) Afferents to the zona incerta in the rat: A combined retrograde and anterograde study. *J Comp Neurol* 241(4):480–492.

Romanski LM, LeDoux JE (1993a) Information cascade from primary auditory cortex to the amygdala: corticocortical and corticoamygdaloid projections of temporal cortex in the rat. *Cereb Cort* 3(6):515–32.

Romanski LM, LeDoux JE (1993b) Information Cascade from Primary Auditory Cortex to the Amygdala: Corticocortical and Corticoamygdaloid Projections of Temporal Cortex in the Rat. *Cereb Cortex* 3(6):515–532.

Root CM, Denny CA, Hen R, Axel R (2014) The participation of cortical amygdala in innate, odour-driven behaviour. *Nature* 515(7526):269–273.

Rosato E, Kyriacou CP (2006) Analysis of locomotor activity rhythms in Drosophila. *Nat Protoc* 1(2):559–68.

Rose FD, Dell PA, Love S (1985) Doppler shift radar monitoring of activity of rats in a behavioural test situation. *Physiol Behav* 35(1):85–7.

Rossier O, Abuin L, Fanelli F, Leonardi A, Cotecchia S (1999) Inverse agonism and neutral antagonism at alpha(1a)- and alpha(1b)-adrenergic receptor subtypes. *Mol Pharmacol* 56(5):858–66.

Roth BL (2016) DREADDs for Neuroscientists. *Neuron* 89(4):683–694.

Roy JC, Sequeira H, Delerm B (1993) Neural Control of Electrodermal Activity: Spinal and Reticular Mechanisms In *Progress in Electrodermal Research*, pp. 73–92. Springer US, Boston, MA.

Royer S, Paré D (2002) Bidirectional synaptic plasticity in intercalated amygdala neurons and the extinction of conditioned fear responses. *Neuroscience* 115(2):455–62.

Rubino T, Massi P, Patrini G, Venier I, Giagnoni G, Parolaro D (1994) Chronic CP-55,940 alters cannabinoid receptor mRNA in the rat brain: an in situ hybridization study. *Neuroreport* 5(18):2493–6.

Rubino T, Patrini G, Parenti M, Massi P, Parolaro D (1997) Chronic treatment with a synthetic cannabinoid CP-55,940 alters G-protein expression in the rat central nervous system. *Mol Brain Res* 44(2):191–197.

Rudolph U, Knoflach F (2011) Beyond classical benzodiazepines: novel therapeutic potential of GABAA receptor subtypes. *Nat Rev Drug Discov* 10(9):685–697.

Ruehle S, Rey A, Remmers F, Lutz B (2012) The endocannabinoid system in anxiety, fear memory and habituation. *JPsychopharmacol* 26(1):23–39.

Sadana R, Dessauer CW (2009) Physiological roles for G protein-regulated adenylyl cyclase isoforms: insights

from knockout and overexpression studies. *Neurosignals* 17(1):5–22.

Sah A, Schmuckermair C, Sartori SB, Gaburro S, Kandasamy M, Irschick R, Klimaschewski L, Landgraf R, Aigner L, Singewald N (2012) Anxiety- rather than depression-like behavior is associated with adult neurogenesis in a female mouse model of higher trait anxiety- and comorbid depression-like behavior. *Tran Psychiatr* 2(10):e171.

Sah P, Faber ESL, Lopez De Armentia M, Power J (2003) The amygdaloid complex: anatomy and physiology. *Physiol Rev* 83(3):803–34.

Sahibzada N, Dean P, Redgrave P (1986) Movements resembling orientation or avoidance elicited by electrical stimulation of the superior colliculus in rats. *J Neurosci* 6(3):723–33.

Saloman JL, Scheff NN, Snyder LM, Ross SE, Davis BM, Gold MS (2016) Gi-DREADD Expression in Peripheral Nerves Produces Ligand-Dependent Analgesia, as well as Ligand-Independent Functional Changes in Sensory Neurons. *J Neurosci* 36(42):10769–10781.

Salomone S, Morel N, Godfraind T (1995) Effects of 8-bromo cyclic GMP and verapamil on depolarization-evoked Ca2+ signal and contraction in rat aorta. *Brit J Pharmacol* 114(8):1731–1737.

Samuels BA, Hen R (2011) Novelty-Suppressed Feeding in the Mouse In Gould TD, editor, *Neuromethods Vol. 63: Mood and Anxiety Related Phenotypes in Mice*, chapter 7, pp. 107–121. New York, NY : Humana Press, c2009-c2011.

Sanz E, Yang L, Su T, Morri DR, McKnight GS, Amieux PS (2009) Cell-type-specific isolation of ribosome-associated mrna from complex tissues. *PNAS* 106(33):13939–44.

Sareen J, Henriksen CA, Bolton SL, Afifi TO, Stein MB, Asmundson GJG (2013) Adverse childhood experiences in relation to mood and anxiety disorders in a population-based sample of active military personnel. *Psychol Med* 43(01):73–84.

Sartori SB, Hauschild M, Bunck M, Gaburro S, Landgraf R, Singewald N (2011b) Enhanced Fear Expression in a Psychopathological Mouse Model of Trait Anxiety: Pharmacological Interventions. *PLoS ONE* 6(2):e16849.

Sartori SB, Landgraf R, Singewald N (2011a) The clinical implications of mouse models of enhanced anxiety. *Fut Neurol* 6(4):531–571.

Sartory G, MacDonald R, Gray JA (1990) Effects of diazepam on approach, self-reported fear and psychophysiological responses in snake phobics. *Behav Res Ther* 28(4):273–282.

Sasaki K, Suzuki M, Mieda M, Tsujino N, Roth B, Sakurai T (2011) Pharmacogenetic modulation of orexin neurons alters sleep/wakefulness states in mice. *PloS one* 6(5):e20360.

Sato K, Leidal R, Sato F (1987) Morphology and development of an apoeccrine sweat gland in human axillae. *Am J Physiol* 252(1 Pt 2):R166–80.

Sauer B, Henderson N (1988) Site-specific DNA recombination in mammalian cells by the Cre recombinase of bacteriophage P1. *PNAS* 85(14):5166–70.

Savage MA, McQuade R, Thiele A (2017) Segregated fronto-cortical and midbrain connections in the mouse and their relation to approach and avoidance orienting behaviors. *J Comp Neurol* 525(8):1980–1999.

Savić MM, Obradović DI, Ugrešić ND, Cook JM, Sarma PVVS, Bokonjić DR (2005) Bidirectional effects of benzodiazepine binding site ligands on active avoidance acquisition and retention: differential antagonism by flumazenil and β-CCt. *Psychopharmacology* 180(3):455–465.

Savidge JR, Bristow DR (1997) Distribution of Ca(2+)-permeable AMPA receptors among cultured rat cerebellar granule cells. *Neuroreport* 8(8):1877–82.

Sazanov LA (2015) A giant molecular proton pump: structure and mechanism of respiratory complex I. *NNat Rev Mol Cell Biol* 16(6):375–88.

Scheibner J, Trendelenburg AU, Hein L, Starke K, Blandizzi C (2002) α_2-Adrenoceptors in the enteric nervous system: a study in α_2-adrenoceptor-deficient mice. *Brit J Pharmacol* 135(3):697–704.

Scheithauer N (2016) Measuring fear and anxiety in mice - Establishment of the Mouse Anxiety Fear Inhibitory Avoidance Task. *Unpulished Master 's Thesis, Faculty of Biology, Luwig-Maximilians-Universität München* .

Schenberg LC, Costa MB, Borges PC, Castro MF (1990) Logistic analysis of the defense reaction induced by electrical stimulation of the rat mesencephalic tectum. *Neurosci Biobehav Res* 14(4):473–9.

Schienle A, Schäfer A, Walter B, Stark R, Vaitl D (2005) Brain activation of spider phobics towards disorder-relevant, generally disgust- and fear-inducing pictures. *Neurosci Lett* 388(1):1–6.

Schmuckermair C, Gaburro S, Sah A, Landgraf R, Sartori SB, Singewald N (2013) Behavioral and Neurobiological Effects of Deep Brain Stimulation in a Mouse Model of High Anxiety- and Depression-Like Behavior. *Neuropsychopharmacol* 38(7):1234–1244.

Schneider T, Igelmund P, Hescheler J (1997) G protein interaction with K+ and Ca2+ channels. *Trends Pharmacol Sci* 18(1):8–11.

Scholkmann F, Boss J, Wolf M (2012) An Efficient Algorithm for Automatic Peak Detection in Noisy Periodic and Quasi-Periodic Signals. *Algorithms* 5(4):588–603.

Scholvin J, Kinney JP, Bernstein JG, Moore-Kochlacs C, Kopell N, Fonstad CG, Boyden ES (2016) Close-Packed Silicon Microelectrodes for Scalable Spatially Oversampled Neural Recording. *IEEE Trans Biomed Eng* 63(1):120–30.

Schotzinger RJ, Landis SC (1988) Cholinergic phenotype developed by noradrenergic sympathetic neurons after innervation of a novel cholinergic target in vivo. *Nature* 335(6191):637–9.

Schroeder MP, Weiss C, Procissi D, Wang L, Disterhoft JF (2016) Activity-induced manganese-dependent MRI (AIM-MRI) and functional MRI in awake rabbits during somatosensory stimulation. *NeuroImage* 126:72–80.

Schutter D, van Honk J (2005) The cerebellum on the rise in human emotion. *Cerebellum* 4(4):290–294.

Schwab HM, Bartholomae A, Heimrich B, Feldmeyer D, Druffel-Augustin S, Goebbels S, ..., A NK (2000) Neuronal Basic Helix-Loop-Helix Proteins (NEX and BETA2/Neuro D) Regulate Terminal Granule Cell Differentiation

in the Hippocampus. *J Neurosci* 20(10):3714âĂŞ3724.

Schweckendiek J, Klucken T, Merz CJ, Tabbert K, Walter B, Ambach W, Vaitl D, Stark R (2011) Weaving the (neuronal) web: fear learning in spider phobia. *NeuroImage* 54(1):681–8.

Scully KM, Rosenfeld MG (2002) Pituitary Development: Regulatory Codes in Mammalian Organogenesis. *Science* 295(5563).

Seligman AM, Karnovsky MJ, Wasserkrug HL, Hanker JS (1968) Nondroplet ultrastructural demonstration of cytochrome oxidase activity with a polymerizing osmiophilic reagent, diaminobenzidine (DAB). *J Cell Biol* 38(1):1–14.

Serfilippi LM, Pallman DRS, Gruebbel MM, Kern TJ, Spainhour CB (2004) Assessment of retinal degeneration in outbred albino mice. *Comp Med* 54(1):69–76.

Setlow B, Gallagher, M H PC (2002) The basolateral complex of the amygdala is necessary for acquisition but not expression of CS motivational value in appetitive Pavlovian second-order conditioning. *Eur J Neurosci* 15(11):1841–53.

Shang C, Liu Z, Chen Z, Shi Y, Wang Q, Liu S, Li D, Cao P (2015) A parvalbumin-positive excitatory visual pathway to trigger fear responses in mice. *Science* 348(6242).

Sharma A, Kesari KK, Saxena VK, Sisodia R (2017) Ten gigahertz microwave radiation impairs spatial memory, enzymes activity, and histopathology of developing mice brain. *Mol Cell Biochem* May 3. doi: 10.1007/s11010-017-3051-8. [Epub ahead of print].

Sharma A, Sisodia R, Bhatnagar D, Saxena VK (2014) Spatial memory and learning performance and its relationship to protein synthesis of Swiss albino mice exposed to 10 GHz microwaves. *Int J Radiat Biol* 90(1):29–35.

Sheinin A, Lavi A, Michaelevski I (2015) StimDuino: An Arduino-based electrophysiological stimulus isolator. *J Neurosci Meth* 243:8–17.

Sheldon RS, Wright CI, Duff HJ, Thakore E, Gillis AM, Roach DE (2007) Mechanism of hypotensive transients associated with abrupt bradycardias in conscious rabbits. *Can J Cardiol* 23(9).

Shepherd J, Grewal S, Fletcher A, Bill D, Dourish C (1994) Behavioural and pharmacological characterisation of the elevated "zero-maze" as an animal model of anxiety. *Psychopharmacology* 116(1):56–64.

Shi X, Barchini J, Ledesma HA, Koren D, Jin Y, Liu X, Wei W, Cang J (2017) Retinal origin of direction selectivity in the superior colliculus. *Nat Neurosci* 20(4):550–8.

Shiba K, Umezaki T, Zheng Y, Miller AD (1997) The nucleus retroambigualis controls laryngeal muscle activity during vocalization in the cat. *Exp Brain Res* 115(3):513–9.

Shibuya I, Douglas WW (1993) Indications from Mn-quenching of Fura-2 fluorescence in melanotrophs that dopamine and baclofen close Ca channels that are spontaneously open but not those opened by high [K+]O; and that Cd preferentially blocks the latter. *Cell Calcium* 14(1):33–44.

Shimada-Sugimoto M, Otowa T, Hettema JM (2015) Genetics of anxiety disorders: Genetic epidemiological and molecular studies in humans. *Psychiatry Clin Neurosci* 69(7):388–401.

Shimizu E, Tang YP, Rampon C, Tsien JZ (2000) NMDA receptor-dependent synaptic reinforcement as a crucial process for memory consolidation. *Science* 290(5494):1170–4.

Shinnick-Gallagher P, McKernan MG (1997) Fear conditioning induces a lasting potentiation of synaptic currents in vitro. *Nature* 390(6660):607–611.

Siebert S, Jürgens U (2003) Vocalization after periaqueductal grey inactivation with the gaba agonist muscimol in the squirrel monkey. *Neurosci Lett* 340(2):111–114.

Siegle JH, López AC, Patel YA, Abramov K, Ohayon S, Voigts J (2017) Open ephys: an open-source, plugin-based platform for multichannel electrophysiology. *J Neural Eng* 14(4).

Siegmund A, Wotjak CT (2007) A mouse model of posttraumatic stress disorder that distinguishes between conditioned and sensitised fear. *J Psych Res* 41(10):848–860.

Siemiątkowski M, Sienkiewicz-Jarosz H, CzŁonkowska A, Bidziński A, PŁaźnik A (2000) Effects of Buspirone, Diazepam, and Zolpidem on Open Field Behavior, and Brain [3H]Muscimol Binding After Buspirone Pretreatment. *Pharmacol Biochem Behav* 66(3):645–651.

Siepmann T, Gibbons CH, Illigens BM, Lafo JA, Brown CM, Freeman R (2012) Quantitative pilomotor axon reflex test: a novel test of pilomotor function. *Arch Neurol* 69(11):1488–92.

Sigel E, Steinmann ME (2012) Structure, function, and modulation of GABA(A) receptors. *J Biol Chem* 287(48):40224–31.

Silasi G, Boyd JD, LeDue J, Murphy TH (2013) Improved methods for chronic light-based motor mapping in mice: automated movement tracking with accelerometers, and chronic EEG recording in a bilateral thin-skull preparation. *Front Neur Circ* 7:123.

Silva BA, Mattucci C, Krzywkowski P, Cuozzo R, Carbonari L, Gross CT (2016) The ventromedial hypothalamus mediates predator fear memory. *Eur J Neurosci* 43(11):1431–1439.

Silva BA, Mattucci C, Krzywkowski P, Murana E, Illarionova A, Grinevich V, Canteras NS, Ragozzino D, Gross CT (2013) Independent hypothalamic circuits for social and predator fear. *Nat Neurosci* 16(12):1731–1733.

Simpson PB, Challiss RA, Nahorski SR (1995) Divalent cation entry in cultured rat cerebellar granule cells measured using Mn2+ quench of fura 2 fluorescence. *Eur J Neurosci* 7(5):831–40.

Skultety FM (1962) Experimental mutism in dogs. *Arch Neurol* 6:235–41.

Sloot WN, Gramsbergen JB (1994) Axonal transport of manganese and its relevance to selective neurotoxicity in the rat basal ganglia. *Brain Res* 657(1-2):124–32.

Sotnikov S, Wittmann A, Bunck M, Bauer S, Deussing J, Schmidt M, Touma C, Landgraf R, Czibere L (2014) Blunted HPA axis reactivity reveals glucocorticoid system dysbalance in a mouse model of high anxiety-related behavior. *Psychoneuroendocrinology* 48:41–51.

Sotnikov S, Markt P, Umriukhin A, Landgraf R (2011) Genetic predisposition to anxiety-related behavior predicts predator odor response. *Behav Brain Res* 225(1):230–234.

Sotres-Bayon F, Sierra-Mercado D, Pardilla-Delgado E, Quirk E (2012) Gating of fear in prelimbic cortex by hippocampal and amygdala inputs. *Neuron* 76(4):804–12.

Sparks DL, Hartwich-Young R (1989) The deep layers of the superior colliculus. *Rev Oculomot Res* 3:213–55.

Sperry RW (1963) Chemoaffinity in the Orderly Growth of Nerve Fiber Patterns and Connections. *PNAS* 50:703–10.

Spiegel EA, Kletzkin M, Szekely EG (1954) Pain Reactions Upon Stimulation of the Tectum Mesencephali. *J Neuropathol Exp Neurol* 13(1):212–220.

Spielberg S, Marshall F (1981) Raiders of the Lost Ark.

Staiger JF, Nürnberger F (1991) The efferent connections of the lateral septal nucleus in the guinea pig: projections to the diencephalon and brainstem. *Cell Tissue Res* 264(3):391–413.

Steinberg W (1952) TROPHIC VS. TROPIC. *JAMA* 149(1):82.

Steinhauer SR, Siegle GJ, Condray R, Pless M (2004) Sympathetic and parasympathetic innervation of pupillary dilation during sustained processing. *Int J Psychophysiol* 52(1):77–86.

Steininger TL, Rye DB, Wainer BH (1992) Afferent projections to the cholinergic pedunculopontine tegmental nucleus and adjacent midbrain extrapyramidal area in the albino rat. i. retrograde tracing studies. *J Comp Neurol* 321(4):515–43.

Stephens MD (1986) Drug-induced piloerection in man: an alpha 1-adrenoceptor agonist effect? *Hum Toxicol* 5(5):319–24.

Steriade M (1996) Arousal: revisiting the reticular activating system. *Science (New York, N.Y.)* 272(5259):225–6.

Sternson SM, Roth BL (2014) Chemogenetic Tools to Interrogate Brain Functions. *Ann Rev Neurosci* 37(1):387–407.

Steru L, Chermat R, Thierry B, Simon P (1985) The tail suspension test: A new method for screening antidepressants in mice. *Psychopharmacology* 85(3):367–370.

Stewart IB, McKenzie DC (2002) The Human Spleen During Physiological Stress. *Sports Med* 32(6):361–369.

Stiedl O, Spiess J (1997) Effect of tone-dependent fear conditioning on heart rate and behavior of C57BL/6N mice. *Behav Neurosci* 111(4):703–11.

Stitt CL, Hoffman HS, Marsh RR, Schwartz GM (1976) Modification of the pigeon's visual startle reaction by the sensory environment. *J Comp Physiol Psychol* 90(7):601–19.

Stoff DM, Stauderman K, Wyatt RJ (1983) The time and space machine: Continuous measurement of drug-induced behavior patterns in the rat. *Psychopharmacol* 80(4):319–324.

Strata P (2015) The Emotional Cerebellum. *Cerebellum* 14(5):570–577.

Strause LG, Hegenauer J, Saltman P, Cone R, Resnick D (1986) Effects of long-term dietary manganese and copper deficiency on rat skeleton. *J Nutr* 116(1):135–41.

Stujenske JM, Spellman T, Gordon JA (2015) Modeling the Spatiotemporal Dynamics of Light and Heat Propagation for In Vivo Optogenetics. *Cell Rep* 12(3):525–34.

Suárez N, Eriksson H (1993) Receptor-mediated endocytosis of a manganese complex of transferrin into neuroblastoma (SHSY5Y) cells in culture. *J Neurochem* 61(1):127–31.

Sugiyama Y, Shiba K, Nakazawa K, Suzuki T, Hisa Y (2010) Brainstem vocalization area in guinea pigs. *Neurosci Res* 66(4):359–365.

Sun N, Li Y, Tian S, Lei Y, Zheng J, Yang J, Sui N, Xu L, Pei G, Wilson FAW, Ma Y, Lei H, Hu X (2006) Dynamic changes in orbitofrontal neuronal activity in rats during opiate administration and withdrawal. *Neuroscience* 138(1):77–82.

Sutherland EW, Cori CF (1951) Effect of hyperglycemic-glycogenolytic factor and epinephrine on liver phosphorylase. *J Biol Chem* 188(2):531–43.

Sutton D, Miller JM (1963) Implanted electrodes: cable coupler for elimination of movement artifact. *Science* 140(3570):988–9.

Swanson LW, Petrovicha GD (1998) What is the amygdala? *Trends Neurosci* 21(8):323–331.

Swerdlow NR, Geyer MA (1993) Prepulse Inhibition of Acoustic Startle in Rats After Lesions of the Pedunculopontine Tegmental Nucleus. *Behav Neurosci* 107(1):104–117.

Szego ÉM, Janáky T, Szabó Z, Csorba A, Kompagne H, Müller G, Lévay G, Simor A, Juhász G, Kékesi KA (2010) A mouse model of anxiety molecularly characterized by altered protein networks in the brain proteome. *Eur Neuropsychopharmacol* 20(2):96–111.

Taché Y, Martinez V, Wang L, Million M (2004) CRF1 receptor signaling pathways are involved in stress-related alterations of colonic function and viscerosensitivity: implications for irritable bowel syndrome. *Brit J Pharmacol* 141(8):1321–30.

Taché Y, Perdue MH (2004) Role of peripheral CRF signalling pathways in stress-related alterations of gut motility and mucosal function. *Neurogastroent Motil* 16 Suppl 1:137–42.

Takeda H, Tsuji M, Matsumiya T (1998) Changes in head-dipping behavior in the hole-board test reflect the anxiogenic and/or anxiolytic state in mice. *Eur J Pharmacol* 350(1):21–29.

Tamborini P, Sigg H, Zbinden G (1989) Quantitative analysis of rat activity in the home cage by infrared monitoring. Application to the acute toxicity testing of acetanilide and phenylmercuric acetate. *Arch Toxicol* 63(2):85–96.

Tang X, Wu D, Gu LH, Nie BB, Qi XY, Wang YJ, Wu FF, Li XL, Bai F, Chen XC, Xu L, Ren QG, Zhang ZJ

(2016) Spatial learning and memory impairments are associated with increased neuronal activity in 5XFAD mouse as measured by manganese-enhanced magnetic resonance imaging. *Oncotarget* 7(36):57556–57570.

Tansey EA, Johnson CD (2015) Recent advances in thermoregulation. *Adv Physiol Educ* 39(3):139–48.

Tarpy RM, Murcek RJ (1984) An electronic device for detecting activity in caged rodents. *Behav Res Meth Ins C* 16(4):383–387.

Tasan R, Bukovac A, Peterschmitt Y, Sartori S, Landgraf R, Singewald N, Sperk G (2011) Altered GABA transmission in a mouse model of increased trait anxiety. *Neuroscience* 183:71–80.

Tedford HW, Zamponi GW (2006) Direct G Protein Modulation of Cav2 Calcium Channels. *Pharmacol Rev* 58(4).

Teikari P, Najjar RP, Malkki H, Knoblauch K, Dumortier D, Gronfier C, Cooper HM (2012) An inexpensive Arduino-based LED stimulator system for vision research. *J Neurosci Meth* 211(2):227–36.

Thaung C, Arnold K, Jackson IJ, Coffey PJ (2002) Presence of visual head tracking differentiates normal sighted from retinal degenerate mice. *Neurosci Lett* 325(1):21–24.

Thompson AC, Stoddart PR, Jansen ED (2014) Optical Stimulation of Neurons. *Curr Mol Imag* 3(2):162–177.

Thornton HB, Nel D, Thornton D, van Honk J, Baker GA, Stein DJ (2008) The neuropsychiatry and neuropsychology of lipoid proteinosis. *J Neuropsychiatry Clin Neurosci* 20(1):86–92.

Tinbergen N (1951) *The Study of instinct.* Clarendon Press/Oxford University Press.

Tischler MD, Davis M (1983) A Visual Pathway that Mediates Fear-Conditioned Enhancement of Acoustic Startle. *Brain Res* 276(1):55–71.

Tjälve H, Henriksson J, Tallkvist J, Larsson BS, Lindquist NG (1996) Uptake of manganese and cadmium from the nasal mucosa into the central nervous system via olfactory pathways in rats. *Pharmacol Toxicol* 79(6):347–56.

Tjälve H, Mejàre C, Borg-Neczak K (1995) Uptake and transport of manganese in primary and secondary olfactory neurones in pike. *Pharmacol Toxicol* 77(1):23–31.

Tong Q, Ye C, McCrimmon RJ, Dhillon H, Choi B, Kramer MD, Yu J, Yang Z, Christiansen LM, Lee CE, Choi CS, Zigman JM, Shulman GI, Sherwin RS, Elmquist JK, Lowell BB (2007) Synaptic glutamate release by ventromedial hypothalamic neurons is part of the neurocircuitry that prevents hypoglycemia. *Cell Metabol* 5(5):383–93.

Tovote P, Fadok JP, Lüthi A (2015) Neuronal circuits for fear and anxiety. *Nat Rev Neurosci* 16(6):317–31.

Tovote P, Esposito MS, Botta P, Chaudun F, Fadok JP, Markovic M, Wolff SBE, Ramakrishnan C, Fenno L, Deisseroth K, Herry C, Arber S, Lüthi A (2016) Midbrain circuits for defensive behaviour. *Nature* 534(7606):206.

Tranel D, Hyman BT (1990) Neuropsychological correlates of bilateral amygdala damage. *Arch Neurol* 47(3):349–55.

Trent NL, Menard JL (2010) The ventral hippocampus and the lateral septum work in tandem to regulate rats' open-arm exploration in the elevated plus-maze. *Physiol Behav* 101(1):141–52.

Tsien JZ, Chen DF, Gerber D, Tom C, Mercer EH, Anderson DJ, Mayford M, Kandel ER, Tonegawa S (1996) Subregion- and cell type-restricted gene knockout in mouse brain. *Cell* 87(7):1317–26.

Turner BH, Herkenham M (1991) Thalamoamygdaloid projections in the rat: A test of the amygdala's role in sensory processing. *J Comp Neurol* 313(2):295–325.

Uhlenbruck G (1983) *Ein gebildeter Kranker – Trostund Trutz-Sprüche für und gegen Ängste und Ärzte* Gustav Fischer Verlag, Stuttgart - New York, 2. ergänzt edition.

Ullah F, dos Anjos-Garcia T, dos Santos IR, Biagioni AF, Coimbra NC (2015) Relevance of dorsomedial hypothalamus, dorsomedial division of the ventromedial hypothalamus and the dorsal periaqueductal gray matter in the organization of freezing or oriented and non-oriented escape emotional behaviors. *Behav Brain Res* 293:143–152.

Ulrich-Lai YM, Herman JP (2009) Neural regulation of endocrine and autonomic stress responses. *Nat Rev Neurosci* 10(6):397–409.

Umezu T (1999) Effects of Psychoactive Drugs in the Vogel Conflict Test in Mice. *Jap J Pharmacol* 80(2):111–118.

Urbach E, Wiethe C (1929) Lipoidosis cutis et mucosae. *Virchows Arch A* 273(2):285–319.

Urban DJ, Roth BL (2015) DREADDs (Designer Receptors Exclusively Activated by Designer Drugs): Chemogenetic Tools with Therapeutic Utility. *Ann Rev Pharmacol and Toxicol* 55(1):399–417.

Urban DJ, Zhu H, Marcinkiewcz CA, Michaelides M, Oshibuchi H, Rhea D, Aryal DK, Farrell MS, Lowery-Gionta E, Olsen RHJ, Wetsel WC, Kash TL, Hurd YL, Tecott LH, Roth BL (2016) Elucidation of The Behavioral Program and Neuronal Network Encoded by Dorsal Raphe Serotonergic Neurons. *Neuropsychopharmacol* 41(5):1404–15.

Vale W, Spiess J, Rivier C, Rivier J (1981) Characterization of a 41-residue ovine hypothalamic peptide that stimulates secretion of corticotropin and beta-endorphin. *Science (New York, N.Y.)* 213(4514):1394–7.

Vanuytven M, Vermeire J, Niemegeers CJE (1979) A new motility meter based on the Doppler principle. *Psychopharmacol* 64(3):333–336.

Vermani M, Marcus M, Katzman MA (2011) Rates of detection of mood and anxiety disorders in primary care: a descriptive, cross-sectional study. *Prim Care Companion CNS Disord* 13(2).

Vernon HM (1911a) The indophenol oxidase of mammalian and avian tissues. *J Physiol* 43(1):96–108.

Vernon HM (1911b) The quantitative estimation of the indophenol oxidase of animal tissues. *J Physiol* 42(5-6):402–27.

Vertes RP (2004) Differential projections of the infralimbic and prelimbic cortex in the rat. *Synapse* 51(1):32–58.

Viana M, Tomaz C, Graeff F (1994) The elevated T-maze: A new animal model of anxiety and memory. *Pharmacol Biochem Behav* 49(3):549–554.

Vianna DM, Graeff FG, Landeira-Fernandez J, Brandão ML (2001) Lesion of the Ventral Periaqueductal Gray Reduces Conditioned Fear but Does Not Change Freezing Induced by Stimulation of the Dorsal Periaqueductal Gray. *Learn Mem* 8(3):164–169.

Vianna D, Brandão M (2003) Anatomical connections of the periaqueductal gray: specific neural substrates for different kinds of fear. *Braz J Med Biol Res* 36(5):557–566.

Vidal-Gonzalez I, Vidal-Gonzalez B, Rauch SL, Quirk GJ (2006) Microstimulation reveals opposing influences of prelimbic and infralimbic cortex on the expression of conditioned fear. *Learn Mem* 13(6):728–33.

Violle N, Balandras F, Le Roux Y, Desor D, Schroeder H (2009) Variations in illumination, closed wall transparency and/or extramaze space influence both baseline anxiety and response to diazepam in the rat elevated plus-maze. *Behav Brain Res* 203(1):35–42.

Visser RM, Scholte HS, Beemsterboer T, Kindt M (2013) Neural pattern similarity predicts long-term fear memory. *Nat Neuroscience* 16(4):388–390.

Vogel JR, Beer B, Clody DE (1971) A simple and reliable conflict procedure for testing anti-anxiety agents. *Psychopharmacologia* 21(1):1–7.

Voigts J, Siegle JH, Pritchett DL, Moore CI (2013) The flexDrive: an ultra-light implant for optical control and highly parallel chronic recording of neuronal ensembles in freely moving mice. *Front Sys Neurosci* 7:8.

Võikar V, Kõks S, Vasar E, Rauvala H (2001) Strain and gender differences in the behavior of mouse lines commonly used in transgenic studies. *Physiol Behav* 72(1-2):271–281.

Volchan E, Rocha-Rego V, Bastos AF, Oliveira JM, Franklin C, Gleiser S, ..., Figueira I (2017) Immobility reactions under threat: A contribution to human defensive cascade and PTSD. *Neurosci Biobeha Rev* 76(Pt A):29–38.

von Frisch K (1942) Über einen Schreckstoff der Fischhaut und seine biologische Bedeutung. *Zeitschrift für Vergleichende Physiologie* 29(1-2):46–145.

Walker P, Carrive P (2003) Role of ventrolateral periaqueductal gray neurons in the behavioral and cardiovascular responses to contextual conditioned fear and poststress recovery. *Neuroscience* 116(3):897–912.

Walters AS, Silvestri R, Zucconi M, Chandrashekariah R, Konofal E (2008) Review of the possible relationship and hypothetical links between attention deficit hyperactivity disorder (ADHD) and the simple sleep related movement disorders, parasomnias, hypersomnias, and circadian rhythm disorders. *J Clin Sleep Med* 4(6):591–600.

Wandruszka M (1981) *Angst und Mut* 2. Aufl. Klett-Cotta, Stuttgart.

Wang L, Chen I, Lin D (2015) Collateral Pathways from the Ventromedial Hypothalamus Mediate Defensive Behaviors. *Neuron* 85(6):1344–1358.

Wang S, Redgrave P (1997) Microinjections of muscimol into lateral superior colliculus disrupt orienting and oral movements in the formalin model of pain. *Neuroscience* 81(4):967–88.

Wedler FC, Denman RB, Roby WG (1982) Glutamine synthetase from ovine brain is a manganese(II) enzyme. *Biochem* 21(25):6389–96.

Wei P, Liu N, Zhang Z, Liu X, Tang Y, He X, Wu B, ..., Wang L (2015) Processing of visually evoked innate fear by a non-canonical thalamic pathway. *Nat Comm* 6:6756.

Weinberger NM (2011) The medial geniculate, not the amygdala, as the root of auditory fear conditioning. *Hear Res* 274(1-2):61–74.

Weiner DM, Meltzer HY, Veinbergs I, Donohue EM, Spalding TA, Smith TT, Mohell N, Harvey SC, Lameh J, Nash N, Vanover KE, Olsson R, Jayathilake K, Lee M, Levey AI, Hacksell U, Burstein ES, Davis RE, Brann MR (2004) The role of M1 muscarinic receptor agonism of N-desmethylclozapine in the unique clinical effects of clozapine. *Psychopharmacology* 177(1-2):207–216.

Wendt J, Löw A, Weymar M, Lotze M, Hamm AO (2017) Active avoidance and attentive freezing in the face of approaching threat. *NeuroImage* 158:196–204.

Wetzel DM, Kelley DB, Campbell BA (1980) Central Control of Ultrasonic Vocalizations in Neonatal Rats: I. Brain Stem Motor Nuclei. *J Comp Physiol Psychol* 94(4):596–606.

Whissell PD, Tohyama S, Martin LJ (2016) The Use of DREADDs to Deconstruct Behavior. *Fronts Genet* 7:70.

Whitney G (1970) Ontogeny of sonic vocalizations of laboratory mice. *Behav Genet* 1(3-4):269–273.

Whittle N, Maurer V, Murphy C, Rainer J, Bindreither D, Hauschild M, Scharinger A, Oberhauser M, Keil T, Brehm C, Valovka T, Striessnig J, Singewald N (2016) Enhancing dopaminergic signaling and histone acetylation promotes long-term rescue of deficient fear extinction. *Trans Psych* 6(12):e974.

Whittle N, Hauschild M, Lubec G, Holmes A, Singewald N (2010) Rescue of Impaired Fear Extinction and Normalization of Cortico-Amygdala Circuit Dysfunction in a Genetic Mouse Model by Dietary Zinc Restriction. *J Neurosci* 30(41).

Williams CL, Peterson JM, Villar RG, Burks TF (1987) Corticotropin-releasing factor directly mediates colonic responses to stress. *Am J Physiol* 253(4 Pt 1):G582–6.

Willott JF, Kulig J, Satterfield T (1984) The acoustic startle response in DBA/2 and C57BL/6 mice: relationship to auditory neuronal response properties and hearing impairment. *Hear Res* 16(2):161–167.

Wittchen HU, Jacobi F, Rehm J, Gustavsson A, Svensson M, Jönsson B, ..., Steinhausen HC (2011) The size and burden of mental disorders and other disorders of the brain in Europe 2010. *Eur Neuropsychopharmacol* 21(9):655–679.

Wong-Riley M (1979) Changes in the visual system of monocularly sutured or enucleated cats demonstrable with cytochrome oxidase histochemistry. *Brain Res* 171(1):11–28.

Wong-Riley MT, Merzenich MM, Leake PA (1978) Changes in endogenous enzymatic reactivity to DAB induced by neuronal inactivity. *Brain Res* 141(1):185–92.

Woodhams SG, Chapman V, Finn DP, Hohmann AG, Neugebauer V (2017) The cannabinoid system and pain.

Neuropharmacology 124:105–20.

World Health Organization (1992) *The ICD-10 classification of mental and behavioural disorders: clinical descriptions and diagnostic guidelines.*

Wotjak CT (2005) Role of endogenous cannabinoids in cognition and emotionality. *Mini-Rev Med Chem* 5(7):659–70.

Wotjak CT, Pape HC (2013) Neuronale Schaltkreise von Furchtgedaechtnis und Furchtextinktion. *Neuroforum* 19(3):92–102.

Yajima Y, Hayashi Y, Yoshii N (1982) Ambiguus motoneurons discharging closely associated with ultrasonic vocalization in rats. *Brain Res* 238(2):445–450.

Yamamoto O, Niida H, Tajima K, Shirouchi Y, Masui Y, Ueda F, ..., Kimura K (1998) Inhibition of stress-stimulated colonic propulsion by alpha2-adrenoceptor antagonists in rats. *Neurogastroenterology and Motility* 10(6):523–532.

Yang M, Augustsson H, Markham C, Hubbard D, Webster D, Wall P, Blanchard R, Blanchard D (2004) The rat exposure test: a model of mouse defensive behaviors. *Physiol Behav* 81(3):465–473.

Yates D (2015) Neural Circuits: A nucleus of fear. *Nat Rev Neurosci* 16(3):121–121.

Yen YC, Anderzhanova E, Bunck M, Schuller J, Landgraf R, Wotjak CT (2013) Co-segregation of hyperactivity, active coping styles, and cognitive dysfunction in mice selectively bred for low levels of anxiety. *Front Behav Neurosci* 7:103.

Yen YC, Gassen NC, Zellner A, Rein T, Landgraf R, Wotjak CT, Anderzhanova E (2015) Glycogen synthase kinase-3β inhibition in the medial prefrontal cortex mediates paradoxical amphetamine action in a mouse model of ADHD. *Front Behav Neurosci* 9:67.

Yen YC, Mauch CP, Dahlhoff M, Micale V, Bunck M, Sartori SB, Singewald N, Landgraf R, Wotjak CT (2012) Increased levels of conditioned fear and avoidance behavior coincide with changes in phosphorylation of the protein kinase B (AKT) within the amygdala in a mouse model of extremes in trait anxiety. *Neurobiol Learn Mem* 98(1):56–65.

Yilmaz M, Meister M (2013) Rapid innate defensive responses of mice to looming visual stimuli. *Curr Biol* 23(20):2011–5.

Yizhar O, Fenno LE, Prigge M, Schneider F, Davidson TJ, O'Shea DJ, Sohal VS, Goshen I, Finkelstein J, Paz JT, Stehfest K, Fudim R, Ramakrishnan C, Huguenard JR, Hegemann P, Deisseroth K (2011) Neocortical excitation/inhibition balance in information processing and social dysfunction. *Nature* 477(7363):171–8.

Young CW, Young MS, Li YC, Lin MT (1996) A new ultrasonic method for measuring minute motion activities of rats. *J Neurosci Meth* 70(1):45–9.

Yu CR, Power J, Barnea G, O'Donnell S, Brown HEV, Osborne J, Axel R, Gogos JA (2004) Spontaneous neural activity is required for the establishment and maintenance of the olfactory sensory map. *Neuron* 42(4):553–66.

Yu X, Wadghiri YZ, Sanes DH, Turnbull DH (2005) In vivo auditory brain mapping in mice with Mn-enhanced MRI. *Nat Neurosci* 8(7):961–8.

Yu YH, Blessing WW (1999) Amygdala co-ordinates sudden falls in ear pinna blood flow in response to unconditioned salient stimuli in conscious rabbits. *Neuroscience* 93(1):135–141.

Zacharko RM, Bowers WJ, Kokkinidis L, Anisman H (1983) Region-specific reductions of intracranial self-stimulation after uncontrollable stress: Possible effects on reward processes. *Behav Brain Res* 9(2):129–141.

Zago S, Ferrucci R, Fregni F, Priori A (2008) Bartholow, Sciamanna, Alberti: pioneers in the electrical stimulation of the exposed human cerebral cortex. *Neuroscientist* 14(5):521–8.

Zamponi GW, Currie KP (2013) Regulation of CaV2 calcium channels by G protein coupled receptors. *BBA-Biomembranes* 1828(7):1629–1643.

Zemelman BV, Lee GA, Ng M, Miesenböck G (2002) Selective photostimulation of genetically chARGed neurons. *Neuron* 33(1):15–22.

Zemelman BV, Nesnas N, Lee GA, Miesenbock G (2003) Photochemical gating of heterologous ion channels: remote control over genetically designated populations of neurons. *PNAS* 100(3):1352–7.

Zerucha T, Stühmer T, Hatch G, Park B, Long Q, Yu G, Gambarotta A, Schultz JR, Rubenstein JL, M E (2000) A highly conserved enhancer in the Dlx5/Dlx6 intergenic region is the site of cross-regulatory interactions between Dlx genes in the embryonic forebrain. *J Neurosci* 20(2):709–21.

Zhang F, Prigge M, Beyrière F, Tsunoda SP, Mattis J, Yizhar O, Hegemann P, Deisseroth K (2008) Red-shifted optogenetic excitation: a tool for fast neural control derived from Volvox carteri. *Nat Neurosci* 11(6):631–633.

Zhang SP, Bandler R, Carrive P (1990) Flight and immobility evoked by excitatory amino acid microinjection within distinct parts of the subtentorial midbrain periaqueductal gray of the cat. *Brain Res* 520(1-2):73–82.

Zheng W, Ren S, Graziano JH (1998) Manganese inhibits mitochondrial aconitase: a mechanism of manganese neurotoxicity. *Brain Res* 799(2):334–42.

Zhu H, Pleil KE, Urban DJ, Moy SS, Kash TL, Roth BL (2014) Chemogenetic inactivation of ventral hippocampal glutamatergic neurons disrupts consolidation of contextual fear memory. *Neuropsychopharmacol* 39(8):1880–92.

Zippelius HM, Schleidt WM (1956) Ultraschall-Laute bei jungen Mäusen. *Die Naturwissenschaften* 43(21):502–502.

Zugaib J, Coutinho MR, Ferreira MD, Menescal-de-Oliveira l (2014) Glutamate/GABA balance in ACC modulates the nociceptive responses of vocalization: An expression of affective-motivational component of pain in guinea pigs. *Physiol Behav* 126(1).